DAMAGE TOLERANCE OF COMPOSITE HONEYCOMB SANDWICH PANELS UNDER QUASI-STATIC BENDING AND CYCLIC COMPRESSION

by

MATTHEW CLAIRE TAYLOR

M.S., University of Southern California
(1986)
B.S., University of Minnesota
(1980)

SUBMITTED IN PARTIAL FULFILLMENT

OF THE REQUIREMENTS OF THE

DEGREE OF

MASTER OF SCIENCE

IN AERONAUTICAL AND ASTRONAUTICAL ENGINEERING

at the

MASSACHUSETTS INSTITUTE OF TECHNOLOGY

June 1989

Signature of Author _____ 23 May '89
Department of Aeronautics and Astronautics

Certified by _____
Professor James W. Mar, Thesis Supervisor
Department of Aeronautics and Astronautics, M.I.T.

Accepted by _____
Professor Harold Y. Wachman
Chairman, Department Graduate Committee

ABSTRACT

DAMAGE TOLERANCE OF COMPOSITE HONEYCOMB SANDWICH PANELS

UNDER QUASI-STATIC BENDING AND CYCLIC COMPRESSION

by

Matthew Claire Taylor

Submitted to the Department of Aeronautics and Astronautics
on May 19, 1989 in partial fulfillment of the requirements
for the Degree of Master of Science

The damage resistance and damage tolerance of minimum gauge face sheet sandwich panels subjected to quasi-static four point bending and cyclic column compression, was experimentally investigated for a graphite/epoxy plain weave fabric and Nomex honeycomb core. Face sheets with [0/90], [+-45], [0/90]s, and [+-45]s layups were constructed from AW193PW/3501-6 prepreg graphite/epoxy fabric and three thicknesses of Nomex honeycomb, 1.0", .687" and .375". Four point bending specimens (2.75" x 14") were constructed with three core thicknesses. Undamaged specimens were constructed with a 2" Nomex test section bounded by aluminum honeycomb core for load point reinforcement. Damage was inflicted with a spring propelled rod (.5" diameter hemispherical tup; .105 slug) at five levels of kinetic energy. Visual and x-ray inspection measurements were made to assess damage. Quasi-static four point loading provided failure moment, face sheet buckling stress and specimen deflection data. Damaged and undamaged column specimens (3.25" x 14") with reinforced grip sections were tested for fatigue life under compression-compression cyclic loading (R =.1). Results indicate that damage resistance increases with face sheet thickness and panel thinness. Residual strength of the 2 ply face sheet is dramatically reduced (0/90, 50 %; +-45, 30 %). The Nomex core limits ultimate bending moment in undamaged 2 ply specimens and all 4 ply specimens, with or without damage. Limited fatigue tests indicate a tremendous high load bearing longevity for undamaged 0/90 specimens. Notch sensitivity of the damaged 0/90 specimen cuts its load capability by at least half. Notch insensitivity of the damaged +-45 specimen allows for 60% of critical load to be carried to .5 million cycles.

Thesis Supervisor: James W. Mar
J.C. Hunsaker Professor of
Aerospace Education

AKNOWLEDGEMENTS

I would like to thank all those people who have made this work possible. Captain Robert W. Sherer and Commander James G. Ward gave me moral and financial support for this extracurricular study over the last three years. My thanks to Carl Varnin and Simon Lie who got me started in the TELAC lab and made me feel welcome. I extend my special gratitude to Al Supple who has lead me through many a trying day in the lab, fixed the computer for me and brought me back "on line" as well. Al was there always willing to help in every way. A very warm and heartfelt thankyou is extended to Professor James Mar who got me interested in composites two years ago and offered an avenue of study that is closed to most part time students. Professor Mar's friendliness and helpful instruction will always represent M.I.T. to me.

Aknowledgements would never be complete without mentioning the "worker bees" - The UROPers. I was lucky to be stuck with such a fine group. All hand selected so they had to call me "Sir". My thanks to Dave Wright who stepped in to help when I needed it down the stretch. My warmest appreciation and gratitude is extended to Chantal Moore who helped me break over a hundred specimens and slugged through hundreds of computer files, always producing a polished result. My eternal appreciation and gratitude has been earned by Teri Centner and Cristina Villella who upon hearing Paul Lagace match their names with me, said "Oh no.. we'll have to call him Sir ". They didn't have to say the "Sir" word in the lab, as long as they worked. And they did! Teri and Cristina constructed specimens through the summer while I was called away to summer training. They did everything that could have been asked for the last 13 months. I couldn't have finished without the dedication demonstrated by these four fine young people.

I am lucky to have three young ladies at home that have earned this degree through as much or more sacrifice as I. My lovely daughters, Autumn and Madeline have never known their father when he hasn't had a book in his hand. They tried so hard to leave me alone to study, but often it wasn't enough and I barked at them. This is the price I wish I hadn't paid for this degree. I can only claim part ownership to this degree. My wife April has put in as much sweat, work and frustration as I have. She has raised the girls and kept up the house without me. She has consoled me, kicked me in the pants and even used child psychology to keep me going. She has typed 99% of this thesis to help me end my ego experience. I hope someday I can repay her. Until then, April you have my eternal loving gratitude and respect.

FOREWARD

This work was conducted at the Technology Laboratory for Advanced Composites (TELAC) in the department of Aeronautics and Astronautics at the Massachusetts Institute of Technology. The work was sponsored by Boeing Helicopters under purchase order TT 70935. The project monitor was Steve Llorente.

TABLE OF CONTENTS

LIST OF FIGURES

LIST OF TABLES

NOMENCLATURE

σ	stress
τ	shear stress
ϵ	strain
γ	shear strain
C	stiffness matrix
S	compliance matrix
ν	Poisson's ratio
E	Young's modulus
Q_{ij}	reduced stiffnesses matrix
G	shear modulus
T	transformation matrix
U_i	invariant constants
θ	ply orientation
t, t_{ply}	lamina thickness
β	deformation angle
x,y,z	cartesian coordinates
u,v,w	cartesian displacements
K	curvature
N_f , N_x	force/unit width in face sheet
M_x	moment/unit width
f	face sheet thickness
h	panel thickness
W,b	panel width
A_{ij}	extensional stiffnesses
B_{ij}	coupling stiffnesses
D_{ij}	bending stiffnesses
r,R	radius of curvature
I	moment of inertia
s	curved path coordinate
P	transverse load
ℓ	moment arm
L	panel deflection section
$\theta_{B,A}$	panel deflection (outboard) angles
q	load / unit length
d	rupture diameter
D	dimple axis length
ξ, ρ, η	bending region coordinates
$\tilde{q}_{mn}$	modal amplitude of generalized displacement
k	core modulus (in z direction)
U	potential energy
W_{ext}	external work
Π	total energy
Hc	fracture parameter
S	standard deviation of a sample
n	population
N	fatigue cycles
R	fatigue ratio

Super-scripts:

"	d^2/dx^2
°	neutral plane or axis

Sub-scripts:

,xx ; ,yy	d^2/dx^2 ; d^2/dy^2
f	face sheet
cr	critical
d	deformed
x,y,z	direction of action with respect to specimen
1,2,3	direction of action with respect to material
o	undamaged, control value

Intentionally left blank for notes:

CHAPTER ONE

INTRODUCTION

The sandwich structure has been studied intensively for the past fifty years in order to understand its stress and strain mechanics; its simple design is used for everything from cardboard boxes to supersonic aircraft control surfaces. The sandwich structure can be constructed from virtually any material in order to satisfy its desired use. The three components for construction are two face sheets which carry in-plane loads and a core bonded between the face sheets. The core provides structural stability by maintaining the load bearing face sheets at a constant separation distance, along with maintaining shear stiffness parallel to the faces and normal stiffness perpendicular to the faces. The face sheets carry the compression and tension loads that resist panel bending.

Beyond the beauty of its simple construction, the sandwich panel's reason for being lies in its high strength to weight ratio and bending stiffness. Thus the sandwich structure has been applied to aircraft construction wherever possible and in whatever combination of materials thought feasible. Face sheet materials have included wood, fiberglass, and metals. The core has consisted of balsa wood, pine, glue pulp, polymen foam and light weight metals. The need to reduce weight led to the invention of another structural form - the honeycomb core.

With the advent of advanced filamentary composite

materials which possess exceptional strength-to-weight advantage and the development of aluminum and Nomex honeycomb cores; it is now possible to construct extremely weight efficient composite honeycomb core sandwich panels for aerospace application. Laminate face sheets can be tailored for specific loading orientations, strengths and durability. The honeycomb core can be made from aluminum, phenolic or Nomex material. It provides flexural stiffness, and shearing resistance through its thickness, shear modulus, and density, respectively. Because honeycomb core panels (HCPs) are typically used for part of the aircraft's external surface, the durability aspect of HCP design is now on a par with strength, stiffness and light weight.

"Durability" is the combination of structural longevity and economics of construction and repair. The filiamentary composite fabric facilitates simplified constuction and thus economic production. Structural longevity refers to damage resistance, damage tolerance, and fatigue life. Filamentary composites have exceptional undamaged characteristics, but their heterogeneous composition and brittle nature make their failure criteria complicated and specific to the structure and its accumulated damage.

This study examines the damage resistance and tolerance of a specific graphite epoxy/honeycomb core sandwich panel under quasi-static bending and compression-compression fatigue loading. The objective is to determine the

characteristics of the panel's resistance to damage, along with its maximum capabilities for various parameters of construction and load orientation.

CHAPTER TWO

PREVIOUS WORK

2.1 BACKGROUND

A great effort has been made in the last fifteen years to determine the fracture principles and mechanics of filamentary composites. Work has focused on the factors that tend to degrade composite laminate structure and the composite material structures.

Composites have some unique problems in that they are susceptible to damage at low levels of imparted energy such as might happen from runway debris, tool drops or hail. Further, this damage from impact may not be visually detectable. Often the damage inflicted to a sandwich composite panel is below the surface between plies and at the laminate core interface.

2.2 IMPACT DAMAGE AND RESIDUAL STRENGTH STUDIES

Many investigators have conducted controlled impact tests on composite sandwich panels to determine damage infliction at prescribed energy levels. Oplinger and Slepetz [1] impacted graphite and S-glass epoxy HCP's with a 2 inch diameter steel ball. They found that graphite epoxy was very brittle compared to S-glass because of its low strain to fracture (less than 1% for G/E, about 3% for S-glass). The Nomex was found crushed under the impact due to the graphite face rupturing, while the S-glass face sheet

bridged the crushed core's indentation to remain intact and absorb some of the impact. The graphite face sheets absorbed energy by progressive fracture along planes defined by the laminate fiber orientations due to the low strain capability relative to the indentor radius. The authors point out the need for a larger strain to failure level for graphite to be damage resistant and suggest that a tougher core (more dense) will prevent large impact damage at a weight penalty. Oplinger et al also suggests a hybrid face sheet of graphite and S-glass to improve resiliency at the cost of ultimate strength.

Rhodes [2] also recommended a hybrid face sheet as a means of raising the damage threshold for graphite sandwich structures. He compared graphite epoxy to Kevlar-491 epoxy under projectile impacts. Once again graphite was found to be more susceptible to breaking. Rhodes found that core indentation (crushing) during impact causes high local stresses in the face, which precipitates buckling. He also impacted panels under compression and was able to cause buckling at impact energy levels well below that required to initiate visible damage. Rhodes suggests a stiffer core as did Oplinger and Slepetz, as well as thicker face sheets to reduce the "bearly visible impact damage" (BVID) threshold. Rhodes maintains that a visual inspection for damage is inadequate.

The work of Adsit and Waszezak [3] supports Rhodes recommendation. After performing impacts with stones, a

.63cm tip radius and 2.54cm tip radius, Adsit et. al. found a panel strength reduction of up to 50% at the BVID (barely visible impact damage) level. Compressive residual strength decreased as impact energy was increased, regardless of impactor head. The Heat Resistant Phenolic honeycomb core (88kg per cubic meter) was not impact resistant, which resulted in core crushing and face sheet delaminations. Both forms of damage cause a localized loss of stability and make face wrinkling more possible. Adsit et. al. also found that distributing the impact energy over a broader surface (ie: .63cm to 2.54cm impactor radius) will add approximately 25% to the compressive residual strength. Data also implies that impact energy with the wide blunt tip can be doubled with no increase in panel damage or reduction in residual strength.

Gwynn and O'Brien [4] and Husman, Whitney and Halpin [5] each arrived at the same conclusion regarding impact energy's effect on compressive failure stress. There is a minimum plateau of residual strength (minimum stress) where greater impact energy will not create further damage. Husman et. al. [5] predicts this at less than face sheet penetration velocities. For velocities at penetration and higher, the residual failure stress approximates that of a hole of similar size. Gwynn et. al. [4] demonstrates that thick laminates have higher failure strains than thin laminates, after each is impacted at the same energy per laminate thickness. Thicker laminates dissipate impact

energy through matrix cracking and not local bending and stretching of fibers because of impact displacement. Delaminations within the face sheet were also associated with impact induced matrix cracking. The delaminations are peanut shaped and oriented (long axis) with the filament direction in each ply. once again, a source of localized buckling instability. Bernard and Lagace [6] examined the impact resistance of sandwich panels utilizing (+-45/0]s AS4/3501-6 graphite epoxy and three different core materials; Rohacell, Nomex and aluminum honeycomb. They established the BVID level at 1 Joule of impact energy; Nomex damage threshold at .4 Joules; and confirmed core crushing to be cell wall buckling. Panels with stiff cores like the aluminum had equal amounts of debonding and face sheet damage while Nomex debonding increases with core stiffness. Bernard also implanted delaminations in the laminates and debonds between face and core to compare against impacted panels. The result was a loss in local stiffness and a reduction in buckling stress threshold. Overall, the buckling load dropped by 8 to 19% for damaged panels and was found to be independent of the core material. This result may simply be a coincidence, because it violates Lie's [7] analytical buckling equation for an undamaged panel; which calls for the flexural rigidity term EI (Young's modulus times the beam's moment of inertia). If the cores were the same thickness this could be explained by negligible core density and stiffness compared to the face

laminates.

Lie [7] performed impacts at three energy levels and measured the dynamic strains of the panel during impact. With this data he compared it against an analytical computer model derived from Hertzian contact theory. Damaged panels of various thickness (all Nomex cores) were tested for residual strength under compression and compared with the afore mentioned critical buckling equation and the Mar-Lin residual strength relation. He found the [+-45] face sheets to be notch insensitive and fail at constant net-section stress. The [0/90] laminates were notch sensitive and so failure ocurred at stress levels lower than the net-section stress. Lie's impact tests found ,7 ft-lbs to be the damage threshold where core crushing begins, followed by matrix cracks, delamination and fiber rupture at 1.5 ft-lbs.

2.3 IMPACT DAMAGE EFFECT ON LONGEVITY

Ramkumar [8] examined the effect of low velocity impacts on laminate columns of 42 and 48 plies. His conclusions are:

- -Tension provides less threat to impact damaged laminates.
- -Delaminations propagate to cause early failure in compression-compression fatigue loading. This also provides the lowest strain failures. (Fatigue test $R = \infty$).
- - Recommends ultrasonic imspections to detect

delamination propagation.

Componeschi et. al. [9] studied stiffness reduction as an indicator of fatigue damage. He concludes that [0,90]s laminates don't experience a loss of longitudinal stiffness. The stiffness is degraded when the 90 degree ply is damaged. Camponeschi et. al. concludes that E_x in quasi-isotropic laminates reduces to an equilibrium state where no significant damage occurs until failure. They also claim that the major degradation in shearing stiffness occurs early in the panel's fatigue life.

"Sudden - Death" and "Degradation" fatigue models were proposed by Chou et. al. [10] to predict residual strength throughout the laminate's fatigue life. Tests indicate that the "Sudden - Death" model where residual strength doesn't degrade, provides a good model for laminates with a large majority of on-axis uni-plies. The "Degredation" model describes increasing strength reductions throughout the fatigue life. It predicts residual strength for off-axis uni-ply laminates.

Finally, Reifsnider, Schulte and Duke [11] propose three regions of damage: a stage of adjustment; coupling and growth; and final damage to failure. Fatigue failure modes and damage development is described for each.

Asit [3] performed fatigue testing on sandwich panels with a necked test section. He used a 4 point bending jig that oscillated at 1 Hz. to fatigue impacted panel test sections. Results indicate that increases in impact energy

shorten the specimen fatigue life, and ruptured fibers from impact have a greater effect on life than delaminations from a blunt impact.

2.4 THE INVESTIGATION

This investigation follows the work of Simon Lie [7]. In order to maintain a consistent data base, similar materials, dimensions, impact and test methods are employed. Residual strength will be tested through a bending test as used by Adsit [3]. However, the fatigue portion will be a follow-on study to Lie's static strength experiments. Similar specimens will be impacted, examined and then fatigued under compression-compression (c-c) loading at various peak loads. Damage propagation will be observed and measured.

CHAPTER THREE
ANALYTICAL MODELS

3.1 INTRODUCTION

This chapter examines the properties and mechanics of orthotropic symmetric laminates and their influence as face sheets of a honeycomb sandwich panel. Material properties will be based on previous tests and classical lamination plate theory. The characteristics of the woven lamina used in this investigation will be discussed. Stress and strain relations within the laminate will be developed and extended to the panel under pure bending. The derivation of homogeneous beam bending and its application to the four - point bending problem will be reviewed. A residual strength face sheet damage propagation under compression because of panel bending will be discussed. And finally, a global buckling model for one face sheet will be proposed.

3.2 STRESS - STRAIN RELATIONS IN AN ORTHOTROPIC LAMINATE

Principle material directions will be oriented to the three dimensional global coordinate system x, y and z, defined by test specimen geometry, illustrated in Figure 3.1, Global Coordinate System. Specimen axes will be parallel or coincident to an orthogonal coordinate axis as follows:

x - longitudinal
y - transverse
z - normal (to panel face)

Principle material directions or axes will be assigned

numbers 1, 2, and 3. The direction of filaments in a uni-ply or the "fill" filament direction in a woven ply will be refered to as the principal material axis 1. The perpendicular axis to 1 which lies in the ply's plane will be axis 2. The "right hand rule" will define the third axis which is normal to the reference ply. Tensor and contracted notation using x, y, z and 1, 2, 3 as subscripts will be used throughout this report to define directions and states of stress - strain.

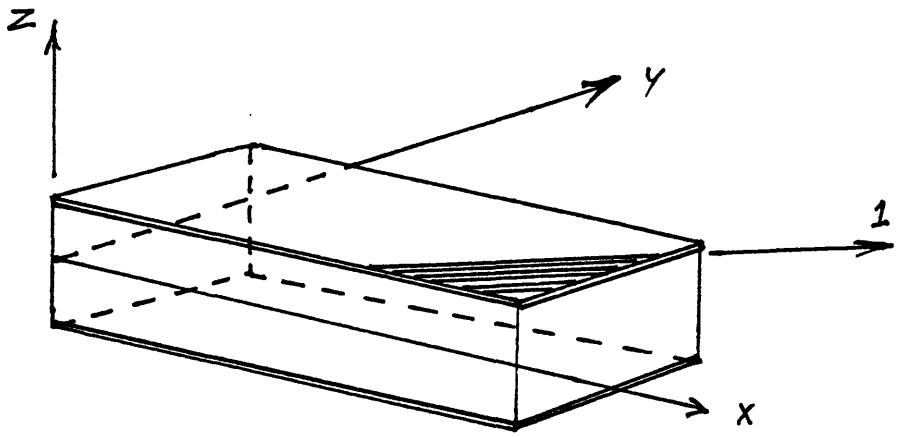

Figure 3.1 Global Coordinate System

Jones [12] provides a discussion of background material on this subject. A plane stress state is defined by assuming that $\sigma_z = 0$, $\tau_{yz} = 0$, $\tau_{zx} = 0$. This assumption is reasonable for a thin laminate. An orthotropic material allows for the reduction of 27 independent stiffness constants from the stiffness matrix C_{ij}. for the general case (anisotropic material). Where;

$$\sigma_i = C_{ij}\,\varepsilon_j \quad i,j = 1,\ldots 6 \qquad (3.2.1)$$

$$\begin{Bmatrix} \sigma_1 \\ \sigma_2 \\ \sigma_3 \\ \tau_{23} \\ \tau_{31} \\ \tau_{12} \end{Bmatrix} = \begin{bmatrix} C_{11} & C_{12} & C_{13} & 0 & 0 & 0 \\ C_{21} & C_{22} & C_{23} & 0 & 0 & 0 \\ C_{31} & C_{32} & C_{33} & 0 & 0 & 0 \\ 0 & 0 & 0 & C_{44} & 0 & 0 \\ 0 & 0 & 0 & 0 & C_{55} & 0 \\ 0 & 0 & 0 & 0 & 0 & C_{66} \end{bmatrix} \begin{Bmatrix} \varepsilon_1 \\ \varepsilon_2 \\ \varepsilon_3 \\ \gamma_{23} \\ \gamma_{31} \\ \gamma_{12} \end{Bmatrix} \quad (3.2.2)$$

can be reduced further with the plane stress state assumptions.

$$\begin{Bmatrix} \sigma_1 \\ \sigma_2 \\ \tau_{12} \end{Bmatrix} = \begin{bmatrix} C_{11} & C_{12} & 0 \\ C_{21} & C_{22} & 0 \\ 0 & 0 & C_{66} \end{bmatrix} \begin{Bmatrix} \varepsilon_1 \\ \varepsilon_2 \\ \gamma_{12} \end{Bmatrix} \quad (3.2.3)$$

Note: $C_{12} = C_{21}$ due to orthotropic symmetry.

The above relation can also be expressed in the compliance form.

$$\varepsilon_i = S_{ij}\,\sigma_j$$

$$\begin{Bmatrix} \varepsilon_1 \\ \varepsilon_2 \\ \gamma_{12} \end{Bmatrix} = \begin{bmatrix} S_{11} & S_{12} & 0 \\ S_{12} & S_{22} & 0 \\ 0 & 0 & S_{66} \end{bmatrix} \begin{Bmatrix} \sigma_1 \\ \sigma_2 \\ \tau_{12} \end{Bmatrix} \quad (3.2.4)$$

Where: $S_{11} = 1/E_1$ $S_{12} = -\nu_{12}/E_1 = -\nu_{21}/E_2$ $S_{22} = 1/E_2$ $S_{66} = 1/G_{12}$

The stiffness matrix for the orthotropic plane stress state can be determined more easily from the reduced stiffnesses form.

$$\begin{Bmatrix} \sigma_1 \\ \sigma_2 \\ \tau_{12} \end{Bmatrix} = \begin{bmatrix} Q_{11} & Q_{12} & 0 \\ Q_{12} & Q_{22} & 0 \\ 0 & 0 & Q_{66} \end{bmatrix} \begin{Bmatrix} \varepsilon_1 \\ \varepsilon_2 \\ \gamma_{12} \end{Bmatrix} \quad (3.2.5)$$

Where the reduced stiffnesses are:

$$Q_{11} = S_{22}/(S_{11}S_{22}-S_{12}^2) \qquad Q_{12} = -S_{12}/(S_{11}S_{22}-S_{12}^2)$$

$$Q_{22} = S_{11}/(S_{11}S_{22}-S_{12}^2) \qquad Q_{66} = 1/S_{66} \quad (3.2.6)$$

In terms of engineering constants

$$Q_{11} = E_1/(1-\nu_{12}\nu_{21}) \qquad Q_{12} = \nu_{12}E_2/(1-\nu_{12}\nu_{21}) = \nu_{21}E/(1-\nu_{12}\nu_{21})$$

$$Q_{22} = E_2/(1-\nu_{12}\nu_{21}) \qquad Q_{66} = G_{12} \quad (3.2.7)$$

Thus four independent material properties, E_1, E_2, ν_{12} and G_{12}

will determine the stress - strain relations in a "special orthotropic lamina". That is, the principle material axes 1 and 2 are aligned with the natural body loading axes x and y.

3.3 STRESS - STRAIN RELATION FOR ARBRITRARY LAMINA

3.3.1 Orientation

A stress - strain relation must be developed for lamina constructed from orthotropic plies of arbitrary orientation with respect to the geometrically natural coordinate directions. In this experimental work, 2 and 4 ply lamina facesheets will be subjected to compressive loads oriented in the direction of the specimen's longitudinal axis. Individual ply orientation can range from -90 to +90 with respect to the longitudinal or loading axis, x.

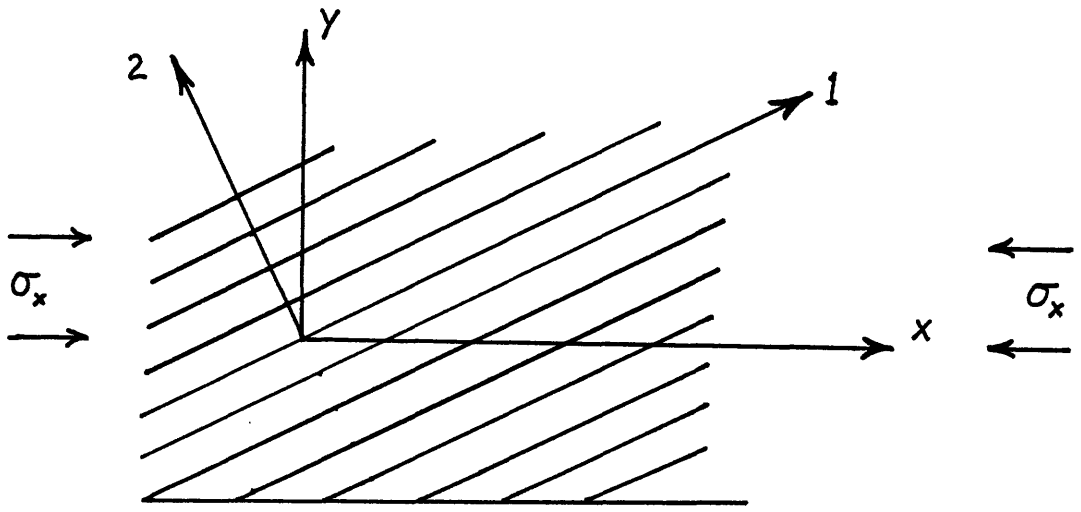

Figure 3.2 Ply Orientation With Respect to Loading Axes

Stress and strain transformations express the stresses

and strains of an x-y coordinate system in a 1-2 coordinate system. The transformations are commonly written as

$$\begin{Bmatrix} \sigma_x \\ \sigma_y \\ \tau_{xy} \end{Bmatrix} = [T]^{-1} \begin{Bmatrix} \sigma_1 \\ \sigma_2 \\ \tau_{12} \end{Bmatrix} \qquad \begin{Bmatrix} \varepsilon_x \\ \varepsilon_y \\ \gamma_{xy}/2 \end{Bmatrix} = [T]^{-1} \begin{Bmatrix} \varepsilon_1 \\ \varepsilon_2 \\ \gamma_{12}/2 \end{Bmatrix} \qquad (3.3.1)$$

where

$$[T] = \begin{bmatrix} \cos^2\theta & \sin^2\theta & 2\sin\theta\cos\theta \\ \sin^2\theta & \cos^2\theta & -2\sin\theta\cos\theta \\ -\sin\theta\cos\theta & \sin\theta\cos\theta & \cos^2\theta-\sin^2\theta \end{bmatrix}$$

and the inverse

$$[T]^{-1} = \begin{bmatrix} \cos^2\theta & \sin^2\theta & \sin\theta\cos\theta \\ \sin^2\theta & \cos^2\theta & -\sin\theta\cos\theta \\ -2\sin\theta\cos\theta & 2\sin\theta\cos\theta & \cos^2\theta-\sin^2\theta \end{bmatrix}$$

The reduced stiffness matrix for any ply orientation θ can be found through matrix multiplication.

$$[\bar{Q}] = [T]^{-1} [Q] [T]^{-T} \qquad (3.3.2)$$

where $\bar{Q}_{ij}$: transformed reduced stiffnesses

$[T]^{-T}$: inverse transpose of [T]

The orthotropic lamina becomes generally orthotropic after transformation.

$$\begin{Bmatrix} \sigma_x \\ \sigma_y \\ \tau_{xy} \end{Bmatrix} = \begin{bmatrix} \bar{Q}_{11} & \bar{Q}_{12} & \bar{Q}_{16} \\ \bar{Q}_{12} & \bar{Q}_{22} & \bar{Q}_{26} \\ \bar{Q}_{16} & \bar{Q}_{26} & \bar{Q}_{66} \end{bmatrix} \begin{Bmatrix} \varepsilon_x \\ \varepsilon_y \\ \gamma_{xy} \end{Bmatrix} \qquad (3.3.3)$$

The stiffness constants are simplified by Tsai and Pagano [13].

$$\begin{aligned} \bar{Q}_{11} &= U_1 + U_2 \cos 2\theta + U_3 \cos 4\theta \\ \bar{Q}_{12} &= U_4 - U_3 \cos 4\theta \\ \bar{Q}_{22} &= U_1 - U_2 \cos 2\theta + U_3 \cos 4\theta \\ \bar{Q}_{16} &= (1/2)U_2 \sin 2\theta + U_3 \sin 4\theta \\ \bar{Q}_{26} &= (1/2)U_2 \sin 2\theta - U_3 \sin 4\theta \\ \bar{Q}_{66} &= U_5 - U_3 \cos 4\theta \end{aligned} \qquad (3.3.4)$$

in which

$$
\begin{aligned}
U_1 &= [3Q_{11} + 3Q_{22} + 2Q_{12} + 4Q_{66}]/\ 8 \\
U_2 &= [Q_{11} - Q_{22}]/\ 2 \\
U_3 &= [Q_{11} + Q_{22} - 2Q_{12} - 4Q_{66}]/\ 8 \\
U_4 &= [Q_{11} + Q_{22} + 6Q_{12} - 4Q_{66}]/\ 8 \\
U_5 &= [Q_{11} + Q_{22} - 2Q_{12} + 4Q_{66}]/\ 8
\end{aligned}
\qquad (3.3.5)
$$

Note that the $\bar{Q}_{ij}$ are composed of invariant terms U_i, which are independent of ply orientation and dependent on material stiffnesses, only.

Using material constants determined for AW193PW/3501-6 graphite epoxy fabric, within TELAC and Boeing Helicopters, [Q] can be determined.

TABLE 3.1

Material Properties of AW193PW/3501-6 Graphite/Epoxy

	E_1	E_2	ν_{12}	$E_{(\theta = 45°)}$	ν_{21}
TELAC	9.09 Msi	8.72 Msi	.087	2.99 Msi	.083
Boeing	9.36 Msi	9.30 Msi	.050	3.00 Msi	.050

Recall that $\nu_{12}E_2 = \nu_{21}E_1$

so $\nu_{21} = \nu_{12}E_2/E_1$ (8.72/9.09) .087 = .083 = ν_{21} TELAC

or (9.30/9.36) .05 = .050 = ν_{21} B.H.

TABLE 3.2

Reduced Stiffnesses

TELAC Values: Q_{11} = 9.09/(1-(.083).087) = 9.16 Msi
Q_{22} = 8.72/(1-(.083).087) = 8.78 Msi
Q_{12} = .087 (8.78) = .764 Msi

Boeing Values: Q_{11} = 9.36/ (1- $.05^2$) = 9.38 Msi
Q_{22} = 9.30/ (1- $.05^2$) = 9.32 Msi
Q_{12} = .05 (9.32) = .466 Msi

By substituting the engineering constants into the

compliance matrix and performing transformation for a given ply orientation with respect to the loading axis, we find:

$$1/E_x = 1/E_1\cos^4\theta + (1/G_{12} - 2\nu_{12}/E_1)\sin^2\theta\cos^2\theta + 1/E_2\sin^4\theta$$

$$\nu_{xy} = E_x[\nu_{12}/E_1(\sin^4\theta + \cos^4\theta) - (1/E_1 + 1/E_2 - 1/G_{12})\sin^2\theta\cos^2\theta]$$

$$1/E_y = 1/E_1\sin^2\theta + (1/G_{12} - 2\nu_{12}/E_1)\sin^2\theta\cos^2\theta + 1/E_2\cos^4\theta$$

$$1/G_{xy} = 2(2/E_1 + 2/E_2 + 4\nu_{12}/E_1 - 1/G_{12})\sin^2\theta\cos^2\theta + 1/G_{12}(\sin^4\theta + \cos^4\theta) \qquad (3.3.6)$$

Since this investigator did not measure G_{12} with a specific shear test (such as the Rail Shear test), the above relations will be used to indirectly determine G_{12} from the +-45 compression tests. $E_{\theta=45^\circ}$ was found to average 3.0 Msi by Lie [7] and Boeing Helicopters. By substituting $\theta = 45^\circ$ and $E_x = 3.0$ Msi, we have the following

$$1/E_x = (1/E_1 - 2\nu_{12}/E_1 + 1/G_{12} + 1/E_2)/4 = 1/E_y \qquad (3.3.7)$$

where G_{12} is the only unknown.

Solving for G_{12}

$$G_{12} = [4/E_x - 1/E_1 - 1/E_2 + 2\nu_{12}/E_1]^{-1} \qquad (3.3.8)$$

and substituting:

TELAC values	G_{12} = .887 Msi
Boeing values	G_{12} = .885 Msi

Similarly, G_{xy} can be found for any orientation now that G_{12} is known. For $\theta = +45^\circ$:

$$1/G_{xy} = [2/E_1 + 2/E_2 + 4\nu_{12}/E_1 - 1/G_{12}]/2 + 1/2\,G_{12} \qquad (3.3.9)$$

TELAC G_{xy} = 4.10 Msi Boeing G_{xy} = 4.44 Msi

Since $Q_{66} = G_{12}$, all of the material constants, orientation

transformation equations and stress - strain relations are available to calculate the stresses and strains within a ply at any given orientation θ, with respect to the axes of applied load. This is facilitated with the Tsai & Pagano invariant reduced stiffnesses equations (3.2.5). Substituting engineering material constants into the invariant relations produces the following invariant values.

TABLE 3.3

Invariant Values for AW193PW/3501-6

	U_1	U_2	U_3	U_4	U_5 (Msi)
TELAC	7.36	.19	1.61	2.37	2.50
Boeing	7.57	.03	1.78	2.24	2.66

The reduced stiffnesses calculated from equation (3.3.4) using TELAC values are:

$$\bar{Q}_{11} = 7.36 + .19 \cos 2\theta + 1.61 \cos 4\theta$$
$$\bar{Q}_{12} = 2.37 - 1.61 \cos 4\theta$$
$$\bar{Q}_{22} = 7.36 - .19 \cos 2\theta + 1.61 \cos 4\theta \quad \text{(Msi units)}$$
$$\bar{Q}_{16} = (.19/2) \sin 2\theta + 1.61 \sin 4\theta$$
$$\bar{Q}_{26} = (.19/2) \sin 2\theta - 1.61 \sin 4\theta$$
$$\bar{Q}_{66} = 2.5 - 1.61 \cos 4\theta$$

Reduced stiffnesses are calculated using TELAC values, for given orientations.

TABLE 3.4

Reduced Stiffnesses Based On Orientation

θ =	0°	10°	20°	30°	40°	45°
$\bar{Q}_{11}$	9.16	8.77	7.79	6.65	5.88	5.75
$\bar{Q}_{12}$	.76	1.14	2.09	3.18	3.88	3.98
$\bar{Q}_{22}$	8.78	8.41	7.49	6.46	5.81	5.75
$\bar{Q}_{16}$	0	1.07	1.65	1.48	.64	.095
$\bar{Q}_{26}$	0	-1.00	-1.52	-1.31	-.46	.095
$\bar{Q}_{66}$	.89	1.27	2.22	3.31	4.01	4.11

Values are in Msi or 10^6 psi.

3.4 THE WOVEN LAMINA

Typical laminates are composed of multiple "uni-plies" stacked at various orientations with respect to the chosen principal axis for the laminate. The graphite/epoxy plain weave lamina used in this research is an orthotropic "bi-ply". That is, each ply has two principle directions of fiber orientation, which are approximately perpendicular and have their center of mass within the same plane. The filament tows in each direction are bent in a sinusoidal fashion as they pass over and under cross woven filament tows, as depicted in figure 3.3(a). As long as the fabric of graphite/epoxy is woven tightly with no holes or gaps between tows, each cross-section of a ply will be well populated with load bearing filaments. Note from figure 3.3(b) that these load bearing filaments are divided by the central ply plane throughout the fabric.

Sub-lamina geometry is discussed in Appendix B.

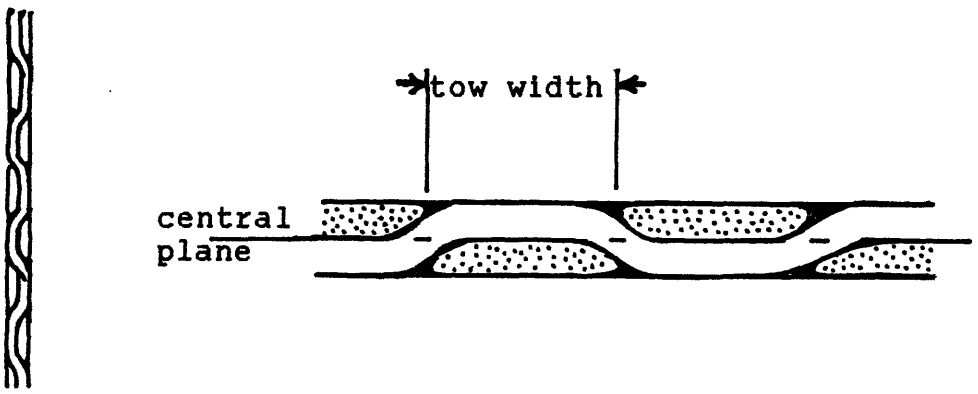

Figure 3.3 Fabric Tow Geometry Within A Lamina

3.5 STRESS - STRAIN VARIATIONS WITHIN A LAMINATE

For thin laminates, it will be assumed that lines originally straight and perpendicular to the central surface of the laminate, will remain straight and perpendicular when the laminate is extended, compressed or bent. This is the Kirchoff hypothesis for plates and the basic assumption of classical laminated plate theory. The result of this assumption is that shearing strains are neglected. (Note that the central surface will be a plane for flat laminates.) Thus, $\gamma_{xz} = \gamma_{yz} = 0$ and normals in the Z direction are assumed to maintain constant length, so $\varepsilon_z = 0$.

The Kirchoff-Love hypothesis for thin shells introduces laminate displacements u, v, and w for coordinate axes x, y, and z, respectively. The laminate occupies the x-y plane and undergoes deformations as illustrated in Jones [12] and reproduced in Figure 3.4 and 3.5. From the figure, line ABCK remains straight under deformation (by definition).

$$U_c = U_o - Z_c \beta \qquad (3.5.1)$$

Subscript O indicates a point on the middle surface. Line ABCD also remains perpendicular to the middle surface, which leads to

$$\beta = \partial w_o / \partial x \qquad (3.5.2)$$

Then, the displacement, u, at any point z through the laminate thickness is

$$u = u_o - z \, \partial w_o / \partial x \qquad (3.5.3)$$

By similar reasoning, $v = v_o - z \, \partial w_o / \partial y$

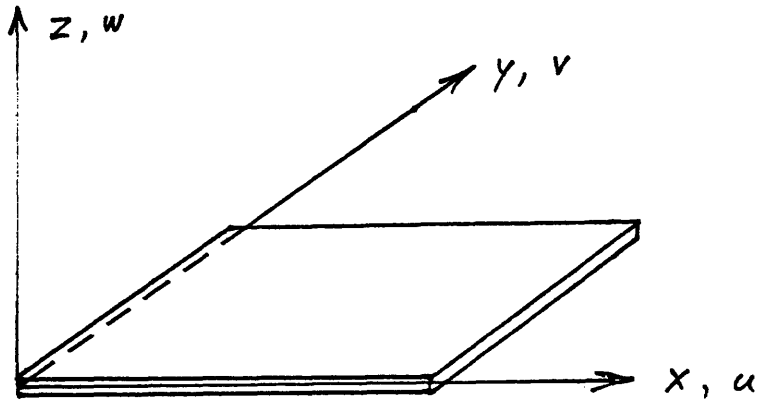

Figure 3.4 Coordinate and Displacement Orientation

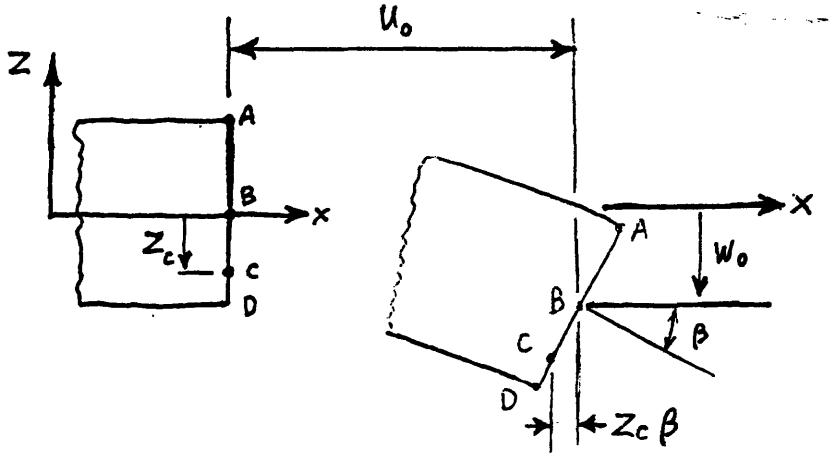

undeformed cross section deformed cross section

Figure 3.5 Geometry of Deformation in the z-x Plane

Non zero strains are defined in terms of displacements.

$$\varepsilon_x = \partial u/\partial x \qquad \varepsilon_y = \partial v/\partial y \qquad \gamma_{xy} = \partial u/\partial y + \partial v/\partial x \qquad (3.5.4)$$

Placing the results of equations (3.5.3) into (3.5.4), the strains become:

$$\begin{aligned} \varepsilon_x &= \partial u_o/\partial x - z(\partial^2 w_o/\partial x^2) \\ \varepsilon_y &= \partial v_o/\partial y - z(\partial^2 w_o/\partial y^2) \\ \gamma_{xy} &= \partial u_o/\partial y + \partial v_o/\partial x - 2z(\partial^2 w_o/\partial x \partial y) \end{aligned} \qquad (3.5.5)$$

Re-writing in matrix form, the strain variation equation is

$$\begin{Bmatrix} \varepsilon_x \\ \varepsilon_y \\ \gamma_{xy} \end{Bmatrix} = \begin{Bmatrix} \varepsilon_x^\circ \\ \varepsilon_y^\circ \\ \gamma_{xy}^\circ \end{Bmatrix} - z \begin{Bmatrix} K_x \\ K_y \\ K_{xy} \end{Bmatrix} \qquad (3.5.6)$$

where the middle surface strains are

$$\begin{Bmatrix} \varepsilon_x^\circ \\ \varepsilon_y^\circ \\ \gamma_{xy}^\circ \end{Bmatrix} = \begin{Bmatrix} \partial u_o/\partial x \\ \partial v_o/\partial y \\ \partial u_o/\partial y + \partial v_o/\partial x \end{Bmatrix} \qquad (3.5.7)$$

and the middle surface curvatures are

$$\begin{Bmatrix} K_x \\ K_y \\ K_{xy} \end{Bmatrix} = \begin{Bmatrix} \partial^2 w_o/\partial x \\ \partial^2 w_o/\partial y \\ 2\partial^2 w_o/\partial x \partial y \end{Bmatrix} \qquad (3.5.8)$$

By substituting the through the thickness strain variation equation (3.5.6) into the orthotropic stress - strain relation, equation (3.3.3); the stresses in any ply k can be determined.

$$\begin{Bmatrix} \sigma_x \\ \sigma_y \\ \tau_{xy} \end{Bmatrix} = \begin{bmatrix} \bar{Q}_{11} & \bar{Q}_{12} & \bar{Q}_{16} \\ \bar{Q}_{12} & \bar{Q}_{22} & \bar{Q}_{26} \\ \bar{Q}_{16} & \bar{Q}_{26} & \bar{Q}_{66} \end{bmatrix}_k \left(\begin{Bmatrix} \varepsilon_x^\circ \\ \varepsilon_y^\circ \\ \gamma_{xy}^\circ \end{Bmatrix} - z \begin{Bmatrix} K_x \\ K_y \\ K_{xy} \end{Bmatrix} \right) \qquad (3.5.9)$$

Since $\bar{Q}_{ij}$ can be different for each ply, the stress variations may not be linear through the thickness, even though the strain variation is linear.

The force and moment per unit length (or width) acting on a laminate is found through integration of the stresses in each layer or lamina through the laminate thickness.

$$N_x = \int_{-f/2}^{f/2} \sigma_x \, dz$$

$$M_x = \int_{-f/2}^{f/2} \sigma_x \, z dz \qquad (3.5.10)$$

where N_x and M_x are the force and moment per unit length. N_y and M_y are the force and moment per unit width, with intergration of σ_y through the thickness, f. Integrating through the laminate for σ_x, σ_y, and τ_{xy} (substituting equation (3.5.9) into (3.5.10)), for both force and moment.

$$\begin{Bmatrix} N_x \\ N_y \\ N_{xy} \end{Bmatrix} = \sum_{k=1}^{m} \left[\bar{Q}_{ij} \right] \left\{ \int_{z_{k-1}}^{z_k} \begin{Bmatrix} \varepsilon_x^\circ \\ \varepsilon_y^\circ \\ \gamma_{xy}^\circ \end{Bmatrix} dz + \int_{z_{k-1}}^{z_k} \begin{Bmatrix} K_x \\ K_y \\ K_{xy} \end{Bmatrix} z dz \right\} \qquad (3.5.11)$$

$$\begin{Bmatrix} M_x \\ M_y \\ M_{xy} \end{Bmatrix} = \sum_{k=1}^{m} \left[\bar{Q}_{ij} \right] \left\{ \int_{z_{k-1}}^{z_k} \begin{Bmatrix} \varepsilon_x^\circ \\ \varepsilon_y^\circ \\ \gamma_{xy} \end{Bmatrix} z dz + \int_{z_{k-1}}^{z_k} \begin{Bmatrix} K_x \\ K_y \\ K_{xy} \end{Bmatrix} z^2 dz \right\} \qquad (3.5.12)$$

where the laminate has m layers or lamina. Recall that middle surface strains and curvatures are not functions of z, but values which can be removed from the summation. Thus equations (3.5.11) and (3.5.12) can be written as

$$\begin{Bmatrix} N_x \\ N_y \\ N_{xy} \end{Bmatrix} = \begin{bmatrix} A_{11} & A_{12} & A_{16} \\ A_{12} & A_{22} & A_{26} \\ A_{16} & A_{26} & A_{66} \end{bmatrix} \begin{Bmatrix} \varepsilon_x^o \\ \varepsilon_y^o \\ \gamma_{xy}^o \end{Bmatrix} + \begin{bmatrix} B_{11} & B_{12} & B_{16} \\ B_{12} & B_{22} & B_{26} \\ B_{16} & B_{26} & B_{66} \end{bmatrix} \begin{Bmatrix} K_x \\ K_y \\ K_{xy} \end{Bmatrix} \tag{3.5.13}$$

$$\begin{Bmatrix} M_x \\ M_y \\ M_{xy} \end{Bmatrix} = \begin{bmatrix} B_{11} & B_{12} & B_{16} \\ B_{12} & B_{22} & B_{26} \\ B_{16} & B_{26} & B_{66} \end{bmatrix} \begin{Bmatrix} \varepsilon_x^o \\ \varepsilon_y^o \\ \gamma_{xy} \end{Bmatrix} + \begin{bmatrix} D_{11} & D_{12} & D_{16} \\ D_{12} & D_{22} & D_{26} \\ D_{16} & D_{26} & D_{66} \end{bmatrix} \begin{Bmatrix} K_x \\ K_y \\ K_{xy} \end{Bmatrix} \tag{3.5.14}$$

where

$$\begin{aligned} A_{ij} &= \sum_{k=1}^{m} (\bar{Q}_{ij})_k \quad (z_k - z_{k-1}) \\ B_{ij} &= 1/2 \sum_{k=1}^{m} (\bar{Q}_{ij})_k \quad (z_k^2 - z_{k-1}^2) \\ D_{ij} &= 1/3 \sum_{k=1}^{m} (\bar{Q}_{ij})_k \quad (z_k^3 - z_{k-1}^3) \end{aligned} \tag{3.5.15}$$

A_{ij} , B_{ij} and D_{ij} are the extensional, coupling and bending stiffnesses, respectively.

Equations (3.5.13 - 15) are simplified for symmetric layups, [θ]s or $[\theta]_{2,3}$, ... The perpendicular weave of AW193PW/3501-6 makes [0/90], [+ - 45], [0/90]s and [+ - 45]s symmetric also. This would not be true for uni-ply construction. These lay-ups are equivalent to $[0]_{z,y}$ and $[45]_{z,y}$. Thus $\bar{Q}_{ij}$ for each ply in the laminate is the same and the summation is over the distance z from the middle surface. All coupling terms B_{ij} , are zero because of symmetric lamina orientation about the middle surface.

Table 3.5

Stiffnesses for Orthotropic Plain Weave Laminates

	Extensional	Coupling	Bending
	A_{ij}	B_{ij}	D_{ij}
[0/90],[+-45]	$2\ \bar{Q}_{ij}\ t_{ply}$	0	$2/3\ \bar{Q}_{ij}\ t^3_{ply}$
[0/90]s,[+-45]	$4\ \bar{Q}_{ij}\ t_{ply}$	0	$16/3\ \bar{Q}_{ij}\ t^3_{ply}$

Using the nominal ply thickness, t_{ply} = .0076 inch and reduced stiffnesses $\bar{Q}_{ij}$ from Table 3.4, one .can calculate the extentional and bending stiffnesses for use in equations (3.5.13) and (3.5.14). Measurement of strains and curvatures will permit the calculation of extentional forces (N_x, N_y), in-plane shearing forces (N_{xy}), moments (M_x ,M_y) and torsion (M_{xy}).

3.6 BEAM DEFLECTION UNDER TRANSVERSE LOADING

To this point, the plane weave laminate has been considered as a perfectly bonded stack of orthotropic plies with special characteristics because of it's weave, symmetric lay-up and material axis orientation. In order to study the interaction of plain weave laminate facesheets and honeycomb cores under bending, the global model of a homogeneous thin beam or panel under transverse loading will be examined. This loading method was the experimental means for determining panel capabilities and failure characteristics.

Timoshenko [14] described the deflection of a thin homogeneous beam supported by two fixed pivot points under transverse loads or bending moments. Timoshenko assumed that the beam has a thin rectangular cross section and its neutral axis lies in the middle surface.

Neglecting the small effect of shearing force, the curvature at any point depends only on the magnitude of the moment M at that point.

The resulting relation for pure bending:

$$1/r = M/EI_y \qquad (3.6.1)$$

where: r is the radius of curvature

M is the moment of external forces

E is Young's Modulus for a homogeneous beam

$$I_y = \int z^2 dA \qquad (3.6.2)$$

I_y is the moment of inertia for the cross section with respect to the neutral axis.

Combining equations (3.6.1) and (3.6.2) yields

$$M_r = EI_y/r = E/r \int z^2 dA = \int E/r\, z^2 dA \qquad (3.6.3)$$

where EI_y: flexual rigidity

Thus the bending moment is inversely proportional to the radius of curvature by a factor of the beam's flexural rigidity, a constant for a given material cross section.

Any beam or panel which is not constrained on its edges will exhibit anticlastic curvature through lateral extension and longitudinal contraction in the surfaces of the beam

which lie on the concave side of the neutral surface, during bending. The opposite is true for the convex side of the neutral surface. The neutral surface as its name implies, does not contract or extend in any direction as it bends in orthogonal directions. Figure 3.6 illustrates the anticlastic curvature in a thick homogeneous beam as it curves in orthogonal directions due to conservation of beam mass and material density. The top surface or concave side of the beam is in a state of lateral extension and longitudinal contraction. That is, ε_y is positive and ε_x is negative.

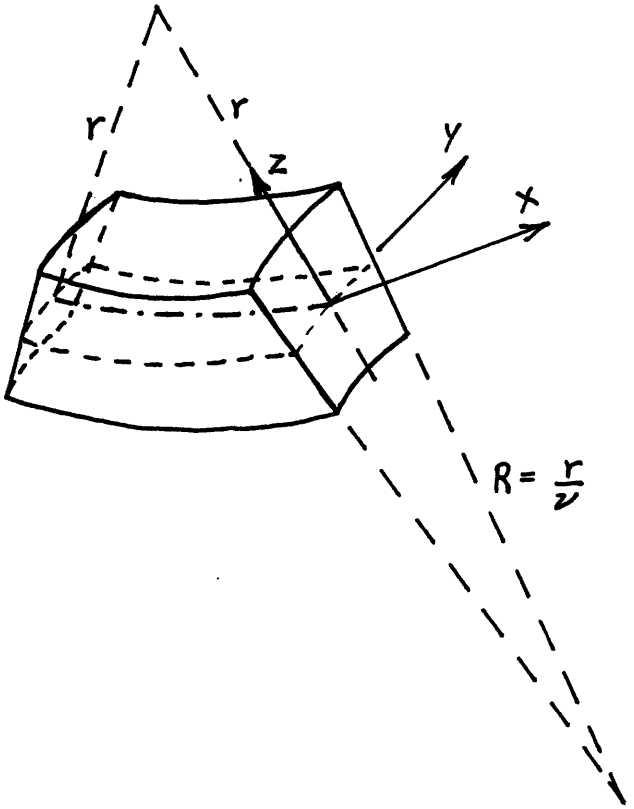

Figure 3.6 Anticlastic Curvature Under Pure Bending

Surface strains within an element of intact material are related by Poisson's ratio. The unit strain in the lateral direction is

$$\varepsilon_y = -\nu_{yx}\,\varepsilon_x = -\nu_{yx}\,z/r \qquad (3.6.4)$$

where z is the distance from the neutral surface to the surface and r is the radius of longitudinal curvature being considered. Due to the distortion, material lines in the cross section originally parallel to the y axis will curve and remain normal to the sides of the beam. Their radius of curvature R will be larger than r by the same proportion as ε_x is to ε_y. A more useful form is

$$R = r/\nu \qquad (3.6.5)$$

where R : the lateral radius of curvature.

This lateral bending of a beam under an axial bending moment becomes quite apparent for thin sandwich beams under large bending distortion.

The incremental distance ds along a deflected beam's neutral surface can be written as

$$ds = r\,d\theta \qquad (3.6.6)$$

using the small angle assumption,

and for sign convention $1/r = d\theta/ds$ (3.6.7)

Assuming flat deflections $ds \approx dx$, $\theta \approx \tan\theta = dz/dx$

and placing approximate values into equation (3.6.7)

$$1/r = d^2z/dx^2 \qquad (3.6.8)$$

Equation (3.6.1) becomes the differential equation of deflection.

$$EI_y\, d^2z/dx^2 = M \qquad (3.6.9)$$

Large curves prevent the small angle approximation and require a more accurate value for θ:

$$1/r = (d\theta/ds) = d(\arctan(dz/dx))/dx \; dx/ds \qquad (3.6.10)$$

$$1/r = (d^2z/dx^2)/[1 + (dz/dx)^2]^{3/2}$$

where $\theta = \arctan(dz/dx)$.

So equation (3.6.9) becomes

$$EI_y \, (d^2z/dx^2) \; / \; [1 + (dz/dx)^2]^{3/2} = M \qquad (3.6.11)$$

3.7 FOUR POINT BEAM BENDING DEFLECTION

Defining the moment equations from equation (3.6.9) for a four point symmetrically loaded beam.

$$M = EI_y \, (d^2w/dx^2) = \begin{cases} Px ; & 0 \le x \le \ell \\ P\ell ; & \ell \le x \le (L-\ell) \\ P(L-x) ; & (L-\ell) \le x \le L \end{cases} \qquad (3.7.1)$$

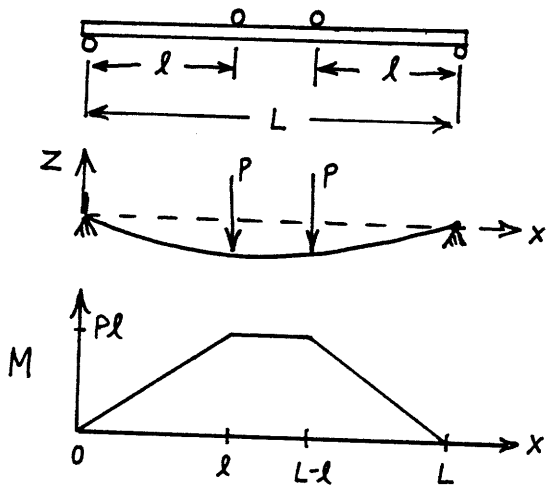

Figure 3.7 Four Point Beam Loading

Integrating the moment equations twice and solving for

associated boundary conditions and compatibility conditions leads to the well known solution.

$$w(x) = \begin{cases} (P/EI_y)[x^3/6 - \ell x(L - \ell)/2] & ; 0 \le x \le \ell \\ (P\ell/EI_y)[x^2/2 - Lx/2 + \ell^2/6] & ; \ell \le x \le (L-\ell) \\ (P/EI_y)[-x^3/6 + Lx^2/2 - x(L^2 - L\ell + \ell^2)/2 \\ \quad + L(L^2 - 3L\ell + 3\ell^2)/6] & ; (L-\ell) \le x \le L \end{cases} \qquad (3.7.2)$$

Maximum Deflection occurs when $dz/dx = 0$ and $x = L/2$, by symmetry

$$(w)_{max} = (P\ell/EI_y)[\ \ell^2/6 - L^2/8\ ] \qquad (3.7.3)$$

The angle on either end of this symmetrically deflected beam is:

$$\theta_A = (dz/dx)_{x=0} = -(P/2EI_y)(\ell^2 - \ell L)$$

$$\theta_B = (dz/dx)_{x=L} = (P/2EI_y)(\ell^2 - \ell L) \qquad (3.7.4)$$

Equations (3.7.3) and (3.7.4) will be used to calculate the flexural rigidity of damaged and undamaged specimens based upon measured values of load, θ_B and mid-beam deflection. The idealized homogeneous beam model must now be examined as a sandwich beam/panel with its 3 dimensional stresses and multiple component parts.

3.8 FLEXURAL STIFFNESS OF THE SANDWICH PANEL

Extending the Kirchoff assumption to a sandwich panel allows equation (3.5.15) to be written in its basic form with the following defined panel dimensions as:

h: panel thickness

f: face sheet thickness

c: core thickness

and

$$A_{ij} = \int_{-h/2}^{h/2} \bar{Q}_{ij}\, dz$$

$$B_{ij} = \int_{-h/2}^{h/2} \bar{Q}_{ij}\, z dz \qquad (3.8.1)$$

$$D_{ij} = \int_{-h/2}^{h/2} \bar{Q}_{ij}\, z^2 dz$$

where $h = c + 2f$ (3.8.2)

t or t_{ply} = one ply

The values for A_{ij} and B_{ij} found in Table 3.6 are simply doubled to account for 2 face sheet laminates and a negligible core stiffness in the x - y plane.

[0/90], [+-45]: $A_{ij} = 4\bar{Q}_{ij}\, t_{ply} = 2\bar{Q}_{ij}\, f$ $B_{ij} = 0$

[0/90]s, [+-45]s: $A_{ij} = 8\bar{Q}_{ij}\, t_{ply} = 4\bar{Q}_{ij}\, f$ $B_{ij} = 0$ (3.8.3)

The bending stiffness becomes (3.8.4)

$$D_{ij} = 1/3\ \bar{Q}_{ij}\left\{\left[Z^3 \Big|_{c/2}^{h/2} + \left[Z^3 \Big|_{-h/2}^{-c/2}\right\} + 1/3\ \bar{Q}_{ij_{core}}\left[Z^3 \Big|_{-h/2}^{+c/2}\right.\right.$$

Since $\bar{Q}_{ij\ core}$ is negligible it can be removed to leave

$$D_{ij} = 2/3\ \bar{Q}_{ij}\ (h^3/8 - c^3/8) = 1/12\ \bar{Q}_{ij}\ (h^3 - c^3) \qquad (3.8.5)$$

This bending stiffness equation is applicable to all symmetric sandwich panels with negligibly stiff cores and face sheets with constant orientation for every ply.

Equations (3.5.13) and (3.5.14) can now be written in simplified matrix form for these specific panels.

$$\{N\} = 2f\ [\bar{Q}_{ij}]\ \{\varepsilon^{\circ}\} \qquad (3.8.6)$$

$$\{M\} = (h^3 - c^3)/12\ \ [\bar{Q}_{ij}]\ \{K\} \qquad (3.8.7)$$

For a sandwich panel under pure bending, the mid-plane will experience no extension, only bending curvature. Hence $\{\varepsilon^{\circ}\} = 0$ and $\{N\} = 0$. If we substitute equation (3.5.8) into (3.5.5) and assume no mid-plane extension (or contraction), equation (3.5.5) becomes

$$\begin{aligned} \varepsilon_x(z) &= -zK_x \\ \varepsilon_y(z) &= -zK_y \\ \gamma_{xy}(z) &= -zK_{xy} \end{aligned} \qquad (3.8.8)$$

where the curvatures are constant through the panel by the Kirchoff assumption. Rearranging equation (3.6.9) into matrix form, we have the curvature relation

$$\begin{Bmatrix} K_x \\ K_y \\ K_{xy} \end{Bmatrix} = -1/z \begin{Bmatrix} \varepsilon_x \\ \varepsilon_y \\ \gamma_{xy} \end{Bmatrix} \qquad (3.8.9)$$

Measured face sheet strains ε_x, ε_y and γ_{xy} can be placed into equation (3.8. 9) along with $z = h/2$, to provide the panel curvatures. $\{M\}$ can then be calculated from equation (3.8.7).

Note: Sign convention

Curvatures are positive when the concave normal is in the positive x,y, or z direction. Positive moments create positive curvatures.

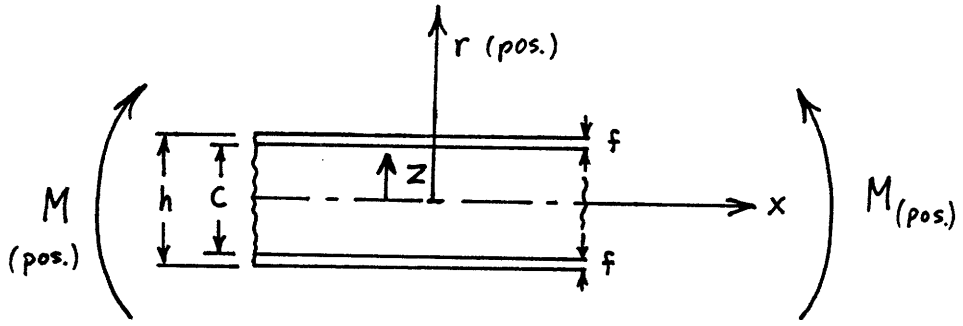

(a) General Panel

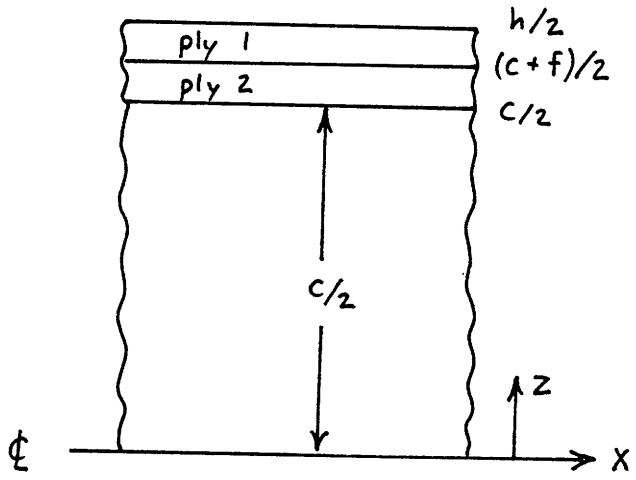

(b) Top Face of 2 Ply Panel

Figure 3.8 Panel Side View

3.9 LOCAL BUCKLING OF FACESHEET AND CORE

If a sandwich panel is bent and it has been assumed that the bending moment is carried by the axial forces in the face sheets only, then an element in its deformed state is loaded as depicted in Figure 3.9 (a). The left hand and right hand forces in the face sheets are rotated through a deflection angle of w" dx with respect to each other, the core element is compressed in the vertical direction by a force N_f w" per unit run as illustrated in Figure 3.9 (b) and expressed as

$$q\,dx = N_f\,(d^2w/dx^2)\,dx \qquad (3.9.1)$$

This force compresses the core and c is reduced.

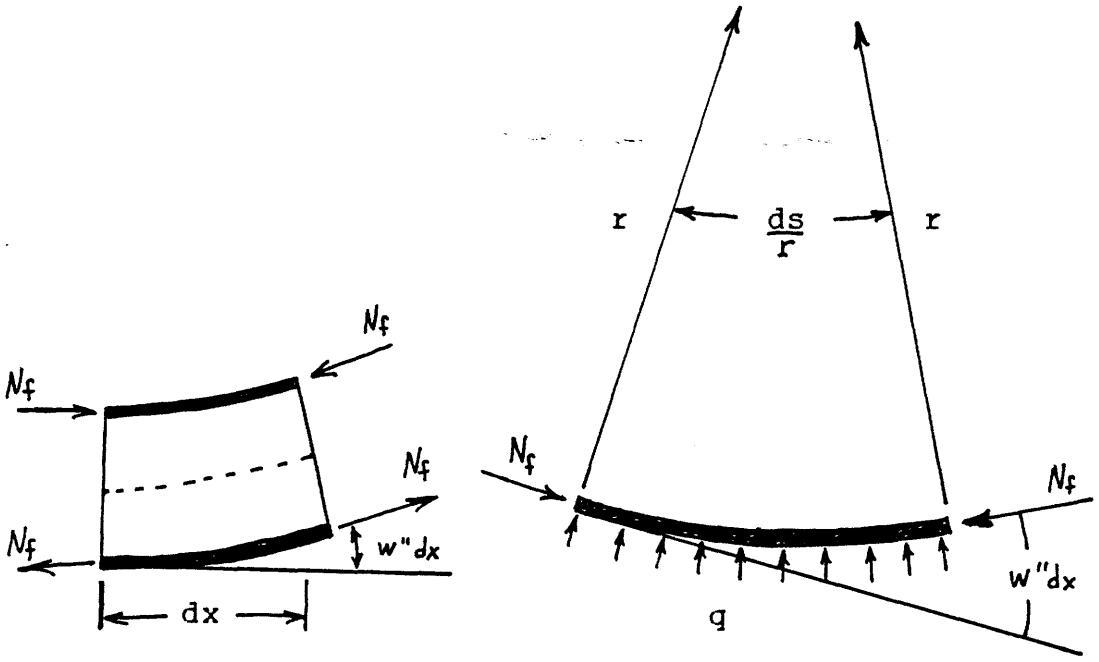

(a) Panel Element Bending

(b) Face Element Loading Curvature

Figure 3.9 Honeycomb Core Loading

Concentrated loading in the vertical (z direction) causes an additional compression. As core thickness c reduces in-plane face sheet loads increase under a constant moment. Increased face sheet loads will increase the normal load on the core once again.

A honeycomb core provides resistance to vertical deformation until its buckling load is approached; at which time the cell walls start to buckle, crimp and finally crush. Figure 3.10 is a typical honeycomb core load diagram to failure. The core loading deformation can be ignored until O approaches the core's wrinkling and cell buckling stress.

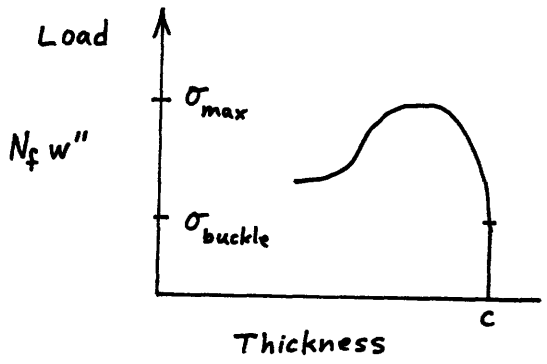

Figure 3.10 Core Deformation Load Diagram

Researchers working with thin face sheets have found face sheet wrinkling and dimpling to occur with honeycomb panels subjected to critical in-plane loading; where the dimple appears within the confines of the core cell. Dimpling is essentially a localized buckling phenomenon of the face element over a cell, which is supported at all edges of the cell. Weikel and Kobayashi [15] proposed a relation between the critical stress and a characteristic

dimension f/d.

where d is the length of a square cell and f is the face sheet thickness.

$$\sigma_{cr} = 2.5.E_f(f/d)^2 \qquad (3.9.2)$$

The 2.5 factor assumes a Poisson value of .3 for the face sheet. Compressive loads were parallel to the square cell's diagonal.

For hexagonal cell sandwiches, Plantema [16] compared the test results of Norris/Kommers [50-5] and Kuenzi [51-17], and found that the exponent for the characteristic dimension f/d, was 1.7 and 2.4, respectively. By settling for the compromise value of 2 and simpler formula:

$$\sigma_{cr} = 3Er(f/d)^2 \qquad (3.9.3)$$

Plantema found a +-8% deviation from Kuenzi's experimental results.

The normal panel loading qdx applied to an undamaged core during sandwich panel bending is $N_f w''$ dx from equation 3.9.1. In most cases $w''dx$ will be quite small (if c/f is greater than 10) and so will the normal loading q applied to the core. Now consider the length-wise cross section of a panel with a face sheet indentation. With the panel perfectly flat and undeformed, fibers of the face sheet running through the indentation are out of the face sheet plane and susceptible to buckling under compressive in-plane loading. When the panel is bent with the dented face under compression, localized normal loading/unit area increases beneath the facial indentation.

Where w_d'' is the local curvature within the face sheet indentation. w_d'' is a function of position within the indentation, as illustrated in Figure 3.11(b). If the tows continue to carry N_f (or σ_x) in their deformed condition, one can see from equation (3.9.4) that σ_z is larger than the undamaged core load, $\sigma_z = N_f w''/dx$ by a factor of $(w'' + w_d''/w'')$.

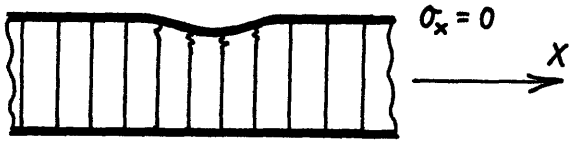

(a) Side View

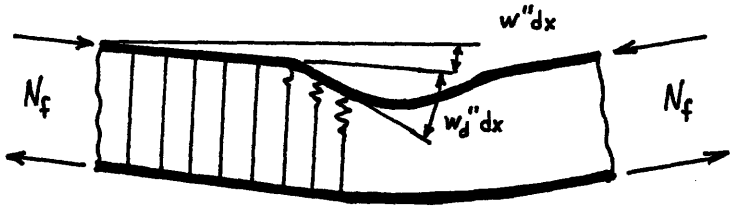

(b) Tow Deflection

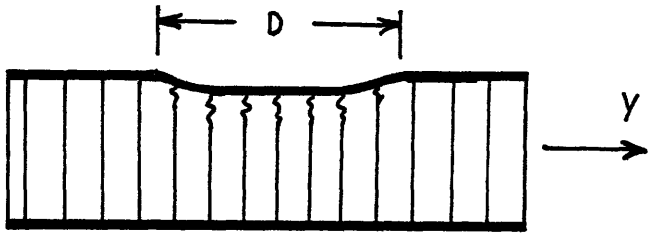

(c) Cross Sectional View

D: Dimple axis length

Figure 3.11 Cross Sectional View of a Dimpled Face Sheet Under Compression

3.10 RESIDUAL STRENGTH MODEL

Once the damage has been assessed and regional damage growth forecast, a practical global model is required to predict panel buckling loads and modes. The buckling load for the undamaged panel is the first step.

A sandwich panel loaded under four point bending as illustrated in Figure 3.7, is subjected to a pure bending moment $M_x = P\ell$, between the two interior load points, as described in section 3.7. The top laminate face sheet will be subjected to a compressive force $N_x = P\ell/(c+f)W$, and modeled as an orthotropic plate restrained by a stiff elastic foundation. The film adhesive embedded in the Nomex foundation adds considerable stiffness to the laminate and thus must be considered in the model.

It is assumed that the Nomex foundation modulus and panel bending stiffness are constant through the pure bending test section. In addition, the panel is simply supported at x = a, o and displays minimal anticlastic curvature. The final approximation neccessary for simplification is that the face sheet bending moment M_{f_x}, due to face curvature, is insignificant compared to the bending moment of the sandwich panel.

In order to simplify the plate-mode calculations, a new coordinate system parallel to the existing x-y-z system will be defined as ξ, ρ, η, respectively. The ξ and ρ axes will bound two sides of the pure bending test section of the panel and η will be the face sheet deflection parallel to

the z axis, from the $\xi - \rho$ datum plane. Refer to Figure 3.1^ for an illustration of the coordinate systems positioning.

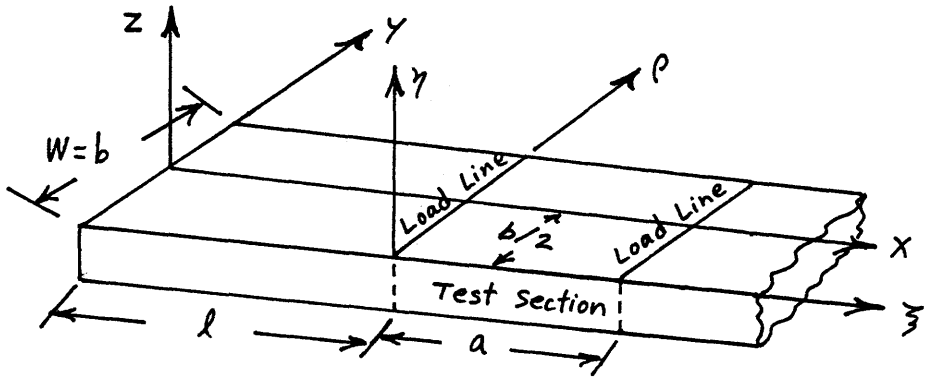

Figure 3.12 Bending Region Coordinate System

The bending region coordinate system has the following relations:

$$\xi = x - \ell$$

$$\rho = y - W/2 = y - b/2 \qquad (3.10.1)$$

where: $W = b$

and from the deflection equation (3.7.7) for the entire panel

$$w = -(Pl/EI_y)[x^2/2 - Lx/2 + \ell^2/6] \; ; \quad l \leq x \leq (L-\ell) \qquad (3.10.2)$$

we gain the deflection relation

$$\eta = w(x) + P\ell^2/EI \; [(2/3)\ell - L/2 \,] \qquad (3.10.3)$$

and assuring a small anticlastic curvature we can shift the deflection relation to $y = -W/2$, the edge of the panel. Now deflection errors become more critical as the defection function η is defined by position (ξ, ρ).

The bending region has dimensions:

$a = L - 2\ell$ $\qquad$ $b = W =$ width

$$\eta(\xi) = -Pl/EI_y[\,\xi^2/2 + (\ell - L/2)\xi\,] \qquad (3.10.4)$$

As expected, η_{max} occurs at $x = L/2$ or $\xi = (L/2) - \ell$

$$\eta_{max}(L/2 - \ell) = Pl/2EI_y[\,L^2/4 - L\ell + \ell^2\,] \qquad (3.10.5)$$

The boundary conditions for the bending region are:

$$\xi = 0, a; \quad \eta = 0; \quad \delta M_{x_f} = -D_{11}\delta\eta_{,xx} - D_{12}\delta\eta_{,yy} \simeq 0$$

by the assumption of insignificance compared to the panel's moment.

$\rho = 0, b$; $\delta\eta = 0$ because the plate is in a curved equilibrium state;

$$\eta(\xi) = -Pl/2EI_y(\,\xi^2 - a\xi\,) \qquad (3.10.6)$$

and $\delta M_y = -D_{12}\delta\eta_{,xx} - D_{22}\delta\eta_{,yy} = 0$ for specially orthotropic plates.

The Rayleigh-Ritz method of assumed modes will be used to predict critical loads and failure modes. The displacements $\eta(\xi, \rho)$ are modeled as:

$$\eta(\xi, \rho) = \sum_{m=1}^{\tilde{m}} \sum_{n=1}^{\tilde{n}} \tilde{q}_{mn} \sin\frac{m\pi\xi}{a} \sin\frac{n\pi\rho}{b} \qquad (3.10.7)$$

where: m and n are the total munber of modes,

$\tilde{q}_{mn}$ is the modal amplitude (the generalized displacements),

ξ is the coordinate along the panel's edge (parallel to x the loading axis),

ρ is the lateral coordinate (parallel to the y axis), and constants K is the modulus of the core.

N_x is the effective end load.

a and b are the length and width of the bending

Boundary conditions are satisfied in that the plate is in a state of variational equilibrium $\delta\eta = 0$ along all sides, prior to buckling.

The total potential energy of the system is given by:

$$\Pi = U_{bending} + U_{spring} - W_{ext}$$

$$\Pi = 1/2\int_0^b\int_0^a \left[EI_y \left(\frac{\partial^2\eta}{\partial\xi^2} \right)^2 + EI \left(\frac{\partial^2\eta}{\partial\rho^2} \right)^2 \right] d\xi\, d\rho \qquad (3.10.8)$$

$$+ 1/2\int_0^b\int_0^a K\eta^2 d\xi\, d\rho - 1/2\int_0^b\int_0^a N_x \left(\frac{\partial\eta}{\partial\xi} \right)^2 d\xi\, d\rho$$

Substituting the assumed deflection function (3.10.7) into (3.10.8) and carrying out integration over the test region, we find a simplified form due to orthogonality of modes.

$$\Pi = \sum_{m=1}^{\tilde{m}} \sum_{n=1}^{\tilde{n}} \frac{ab}{8} \left[\left(\frac{m\pi}{a}\right)^4 EI_y + \left(\frac{n\pi}{b}\right)^4 EI_x + K - \left(\frac{m\pi}{a}\right)^2 N_x \right] \tilde{q}_{mn} \qquad (3.10.9)$$

Applying the Principle of Stationary Potential Energy requires that

$$\partial\Pi/\partial\tilde{q}_{mn} = 0 \qquad (3.10.10)$$

$$\partial\Pi/\partial\tilde{q}_{mn} = \sum_{m=1}^{\tilde{m}} \sum_{n=1}^{\tilde{n}} \frac{ab}{8} \left[\left(\frac{m\pi}{a}\right)^4 EI_y + \left(\frac{n\pi}{b}\right)^4 EI_x + K - \left(\frac{m\pi}{a}\right)^2 N_x \right] \delta_{mn}\, 2\tilde{q}_{mn} = 0 \qquad (3.10.11)$$

where the Kronecker Delta $\delta_{mn} = \begin{cases} 1, & \text{if } m = n \\ 0, & \text{if } m = n \end{cases}$

The summation terms can be discarded as there will be only one non-trivial term per choice of m and n. Rewriting equation (3.10.11) and dropping non-zero factors.

$$\partial \Pi / \partial \tilde{q}_{mn} = \left\{ \left(\frac{m\pi}{a}\right)^2 EI_y + \left[\left(\frac{n\pi}{b}\right)^4 EI_x + K \right] \left(\frac{a}{m\pi}\right)^2 - N_x \right\} \tilde{q}_{mn} = 0 \tag{3.10.12}$$

This equation is of the form

$$(B_{mn} - N_x) \tilde{q}_{mn} = 0 \tag{3.10.13}$$

where $B_{mn} = \left(\frac{m\pi}{a}\right)^2 EI_y + \left[\left(\frac{n\pi}{b}\right)^4 EI_x + K \right] \left(\frac{a}{m\pi}\right)^2$

and can be written in matrix form as

$$\left[B_{mn} - N_x \right] \left[\tilde{q}_{mn} \right] = \{0\} \tag{3.10.14}$$

For each selection of m there exists a diagonal matrix in n

$$\begin{bmatrix} (B_{m1} - N_x) & 0 & \cdots & 0 \\ 0 & (B_{m2} - N_x) & \cdots & 0 \\ \vdots & \vdots & \ddots & \vdots \\ 0 & 0 & \cdots & (B_{m\tilde{n}} - N_x) \end{bmatrix} \begin{Bmatrix} \tilde{q}_{m1} \\ \tilde{q}_{m2} \\ \vdots \\ \tilde{q}_{m\tilde{n}} \end{Bmatrix} = \{0\} \tag{3.10.15}$$

which provides a non-trivial solution if and only if the determinant of the diagonal matrix is zero. Hence,

$$(B_{m1} - N_x)(B_{m2} - N_x) \cdots (B_{m\tilde{n}} - N_x) = 0 \tag{3.10.16}$$

From equation (3.10.16) one can see that the term which equals zero at the lowest value of B_{mn} will be the critical buckling load for the selected mode value of m. Equations (3.10.14-16) can be used for each iteration of m, m+1, m+2, etc. until a complete matrix has been calculated.

$$N_{cr_{mn}} = \min \left(\frac{m\pi}{a}\right)^2 EI_y + \left[\left(\frac{n\pi}{b}\right)^4 EI_x + K \right] \left(\frac{a}{m\pi}\right)^2 \tag{3.10.17}$$

where N_{cr} is the buckling or face sheet wrinkling load. Notice that the buckling load depends on panel flexural rigidity in two directions, test section dimensions, foundation stiffness modulus and modal combinations.

The failure load for damaged panels will be estimated, based upon the critical load of undamaged panels, calculated from equation (3.10.17) This undamaged failure load N will

be converted to an equivilent stress σ_o. Two methods will be used to approximate the residual strength of a damaged panel:

1) Constant net-section stress (upper bound)

2) Mar - Lin relation [17] (lower bound)

Lie [7] describe this bounding method for predicting residual strength.

For panels which are insensitive to notches, the net-section on both sides of the damage is assumed to carry a constant stress:

$$\sigma_{cr} = \sigma_o \, (b-d)/d \qquad (3.10.18)$$

where: σ_{cr} is the failure stress of the damaged panel,

σ_o is the failure stress of an undamaged panel,

b is the panel width, and

d is the ruptured face sheet diameter.

If the panel is notch-sensitive, then the Mar-Lin[17] relation is used to predict the failure stress:

$$\sigma_{cr} = Hc \, (d)^{-.28} \qquad (3.10.19)$$

where: Hc is the experimentally determined composite "fracture parameter".

Equation (3.10.19) is an empirically derived formula which is based on two material properties and the dimension of cross sectional damage. The fracture toughness depends on laminate lay-up , ratio of matrix to laminate elasticity moduli, yielding stress, and original length of the discontinuity, d. However, the exponential value -.28 which Lin denotes as -m represents the order of singularity of a

crack within a matrix. Lin requires that m depend on the constituent properties of the filament and matrix. Lin's study provided values of -.28 and -.30 for Hercules graphite filaments and epoxy matrix 3501-6. Hence, the value for m the order of singularity, is used in equation (3.10.19), but fracture parameter Hc, is left to experimental derivation.

Lie [7] uses Federson's [18] tangent line correction technique to bound the domain where d/b provides an impractical result from equation (3.10.19), (ie: As d approaches 0, σ_{cr} increases without bound; and as d approaches b, σ_{cr} does not approach a zero value). Figure 3.13 illustrates the Mar-Lin Relation with Lie's Constant Net - Stress and tangent corrections. The two methods depicted provide upper and lower bounds for predicting residual strength of damaged laminates in compression, for a given damage-to-width ratio. The failure stress for panel bending failure will be compared with these in-plane column compression predictions.

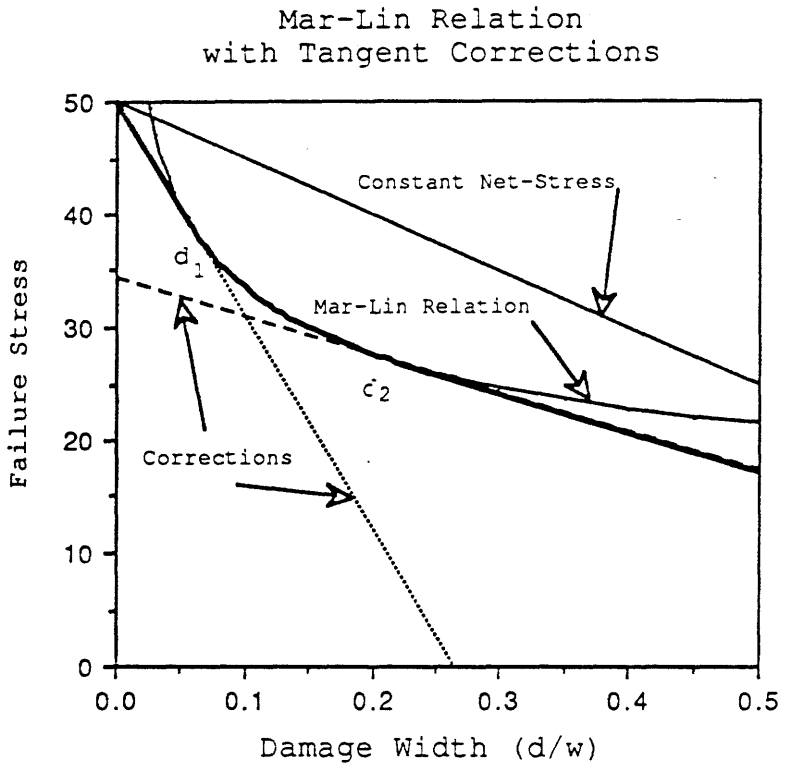

Figure 3.13 Mar - Lin Relation with corrections

CHAPTER FOUR

EXPERIMENTAL PROCEDURE

4.1 EXPERIMENTAL PARAMETERS

The objectives of the residual strength experimentation was to isolate and examine the contribution of various parameters to the residual strength of a damaged HCP (honeycomb core panel). Both material and experimental parameters were fixed to reduce the enormity of the experimental task. The fixed parameters were:

- specimen width and length
- face sheet material
- core material and density
- impactor mass, shape and size
- bonding epoxy
- age within specimen's life
- temperature and humidity (normal room temperature and humidity)
- dual cantilever clamping during impact

The parameters which were isolated, measured and varied were:

- core thickness
- impact energy
- face sheet thickness
- face sheet orientation (relative to load application and core ribbon direction)
- strain measurement positions

The method of testing was tailored to isolate and

evaluate certain parameters and characteristics of the HCP. Four point bending evaluated flexual rigidity, maximum deflection and curvature, anticlastic curvature, failure moment, damage/dimple propagation, and failure modes. Panel compression tests were performed to evaluate ultimate face sheet strength in compression and extent of edge effects. The final series of tests examined the fatigue life of specimens with various states of damage, under panel compression-compression loading, because of the impracticality of fatigue bending.

4.2 TEST PROGRAM

The test program called for the fabrication of HCP's of various "types" (ie: face sheet layup, core thickness and core composition) for impact testing, four point bending and column compression under quasi-static and cyclic loading. Table 4.1 describes the four point bending residual strength test matrix. The tests were performed under slow ramp speeds to simulate static strength conditions. Note that some undamaged specimens were fabricated with a composite aluminum and Nomex core, so that the core would not crush under the loading tabs and the Nomex test section could be brought to its ultimate bending moment. Table 4.1 specifies the impact energy for each specimen and thus contains part of the impact test matrix. The remaining impact test matrix is included within the fatigue test matrix.

TABLE 4.1

FOUR POINT BENDING RESIDUAL STRENGTH TEST MATRIX

FOUR POINT BENDING; Damaged Laminate Under Compression

Layup	Core Thickness (in)		Impact Energy (ft-lb)	# of Specimen
+-45	.375	(N/A)	0.0	4
+-45	.375		0.0	3
+-45	.375		1.0	5
+-45	.375		1.2	4
+-45	.375		2.0	5
+-45	.687	(N/A)	0.0	4
+-45	.687		1.0	5
+-45	.687		2.0	4
+-45	1.00	(N/A)	0.0	4
+-45	1.00		0.0	3
+-45	1.00		1.0	6
+-45	1.00		1.2	4
+-45	1.00		2.0	6
[+-45]s	1.00		2.0	3
[+-45]s	1.00		2.5	2
[+-45]s	1.00		3.15	3
0/90	.375	(N/A)	0.0	4
0/90	.375		0.0	3
0/90	.375		1.0	5
0/90	.375		1.2	4
0/90	.375		2.0	5
0/90	.687	(N/A)	0.0	4
0/90	.687		0.0	2
0/90	.687		1.2	5
0/90	.687		2.0	4
0/90	1.00	(N/A)	0.0	4
0/90	1.00		1.0	6
0/90	1.00		1.2	4
0/90	1.00		2.0	6
[0/90]s	1.00		2.0	2
[0/90]s	1.00		2.5	1
[0/90]s	1.00		3.15	2
			Total	126

Note: (N/A) indicates a reinforced Nomex/aluminum core

The Panel Compression Test Matrix in Table 4.2 was employed to evaluate the ultimate in-plane compression failure load for the face sheets at two orientations. A thick core of light weight aluminum honeycomb may prevent premature buckling through greater normal stiffness and width; and also contribute negligibly to longitudinal stiffness.

TABLE 4.2

UNDAMAGED PANEL STRENGTH TEST MATRIX

PANEL COMPRESSION; Laminate Compression Limits

Layup	Core Thickness	Core Material	# of Specimens
+-45	1.00	Low Density Aluminum Core	4
0/90	1.00	Low Density Aluminum Core	4

The fatigue test program was limited in scope and variables because of the enormity of a multi-variable investigation. As mentioned previously, panel specimens were tested under sinusoidal cyclic compression as a practical substitute for four point bending oscillatory deflections. The specimen's deflection amplitude under the four point bending stroke would be too large. A shorter beam specimen would have a smaller deflection, but require greater loads at the loading points to meet the desired maximum moment for cyclic bending and cause premature if not immediate localized core crushing under the loading tabs. The result of panel fatigue testing is that the longevity

of the core under bending fatigue is not considered. However, this panel fatigue test program as described in Table 4.3, is implicitely applicable to the longevity of the HCP compression face sheet under bending and directly applicable to in-plane compression of the HCP. In fact this longevity study was intended as a continuance to the quasi-static panel compression investigation of Lie [7], using similar panels and impact damage.

4.3 SPECIMEN DESCRIPTION

Four types of sandwich honeycomb panel specimens were constructed for this investigation; the basic sandwich, reinforced sandwich, static compression panel, and fatigue panel. The face sheet for each specimen consisted of two or four plies of an AS4 graphite epoxy plain weave fabric. Face sheet orientation and thickness was prescribed by the test matrix for a given core material and thickness. Face sheets were bonded to a homogeneous or composite honeycomb core:

SPECIMEN TYPE	CORE MATERIAL
Basic	Nomex Honeycomb
Reinforced	Nomex/Aluminum honeycomb composite
Static Panel	Aluminum honeycomb composite
Fatigue Panel	Nomex honeycomb composite

Both types of panel specimens have Scotch ply loading tabs bonded to both face sheets at either end and a high density aluminum honeycomb core between the loading tabs. Figures 4.1,2,3 and 4 illustrate the specimen configuration.

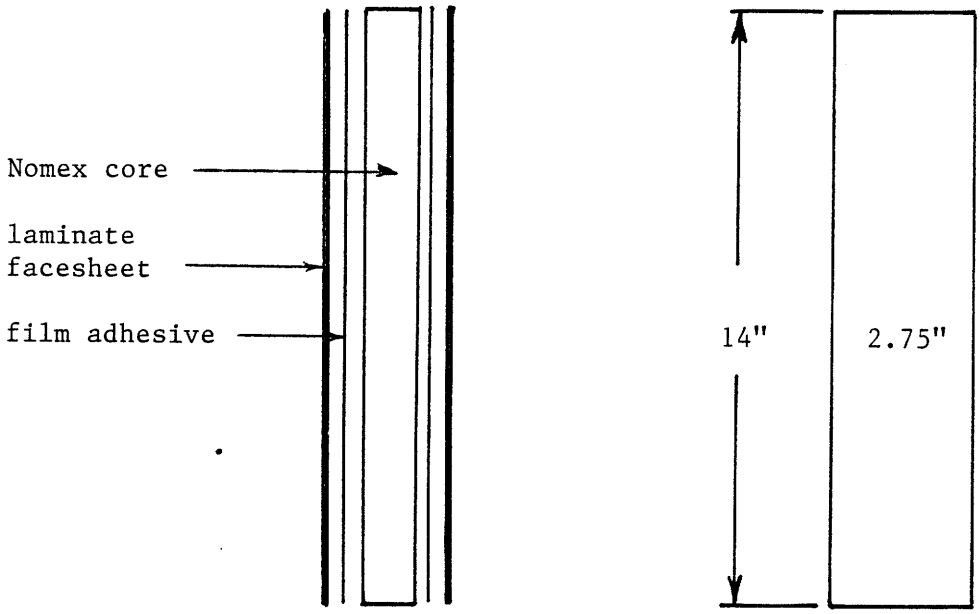

Figure 4.1 Basic Sandwich Panel

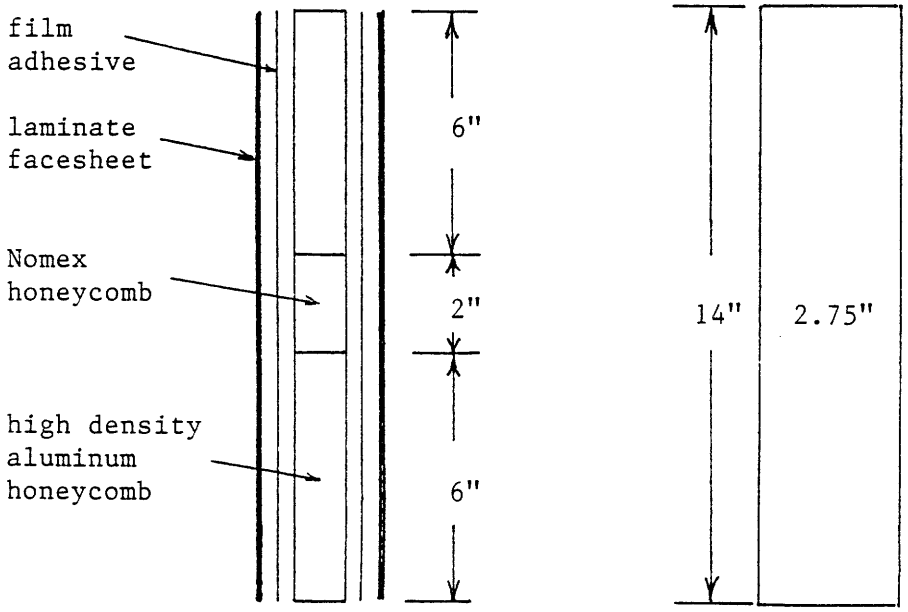

Figure 4.2 Reinforced Sandwich Panel

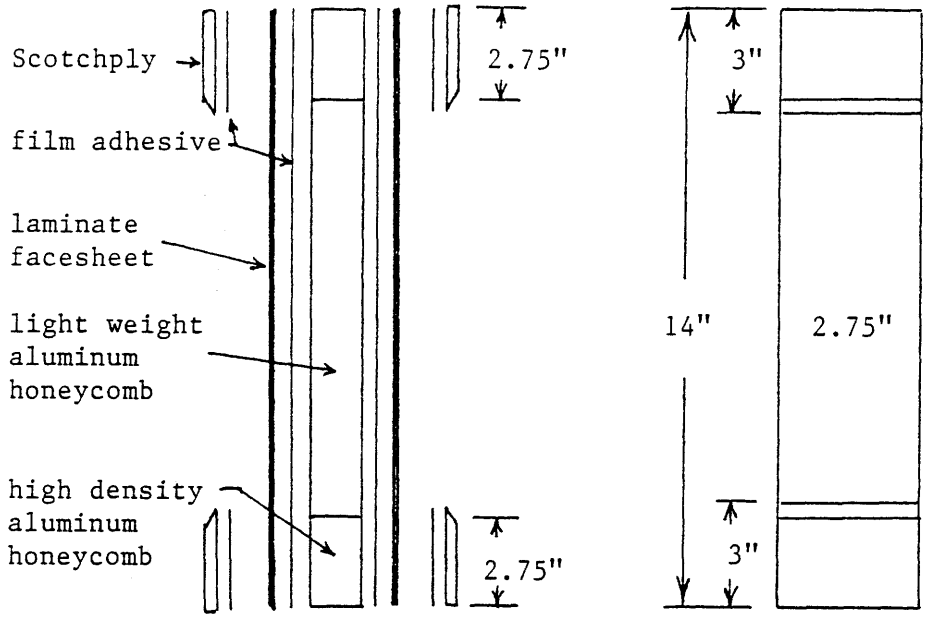

Figure 4.3 Static Compression Sandwich Panel

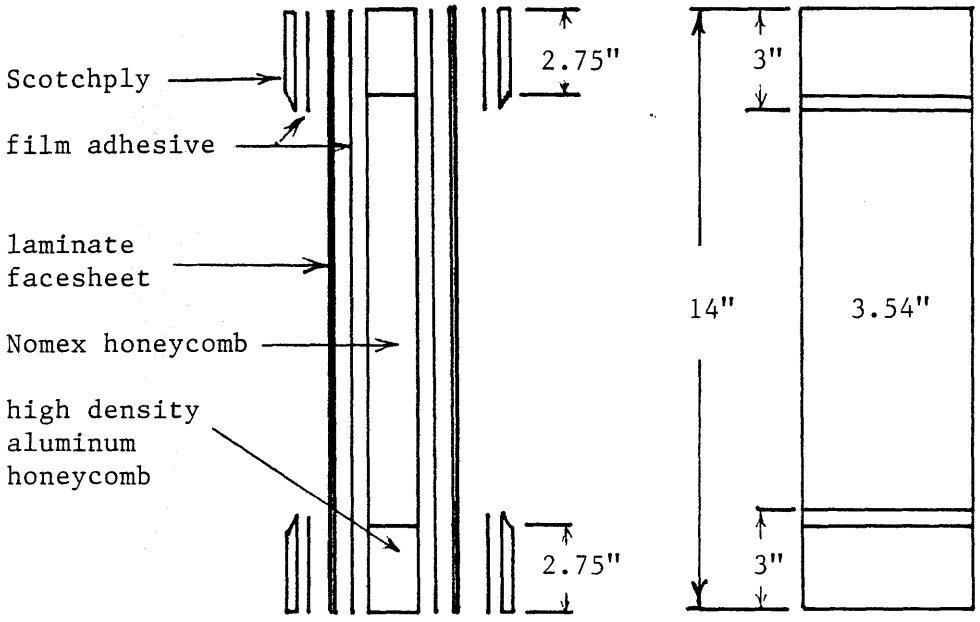

Figure 4.4 Fatigue Sandwich Panel

TABLE 4.3

PANEL LONGEVITY TEST MATRIX

Test: Panel Compression - Compression Oscillation

Face sheet Layup	Panel Thickness (in)	Impact Energy (ft-lb)	# of Specimens
+-45	.375	2.0	1
+-45	.687	0.0	2
+-45	.687	1.0	3
+-45	.687	2.0	3
+-45	1.00	0.0	2 (P:1)
+-45	1.00	1.0	2
+-45	1.00	2.0	1
0/90	.375	2.0	1
0/90	.687	0.0	3
0/90	.687	1.0	3
0/90	.687	2.0	2
0/90	1.00	0.0	1 (P)
		TOTAL	24

(P):Specimen of width 70mm and non-standardized fabrication of grip reinforcement.

4.4 MANUFACTURING PROCEDURES

The fabrication of the test specimens involved as many as nine separate operations: layup, laminate cure, post cure, trimming, core assembly, sandwich panel bond, tab bond, machining, and strain gauge application.

4.4.1 Layup

All face sheets are made from a AS4 graphite filament plain weave fabric impregnated with 3501-6 epoxy. This pre-preg is a net-resin system with a 34% resin content, by

volumn. The pre-preg fabric is supplied by Hercules and Fiberite and known as AW193PW/3501-6. The Hercules product contains red and yellow tracer fibers. The Fiberite fabric uses white tracer fibers. Both materials have very similar properties.

The pre-preg fabric is removed from its freezer storage 30 minutes before cutting. Once the material approaches room temperature it can be removed from its air tight bag with minimal condensation formation. Normal room temperature makes the fabric tacky and easy to cut. High humidity and room temperature makes the pre-preg too tacky and troublesome to layup.

A 12 by 14 inch aluminum plate covered with non-stick tape provides the template for cutting pre-preg plies with a Stanley utility knife. The template can be oriented at desired angles with respect to the fabric's longitudinal tracer fibers with pre-cut angular templates. This experiment required only the 0/90 and 45 degree templates to cut the four layups used: [0/90]; [+-45]; [0/90]s; and [+-45]s. A sheet of Teflon FEP flourocarbon film is then applied to each face of the pre-preg layup.

4.4.2 Laminate Cure

The cure layup is depicted in Figure 4.5 and consists of the aluminum cure base plate, non-porous Teflon, a frame work of aluminum T dams and cork, the pre-preg layup surrounded by the FEP flourocarbon film, a second layer of

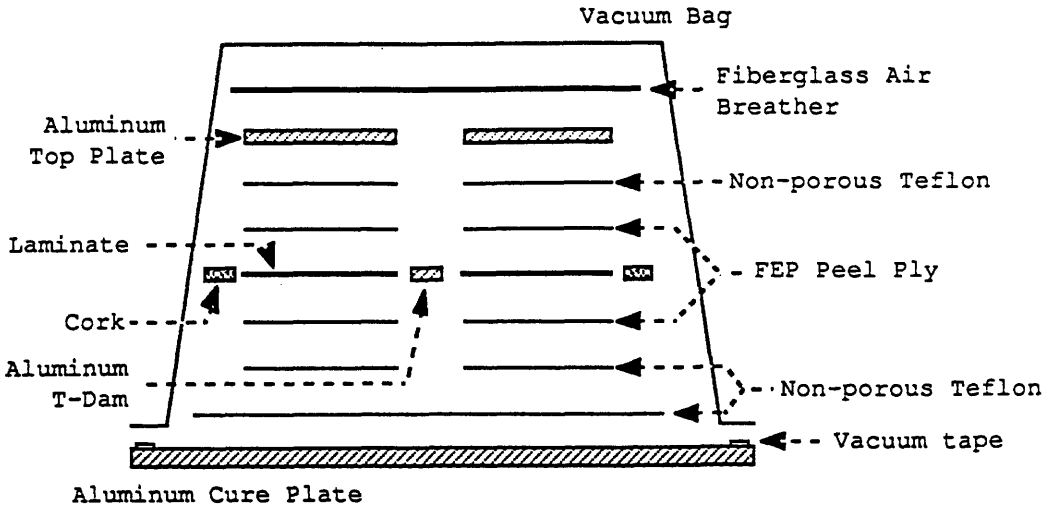

Figure 4.5 Laminate Cure Layup

non-porous Teflon and an aluminum top plate. No paper bleeder plies are required. It is recommended that the Teflon be wrapped tightly around the edges of the top plate to prevent resin bleed. The entire assembly is covered with a fiberglass cloth and then enclosed under a vacuum film bag secured at the edge of the cure base plate by vacuum tape, for an air tight seal.

The laminates are cured under a 135 psi pressure differential (15 psi vacuum and 120 psig autoclave pressure) using a two step process. The first stage is the resin flow throughout the fabric at 225 °F for 60 minutes. The second stage cures the resin at 350 °F for 2 hours. Temperature increases and reductions are conducted at 5 °F per minute to avoid thermal shock. A cure cycle time history is presented in Figure 4.6 Laminate Cure Cycle.

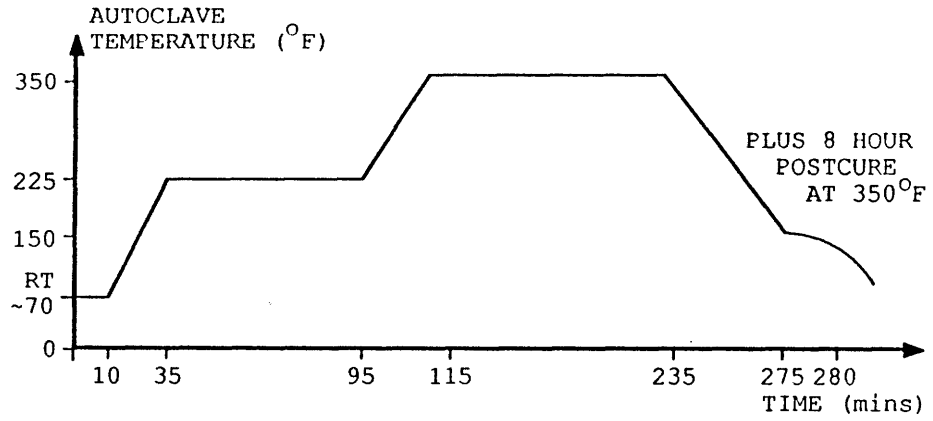

Figure 4.6 Laminate Cure Cycle

4.4.3 Post-Cure

The post-cure procedure is to cure the laminate in a non-pressurized oven at 350°F for 8 hours. This extended cure maximizes the epoxy matrix capabilities.

4.4.4 Trimming

Following the post-cure, the laminate is trimmed and squared on all four edges with a diamond grit cutting wheel mounted on a milling machine. The wheel is cooled with a low velocity stream of water, which also carries away debris during the cutting. The 5 inch wheel rotates at 1100 rpm as the cutting table advances the laminate at 11 inches per minute.

4.4.5 Core Assembly

The core assembly for the basic sandwich specimen is simply the cutting of an oversized 12 by 14 inch piece of Nomex honeycomb, with a nominal density of 3.0 pcf. Excess core material is trimmed following panel bonding.

The reinforced sandwich specimen requires aluminum honeycomb on both sides of a mid beam 2 inch Nomex test section, as illustrated in Figure 4.2. The aluminum core with a density of 22.0 pcf will not wrinkle and crush under the loading tabs as does the Nomex.

The static compression column is composed of a low density (3 pcf) aluminum honeycomb core test section bounded by two inch high density aluminum honeycomb sections (refer to Figure 4.3). The fatigue compression column has similar end sections bounding a Nomex honeycomb test section. The high density aluminum end sections are neccessary to withstand the test machine grip pressure.

All of the composite core joints are cemented with Hysol Clear Epoxy-Patch with the aid of an assembly jig. The epoxy cures in 8 hours at room temperature.

4.4.6 Bond Cure

The face sheets are bonded to the cores with American Cyanimid's FM-123-2 film adhesive (density: .06 lb/ft). Non-porous Teflon sheets cover the panel on both sides. Steel top plates are then placed on top of the Teflon followed by fiberglass air-breather. An aluminum bar is

placed along the side of exposed Nomex core material in order to protect it from the 40 psi crushing effect of the vacuum bag. The panel bond cure arrangement is shown in Figure 4.7.

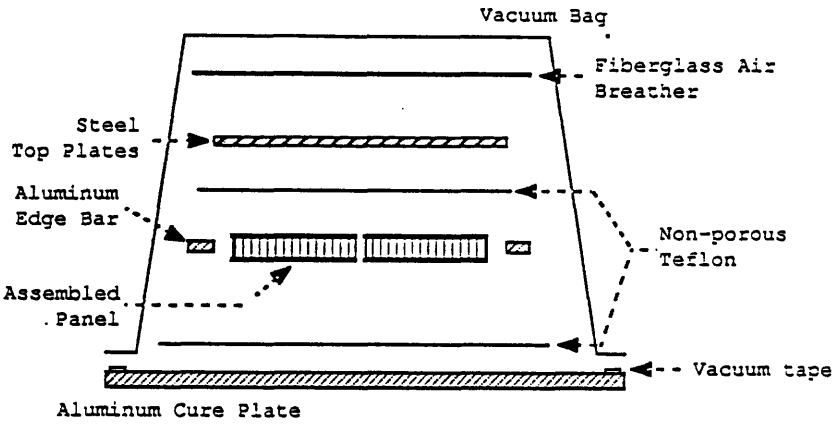

Figure 4.7 Panel Bond Cure Layup

The dog-eared vacuum bag is left vented to the atmosphere as autoclave pressure is brought to 40 psi and the temperature reaches 225 °F. This single stage is held for 2 hours. Note that a vacuum drawn under the vacuum bag would cause a pressure diffential between the internal bag and the atmospheric pressure trapped within each core cell. This differential has been known to cause core damage.

4.4.7 Load Tab Cure

Pre-cured fiberglass crossply loading tabs are used to distribute test machine grip pressure evenly and thus avoid grip induced damage. These tabs are cut from 3M Scotchply Type 1002 Crossply material. The tabs are 7 plies thick

with a nominal thickness of .07 inches. They are bonded to the panels with the same adhesive and procedure used to bond the face sheets to the cores.

4.4.8 Panel Machining

After the bond cure, the panels are cut length wise into four 2.75 inch (70mm) or three 3.54 inch (90mm) wide beams for bending and panel tests, respectively. An 11 inch diamond grit wheel rotating at 700 rpm, cuts the panel at a feed rate of 5 inches per minute. The cut specimens have nominal dimensions of:

2.75 by 14 inches; basic and reinforced panels, and and static compression column

3.54 by 14 inches; fatigue column

The disassembled specimens are illustrated in Figures 4.1,2,3 and 4.

4.4.9 Coupon Machining

Twelve static panel coupons 2.75 inches square, were cut with the 11 inch wheel, from spare panels. Two coupons from each of the three core thickness types (1.0", .687", and .375") were then cut through the top face sheet to the interface of the laminate/core bond. A second parallel cut and removal of debris results in a slit between 2.0 and 3.5 mm in width. One slit is cut parallel to the honeycomb core's ribbon direction. Figure 4.8 illustrates the three types of static compression and indentation coupons.

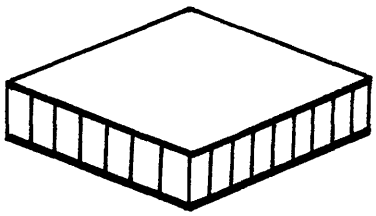

Core Compression
Coupon

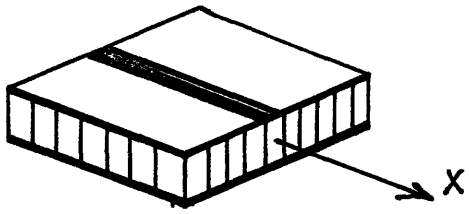

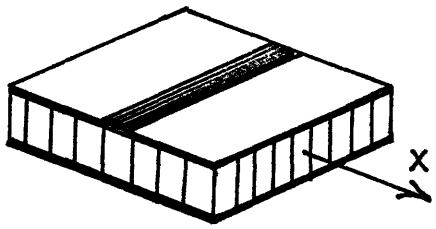

Parallel Slit Perpendicular Slit

Figure 4.8 Static Core Compression and Indentation Coupons

4.4.10 Strain Gauging

The final step in the manufacturing process is the application of strain gauges. Since this investigation deals with post-impact damage and residual strength, it was not necessary to mount strain gauges until after the impact event. This procedure saved undue wear and tear on the delicate gauges.

Micro-Measurements type EA-06-125AD-120 and EA-06-125TM-120 strain gauges are mounted to specimen face sheets with a cyanoacrylate adhesive according to the manufacturer's instructions. The gauge locations specified for six test configurations, as shown in Figure 4.? . Each strain guage configuration is labeled with a Roman numeral and each gauge is assigned a number within the

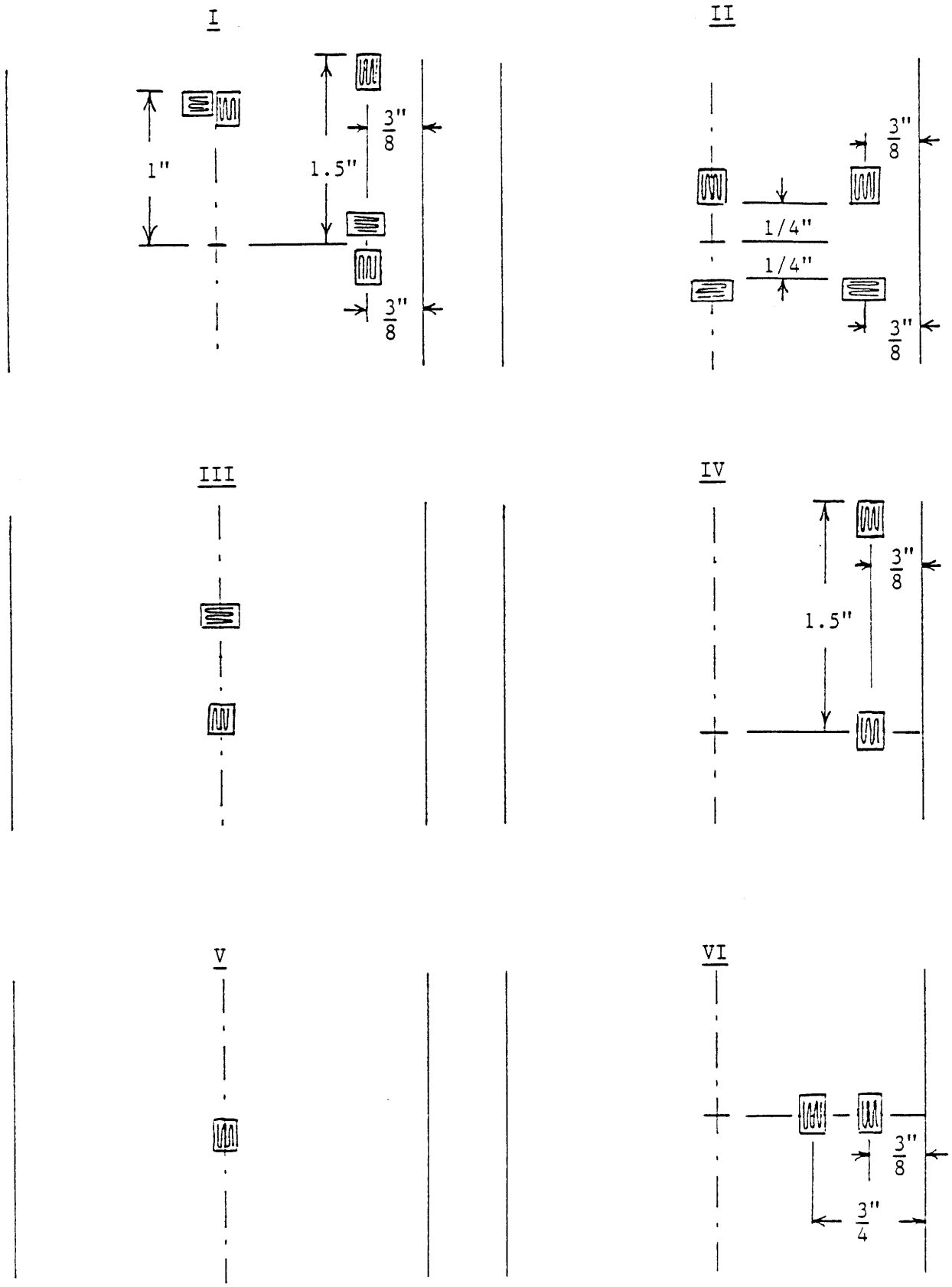

Figure 4.9 Strain Gauge Configurations

numbers (1,3 and 5) to gauges mounted in the specimen's longitudinal direction. Even numbers are mounted in the transverse direction. Static compression column specimens are mounted with two strain gauges (configuration III) on both face sheets. Bending specimens have gauges mounted only on the compression face. Fatigue column specimens require no strain gauges.

4.5 TESTING PROCEDURE AND DATA ACQUISITION

Five types of tests were performed: static beam bending, static column compression, impact measurement, static indentation and core compression, and column compression fatigue tests. Specimens that were to be tested for residual strength or longevity, were first subjected to a prescribed impact and damage assessment inspection. The damage assessment consisted of visual measurements under magnification and x-ray photography. One specimen from each test type and damage level was dissected to measure core and bond damage. Specimens with and without damage were then tested for ultimate and residual strength, or longevity under compression-compression cyclic loading.

4.5.1 Impact Tests

Specimens to be impacted are mounted in a holding jig which is designed to provide clamped boundary conditions along the short edges and leave the long edges free. Figure

4.10 depicts the holding jig. The jig uses 4 sets of aluminum bars to clamp the specimen. The jig is supported by a rigid steel frame.

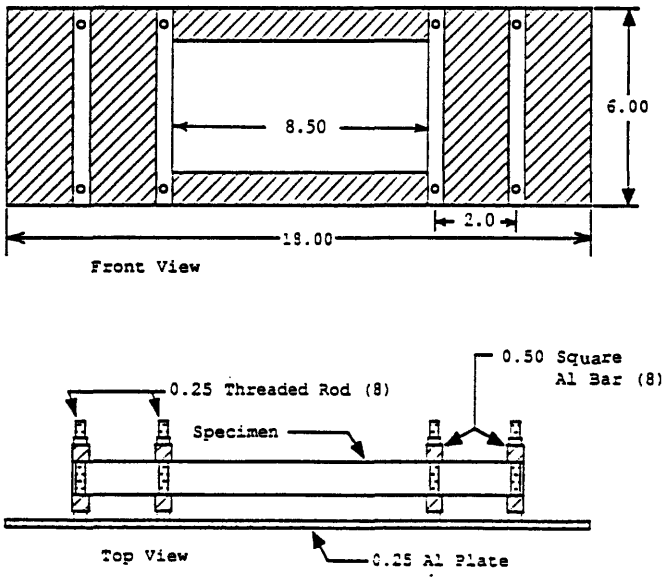

Figure 4.10 Specimen Holding Jig

The impactor mechanism is a spring driven 26 inch steel rod mounted on linear bearings so that it may have free travel along its axis. The rod has a mass of .105 slugs. The main spring of the striker unit is compressed when the striking mechanism's end plate is coupled to activated electromagnets and the magnet mechanism is drawn back with a hand winch. Figure 4.11 illustrates the striking unit. Figure 4.12 illustrates the impacting rod mehanism. The entire device is known as FRED within the TELAC laboratory. The name has no significance other than identification.

The striking unit can be drawn back with the winch to any net deflection of the main spring at any time. Thus impacts are repeatable based on spring compression distance.

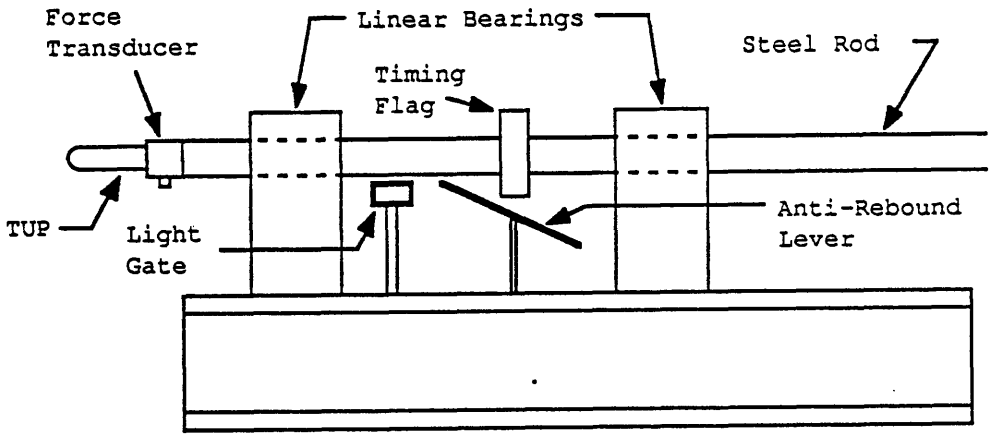

Figure 4.11 FRED's Striking Unit

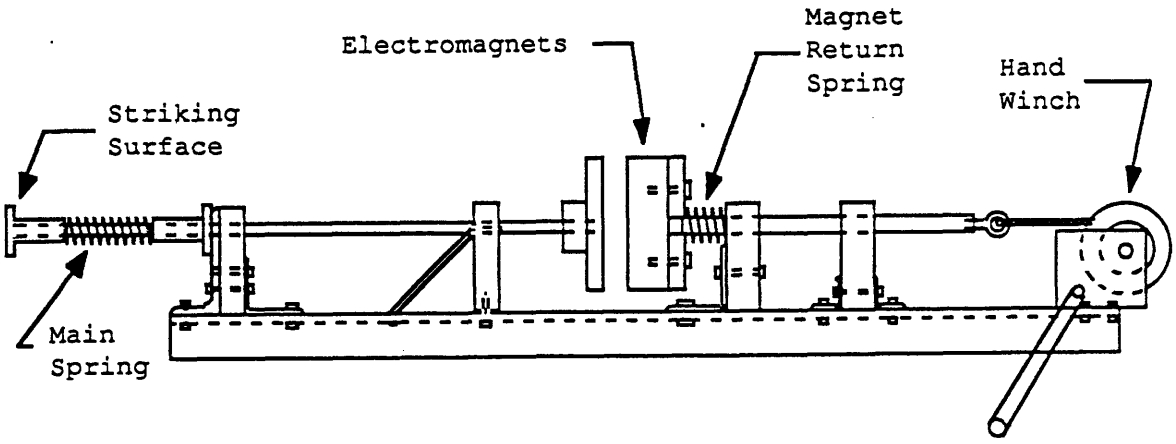

Figure 4.12 FRED; Impacting Rod Mechanism

The striking unit is set in motion when the electromagnets are de-energized. The striking surface is then driven forward by the compressed main spring until it strikes the impactor rod, which in turn is propelled at the target specimen in the holding jig. The impactor rod trips a CENCO Model 31709 photo electric timing gate with a 13 mm rubber "doughnut" timing flag. The photo-electric sensors start and stop a digital timer as the flag interrupts the

beam of light. The photo-electric cells trigger at .5mm into the flag and at 12.5mm, resulting in an effective timing flag of 12mm.

The impacting rod mechanism is equipped with an anti-rebound lever which prevents the impactor from rebounding and striking the specimen and passing through the light gate a second time. Attached to the impacting rod is a PCB Model 208A05 force transducer and a 1/2 inch diameter hemispherical stainless steel impact head known as a tup. The transducer measures force during the impact with the specimen.

Data is collected by a DEC Micro PDP-11/23 computer equipped with a Data Translation DT-3382-G-32DI analog to digital converter. The signal from the force transducer is sampled at a rate of 25 kHz and this data is stored for later analysis. Data collection is triggered by the falling edge of the signal from the CENCO timing unit.

Impact velocity and force over time are recorded and filed for each specimen impact. The specimen must now be examined for damage and quantified relative to the impact history.

4.5.2 Damage Assessment

Impacted specimens are inspected visually under 15 to 1 magnification to measure the cross sectional width of ruptured fibers and is also subjected to x-ray photography. An x-ray opaque dye, 1,4-Dilodobutane is applied to the

perimeter of the damage with a hypodermic needle, one tiny drop at a time. The dye is allowed to penetrate the laminate's deepest cracks through capillary action for 2 hours. After the absorbtion period, the specimen is placed damaged face down on a sheet of Polaroid Type 52 Polapan 4 5 Instant Film inside a Scanray Torrex 150D X-Ray Inspection System cabinet. The x-ray machine operates at 50 kVolts and is set to expose the film to 240 mrad using the "TIMERAD" control. After exposure, the film is processes according to the manufacturer's instructions. The resulting black and white photograph displays a full size image of the damaged area. The photograph can be measured to provide dimensions and area of the delamination.

Specimen dissection is accomplished with the same milling procedure as used in fabrication. The specimen is sectioned through the center of the impact site, and inspected for debonding and core indentation.

4.5.3 Four Point Bending

The residual strength of damaged specimens and the ultimate strength of undamaged specimens are tested under bending provided by a four-point bending installation mounted in the MTS-810 uniaxial test machine. The installation illustrated in Figure 4.13, consists of two aluminum I beams with two loading roller cradles on each. The upper I beam has a grip block bolted to it, which holds the I beam in place when the MTS-810's upper gripping jaws

are pressurized. The loading point cradles are adjustable for any loading point placement. Four one inch diameter cold roll steel rollers are placed in the loading cradles to act as non-fixed loading points. Loading tabs 5/8 inch wide are mounted to each specimen's loading points with double faced tape. The loading points can vary throughout the test series, but symmetry about the specimen mid-point should be maintained.

The bending specimen is loaded for testing by placing the beam on the bottom two rollers and aligning the specimen edge with the I beam with the use of a straight edge. This assures that the loading rollers (loading lines) are perpendicular to the specimen's longitudinal axis. The 15 inch strain gauge lead wires are then connected to the strain box terminals which send strain measurement as data to the DIGITAL 1134 digital computer. The strain gauges are then calibrated for a 40,000 micro-strain range and zeroed. An angular deflection indicator is now attached to the top face of one end of the specimen, with double faced tape. The indicator, constructed from wood, Nomex and toothpicks, is tailored for each specimen thickness. The indicator is aligned with the zero degree mark and pivot point of a protractor mounted to the lower I beam cradle. The lower I beam with specimen is then raised to the starting position with the MTS-810 manual stroke control, the loading points and I beams aligned, and the top two rollers are inserted between cradle and loading tab.

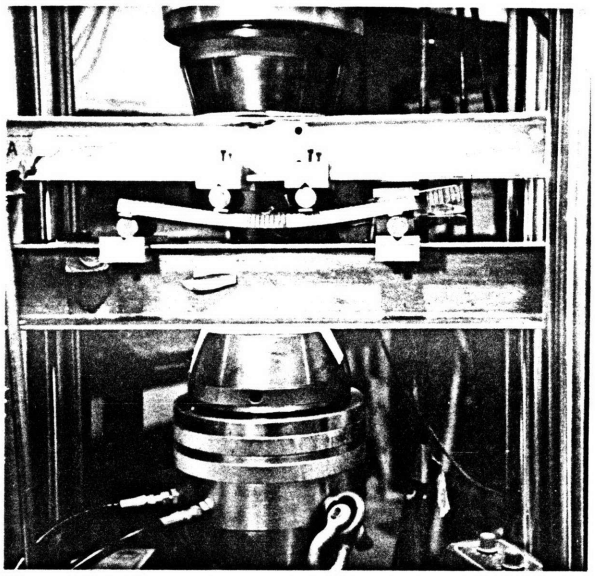

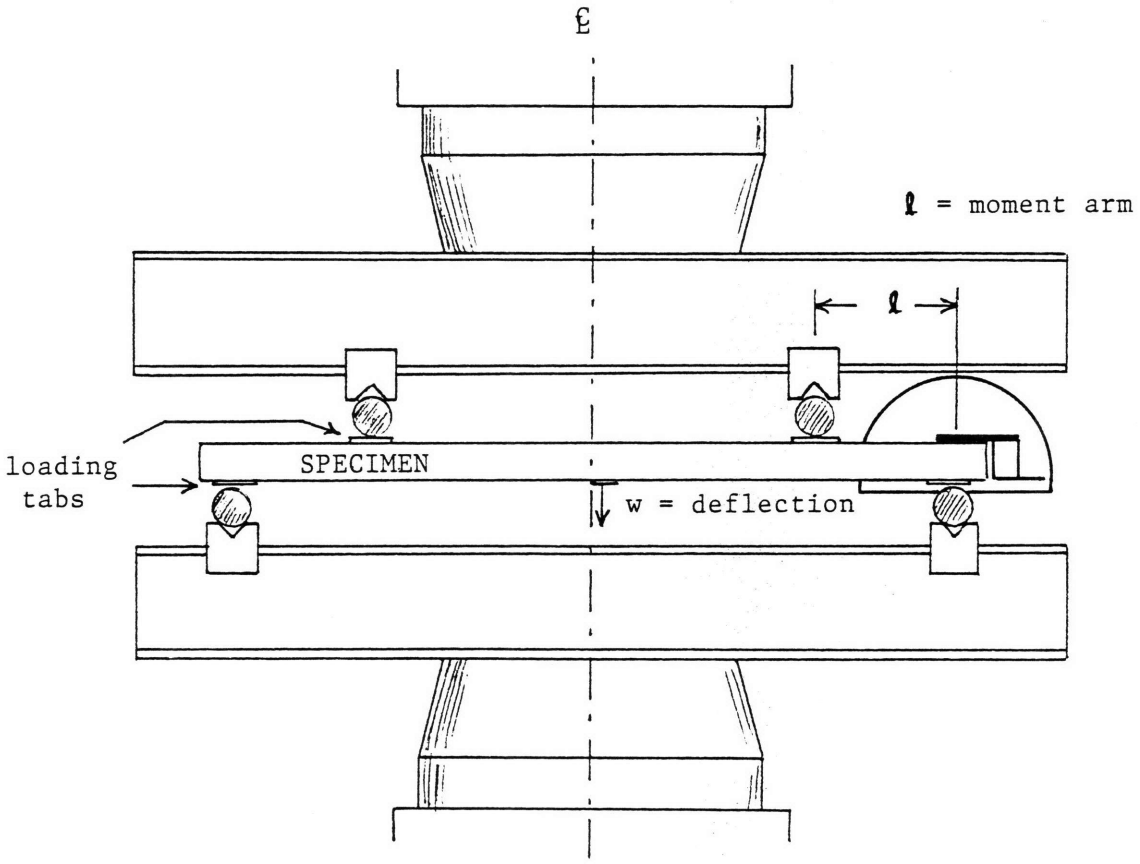

Figure 4.13 Four Point Bending Installation

from the indicator and protractor (the net change in angle is of interest) and the distance between the bottom I beam and the specimen's mid-point center line is measured with calipers. A digital indicator connected to a stroke output terminal on the MTS-810, provides constant stroke displacement at 1.0 volt per half inch. The MTS-810 is placed in stroke control with ramp compression speeds between .00125 and .00250 inches per second, depending on specimen stiffness and manual measurement speed. The MTS-810 and DIGITAL 1134 are started simultaneously. The MTS-810 providing constant stroke displacement and load from two digital indicators and the computer recording the average of 3 data samples every second for all strain gauges, and load and stroke transducers. Specimen mid-point and angular deflection at the end loading point are measured and recorded along with the applied load, at pre-determined stroke intervals (typically .0625 or .125 inches). Photographs of the damaged face sheet can be taken during bending with a 2 inch wide mirror strip taped to the top I beam and hung down at approximately 45 degrees. A tripod mounted 35mm camera with ASA 400 film is then focused on the image in the mirror. Length measurements of damage propagation can also be made with a thin ruler and a keen eye. Measurements and observations can be continued until failure.

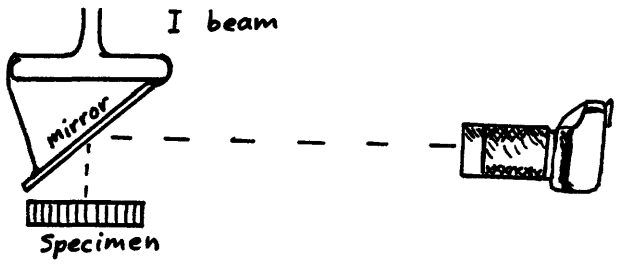

Figure 4.14 Face Sheet Damage Photography

Failure is defined as a substantial drop in load bearing capacity and is caused by:

- core crushing, wrinkling, or shearing
- debonding between face sheet and core
- face sheet folding or buckling

4.5.4 Static Panel Compression

Two groups of panel specimens with aluminum honeycomb cores were tested under compression to determine their ultimate buckling load and face sheet stresses. The testing procedure is the following.

The panel are loaded in the MTS-810 by aligning the panel in the upper grip with a square so that the specimen's axis is parallel to the machine's loading axis. The top grip is then activated and the column is held by textured flat grips under 500 psi pressure. The strain gauges are then connected, calibrated and zeroed as in the bending procedure. With stroke control selected, the lower grip is raised and clamped to the lower grip section of the column. After checking that the applied load is zero, the computer and test machine are started. Again, the stroke rate can be

selected between .00125 and .00250 inches per second. The test is terminated upon column buckling.

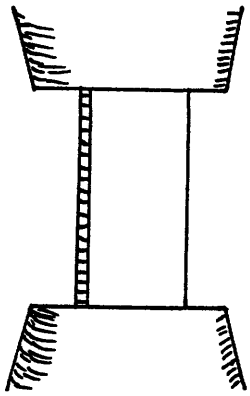

Figure 4.15 Panel Compression Test

4.5.5 Core Compression and Indentation

The core compression test procedure is to place the test coupon on a steel plate, which lies on the lower grip mount of the MTS-810 test machine. An identical steel plate is then placed on top of the coupon and the lower grip and stack are raised to the starting position with the stroke control. Once again the computer and test machine are started simultaneously, with a stroke rate of .0025 in/sec. As the 2.75 X 2.75 inch coupon core is compressed, the load cell and stroke transducers provide continuous data to the computer, which samples and averages 3 times per second. Significant core wrinkling is observed and identified during the test by a mark placed in the test data history. A second mark is made when significant crushing is determined.

Both marks are subjective judgements on the part of the observer. The test is terminated when core crushing is pronounced and the load has dropped significantly.

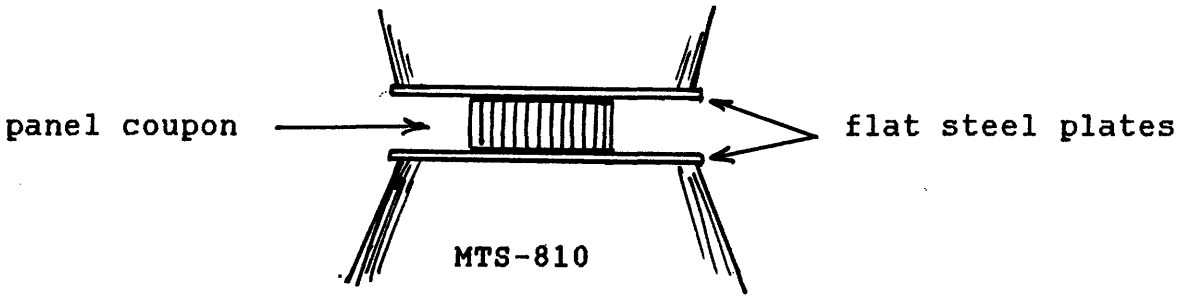

Figure 4.16 Core Compression Test

The core indentation test using coupons with slits across one face sheet laminate is designed to simulate the impinging core crushing pressure of a face sheet indentation (dimple) as it propagates laterally from the face sheet's compressive loading axis. The slit is cut to a prescribed width to provide an incident angle between the indentor and honeycomb cell axis. The slit also prevents the face sheet from providing z axis support to the core through tension.

The core indentation test begins with the placement of the test coupon on the steel plate used in the core compression test. Next, a 4 inch long steel cylinder, 1.5 inches in diameter, is laid length wise in the coupon's slit. The lower grip and specimen configuration is then raised with stroke control, until the cylinder touches the upper grip housing face. Once again the computer and test machine work in concert at the usual stroke rate. The

observer monitors the propagation of the point of face sheet deflection. Marks are place in the data history and loads recorded when the deflection propagation along the face sheet reaches pre-determined distances from the slit center. The test is terminated when the propation reaches a specified distance.

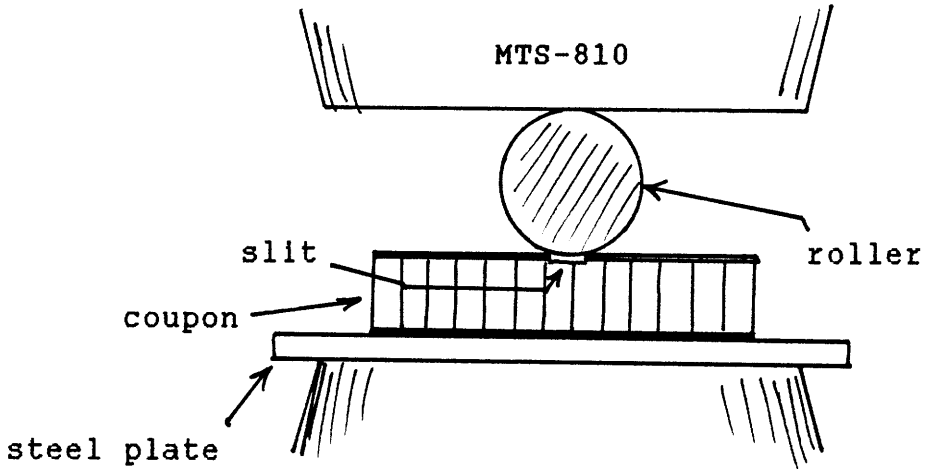

Figure 4.17 Core Indentation Test

4.5.6 Panel Fatigue

Damaged and undamaged panel specimens are placed into the MTS-810 grips in the same manner as the static compression panel. Strain gauges and the computer are not needed for this test. The MTS-810 is placed in load control and the loading force is fine tuned to ten percent of the desired compression amplitude with the "Set Control" dial. The load can be read directly from the digital indicator with "DC" selected. The difference between the selected amplitude and the 10% set point is then dialed into the

"SPAN 1" control. The machine is then set to the oscillatory mode, "REMOTE" selected and "HAVERSINE" and "INVERT" are depressed. The final preparation step is to reset the cycle counters to zero.

Damage dimensions must be monitored throughout the test. A damage width measurement using a ruler was made with no load, the "Set Point" load and the amplitude load, at the beginning of the fatigue test. The amplitude measurement can be taken quite easily by setting the oscillation speed to .1 Hz and adjusting the amplitude load with "SPAN 1", while "PEAK READ" is selected in the digital indicator. If the damaged indentation does not propagate, the cycle frequency can be increased incrementally and the load amplitude fine tuned with "SPAN 1". A high intensity photographic lamp will aid in measuring the dimple length of the damaged region as well as photography. Dimple length and cycle number are recorded throughout the life of the specimen. The test terminates when the specimen can no longer carry the selected load. The MTS-810 can be set with stroke limits which automatically disconnect hydraulic power when the limit is reached. A quarter inch of stroke travel is the recommended limit for these columns.

CHAPTER FIVE

EXPERIMENTAL RESULTS

5.1 IMPACT TEST RESULTS

Impact events were conducted for specimens of three core thicknesses, 4 different face sheet layups using 5 impact energy levels. A 8.5" test section between a cantilever clamping arrangement as depicted in Figure 4.10 allowed for dynamic response to impact. The damage inflicted had generally the same characteristics within the same impact energy level. The impact tests and damage assessment is reported for individual specimens in Appendix A.

5.1.1 Impact Velocity and Energy

The spring driven impact test machine (FRED), was employed at five different spring displacements; 40, 43, 50, 55, and 60mm. FRED propelled the .105 slug impactor rod at impact velocities between 4.4 and 8.7 feet per second. Figure 5.1, Impact Velocity/Energy versus Spring Displacement, displays the impact energies and velocities recorded during testing for each spring displacement setting. Table 5.1, Mean Impact Energy, reports the average impact energy, sample size and standard deviation within the sample. Standard deviations for samples will be calculated throughout this report using

$$S = \sqrt{\sum_i (\bar{x}_i - \bar{\bar{x}})^2/(n-1)} \qquad (5.1.1)$$

where n is the number of elements in the sample and x is the sample mean.

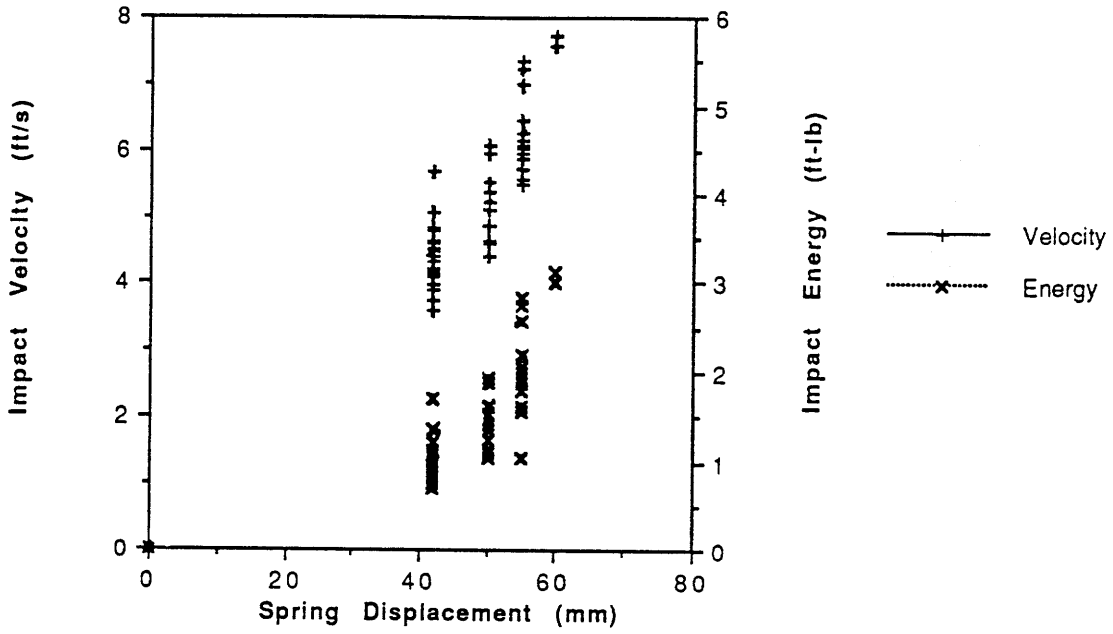

Figure 5.1 Impact Velocity/Energy vs. Spring Displacement

TABLE 5.1
Spring Displacement Versus Kinetic Energy

Spring displacement:	40mm	43mm	50mm	55mm	60mm
Mean (ft-lb):	.99	1.14	1.94	2.47	3.17
Std. devation(ft-lb):	.17	.29	.42	.11	.14
Sample size:	41	16	46	5	7

5.1.2 Impact Force

The force transducer in the tup provided force values throughout the impact event. Table 5.2, Maximum Impact Forces, displays the average peak forces recorded through the tup force transducer for specific specimen type and energy level (spring displacement).

TABLE 5.2

Maximum Impact Forces

	1 inch	.687 inch	.375 inch
[+-45]			
40mm	140 [11] (6)	148 [12] (7)	130 [2.9] (4)
43mm	145 (1)		151 [8.4] (3)
50mm	144 [25] (4)	157 [18] (7)	154 [10] (4)
[0/90]			
40mm	122 [34] (3)	126 [12] (7)	124 [33] (4)
43mm	120 [12] (4)		137 [16] (4)
50mm	283 [31] (3)	152 [26] (4)	148 [22] (5)
[0/90]s			
50mm	155 [15] (3)		
55mm	280 [.7] (2)		
60mm	282 [20] (3)		
[+-45]s			
50mm	144 [24] (4)		
55mm	239 [64] (2)		
60mm	255 [11.6] (5)		

Notes:
- Maximum force in lbs.
- [ ] Standard deviation within sample in lbs.
- ( ) Population of sample
- skewed data are not included

Force versus time histories were recorded by the computer during the impact event. Figure 5.2, Force-Time History: Impact Spectrum, illustrates the force-time histories of three [+-45] 1 inch specimens, (#29, 30, and 31) impacted at 2.12, 1.31 and 1.10 ft-lbs, respectively. Their peak forces were all about the same, 131 to 145 lbs. The plateau of force oscillations following the maximum peak evident in #29 is reduced in #30 and bearly evident in #31. The impactor contact time as denoted by the width of the graph's base was .030 seconds for specimen #29 and .025 seconds for specimen #'s 30 and 31. Most low energy impacts only dented the face sheet and did not break many fibers.

FORCE-TIME HISTORY FOR

HIGH, MEDIUM AND LOW ENERGY DYNAMIC IMPACTS

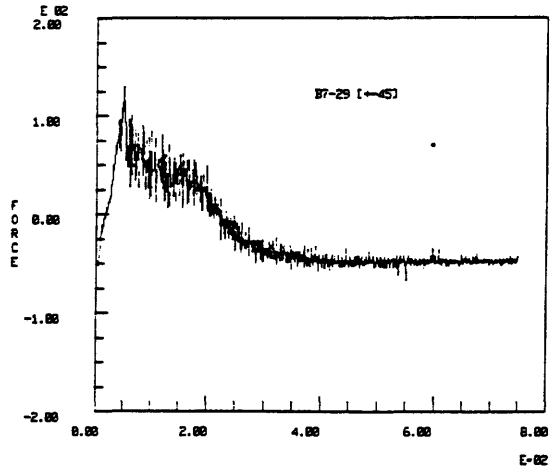

Spec. # 29
2.12 ft-lb Impact
d/W = .186
Area .270 sq. in.

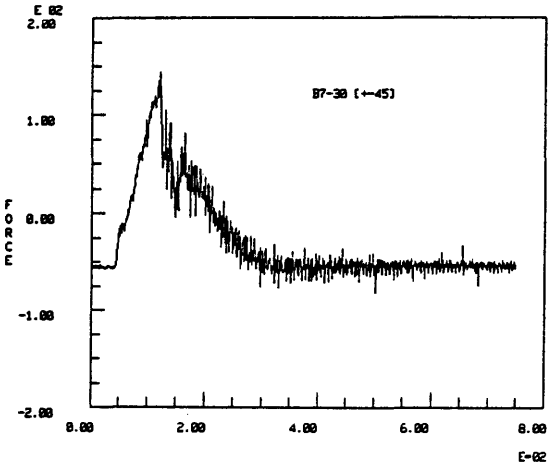

Spec. # 30
1.31 ft-lb Impact
d/W = .043
Area .130 sq. in.

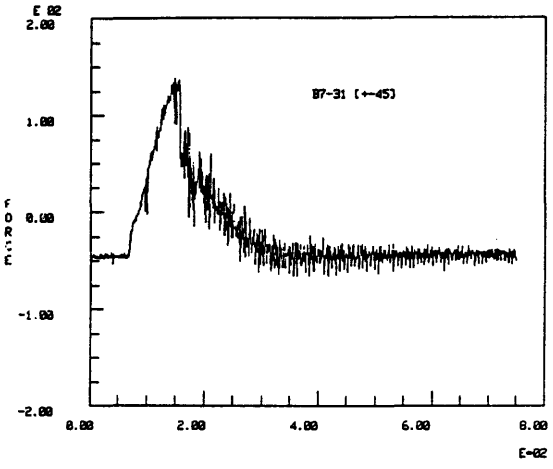

Spec. # 31
1.10 ft-lb Impact
d/W = .057
Area .136 sq. in.

Figure 5.2 Force-Time History: Impact Spectrum

30

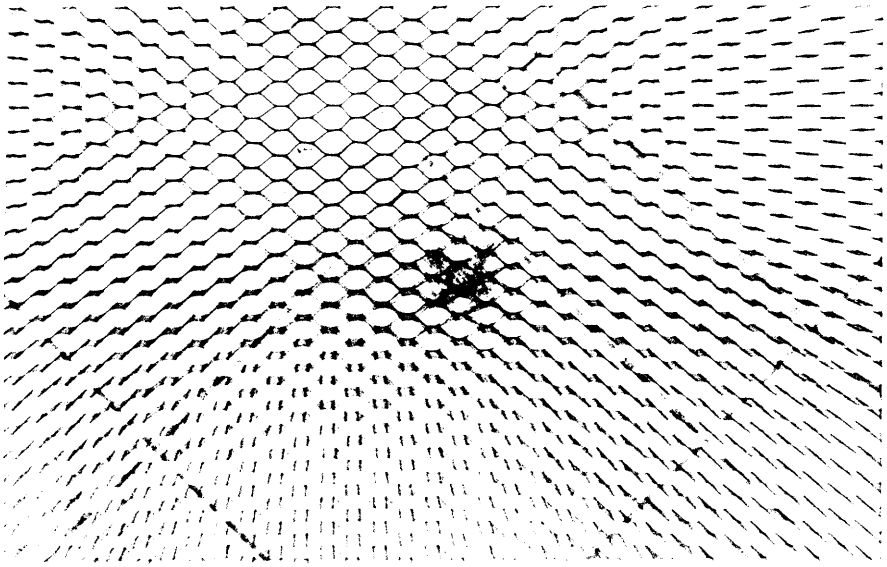

Specimen # 30; Delamination Area = .13 sq. in.

31

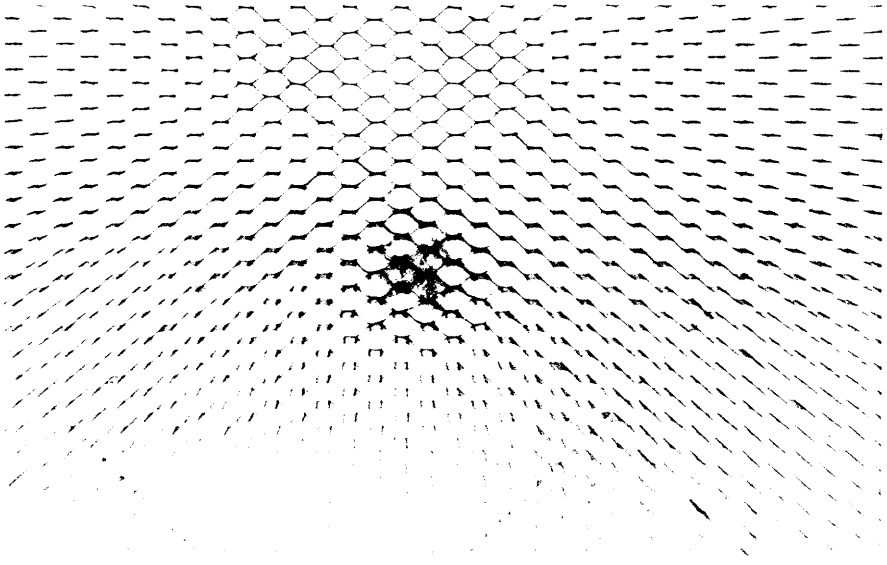

Specimen # 31; Delamination Area = .136 sq. in.

Figure 5.3a Impact Spectrum - Damage

The force oscillation "plateau" can be used as a measure of the level of damage being inflicted.

Figure 5.3 Damaging Impacts, illustrates the force "plateau" effect associated with ruptured fibers and delamination area as found to occur in the 2 and 4 ply face sheets and for different panel thicknesses. Low energy impacts which did not rupture the face sheet (refer to specimen # 204 and 301), leaving only a dent, were found to have force-time graphs. Similar in shape to a negative parabola. Specimen numbers 29, 212 and 309 each sustained varying degrees of impact damage as denoted by d/W. The "plateau" width decreases with d/W until the shape of #309 approaches the parabolic shape associated with minimal fiber rupture.

5.1.3 Impact Energy

Impact energy was calculated from each impact velocity measured during the impact testing. Impact evergy is presented in Tables A.1-8 in Appendix A for individual specimens and plotted against inflicted damage measurements in Figures 5.5-9. These results will be discussed in Chapter 6.

FORCE-TIME HISTORY

.375 in. Specimens

[0/90]
Spec. # 212
1.93 ft-lb Imp.
d/W = .143
Area = .174 sq. in.

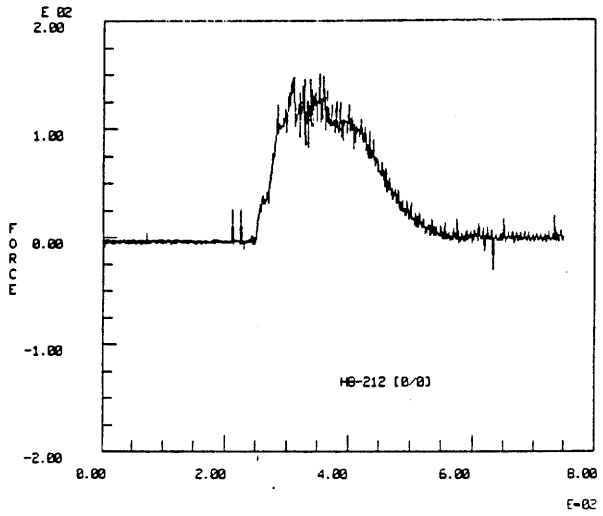

[0/90]
Spec. # 204
.98 ft-lb Imp.
d/W = .014
Area = .013 sq. in.

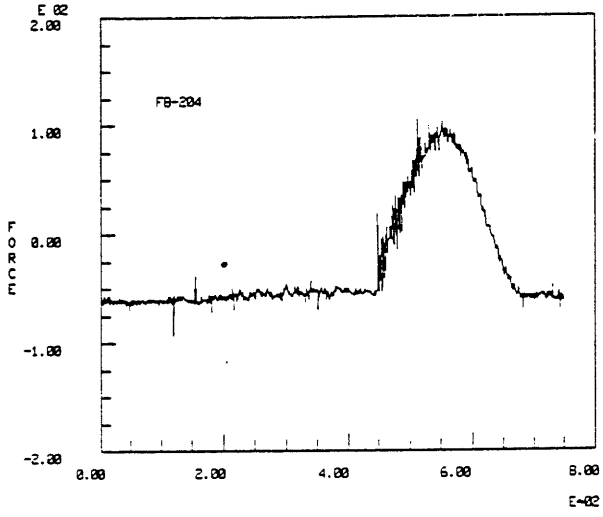

1.0 in. Specimens

[+-45]s
Spec. # 309
3.01 ft-lb Imp.
d/W = .086
Area = .234 sq. in.

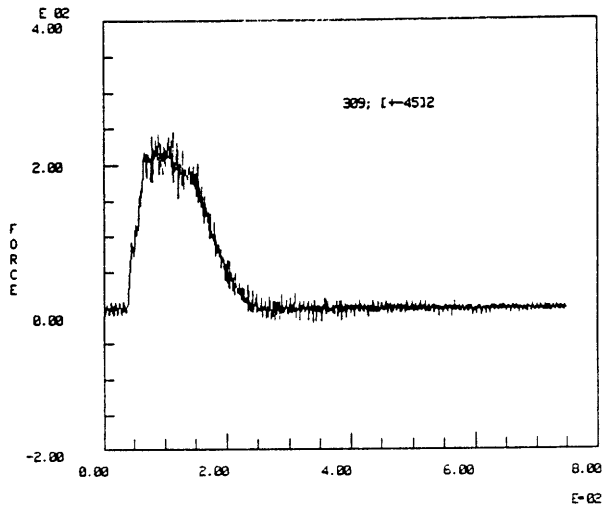

[+-45]s
Spec. # 301
2.12 ft-lb Imp.
d/W = .014
Area = .197 sq. in.

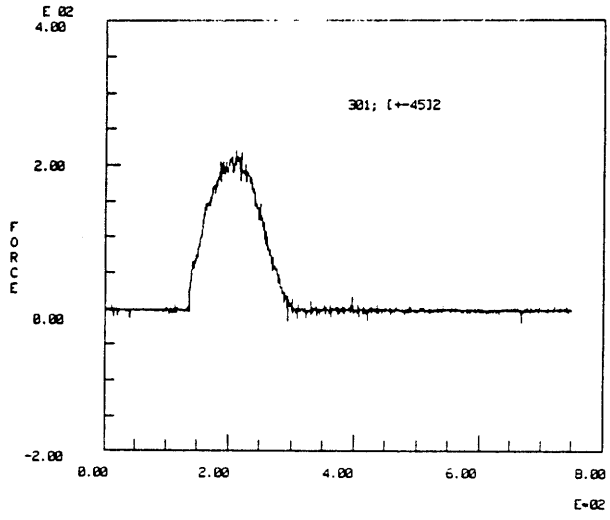

Figure 5.3 Force-Time History - Damaging Impacts

5.2 DAMAGE ASSESSMENT

Following the impact event, each specimen was x-rayed and inspected visually as described in section 4.5.2. The x-ray photographs provided excellent resolution of inter-ply delaminations. Cracks and delamination regions appeared as gray lines or shaded areas. Dye accumulation around core cells was quite evident in some photographs. Core and face debonding was not evident from these photographs.

The area of damage defined by gray cracks and shading (delamination) was determined by placing a transparent grid mesh over the photograph and counting 2mm x 2mm squares that contained damage. The resulting damage area is reported by specimen in Appendix A, Tables A.1 through A.8.

The cross-sectional rupture diameter d was measured under 15 to 1 magnification and is reported as a ratio over the specimen's nominal width, W. The cross-sectional damage ratio d/W is reported by specimen in the tables of Appendix A.

Both damage measurement techniques require subjective evaluation on the part of the investigator. Individual cracks within the laminate were assigned a fraction of the unit square area that they occupied. Filament tows which displayed signs of partial or complete breakage beneath an obscurring tow were assigned as a complete or partial break. It was found that tows fracture from center outward. The measurement of d simply involved choosing the rupture limits

on each side of the inclusion, which were furthest from the specimen's centerline and projecting a distance d on the transverse mid-line of the specimen. Figure 5.4 illustrates this projection technique.

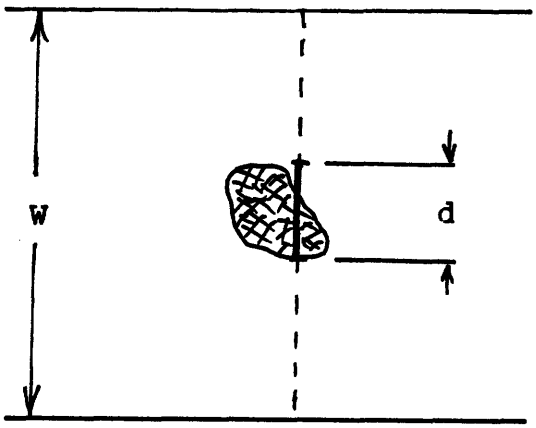

Figure 5.4 Cross-Sectional Damage Projection

Fiber rupture for 2 ply laminates begins at approximately 1.0 ft-lbs of impact for this half inch hemispherical impactor. Four ply face sheets exhibit a minimum .05 square inches of delamination area after a 1.93 ft-lb impact. Actual surface filament rupture was not observed until 2.42 ft-lb of impact for the 4 ply laminates. Specimens with a d/W value of .014 have a .5mm hole in the center of the impact site. The hole was drilled to inject dye for sub-lamina x-ray inspection of intact face sheets. The .5mm hole was unimportant to damage propagation or residual strength.

The fiber rupture threshold proposed by Lie [7], of 1.4 ft-lbs is high because he measured velocity using a 13mm timing flag unaware that a 1mm error existed in triggering

the timing light gate. This investigator is using an "effective" timing flag of 12 mm, which reduces comparable speeds by 8% and impact energies by 15%. This leaves just a .19 ft-lbs difference between Lie's threshold estimate of 1.19 ft-lbs and 1.0 ft-lbs proposed here. This differential is within subjective visual inspection and experimental error.

Core indentation in the form of wrinkled and buckled honeycomb cells was found to occur with the initiation of delamination, at approximately .70 ft-lbs of impact. Sectioned impact specimens were measured for core indentation depth and the diameter of core/face sheet debonding. The measurements are provided in Table A.9 of Appendix A.

Specimen 29 listed in Table A.9, suffered severe core damage due to face sheet penetration. The core indented 3mm and had a 12mm core/face debond diameter. The face sheet had a rupture diameter of 13mm. Other specimens had larger core debonds than face sheet ruptures.

The typical indentation from a 2.0 ft-lb impact upon a 2 ply face sheet is between 1.2 and 3 mm(ie: specimens 29 & 55). 2.0 ft-lbs represents the 2 ply face sheet penetration threshold. If the face sheet holds, core indentation is less than 1.2mm. Core indentation is reduced further by the 4 ply face sheet, as evidenced by a .8mm indentation umder impacts of 3.01 and 3.26 ft-lbs, for specimens 321 and 307, respectively.

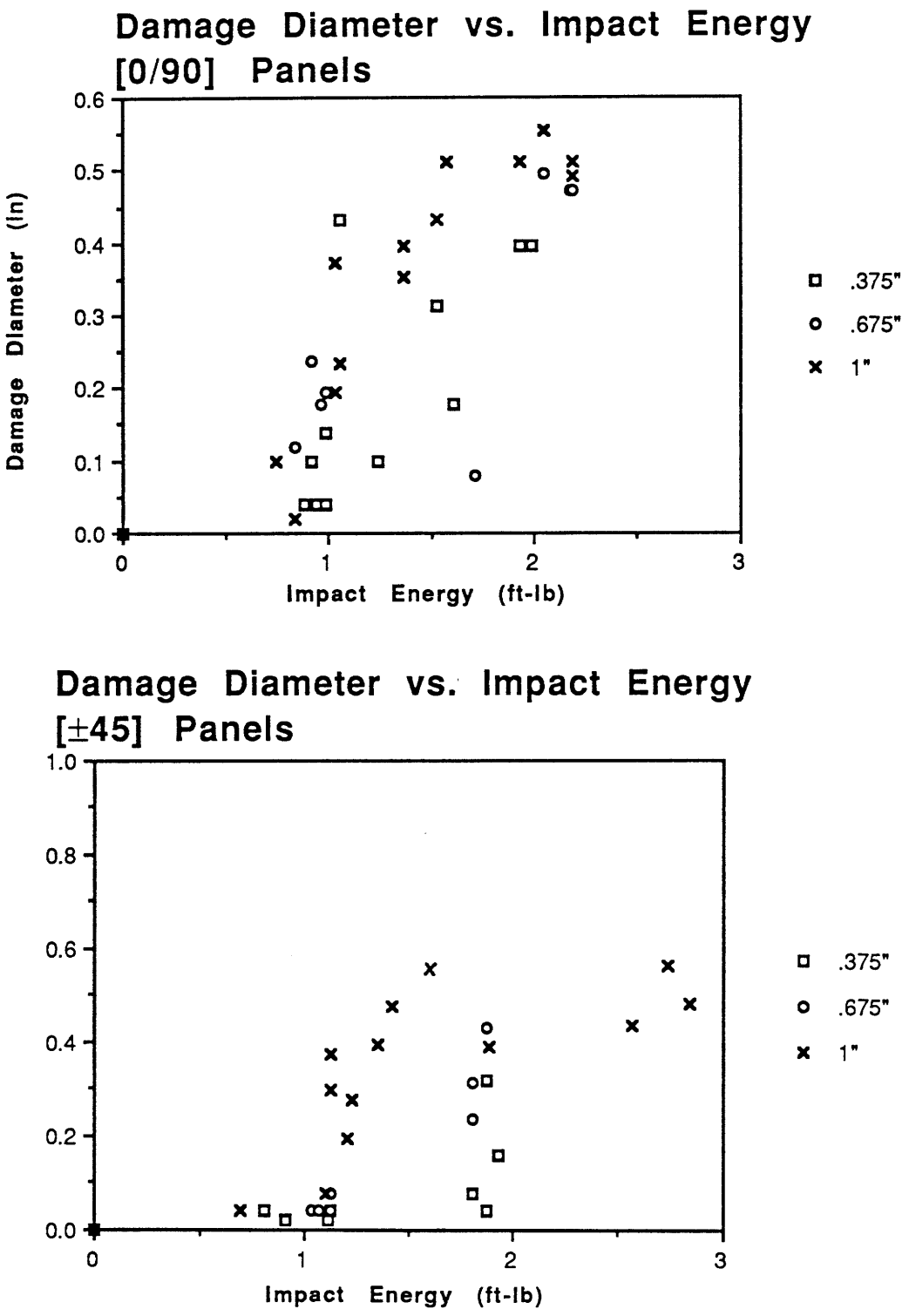

Figure 5.5 Damage Diameter vs Impact Energy

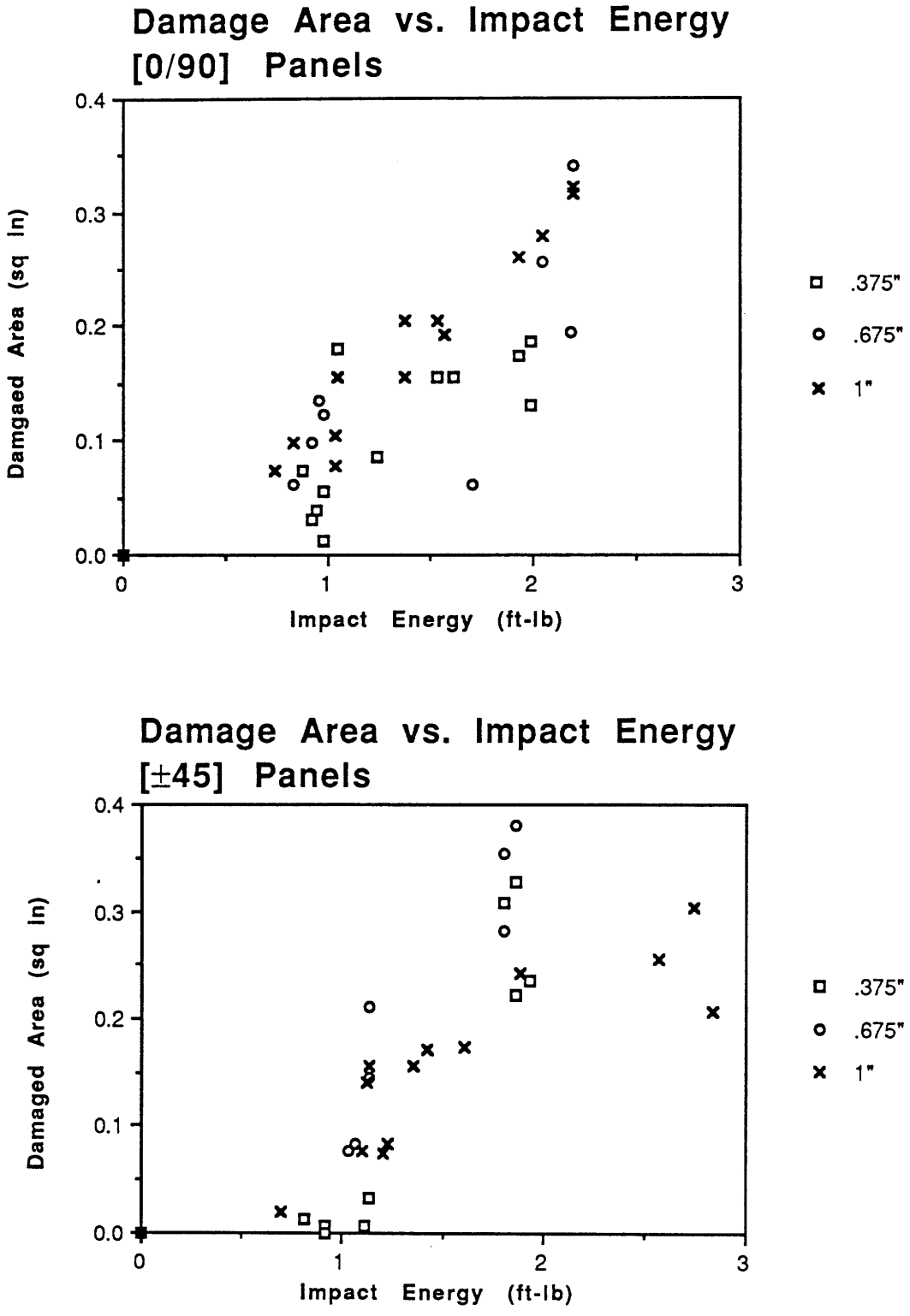

Figure 5.6 Damage Area vs Impact Energy

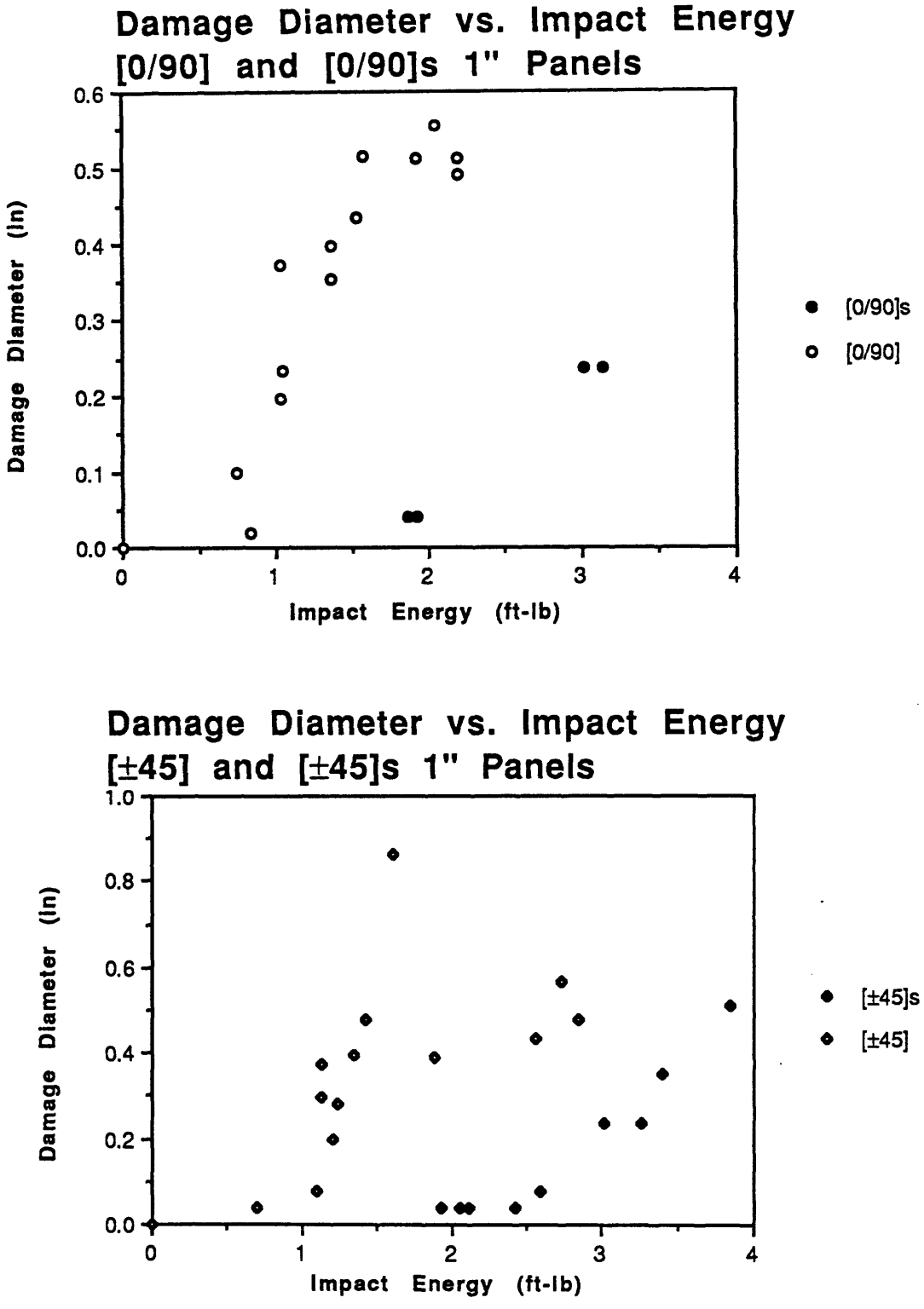

Figure 5.7 Damage Diameter vs Impact Energy: 2 and 4 ply, 1" Panels

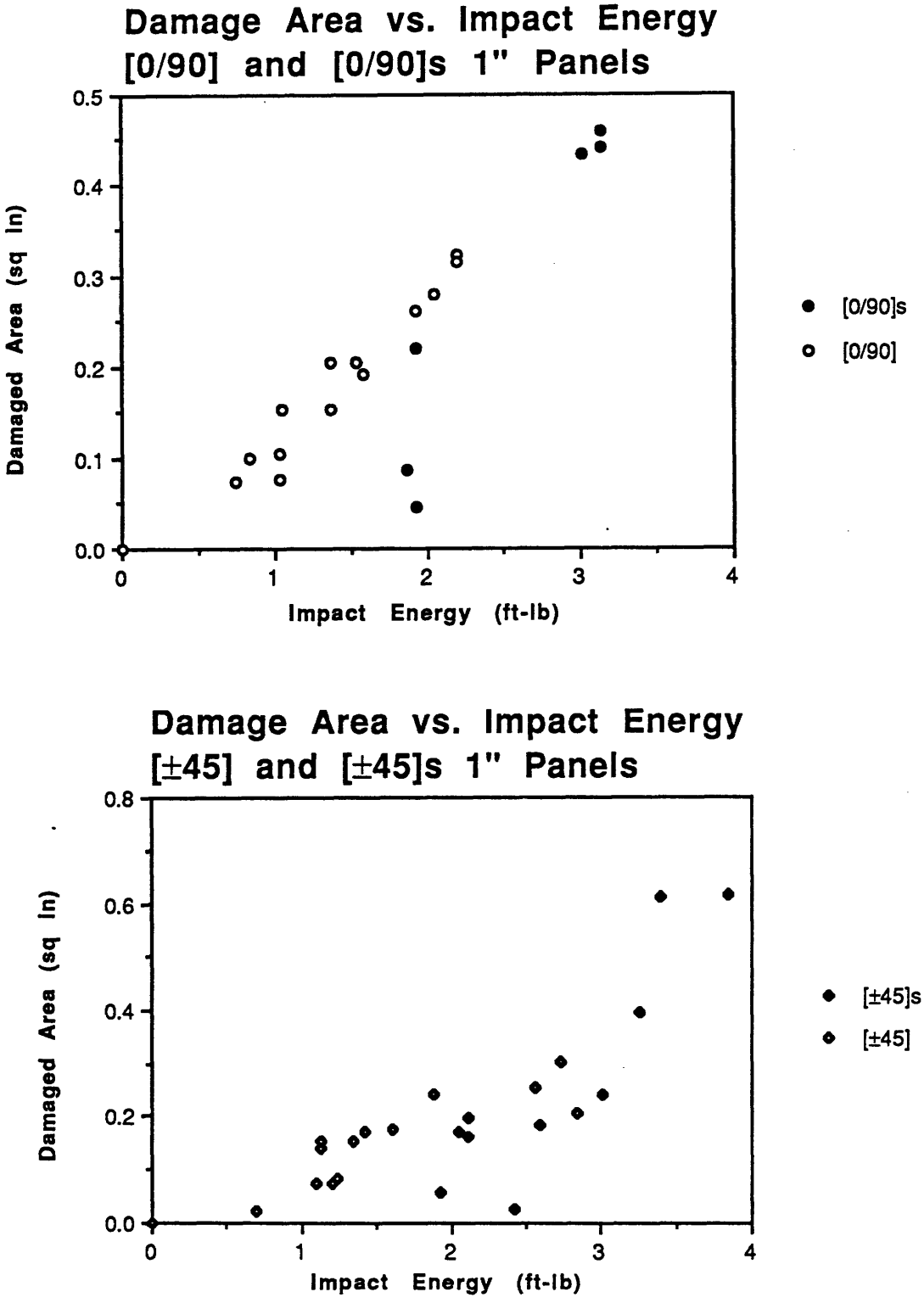

Figure 5.8 Damage Area vs Impact Energy: 2 and 4 ply, 1" Panels

A sample of x-ray photographs depicting the delamination within damaged face sheets is provided in Figures A.1,2,3,4, and 5 of Appendix A. The photographs do not provide any information regarding core indentation or debonding. But they do show the shape of the honeycomb cells under and around the inclusion.

5.3 QUASI STATIC FOUR POINT BENDING

Nomex sandwich panels and reinforced sandwich panels were tested to failure. Damaged panels usually buckled through the inclusion on the compression face sheet as expected. Undamaged panels with no aluminum core reinforcement suffered core buckling and crushing under the interior loading points. Reinforced undamaged panels experienced face sheet buckling in the 2 inch Nomex core test section. The 4 ply face sheet panels typically failed with core buckling or shearing, despite moderate face sheet damage. The specimens which failed due to core crushing or face sheet debonding are reported with the specimens which failed through the damage site. The sandwich panel is only as strong as its weakest element, which justifies the report of core and bond failure.

Tables A.1 through A.8 in Appendix A report four catergories of information about each test specimen:

1.) degree of impact - velocity and energy of the impact

2.) degree of damage - delamination size and ruptured cross-section

3.) parameters at failure - moment, stress and strain

4.) mode of failure - laminate buckling failure was predominant and can be assumed unless actual failure mode is stated.

5.3.1 Failure Modes

Two typical modes of fracture were observed for the two ply damaged panels. The 0/90 face sheets fractured laterally through the damage site with in-plane splicing and "brooming" between plies. The +-45 face sheet also fractured through the damage, but the fracture line would run parallel to tows (+45 or -45) in a fine toothed zigzag fashion or in large splits up to 1 inch in length. Other modes included "turn down" buckling where the laminate fractures and bends down into the core. Lateral stair step (for the 0/90) is the fracture along tow boundaries predominantly in the lateral direction. Delamination of the face sheet and core following fracture also occured. Combinations of these modes were also observed and are illustrated in Figure 5.9.

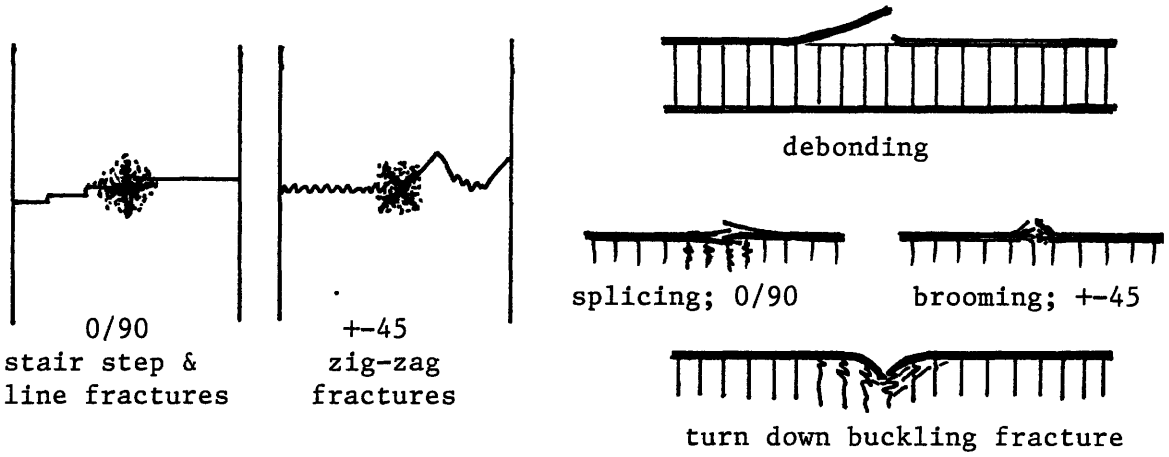

Figure 5.9 Compressive Fracture Modes for Damaged Face Sheet

An elliptical indentation or dimple would usually become visible around the damage site of 2 ply face sheets as the in-plane compressive load reached 75% of its critical load. The dimple expanded laterally across the specimen as load increased. Figures A.6,7,8, & 9 contain photographs of Specimen # 235 at four loads. Dimple length increases with stress. Dimple length was measured visually at the instant of specimen fracture for a number of specimens. The longest dimples recorded were 38mm measured from three [0/90] .375in specimens and one [0/90] .687in specimen. The longest dimple among the +-45 face sheets was 30mm in a .375in specimen. The average dimple lengths at fracture are recorded in Table 5.3.

TABLE 5.3

Dimple Lengths at Fracture Load

Core Thickness:	1 "	.687 "	.375 "
0/90	18(2)	31(2)	32(8)
+-45	23(4)	24(4)	27(8)

lengths in millimeters

( ) number in sample

No dimples were observed in any four ply laminate face sheets.

In some cases, the dimple prescribed the failure mode pattern. Specimens which developed long dimple indentations often fractured with "turn down" buckling over the length occupied by the dimple and in-plane straight line fracture at either side. This result is not surprising in that the face sheet is turned down into the core by the indentation prior to fracture.

The typical mode of fracture for the undamaged reinforced specimen was face sheet fracture (buckling presumed) within the 2 inch Nomex test section. Figure A.10 illustrates a test section buckling fracture for Specimen # 61 at 55.45 Ksi. Some failures occured on or next to the Nomex/aluminum core joint. Tables A.1 - 6 contain undamaged specimen failure bending moments, stresses strains and failure mode. Specimen # 117 failed prematurely because of face sheet debonding. The [+-45] .375 in. reinforced specimens (Table A.5: #'s 230, 231 & 233) could not be deflected enough to gain fracture. Figure A.11 is a

photograph of Specimen # 232 impinging on the assembly at either end because of excessive deflection. The stresses and strains are recorded for their maximum deflections of 38mm and 21 degrees at the outboard support.

The damaged 4 ply face sheet specimens (300 series in Table A.7 & 8) and the undamaged 2 ply face sheet specimens (Tables A.1-6) typically failed due to core shearing, crushing or the combination of both. Only three of the 4 ply 300 series specimens (#'s 301, 322, & 323) failed because of laminate fracture through a damage site. The core was placed under great shearing stress in the 300 series tests because the face sheets were twice as stiff in compression, eight times stiffer in bending and the core was one inch thick. Shearing strain of the core was observed in the x axis followed by compressive buckling and crushing of the core's cells, for all of the 300 series core failures. Figures A.12-14 depict core ripping, crushing and shearing failures.

The undamaged 2 ply face sheet specimens typically failed with core shearing and crushing or face sheet buckling under one of the inner loading points. Core buckling under these loading points either initiated face fracture or continued into further core crushing. Figure 5.10 illustrates observed core failure modes

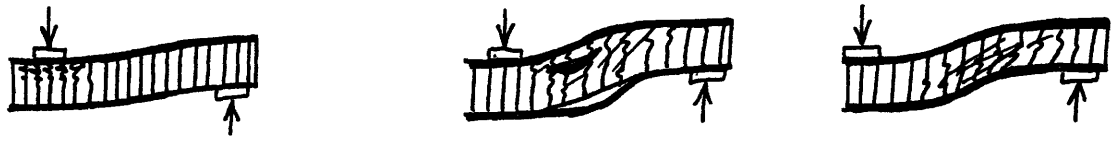

core crushing failure

core shearing (rip) and debonding failure

core shearing and buckling failure

Figure 5.10 Core Failure Modes

5.3.2 Panel Deflection Under Load

Mid-point deflection and angular deflection at the outboard loading point were measured and recorded throughout the quasi-static bending test. The mid-point deflection, and deflection angle, θ_β are plotted versus the applied deflection load for each type of specimen tested, and reported in Appendix C. The curves are provided as raw data for these specific specimens and loading point placement. From Figure 3.7 Four Point Beam Loading, the loading points are:

2 ply face sheet specimens - ℓ = 110mm moment arm
L = 320mm

4 ply face sheet specimens - ℓ = 130mm moment arm
L = 330mm

Taking P to equal half of the applied experimental load and placing experimental data for deflection w_{max} and deflection angle θ_β into equations (3.7.3) and (3.7.4) respectively,

will produce the specimen's flexural rigidity EI_y. The small angle assumption limits the accuracy of these equations for anything but small deflections.

5.3.3 Failure Stresses and Strains

Stresses at failure were calculated for σ_x in the compression face sheet using the following four point symmetric bending equation.

$$\sigma_x = P\ell / \{2fW[h-f]\} \qquad (5.3.1)$$

The far field stress values recorded in Appendix A come directly from equaiton (5.3.1). Local failure stress is the far field stress times a net cross-section correction factor.

$$\sigma_{x\,local} = \sigma_{x\,far\ field}\,[1/(1 - d/W)] \qquad (5.3.2)$$

The average failure stresses for actual face sheet fracture are presented in Table 5.4. Specimens which failed through other modes have been excluded. Table 5.4 provides a basis for residual strength comparisons between impact energy effects and specimen parameters, thickness and face sheet orientation. Far-field failure stress is plotted versus impact energy and cross-sectional damage for all test specimens, in Figures 5.11,12,13 and 14.

TABLE 5.4

Mean Face Sheet Failure Stresses

Damage Level	1 in.	.687 in.	.375 in.
0/90 zero	64.39 (4)	58.11 (4)	67.09 (4)
0/90 high	21.52 (6) [28.76] (6)	31.28 (3) [37.86] (3)	29.76 (3) [34.93] (3)
0/90 Med.	25.16 (4) [28.76] (4)		35.44 (5) [32.60] (5)
0/90 Low	31.07 (3) [34.87] (3)	37.32 (5) [38.62] (5)	31.76 (5) [32.60] (5)
+-45 Zero	35.97 (4)	36.58 (3)	50.00+ (3)
+-45 High	25.66 (3) [33.52] (3)	23.28 (2) [25.88] (2)	20.85 (4) [22.06] (4)
+-45 Med	25.79 (2) [30.10] (2)		24.27 (2) [24.52] (2)
+-45 Low	26.53 (5) [29.17] (4)	24.23 (3) [24.70] (3)	23.70 (3) [23.87] (3)

All stresses are in Ksi units.
[ ] local stresses
( ) number in sample

5.4 PANEL COMPRESSION RESULTS

The aluminum honeycomb panel test specimens had fabrication flaws which caused premature failures. The results of Lie's [7] Nomex panel compression tests are more suitable for determining face sheet failure loads.

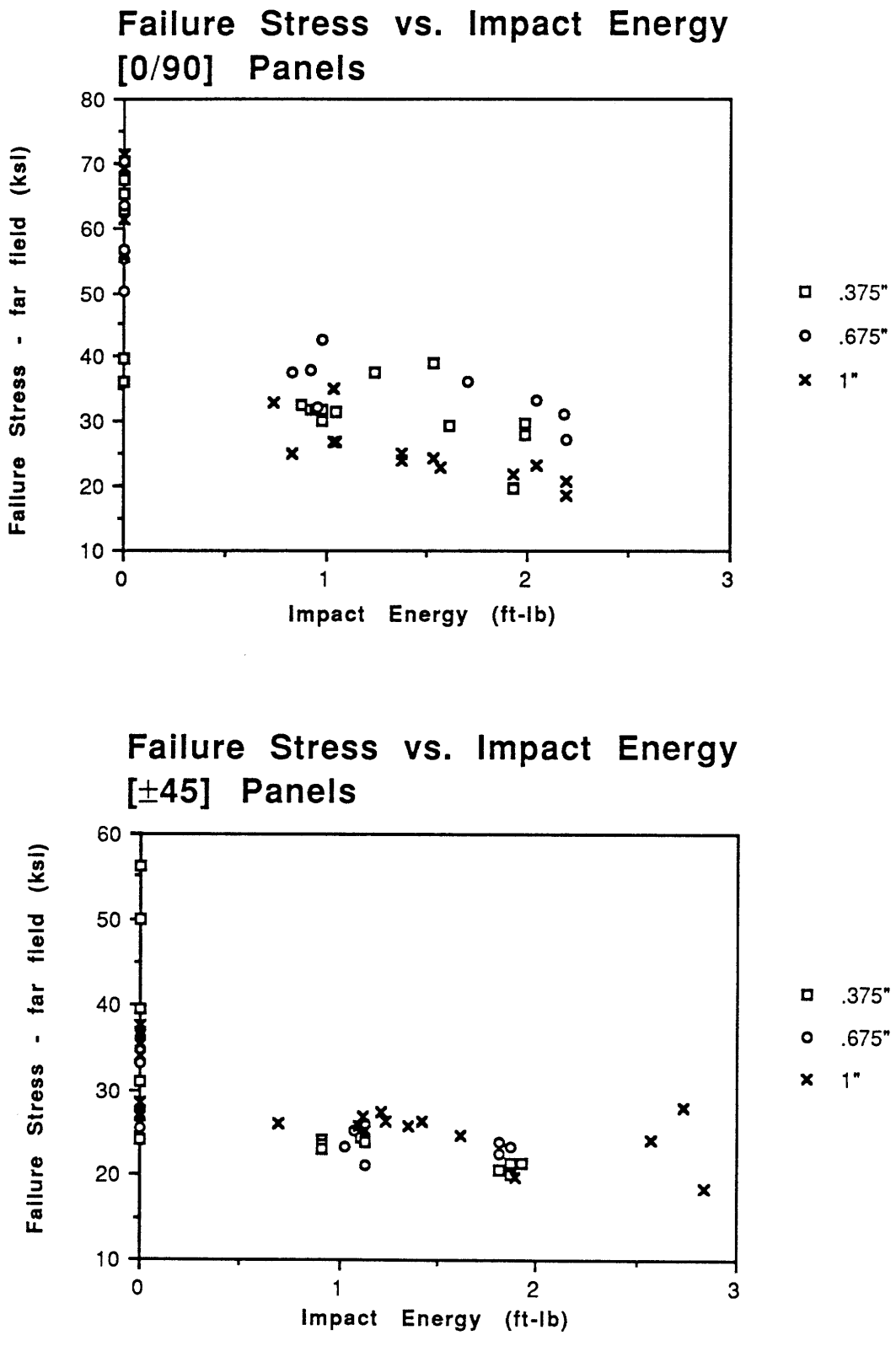

Figure 5.11 Failure Stress vs Impact Energy

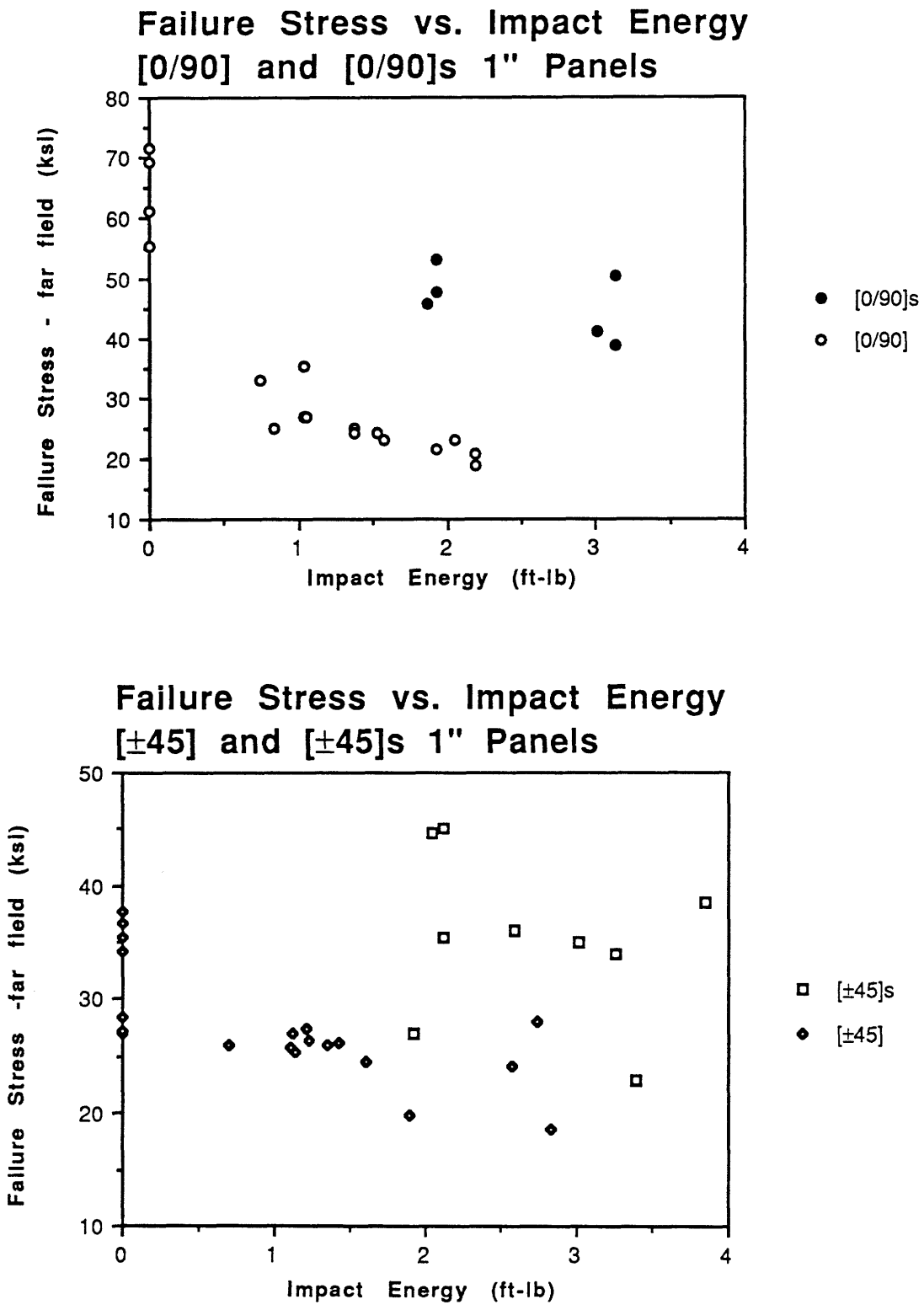

Figure 5.12 Failure Stress vs Impact Energy: 2 and 4 ply, 1" Panels

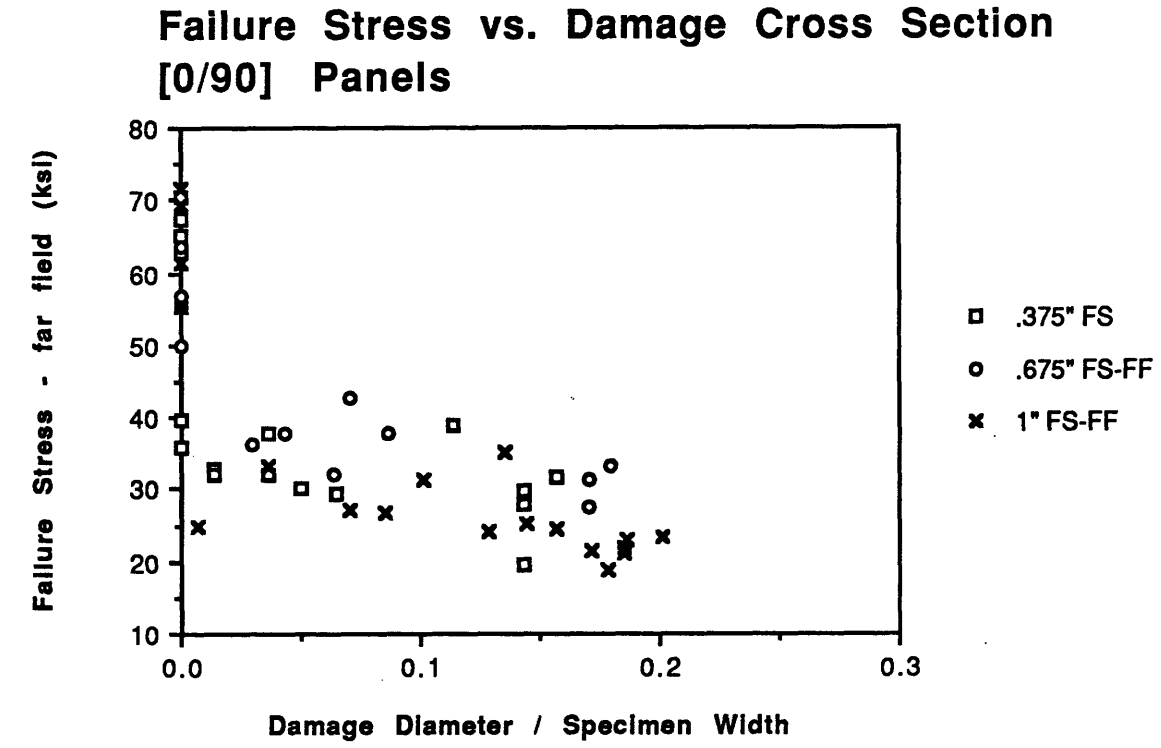

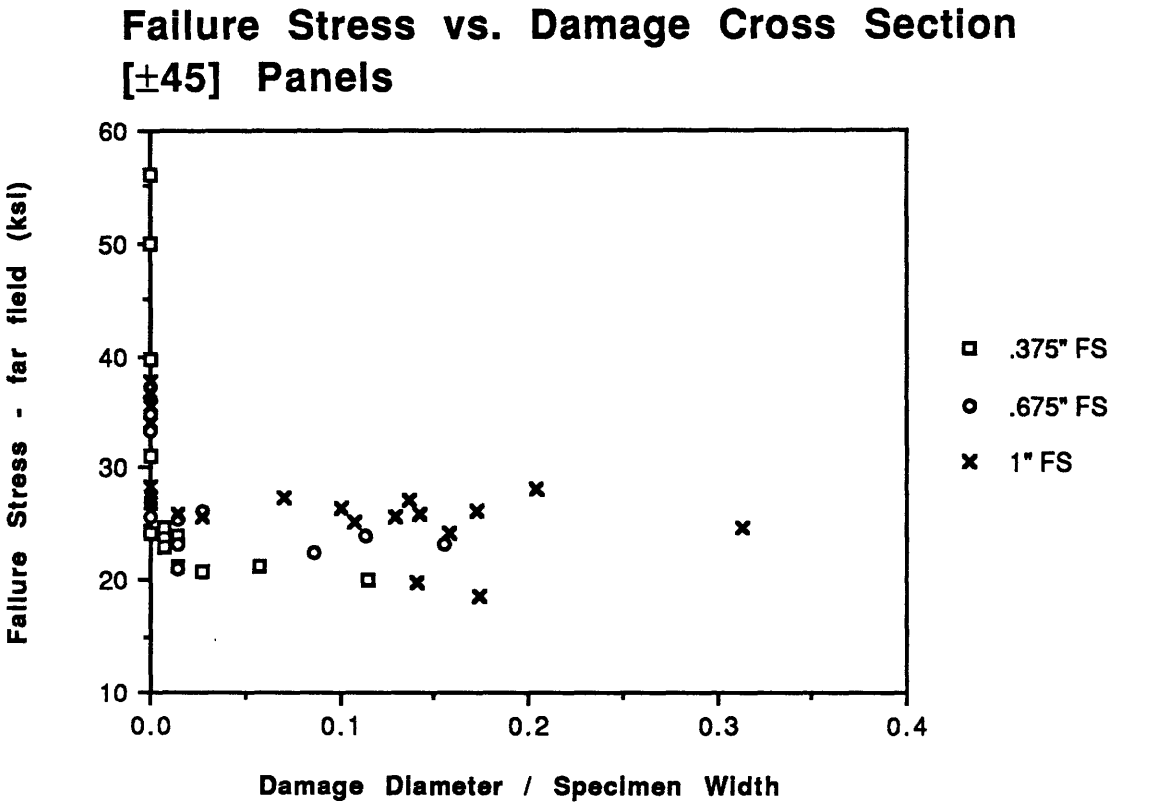

Figure 5.13 Failure Stress vs Damage Cross Section

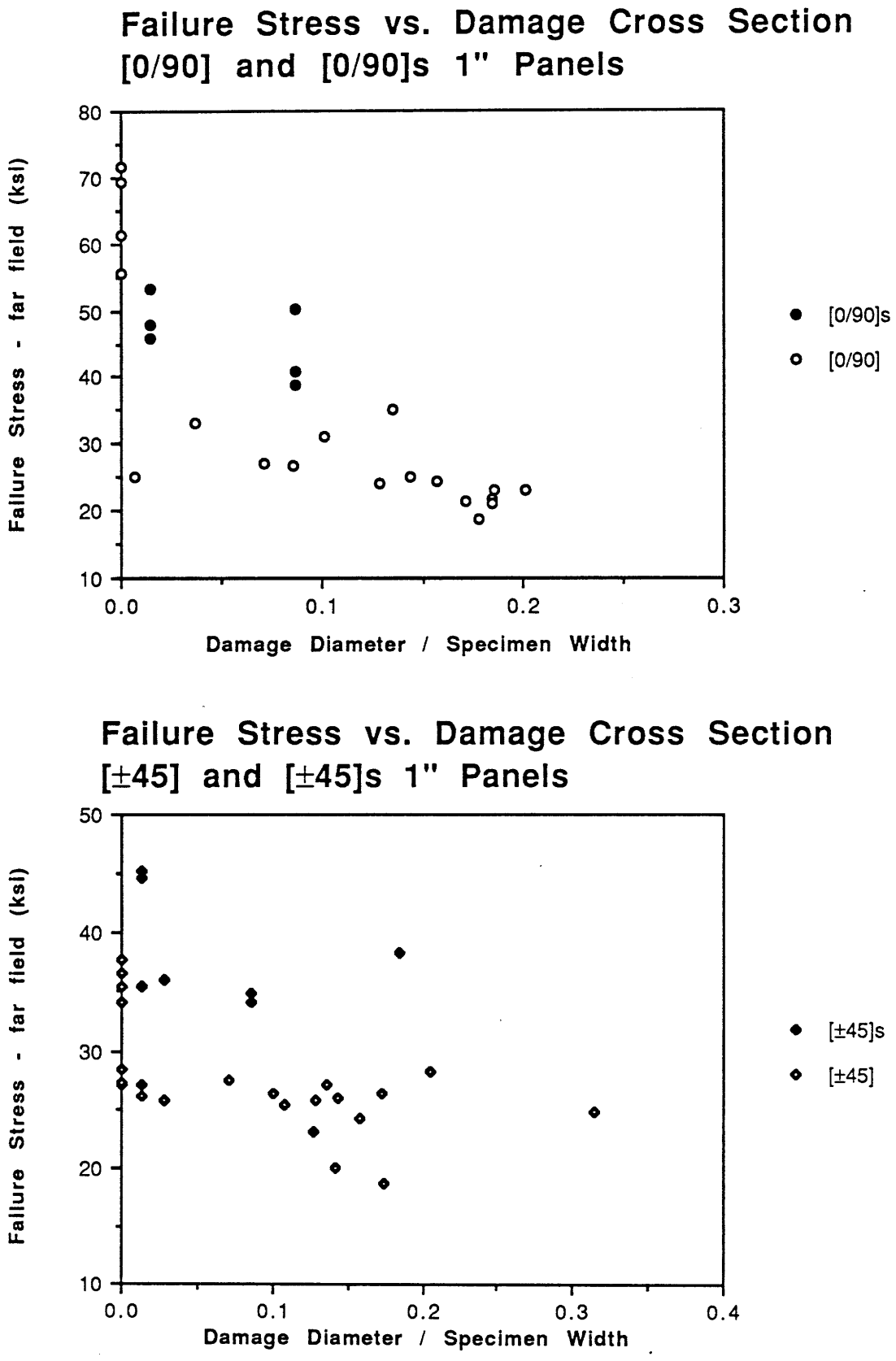

Figure 5.14 Failure Stress vs Damaged Cross Section: 2 and 4 ply, 1 inch Panels

5.5 CORE COMPRESSION RESULTS

Six Nomex coupons with 2 ply laminate face sheets were tested for core buckling threshold. The onset of core buckling was determined by noticable waves through the sectioned honeycomb cell walls. The average buckling stress (from two samples) for each Nomex thickness is:

1.0 inch	218 psi
.687 inch	221 psi
.375 inch	205 psi

The critical load for Nomex buckling appears to be independent of thickness and approximately 210psi

5.5.1 Core Indentation Results

Six Nomex sandwich coupons were tested for core indentation resistance. The objective was to determine the load/unit area required to buckle a single row of honeycomb cells at an impinging load angle of 8 to 12 degrees. A steel cylinder 38.04mm in diameter acted as the indentor. The results are summarized below in Table 5.5.

TABLE 5.5

Core Indentation Impinging Loads

	Perpendicular to Ribbon	With Ribbon
Impinging Angle:	3 - 8 degrees	3.5 - 10.4 degrees
1 inch core	210psi	262psi
.687 inch core	210psi	222psi
.375 inch core	214psi	208psi

The data is very close to the normal load/unit area for the core as determined with the core compression test.

5.6 PANEL FATIGUE RESULTS

An introductory series of twenty eight Nomex honeycomb panel specimens were tested for damaged and undamaged fatigue life under cyclic compression (R=.1). The results of twenty four specimen tests are reported in Tables A.10 and A.11 of Appendix A. The impact energy and damage dimensions are listed by specimen number. The maximum compression stress amplitude is reported as a percentage of the undamaged critical stress as determined by Lie [19], for each damage state. Table 5.6 summarizes Lie's residual strength estimates.

TABLE 5.6

Residual Strength Estimates (Ksi)

Layup	Core Thickness	Damage Level zero	low	medium	high
0/90	.687 in.	45.05	35.67	32.99	24.95
+-45	.687 in.	29.37	26.92	26.22	24.12
0/90	1.00 in.	48.81	38.46	35.50	26.62
+-45	1.00 in.	30.31	27.25	26.38	23.75
0/90	.375 in.	44.86	35.08	32.37	23.88
+-45	.375 in.	27.76	25.29	24.58	22.46

The undamaged strength estimates are provided as foot notes in Tables A.10 and A.11.

The maximum stress amplitude was altered for some specimens during their fatigue life because damage was inflicted immediately as with specimen 260, or the specimen was continuing past reasonable life expectations. Cycles at each specific stress amplitude is recorded in the Cycles @ Stress Amplitude column of Tables A.10 and 11. The sum of the cycles at each stress amplitude is recorded in the Life Cycles column.

CHAPTER SIX

DISCUSSION

6.1 IMPACT RESULTS

6.1.1 Impact Force

Refering to Table 5.2, Impact force increases with energy level for all two ply face sheets and specimen thicknesses. However, the 4 ply specimens exhibit a high force level that remains constant through escalating impact energy. The impact forces listed in Table 5.2 are fairly constant across specimen thicknesses for a given impact energy level.

A comparison between specimens of constant impact energy and core thickness suggests that 10 to 20 more pounds is exerted on the +-45 specimen for every thickness and low to medium energy level. Since the 0/90 and +-45 face sheets are exactly the same, this phenomena may depend on face sheet orientation and the clamped boundary at either end. The flexural stiffness of the panel depends on face sheet orientation and core thickness. Table 5.2 data suggests that force is not influenced by panel thickness. Fiber rupture or breakage does not explain the effect because it occurs in face sheets with only a slight indentation as well as rupture. The answer may lie in the face sheet bending stiffness. The 0/90 orientation has bending stiffness parameters $D = 2.68$ in-lb and $D = 2.57$ in-lb. These bending stiffness parameters do not support the

phenomena. One conclusion is clear. Thicker face sheets provide a greater resisting force to impact.

Force versus time histories of impact events support Lie's [7] explaination of sudden force drops due to fiber rupture at critical strains and the on set of vibrations within the face sheet. Impacts which result in damage such as penetration or fiber rupture have force-time history's with a steep peak followed by a slight drop to a plateau of force oscillations, which then dampens to zero.

6.1.2 Force - Time History

Specimens with parabolically shaped force - time histories without oscillations typically have limited filament breakage.

The large impact energies exerted on the 4 ply laminate face sheets (Figure 5.3) can be seen in the force vibrations following the peak. These vibrations may be caused in part by the strain energy released by the delaminations that had just occured during impact. The second part of the vibration phenomenon is the natural vibration modes of a plate on an elastic foundation.

The highly damaged 4 ply face sheets of specimens #'s 306 and 308 have significant filament damage. They also have characteristic plateaus and slow dampening curves with oscillations. It appears that delamination and natural plate vibrations contribute to force oscillations and that filament fracture causes a plateau of constant oscillation

followed by slow dampening to zero. Lie [7] made the same conclusion.

6.1.3 Impact Energy and Damage Assessment

The data plotted in Figures 5.5 and 5.6 provide some insight into the relationship between impact energy and damage to thin face sheet panels. Increased impact energy will usually cause more delamination, fiber rupture and core damage. The data variance indicates that theoretical predictions will be subject to large deviations. A band of values may be an appropriate empirical estimation.

It is evident from both damage plots that the .375 inch panel and the .687 inch panel, resists fiber rupture and delamination better than thicker panels. This is due to the thin panel's reduced flexural rigidity which allows it to flex and absorb the impact through a larger deflection distance (in the impactor's direction of force) and thus absorb the impact energy through global strains instead of localized failure strains. The +-45 orientation would be more damage resistant than the 0/90 layup by the same stiffness argument. This face sheet flexibility is evident in the data plots for the .375 in. and the .687 in. panels. The 1 in. panel is not influenced significantly by face sheet bending compliance, because of its stiffness.

The 4 ply face sheet has a much greater resistance to surface filament rupture,than the 2 ply laminate, as illustrated in Figure 5.7. The delamination area for the

4 ply converges with the delamination area plot for the 2 ply face sheet (Fig. 5.8), after the 1.8 ft-lb threshold is attained. The threshold impact energy for filament rupture is almost 3 times greater for the 4 ply, and 2 times greater for the initiation of delamination. Note: 4 ply damage diameters which are less than .1 are artificially induced for dye injection and should be ignored for damage assessment.

Face sheet thickness is instrumental in protecting the core from indentation and penetration. A 2.0 ft-lb impact will rupture a 2 ply face sheet. A 3.0 ft-lb impact will penetrate a 2 ply face sheet into the core, but will only make a small .8mm dent in a 4 ply face sheet.

6.1.4 Damage

Face sheet damage occurs in an increasing sequence of damage levels as follows:

1) No external damage may hide small delaminations and core indentation may be hidden under an unmarked laminate surface.

2) External matrix cracks between tows and a slight dimple indicate some delamination, slight core indentation and debonding.

3) A significant dimple with matrix cracks may contain individual filament beakage, and will certainly contain delamination and core indentation on the order of .8mm.

4) Ruptured tows will be accompanied by many matrix cracks in the dimple and core indentation depth of 1mm.

5) Face sheet rupture will be evidenced by four triangular flaps bending down into the dimple.

6) Face sheet penetration will have a core indentation greater than 1.5mm and significant cracking around the shoulder of the dimple. The core may be visible.

X-ray photographs of specimens 208, 66 and 29 provided in Figure A.1, 2, 3 of Appendix A, display damage levels 2, 4 and 6, respectively. Figures A.4 & 5 are x-ray photographs of 4 ply specimens 303 and 321, which display damage levels 3 and 5, respectively.

All of these x-ray photographs (except for severe rupture in Figure A.3) display face sheet orientation through an accumulation of delamination parallel to the tows. This shows up as dark perpendicular axes. Note that specimens 29 and 303 are oriented to +-45 and the others to 0/90. Figure A.2 containing specimen 66 also displays delaminations perpendicular to the ends of each central axis. These delaminations at damage level 4 are caused by tows bending excessively at the shoulder of the dimple. The delamination relieves filament strain and prevents further rupture as in damage level 6, penetration.

6.2 RESIDUAL STRENGTH

6.2.1 Analytical Comparisons

The basis for residual strength predictions lies in the ability to accurately calculate loads, moments and stresses from predicted or measured failure strains. In order to establish confidence in the analytical method, a few calculations will be discussed.

Equation (3.8.7) was used with the TELAC and BOEING reduced stiffnesses matrices to calculate the bending moment M_x , for the [0/90] 1" specimens. Strain gauge values at failure were used to calculate the far field and local (at the fracture site) bending moments. The analytical moment was then compared to the measured failure moment to determine the differential. The results are:

	TELAC	BOEING
M_x far field differential	-.86%	1.64%
std deviation	8.76%	9.95%
sample size	16	18
M_x local field differential	6.65%	10.99%
std. deviation	12.46%	13.64%
sample size	13	13

The local errors in M_x of 6.65 and 11% indicate that the specimens are failing at a lower load than their strain gauges would indicate. The thin face sheet laminate becomes alastic - plastic very quickly which would account for this

loss of load bearing per unit of strain. The greatest plastic stretching occurs in the local failure cross section either side of the inclusion.

The stress-strain relation $\{\sigma_i\} = [Q_{ij}]\{\varepsilon_j\}$ was calculat- using experimental strains and TELAC Q_{ij} values, for both 1" panel groups and the [0/90] .687" specimens. The deviation results from experimental stresses are:

Core	Face sheet	Percent Difference σ_x (far field)	σ_x (local)
1 in.	0/90	1.3 [9.9] (17)	-.59 [5.8] (9)
1 in.	+-45	-2.6 [19] (10)	121.0 [52] N/A
.687 in.	0/90	-4.9 [9.6] (8)	3.5 [17.7] (8)

[ ] Sample standard deviation in percent

( ) Sample size

The +-45 panel has a very non-linear local region refering to its 121% error between gauge computations and actual stress. The large standard deviations in strain measurement on the +-45 face sheet is probably due to gauge orientation diagonally on the laminate's weave where slight shear strains become large extensional strains.

6.2.2 Failure Stress and Impact Energy

Figure 5.11 shows a pattern of decreasing failure stress as impact energy increases. The data indicates that core thickness is significant in determining far field

failure stress for the 0/90 panels, but not for the +-45 panels. The +-45 data points in Figure 5.11 are practically independent of thickness and marginally influenced by impact energy. Figure 5.13 data indicates that the +-45 panel is independent of damage diameter. This leads to Lie's [7] conclusion that +-45 laminates are notch insensitive. That is, loads are easily carried around damaged areas.

The +-45 orientation of tows can transfer loads effectively around damage sites as long as the matrix stays intact. When the matrix starts to crack at large stresses, the tows cannot carry load without inducing shearing strain which further damages the matrix. The matrix dependent nature is the key to the +-45 panels damage tolerance and also its limit on strength.

The 0/90 panel's stiffness contributes to its damage susceptability and reduced residual strength. A damaged 0/90 panel 1 in. thick loses 50% of its strength from a threshold impact of .9 ft-lbs. Thinner panels are more damage resistant but still loose approximately 40 to 50% of their strength from a threshold impact. Notch sensitivity is demonstrated by the huge drop in residual strength due to a damage diameter of any size.

Doubling the face sheet thickness makes both layup orientations more damage resistant and damage tolerant. The [0/90]s laminate is more tolerant of surface fiber rupture than the 2 ply version. The [+-45]s has a greater modulus of elasticity (determined through linear regression of

stress-strain data) than the 2 ply laminate. Both improvements are the result of the extra support and stiffness provided by more matrix and filament fabric. Buckling instability and matrix cracking are reduced through greater stiffness.

6.2.3 Damage Propagation

Face dimpling was observed during testing, but only for face sheets with observed damage. No dimples on the order of a cell's size were observed. The graphite/epoxy face sheet used is too stiff through its thickness (in the z axis) and the characteristic dimension f/d described by Weikel et. al. [15] is too large for any 1/8 inch dimples to appear before global buckling takes place. The indentations that did appear were supported by the perimeter of an indentation in the core (typically 1/2 inch in diameter). Experiments demonstrated that a small indentation or rupture in the face sheet due to an impact, propagates as an elliptical dimple transverse to the loading axis in both bending and column compression tests, [7]. Once the elliptical dimple reaches a critical length, face sheet buckling occurs.

The following hypothesis is offered to explain the experimental observations. Damage propagates transverse to loading because of maximum principle stress at the lateral edges of a damage inclusion. Local buckling occurs in the damage inclusion over a weakened core, which causes the

plate to deflect into the third dimension (of least resistance). Because the panel is in bending, the compressed plate will deflect (locally) in the direction of greater radius of curvature (ie: into the honeycomb core). As the dimple elongates in the transverse direction, the core is crushed down and slightly from the side by the tip of the expanding dimple deflection. The thin cell walls of the honeycomb core are buckled at the tip of the elliptical damage propagation. The cells can no longer support local stresses normal to the core face (parallel to the cell axis), and the sandwich panel cannot transfer loads properly in the dimple indentation. The face sheet finally buckles due to the loss of effective load bearing cross-section.

The dimple does not expand in the direction of load. Figure 6.1, Longitudinal Section of Dimple Indentation, illustrates the unloaded and loaded condition of filament tows which pass through the damage dimple. The core has pre-existing damage from the impact event which produced the indentation. Core cells beneath an unloaded face sheet indentation are crushed further during bending by greater face fiber deflection and localized load/unit area, σ_z. The localized load/unit area on the crushed core will decrease when the deflected tow's load σ_x is reduced. Thus an equilibrium between the core's damage resistance threshold

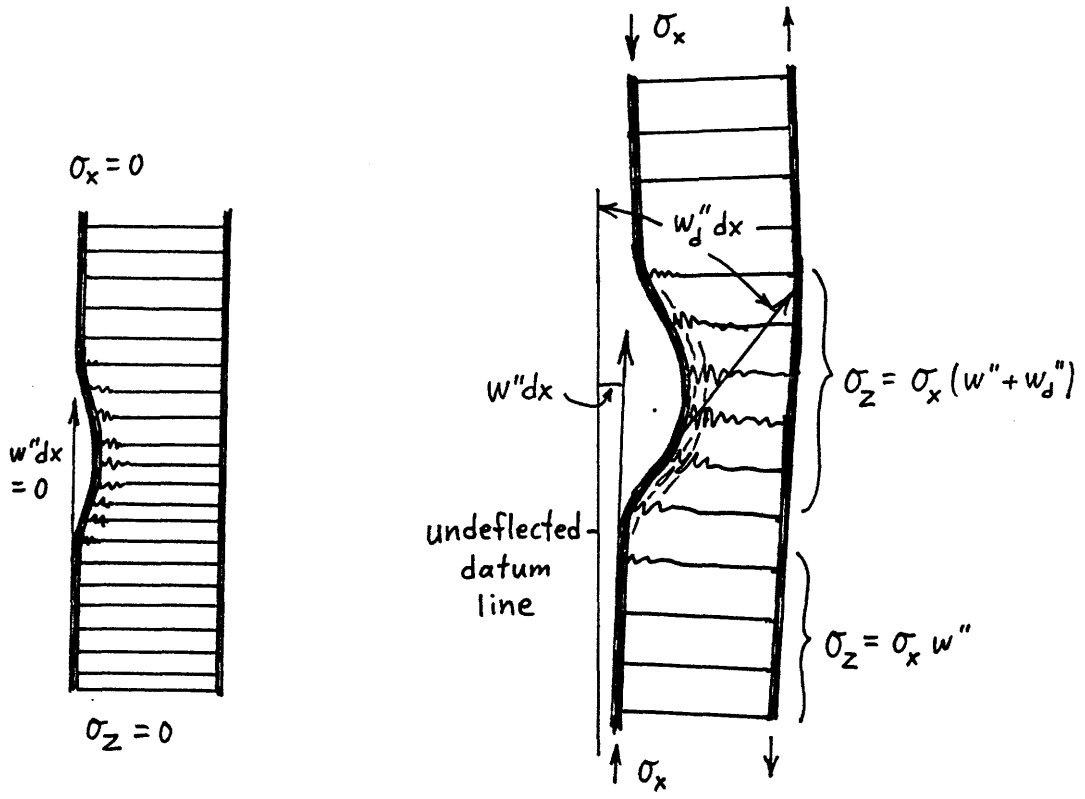

before loading during loading

Figure 6.1 Longitudinal Section of Dimple Indentation

(σ_z to buckle) and the crushing load/unit area $\sigma_z = \sigma_x (w'' + w_d'')$ caused by deflected face sheet tows, arrests further propagation of the deflection in the direction of the fiber/tow axis.

The load carried by a tow fibers which passes through a face sheet indentation will be reduced because of deformation. That excess load must be transmitted to adjacent tows. The means of load transmission in a graphite/epoxy laminate is the epoxy matrix. If longitudinal loads can be shared through the matrix, it

follows that out of plane loads can be transmitted to adjacent tows still in the loading face plane. The woven face sheet fabric used in this experiment makes the lateral transmission of σ_z loads possible through warp tows in addition to the matrix. The lateral transmission of σ_x loads and ultimate tow and face buckling differs with loading orientation.

6.2.4 Mar - Lin Relation

Damage diameter and localized failure stresses for the 1 inch, 2 ply face sheet specimens, were taken from Tables A.1 and 2, and used in equation (3.10.19), the Mar-Lin [17] relation. Solving for Hc, the fracture parameter, the following values were attained:

	Mean Hc	Std. Deviation	Sample Size
0/90, 1" panel	22.55	3.0	12
+-45, 1" panel	23.18	4.2	10

fracture parameter units are 10 lb./cu. in.

The fracture parameters are within 3% of each other, indicating that Hc is dependent on material and not orientation [17].

Figures 6.2 and 6.3 have been plotted using the calculated fracture parameter, equation 3.10.19 and tangent lines as did Lie [7]. Data points have also been plotted to illustrate the accuracy of the approximation.

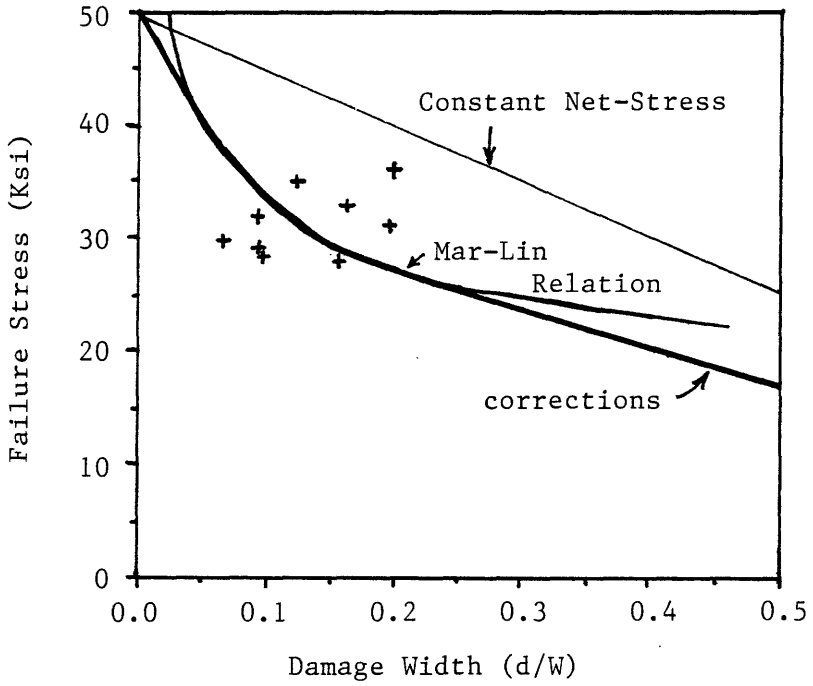

Figure 6.2 Mar-Lin Residual Strength; +-45, 1" Panels

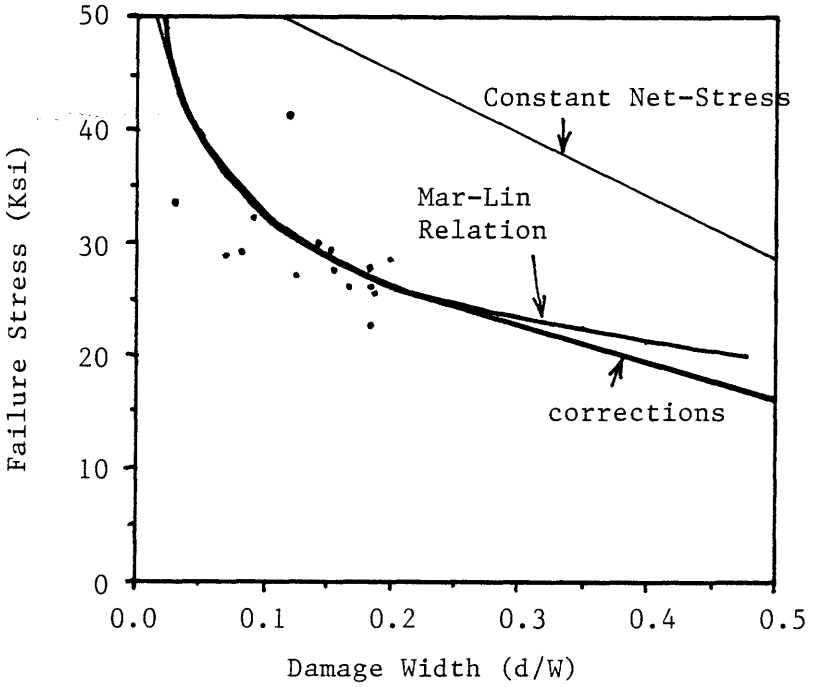

Figure 6.3 Mar-Lin Residual Strength; 0/90, 1" Panels

6.3 PANEL LONGEVITY

Undamaged 0/90 panels have a longevity in excess of 669,000 cycles at loads as high as 90% of buckling. Loads above 90% appear to weaken the matrix after 40,000 cycles, leading to eventual buckling.

The +-45 panels have a reduced life at much smaller loads, because damage accumulates in the matrix as fatigue or stress cracks. The large lateral extension and longitudinal compression of the face sheet as it cycles, induces matrix cracking.

To attain a 100,000 cycle life for a 0/90 panel damaged by a threshold impact of 1.1 ft-lbs., the load amplitude must be 50% or less of the buckling load. The 0/90 orientation demonstrates its inability to transfer loads around damage by not lasting more than 210 cycles at 50% O critical, with a damage diameter of 15mm.

Threshold impacts of 1.1 ft-lbs on +-45 face sheet specimens are tolerated well with almost half a million cycles at 69% and 211,320 cycles at 73% of the critical buckling load. These loads are approximately the same as those carried by the 0/90 columns at 47%. Therefore, because of the +-45 panel's ability to transfer load around ruptured fibers, it can carry moderate loads longer than the 0/90 panels with damage.

Three series of fatigue specimen photographs are provided in Appendix A. Figure A.15 illustrates the growth of a dimple in Specimen # 166 (0/90), maximum load amplitude

2878 lbs (R=.1). The 40mm dimple in the last photograph was measured just before failure. Figure A.16 depicts a +-45 specimen (# 156) at fracture. Figure A.17 is an extended series of photographs and dimple length measurements for Specimen # 164, a 0/90 face sheet. This failure mode was unique in that it propagated in only one direction and then continued to carry the load with one face fractured.

CHAPTER SEVEN

CONCLUSIONS AND RECOMMENDATIONS

7.1 CONCLUSIONS

This investigation accomplished its goals of determining impact damage dimensions, residual strength under a bending moment and failure modes. The effect of panel parameters on damage resistance and damage tolerance was explored. A preliminary investigation of panel longevity identified panel limitations and areas for expanded research.

Test results and experimental observations support the following conclusions about minimum gauge face sheet sandwich panels constructed from graphite/epoxy plain weave fabric and Nomex honeycomb cores of various thickness:

- Increased face sheet thickness increases damage resistance for both the face sheet and core.

- A reduction in core thickness leads to more impact damage resistant due to greater bending flexibility.

- Impact force amplitude increases with increased face sheet thickness because of its inherent plate bending stiffness.

- The +-45 face sheet has some damage tolerance for quasi-static loading because it can transfer loads around a damaged area. Failure loads depend on matrix strength.

- The 0/90 face sheet has limited damage tolerance for quasi-static loading because it cannot transfer loads around

a damaged area.

- The Nomex core was the failing component for most 4 ply panels and undamaged two-ply face sheet panels not reinforced with an aluminum core.

- The Mar-Lin relation provides a good approximation of residual strength for a given damage cross section ratio.

- Face sheet dimple indentation length is a function of load and existing laminate and core damage.

- To attain a 100,000 cycle life for a 0/90 panel damaged by a threshold impact of 1.1 ft-lbs, the load amplitude must be less than 50% of the buckling load.

- The ability of +-45 face sheets to transfer loads around damaged areas allows cyclic compression loads of 60% critical, to reach half a million cycles.

- Face sheet dimple growth can be observed in the 0/90 laminate at cyclic compression loads greater than 50% critical and in +-45 laminates at cyclic compression loads greater than 60% critical.

- The undamaged 0/90 panel has a fatigue life of 669,000 cycles at 90 to 95% critical load.

7.2 RECOMMENDATIONS

The growth of damage in a minimum gauge face sheet sandwich panel made from AW193PW/3501-6 under static and fatigue loading, merits further investigation. Areas that need further exploration include:

- Properties of panels with different layups and loading

orientations.

- Strength properties of other core materials.

- Impact effects on panels subjected to in-plane loads and/or bending moments.

- Development of an analytical model which describes dimple formation and propagation to global failure.

- Fatigue life of damaged panels at low loads.

- Fatigue life of damaged panels under compression - compression, tension-tension and compression-tension cyclic loading.

- Damage development within a panel throughout its fatigue life, as measured by reduced stiffnesses, expanded delamination, crack length, crack population, broken filaments and residual strength.

- Damage resistance and tolerance at various stages of panel life.

- Residual strength and fatigue life of panels subjected to high humidity and water ingestion.

- Damage resistance of hybrid panels with buffer strips and/or modified epoxies at various volume fractions and multiple material lamina.

REFERENCES

[1] Oplinger, D.W. and Slepetz, J.M., "Impact Damage Tolerance of Graphite/Epoxy Sandwich Panels", Foreign Object Impact Damage to Composites, ASTM STP 568, American Society for Testing and Materials, 1975, pp. 30-48.

[2] Rhodes, M.D., "Impact Fracture of Composite Sandwich Structures", AIAA Paper No. 75-748, 16th Structures, Structural Dynamics and Materials Conference., Denver, CO, May 1975.

[3] Adsit, N.R. and Waszczak, J.P., "Effect of Near-Visual Damage on the Properties of Graphite/Epoxy,"Composite Materials: Testing and Design (Fifth Conference), ASTM STP 674, pp. 101-117.

[4] Guynn, E.G. and O'Brien, T.K., "The Influence of Lay-Up and Thickness on Composite Impact Damage and Compression Strength", AIAA Paper No. 85-0646

[5] Husman, G.E., Whitney, J.M. and Halpin, J.C., "Residual Strength Characterization of Laminated Composites Subjected to Impact Loading", Foreign Object Impact Damage to Composites, ASTM STP 568, American Society for Testing and Materials, 1975, pp. 92-113

[6] Bernard, M.L., "Impact Resistence and Damage Tolerance of Composite Sandwich Plates", S.M. Thesis, Massachusetts Institute of Technology, May 1987

[7] Lie, S.C., "Damage Resistance and Damage Tolerance of Thin Composite Facesheet Honeycomb Panels", S.M. Thesis, Massachusetts Institute of Technology, March 1989

[8] Ramkumar, R.L., "Effect of Low-Velocity Impact on the Fatigue Behavior of Graphite/Epoxy Laminates", Long-Term Behavior of Composites, ASTM STP 813, T.K. O'Brien, Ed., American Society for Testing Materials, Philadelphia, 1983, pp. 116-135

[9] Camponeschi, E. T. and Stinchcomb, W. W., "Stiffness Reduction as an Indicator of Damage in Graphite/Epoxy Laminates,"Composite Materials: Testing and Design (Sixth Conference), ASTM STP 787, I. M. Daniel, Ed., American Society for Testing and Materials, 1982, pp. 225-246.

[10] Chou, P.C. and Croman, Robert, "Degradation and Sudden-Death Models of Fatigue of Graphite/Epoxy Composites,"Composite Materials: Testing and Design

(Fifth Conference), ASTM STP 674 pp. 431-454.

[11] Reifsnider, K.L., and Duke, J.C., "Long-Term Fatigue Behavior of Composite Materials", Long-Term Behavior of Composites, ASTM STP 813, T.K. O'Brien, Ed., American Society for Testing and Materials, Philadelphia, 1983, pp. 136-159

[12] Jones, R.M., "Mechanics of Composite Materials", Scripta Book Company, Washington, D.C., 1975

[13] Tsai, S.W., Halpin, J.C., and Pagano, N.J. (eds.): "Composite Materials Workshop", Technomic Publishing Co., Wesport, Conn., 1968

[14] Timoshenko, S., "Strength of Materials", D. Van Nostrand Company Inc., New York, N.Y., 1950

[15] Weikel, R.C. and Kobayashi, A.S., "On the Local Elastic Stability of Honeycomb Face Plate Subjected to Uniaxial Compression", J. Aero/Space Sci., 26,10, Oct. 1959, pp. 672-674

[16] Plantema, F.J., "Sandwich Construction", John Wiley & Sons, Inc., New York, N.Y., 1966

[17] Mar, J.W., and Lin, K.Y., "Characterization of Splitting Process in Graphite/Epoxy Composites", Journal of Composite Materials, Vol. 13, October 1979

[18] Federson, C.E., "Evaluation and Prediction of Residual Strength of Center Cracked Tension Panels", Damage Tolerance in Aircraft Structures, ASTM Special Technical Publication 486, 1970

[19] Lie,S.C. and Mar, J.W., "Damage Resistance and Damage Tolerance of Minimum Gauge Honeycomb Structures", TELAC Report 88-10, Dept. of Aero/Astronautics, MIT 1988

[20] Bhatia, N.M., "Strength and Fracture Characteristics of Graphite-Glass Intraply Hybrid Composites, "Composite Materials: Testing and Design (Sixth Conference), ASTM STP 787, I. M. Daniel, Ed., American Society for Testing and Materials, 1982, pp. 183-199.

[21] Williams, J.G. and Rhodes, M.D., "Effect of Resin on Impact Damage Tolerance of Graphite/Epoxy Laminates," Composite Materials: Testing and Design (Sixth Conference), ASTM STP 787, I. M. Daniel, Ed., American Society for Testing and Materials, 1982, pp. 450-480.

APPENDIX A: EXPERIMENTAL RESULTS; TABLES AND FIGURES

This appendix contains experimental results presented in tabular form and photographs.

TABLE A.1

RESIDUAL STRENGTH TEST RESULTS

Spec. #	Impact Vel. [ft/s]	Impact Energy [ft-lb]	Damaged Area [sq in]	d/W	Failure Moment [in-lb]	Failure Stress (far) [Ksi]	Failure Stress (local) [Ksi]
1 Inch Panels; [+-45]							
@ 1	7.35	2.84	0.206	0.174	782	18.56	22.47
2	7.23	2.74	0.304	0.205	951	28.12	35.37
3	6.99	2.57	0.256	0.158	1026	24.22	28.76
@ 4	6.01	1.89	0.242	0.141	857	19.87	23.13
17	5.55	1.61	0.174	0.201	1195	24.65	30.81
6	4.64	1.13	0.155	0.108	1068	25.30	28.42
# 7	*	*	0.223	0.129	1085	25.61	28.75
8	5.20	1.42	0.171	0.173	1111	26.28	31.78
9	4.79	1.21	0.140	0.136	1152	27.04	31.32
@ 10	5.08	1.35	0.155	0.143	1161	25.97	35.24
11	4.85	1.23	0.084	0.101	1120	26.31	29.25
12	4.79	1.21	0.074	0.071	1174	27.48	29.59
13	4.59	1.10	0.076	0.028	1119	25.78	26.52
19	3.61	0.69	0.02	0.014	1121	26.04	*
@ 14	0	0	0	0	1144	26.96	
@ 15	0	0	0	0	1163	27.30	
@ 16	0	0	0	0	1217	28.45	
J 36	0	0	0	0	1492	35.37	
37	0	0	0	0	1566	36.64	
38	0	0	0	0	1618	37.72	
39	0	0	0	0	1459	34.15	

* denotes lost data
@ buckling under loading point
# core crushed
J fracture over or adjacent to Nomex/aluminum joint

TABLE A.1 (cont.)

RESIDUAL STRENGTH TEST RESULTS

Spec. #	Net Strain to Failure				
	Gage 1	Gage 2	Gage 3	Gage 4	Gage 5
1 Inch Panels; [+-45]					
1		0.0051	-0.0076	0.00513	-0.00728
2	-0.01215	0.0133	-0.0083	0.00663	-0.00852
3	-0.01123	0.00781	-0.00826	0.00654	-0.00924
4	-0.00728	0.00571	-0.00644	0.00512	-0.00715
17	-0.01686	0.01208	-0.01084	*	-0.01056
6	-0.01407	0.01137	-0.01107	0.01027	-0.01348
7	-0.01185	0.01029	-0.01017	0.00904	-0.01221
8	-0.01084	0.01051	-0.01028	0.00966	-0.01232
9	-0.01252	0.00994	-0.01106	0.00851	-0.01181
10	-0.01369	0.01162	-0.01293	0.01011	-0.01289
11	-0.01231		-0.01018		
12	-0.01234	0.01078	-0.01092	0.00876	-0.01141
13	-0.01459		-0.00968		
19	*	0.010	-0.01101	*	-0.00872
14	-0.01471	0.01221			
15	-0.01508	0.01291			
16	-0.01656	0.01412			
36	-0.02466	0.02164			
37	-0.02525	0.02093	-0.01447	0.01297	
38	-0.02391	0.01987			
39	-0.02194	0.01641	-0.01442	0.01091	

TABLE A.2

RESIDUAL STRENGTH TEST RESULTS

Spec. #	Impact Vel. [ft/s]	Impact Energy [ft-lb]	Damaged Area [sq in]	d/W	Failure Moment [in-lb]	Failure Stress (far) [Ksi]	Failure Stress (local) [Ksi]
1 Inch Panels; [0/90]							
42	5.88	1.81	0.155	0.172	920.01	21.51	25.98
51	6.06	1.93	0.261	0.185	930.95	21.67	26.59
52	6.25	2.05	0.279	0.201	993.73	23.17	28.97
53	6.45	2.19	0.316	0.185	898.47	20.91	25.65
54	6.45	2.19	0.322	0.178	803.01	18.76	22.84
65	5.47	1.57	0.192	0.186	994.01	23.09	28.36
48	5.11	1.37	0.155	0.144	1067.34	25.14	29.37
49	5.11	1.37	0.205	0.128	1037.03	24.12	27.66
50	5.39	1.53	0.205	0.157	1047.86	24.41	28.95
64	4.42	1.03	0.105	0.071	1152	26.98	29.04
41	4.23	.94	0.074	0.101	1334	31.16	34.59
43 @	3.75	0.74	0.074	0.036	1418.07	33.03	34.27
44	4.42	1.03	0.078	0.135	1513.33	35.24	40.74
45 #	3.98	0.83	0.099	0.007	1026.21	24.95	25.12
46	4.47	1.05	0.155	0.085	1140.95	26.81	29.29
60	0	0	0	0	2613.15	61.25	
61	0	0	0	0	2305.72	55.45	
62	0	0	0	0	3056.98	71.53	
63	0	0	0	0	2940.07	69.32	

@ buckling under loading point
# core crushed

TABLE A.2 (cont.)

RESIDUAL STRENGTH TEST RESULTS

Spec. #	Net Strain to Failure				
	Gage 1	Gage 2	Gage 3	Gage 4	Gage 5
1 Inch Panels; [0/90]					
42	-0.00280	.00012	-0.002461		-0.00104
51	-0.00272	.00012	-0.001881	-.00002	-0.001101
52	-0.00334	.00016	-0.002961	.00014	-0.001321
53	-0.00260	.00006	-0.002501	.00008	-0.001261
54	-0.00238	.00012	-0.002421	.000120	
55	-0.00302	.00012	-0.00251		-0.00134
48	-0.00328	.00004	-0.003161	-.00004	-0.001501
49	-0.00328	.00006	-0.002641	.00010	-0.001461
50	-0.00272	.00016	-0.002801	.00008	-0.001401
64	-0.00316	.00014	-0.00268		
41	-0.00718	.00006	-0.00364	*	*
43	-0.00400	.00048	-0.003241	.00070	-0.002581
44	-0.00316	.00063	-0.003501	.00035	-0.002121
45	-0.00236	.00030	-0.002421		-0.002201
46	-0.00358		-0.003161		
60	-0.00711	.00082	-0.007061	.000770	
61	-0.00639	.000334			
62	-0.00845	.000485			
63	-0.00760	.00078	-0.00738	.00014	

TABLE A.3

RESIDUAL STRENGTH TEST RESULTS

Spec. #		Impact Vel. [ft/s]	Impact Energy [ft-lb]	Damaged Area [sq in]	d/W	Failure Moment [in-lb]	Failure Stress (far) [Ksi]	Failure Stress (local) [Ksi]
.687 Inch Panels; [+-45]								
121		5.88	1.81	0.354	0.114	730.01	23.99	27.08
122	@	5.97	1.87	0.381	0.156	689.01	23.28	27.58
123		5.88	1.81	0.282	0.086	667.01	22.56	24.68
113	@	4.42	1.03	0.078	0.014	719.01	24.35	24.69
114		4.52	1.07	0.084	0.014	751.01	25.42	25.78
115		4.63	1.13	0.144	0.028	773.01	26.14	26.89
116		4.63	1.13	0.21	0.014	697.01	21.13	21.43
117	D	0	0	0	0	686.00	25.65	
118		0	0	0	0	1026.00	38.63	
119		0	0	0	0	1005.00	37.81	
120	J	0	0	0	0	983.00	33.31	

* denotes lost data
@ buckling under loading point
D face sheet debonding failure
J fracture over or adjacent to Nomex/aluminum joint

TABLE A.3 (cont.)

RESIDUAL STRENGTH TEST RESULTS

Specimen Number	Net Strain to Failure				
	Gage 1	Gage 2	Gage 3	Gage 4	Gage 5
.687 Inch Panels; [+-45]					
121	-0.011131	.009460	-0.011131		-0.011641
122	-0.012081	.009320	-0.009101	.008080	-0.010421
123	-0.012961	.011180	-0.009401	.007880	-0.010361
113	-0.010861	.008720	-0.009261	.008160	-0.010241
114	-0.011661	.010800	-0.011071	.008780	-0.011461
115	-0.014101	.010900	-0.010741	.008140	-0.001131
116	-0.011141	.008600	-0.008981	.007920	-0.011141
117	-0.012541	.007500			
118					
119	-0.003381	.027961			
120	-0.022781	0.020901	-0.015621	0.017001	

TABLE A.4

RESIDUAL STRENGTH IMPACT RESULTS

Spec. #	Impact Vel. [ft/s]	Impact Energy [ft-lb]	Damaged Area [sq in]	d/W	Failure Moment [in-lb]	Failure Stress (far) [Ksi]	Failure Stress (local) [Ksi]
.687 Inch Panels; [0/90]							
108	6.45	2.18	0.194	0.171	920.01	31.16	37.59
109	6.45	2.19	0.341	0.171	868.01	29.41	35.46
110	6.25	2.05	0.256	0.179	983.01	33.28	40.54
105	4.33	0.98	0.124	0.071	1258.01	42.59	45.85
106	4.28	0.96	0.135	0.064	953.01	32.25	34.46
107	4.19	0.92	0.099	0.086	1059.01	37.85	39.22
111	3.98	0.83	0.062	0.043	1024.01	37.74	36.31
112	5.69	1.71	0.062	0.029	1068.01	36.17	37.25
126	0	0	0	0	1555.00	56.82	
127	0	0	0	0	1724.00	63.54	
128	0	0	0	0	1459.00	55.24	
129	0	0	0	0	1492.00	56.83	
101 @	0	0	0	0	1195	40.47	
102 @	0	0	0	0	1228	41.54	

@ buckling under loading point

TABLE A.4 (cont.)

RESIDUAL STRENGTH TEST RESULTS

Specimen Number	Net Strain to Failure				
	Gage 1	Gage 2	Gage 3	Gage 4	Gage 5
.687 Inch Panels; [0/90]					
108	-0.003351	.000050	-0.003281	.000100	-0.001401
109	-0.005231	.000090	-0.002871	.000080	-0.001021
110	-0.003701	.000100	-0.003331	.000100	-0.001791
105	-0.004811	.000560	-0.003661	.000110	-0.002461
106	-0.004101	.000300	-0.003681	.000780	-0.002001
107	-0.004321	.000480	-0.004321	.000280	-0.002361
111	-0.004741	.000600	-0.003781		-0.002101
112	-0.004421	.000680	-0.004281		-0.002841
126	-0.011131	.000340			
127	-0.005241	.000660			
128	-0.006451	.001020			
129	-0.006641	.000580	-0.005841	-0.00146	
101	-0.00472	.000600			
102	-0.00456	.000440			

TABLE A.5

RESIDUAL STRENGTH TEST RESULTS

Spec #	Impact Vel. [ft/s]	Impact Energy [ft-lb]	Damaged Area [sq in]	d/W	Failure Moment [in-lb]	Failure Stress (far) [Ksi]	Failure Stress (local) [Ksi]
.375 Inch Panels; [+-45]							
223	5.97	1.87	0.328	0.115	327.01	20.01	22.61
239	5.97	1.87	0.223	0.014	349.01	21.35	21.65
240	5.88	1.81	0.308	0.028	338.00	20.70	21.30
241	6.06	1.93	0.236	0.058	349.00	21.35	22.67
237	4.58	1.11	0.007	0.007	403.00	24.59	24.76
238	4.63	1.13	0.033	0.014	392.00	23.94	24.28
221	3.91	0.81	0.013	0.014	not tested		
234	4.14	0.91	0	0.007	370.00	23.06	23.22
235	4.14	0.91	0.007	0.007	381.00	23.70	23.87
236	4.14	0.91	0	0.007	381.00	24.34	24.51
230 $	0	0	0	0	925.00	56.04	
231 $	0	0	0	0	814.00	49.96	
233 $	0	0	0	0	647.00	39.59	

$ discontinued without failure

TABLE A.5 (cont.)

RESIDUAL STRENGTH TEST RESULTS

Spec. #	Net Strain to failure				
	Gage 1	Gage 2	Gage 3	Gage 4	Gage 5
.375 Inch Panels; [+-45]					
223	-0.003021	.000200	-0.005521	.000100	
239	-0.009261	.006681	-0.008281	.006901	-0.009001
240	-0.008601		-0.007481		
241	-0.009231		-0.007731		
237	-0.012841	.009380	-0.009961	.008040	-0.011141
238	-0.009301		-0.008581		
221					
234					
235					
236					
230	-0.023861	.016900			
231	-0.02112	.015920			
233	-0.018741	.014020		.012770	-0.014541

TABLE A.6

RESIDUAL STRENGTH TEST RESULTS

Spec. #	Impact Vel. [ft/s]	Impact Energy [ft-lb]	Damaged Area [sq in]	d/W	Failure Moment [in-lbs]	Failure Stress (far) [Ksi]	Failure Stress (local) [Ksi]
.375 Inch Panels; [0/90]							
212	6.06	1.93	0.174	0.143	667.01	19.63	
217	6.06	1.05	0.181	0.157	518.01	31.71	37.61
218	6.15	1.99	0.186	0.143	466.01	29.76	34.73
219	6.15	1.99	0.131	0.143	444.01	27.82	32.46
209	5.54	1.61	0.155	0.065	487.01	29.46	31.51
210	4.86	1.24	0.087	0.036	624.01	37.79	39.21
211	539	1.53	0.155	0.114	645.01	39.07	44.09
204	4.33	0.98	0.013	0.014	528.01	32.02	32.48
205	4.23	0.94	0.039	0.014	528.01	32.02	32.48
206	4.1	0.88	0.074	0.014	539.00	32.66	33.13
207	4.19	0.92	0.031	0.036	528.00	32.02	33.22
208	4.32	0.98	0.056	0.05	498.01	30.1	31.68
225 J	0	0	0	0	1100.00	67.28	
226 J	0	0	0	0	1068.00	65.29	
227	0	0	0	0	1152.00	70.46	
228	0	0	0	0	1068.00	62.76	
202 @	0	0	0	0	589	36.03	
203 ^	0	0	0	0	814	39.63	

@ buckling under loading point
^ core shear and buckling failure
J fracture over or adjacent to Nomex/aluminum joint

TABLE A.6 (cont.)

RESIDUAL STRENGTH TEST RESULTS

Spec. #	Net Strain to Failure				
	Gage 1	Gage 2	Gage 3	Gage 4	Gage 5
.375 Inch Panels; [0/90]					
212	-0.002021	.000141			
217	-0.004341		-0.003361		
218	-0.004281		-0.003441		
219	-0.005101		-0.003621		
209	-0.003861	.000100	-0.003461	.000120	-0.001761
210	-0.004591	.000650	-0.003871	.000100	-0.002211
211	-0.004971	.000110	-0.004361	.000090	-0.001731
204	-0.007321	.000600	-0.003761	.000260	-0.002521
205	-0.004001	-.003660			
206	-0.004261		-0.004381		
207	-0.004321		-0.003761		
208	-0.00398	.000040	-0.003601	.00012	-0.00206
225	-0.007621	.000680			
226	-0.006961	.000440			
227	-0.007861	.000880			
228	-0.006741	.000580	-0.007041	.000320	
202	-0.00437	.000320	-0.00398	.000420	
203	-0.00449	.000380	-0.00452	.00038	

TABLE A.7

RESIDUAL STRENGTH TEST RESULTS

Spec. #	Impact Velocity [ft/s]	Impact Energy [ft-lb]	Damaged Area [sq in]	d/W	Failure Moment [in-lb]	Failure Stress (far) [Ksi]	Failure Stress (local) [Ksi]
1 Inch Panels; [+-45]s							
308 D	8.03	3.39	0.611	0.127	994.00	23.00	26.38
309 D	7.57	3.01	0.243	0.086	1487.00	34.93	38.22
310 D	7.87	3.26	0.394	0.086	1451.00	34.05	37.25
305 ^	7.03	2.59	0.184	0.028	1555.00	35.97	37.58
306 #	8.56	3.85	0.617	0.185	1661.00	38.42	47.85
312 D	6.79	2.42	0.025	0.014	*	*	*
301	6.35	2.12	0.197	0.014	1533.00	35.48	36.51
302 ^	6.35	2.12	0.164	0.014	1924.00	45.12	45.83
303 #	6.25	2.05	0.171	0.014	1901.00	44.62	45.25
311 ^	6.06	1.93	0.056	0.014	1152.01	26.97	27.32

* denotes lost data
D face sheet debonding failure
^ core shear and buckling failure
# core crushed

TABLE A.7 (cont.)

RESIDUAL STRENGTH TEST RESULTS

Spec. #	Net Strain to Failure				
	Gage 1	Gage 2	Gage 3	Gage 4	Gage 5
1 Inch Panels; [+-45]s					
308	-0.004221		-0.003501	.002970	-0.003461
309	-0.006501				
310	-0.006601	.005300			
305	-0.007341	.005940	-0.007041	.005341	-0.006901
306	-0.008601		-0.007561		
312					
301	-0.008001	.006010	-0.007141	.005400	-0.007401
302	-0.011701	.009670		.011771	-0.017341
303	-0.011621	.009930		.009610	-0.012641
311					

TABLE A.8

RESIDUAL STRENGTH TEST RESULTS

Spec. #	Impact Velocity [ft/s]	Impact Energy [ft-lb]	Damaged Area [sq in]	d/W	Failure Moment [in-lb]	Failure Stress (far) [Ksi]	Failure Stress (local) [Ksi]
1 Inch Panels; [0/90]s							
321 #	7.57	3.01	0.433	0.086	1745.00	40.98	44.84
322	7.72	3.13	0.459	0.086	2137.00	50.20	54.92
323	7.72	3.13	0.441	0.086	1763.00	38.75	43.79
319 ^	6.67	2.34	0.322	0.043	1903.00	44.71	46.72
316 ^	5.97	1.87	0.086	0.014	1893.00	45.87	47.48
317 ^	6.06	1.93	0.046	0.014	2063.00	47.72	49.64
318 ^	6.06	1.93	0.221	0.014	2262.00	53.11	54.24

^ core shear and buckling failure
# core crushed

TABLE A.8 (cont.)

RESIDUAL STRENGTH TEST RESULTS

Spec. #	Net Strain to Failure				
	Gage 1	Gage 2	Gage 3	Gage 4	Gage 5
1 Inch Panels; [0/90]s					
321	-0.002661	.000181	-0.002401	.000221	-0.001421
322	-0.002981	.000180			
323	-0.003001	.000180	-0.0055	.000100	
319	-0.00238	.000060	-0.00211	.000060	-0.00182
316	-0.002241	.000140	-0.002181	.000100	-0.002241
317	-0.002741	.000120			
318	-0.002081	.000160		.000740	-0.002741

TABLE A.9

SPECIMEN SECTION RESULTS

Specimen Number	Layup	Impact Energy (ft-lb)	Core/Face Debond Dia. (mm)	Core Indent. Depth (mm)	Rupture Dia. d (mm)
29	+-45	2.12	12	3	13
31	+-45	1.10	7	1	4
47	+-90	1.03	10	1.3	8
55	+-90	2.05	14	1.2	12.5
66	+-90	1.11	9.2	1	10.5
220	+-90	1.93	13.1	2.5	12
224	+-45	1.87	7.5	.5	2
242	+-90	1.07	0	0	1
307	+-45	3.26	9	.8	9
321	+-90	3.01	10	.8	6

TABLE A.10

FATIGUE TEST RESULTS

[0/90] Columns:

Spec. Number	Impact Energy [ft-lb]	Damaged Area [sq in]	d/W	Stress Amplitude σ/σ crit (%)	Cycles @Stress Amplitude (N)	Life Cycles (N total)
F1	0	0	0	74	515000*	515000*
167	0	0	0	90	669140?	669140?
160	0	0	0	90 #	904260*	
				95	40770	945030
161	0	0	0	95	69640	69640
166	1.10	.132	.114	59	23830	23830
163	1.16	.109	.121	67	100	100
162	1.13	.155	.121	71	192	192
164	2.51	.279	.161	42	30530(1 face fail)	
					123920*	123920*
260	1.87	.100	.078	50 #	(1 cycle-20mm crack)	
				47	70100	70100
165	2.34	.270	.167	50	210	210
					(1st cycle damage)	

load altered
* discontinued
? doubtful fatigue failure

F1 is 1 inch thick and 2.75 inch wide
260 is .375 inch and 3.54 inch wide

Specimen Series	Core	σ critical (undamaged) (Ksi)
1 - 99	1 in	48.81
101-199	.687 in	45.05
201-299	.375 in	44.86

TABLE A.11

FATIGUE TEST RESULTS

[+-45] Columns:

Spec. Number	Impact Energy [ft-lb]	Damaged Area [sq in]	d/W	Stress Amplitude σ/σ crit (%)	Cycles @Stress Amplitude (N)	Life Cycles (N total)
P2	0	0	0	78	153660	153660
71	0	0	0	78 #	34580*	
				82	5000	39580
150	0	0	0	85	118040	118040
151	0	0	0	90	4720	4720
153	1.01	.124	.089	69 #	472700*	
				73	94600	566330
157	1.13	.147	.144	73	211320	211320
152	.80	.019	.011	78 #	1189990	
				80	671890*	1851880*
72	.83	.050	.086	76	302360	302360
73	.75	.050	.014	80	197050	197050
155	2.26	.295	.194	62 #	883340	
				66	15620	898960
154	2.42	.280	.200	66	88870	88870
156	2.20	.264	.178	70	143590	143590
74	1.53	.149	.278	64 #	1036120*	(No dimple
				78 #	171760*	growth)
				72	6160*	
250	1.82	.143	.167	78	210	210

\# load altered
* discontinued

70 series are 1 inch thick and 3.54 inch wide
P2 is 1 inch thick and 2.75 inch wide
250 is .375 inch thick and 3.54 inch wide

Specimen Series	Core	σ critical (undamaged) (Ksi)
1 - 99	1 in	30.31
101-199	.687 in	29.37
201-299	.375 in	27.76

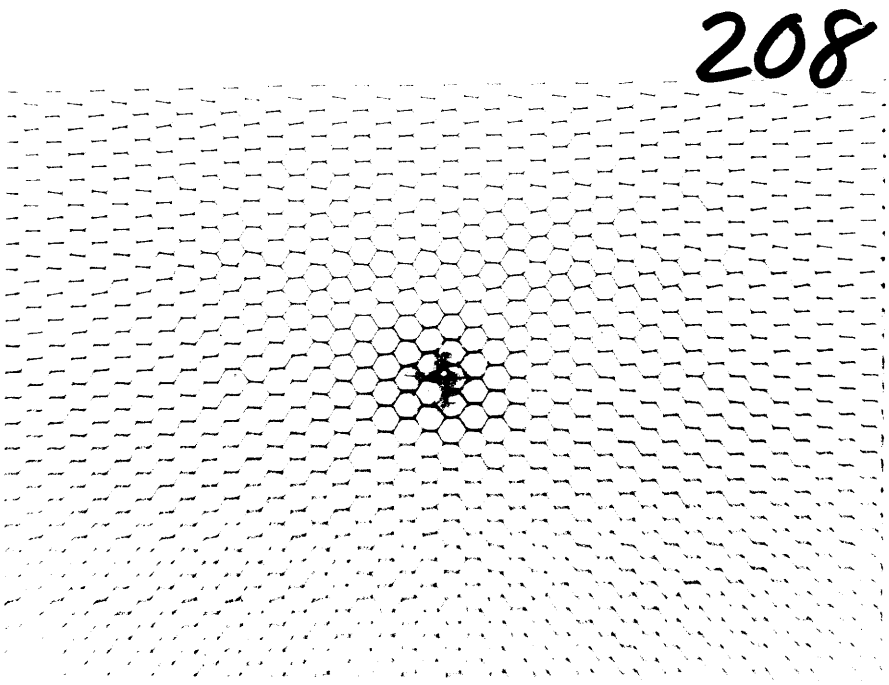

Impact .98 ft-lb Force 145 lb.
d/W = .05 Delam. Area .056 sq. in.

Figure A.1 Specimen 208 - [0/90] .375 Inch Core

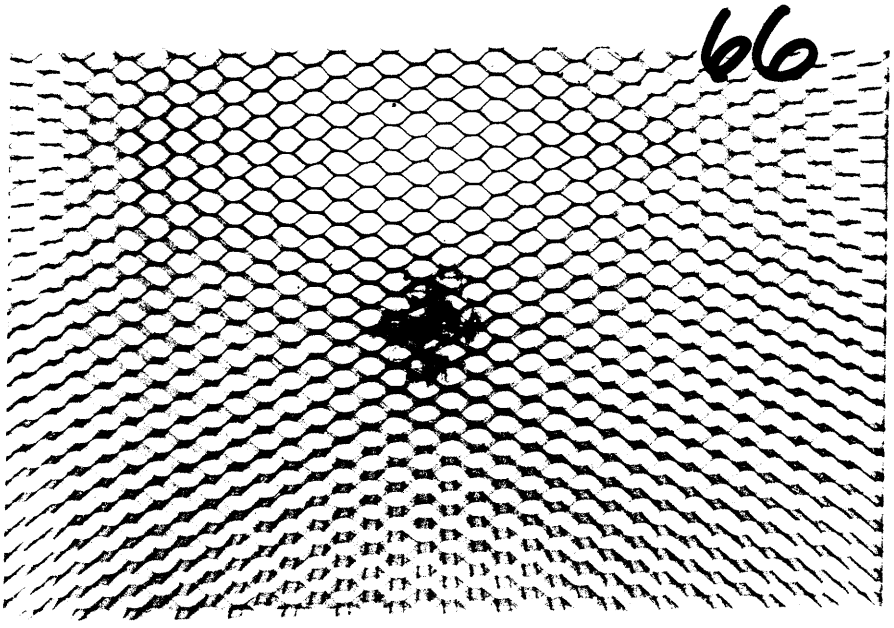

Impact 1.11 ft.-lb. Force 129 lb.
d/W = .150 Delam. Area .205 sq. in.

Figure A.2 Specimen 66 - [0/90] 1 Inch Core

29

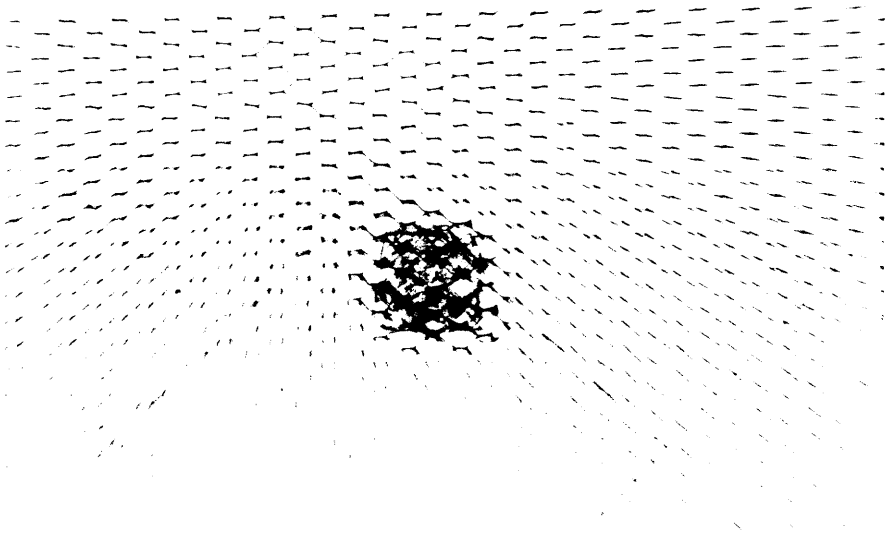

Impact 2.12 ft.-lb.
d/W = .186

Force 131 lb.
Delam. Area .270 sq. in.

Figure A.3 Specimen 29 - [+-45] 1 Inch Core

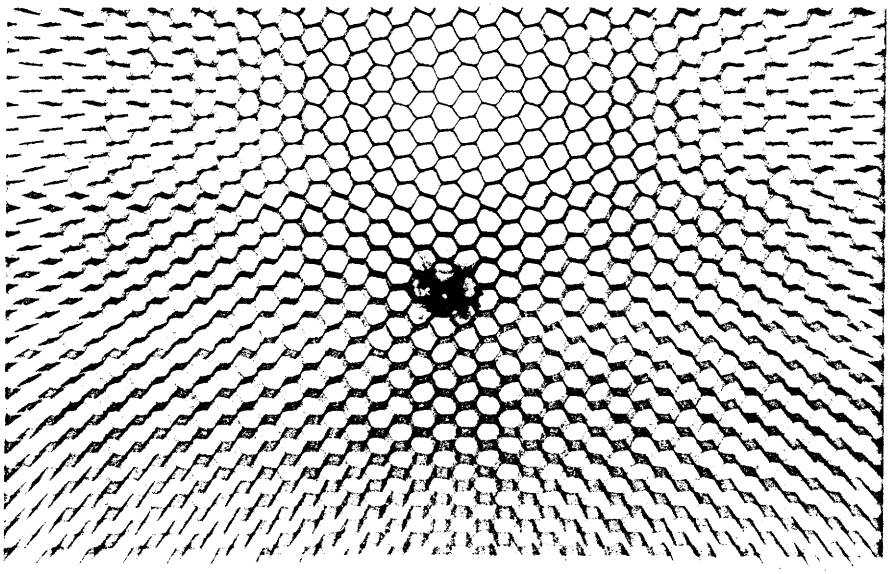

Impact 2.05 ft.-lb.
d/W = .014

Force 259 lb.
Delam. Area .171 sq. in.

Figure A.4 Specimen 303 - [+-45]s 1 Inch Core

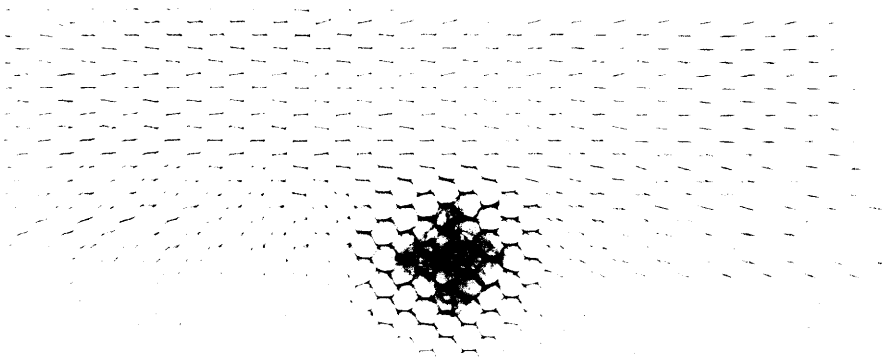

Impact 3.01 ft.-lb.
d/W = .086

Force 305 lb.
Delam. Area .433 sq. in.

Figure A.5 Specimen 321 - [0/90]s 1 Inch Core

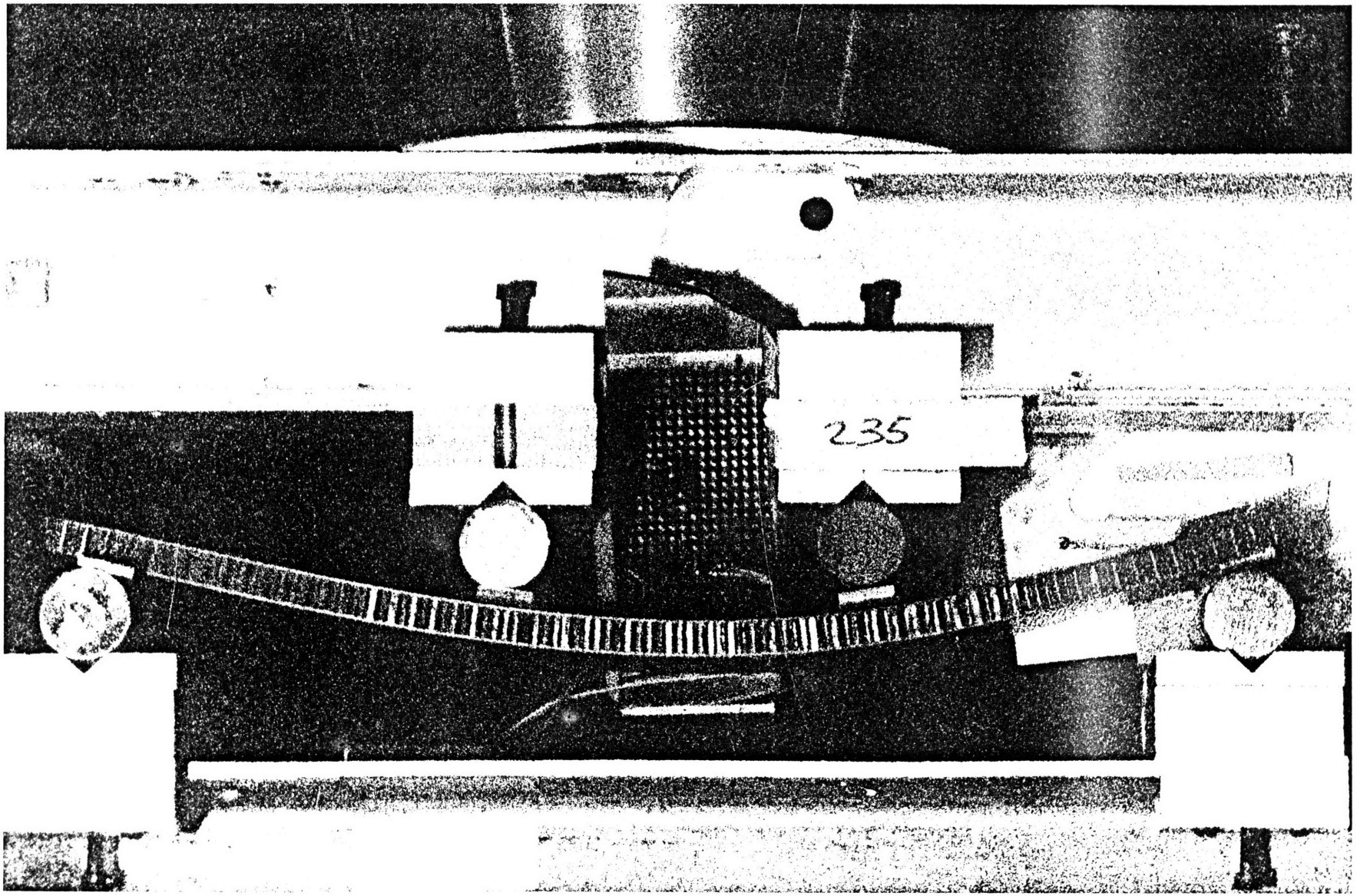

Figure A.6 Specimen # 235, (+-45); Deflected under 150 lbs. Suspended mirror depicts image of dimple indentation. Stress(far field) - 19.67 Ksi

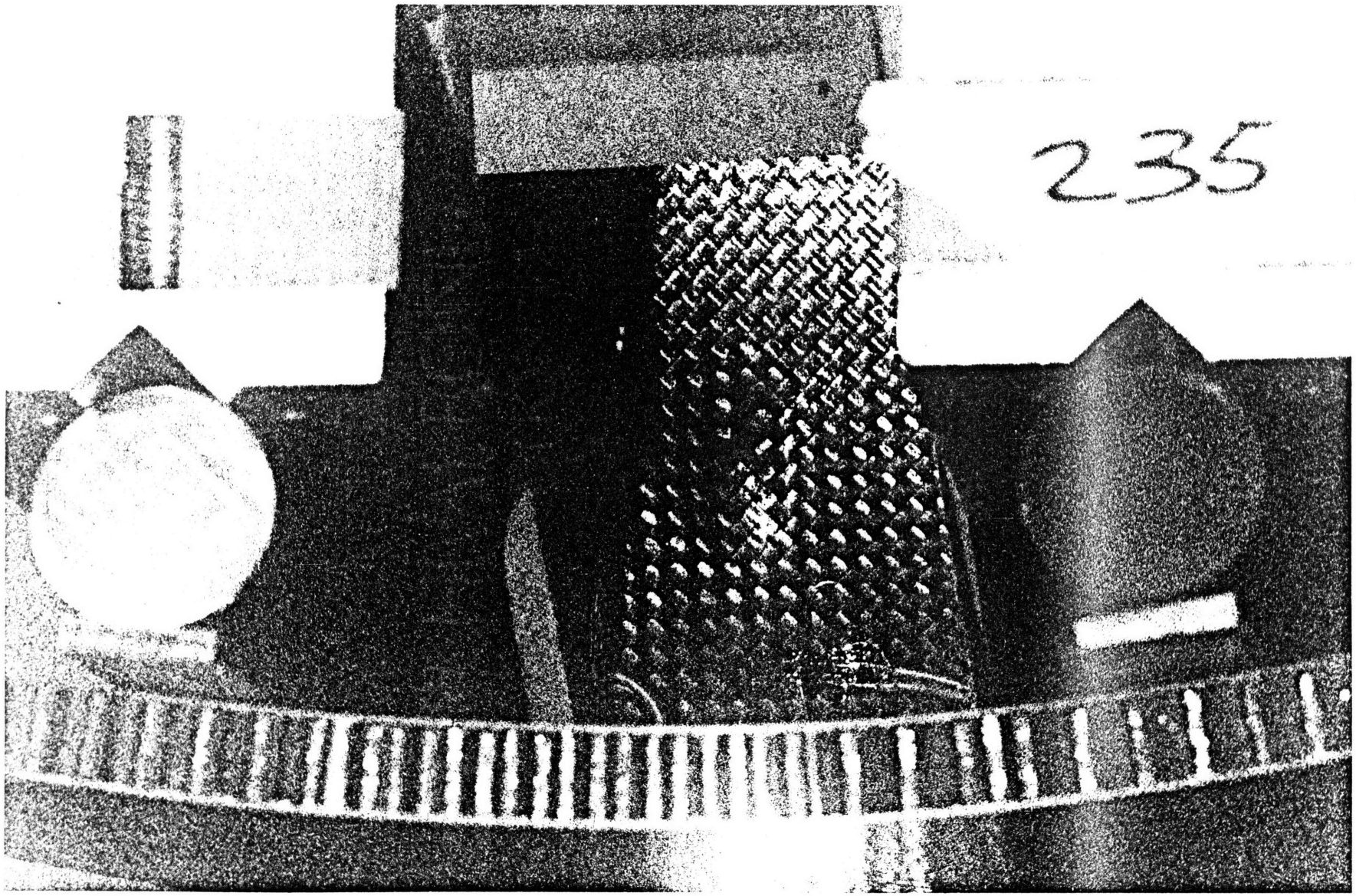

Figure A.7 Specimen # 235; Applied load - 1601bs.; Stress(far field) - 20.98 Ksi.
Dimple length - 7/16 inch

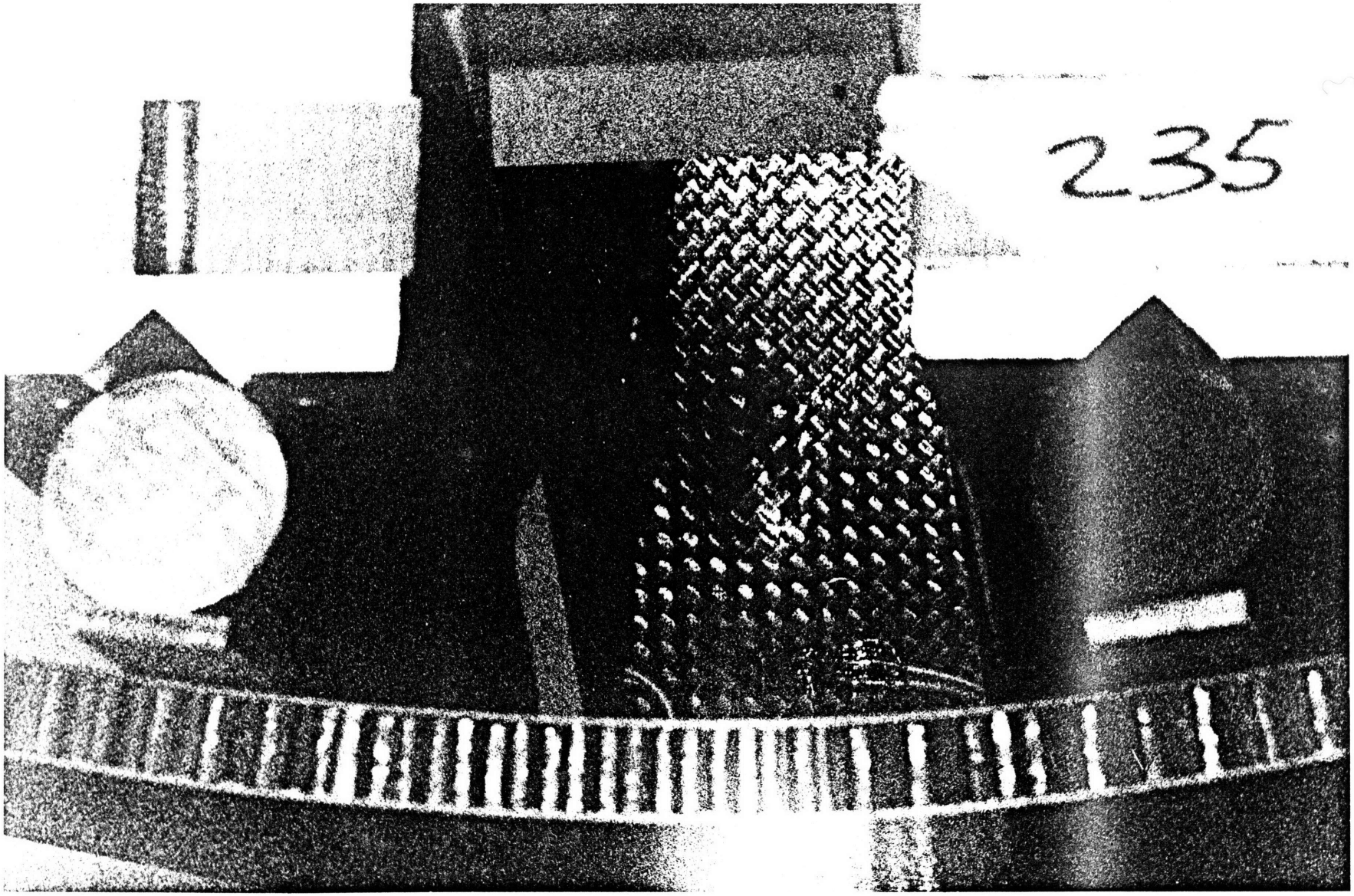

Figure A.8 Specimen # 235; Applied Load - 170 lbs.; Stress(far field) - 22.29 Ksi.
Dimple length - 1/2 inch

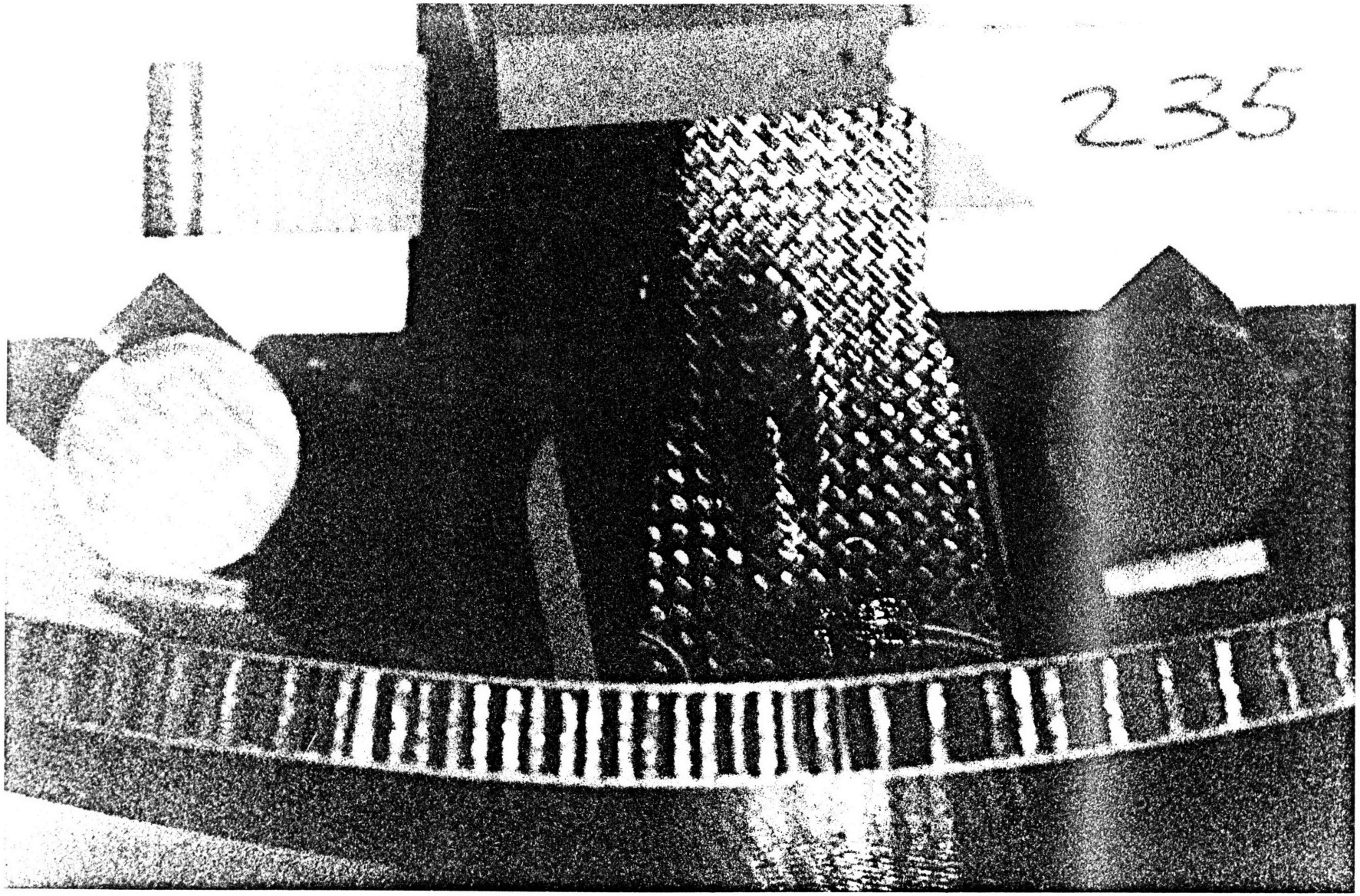

Figure A.9 Specimen # 235; Failure Load - 190 lbs.; Failure Stress - 23.87 Ksi.
Dimple Length - 1 inch

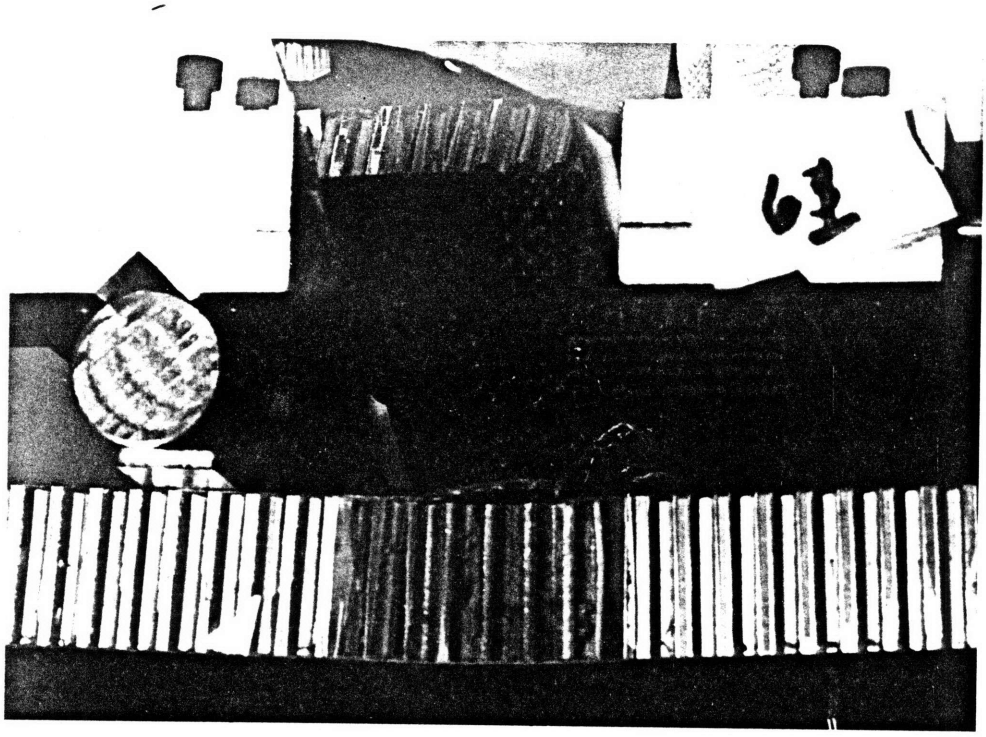

Figure A.10 Specimen # 61, (0/90); undamaged, face sheet fracture and debond
Failed at 55.45 Ksi

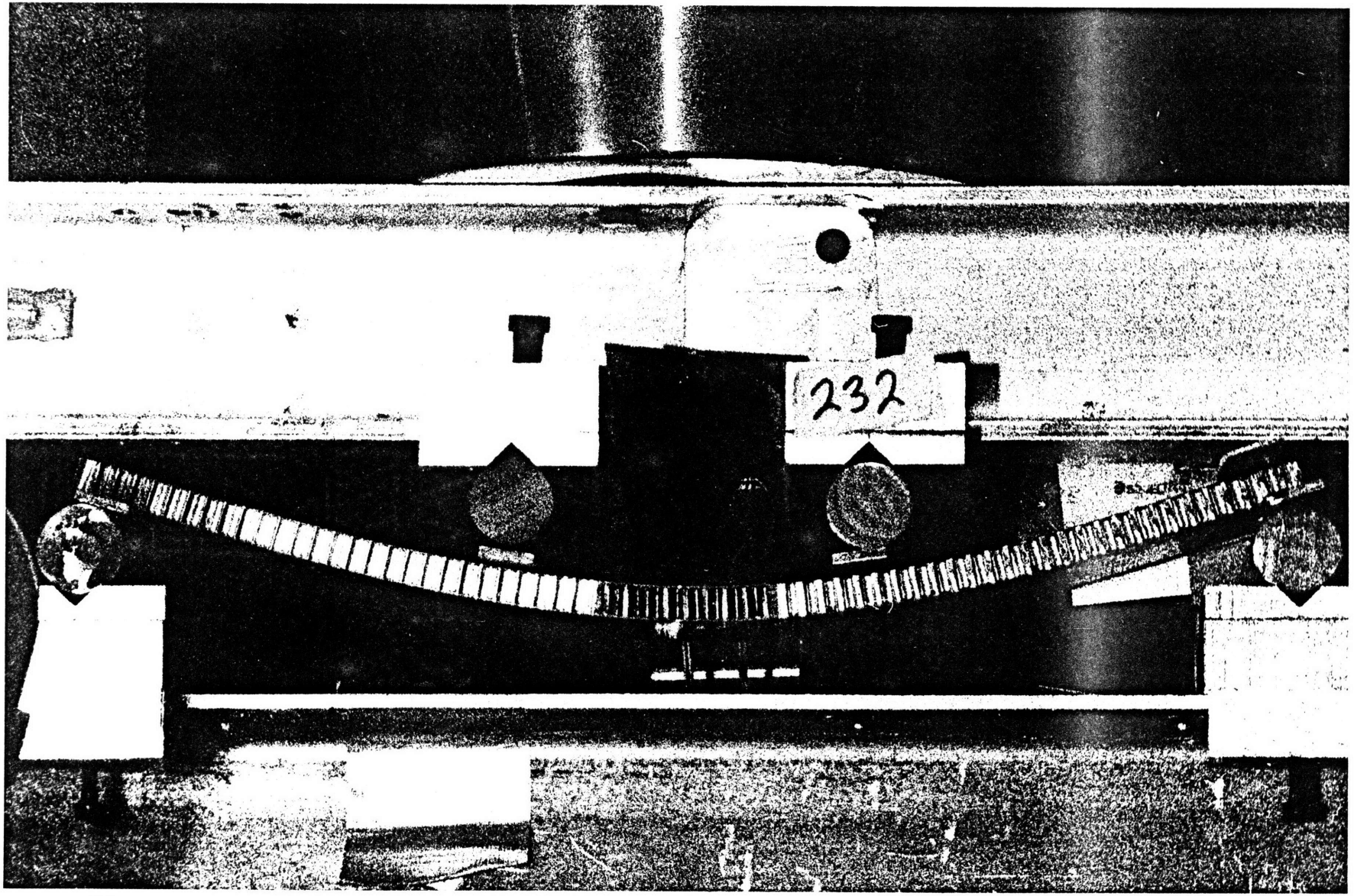

Figure A.11 Specimen # 232, (+-45), reinforced core, undamaged: Specimen impinging on apparatus.

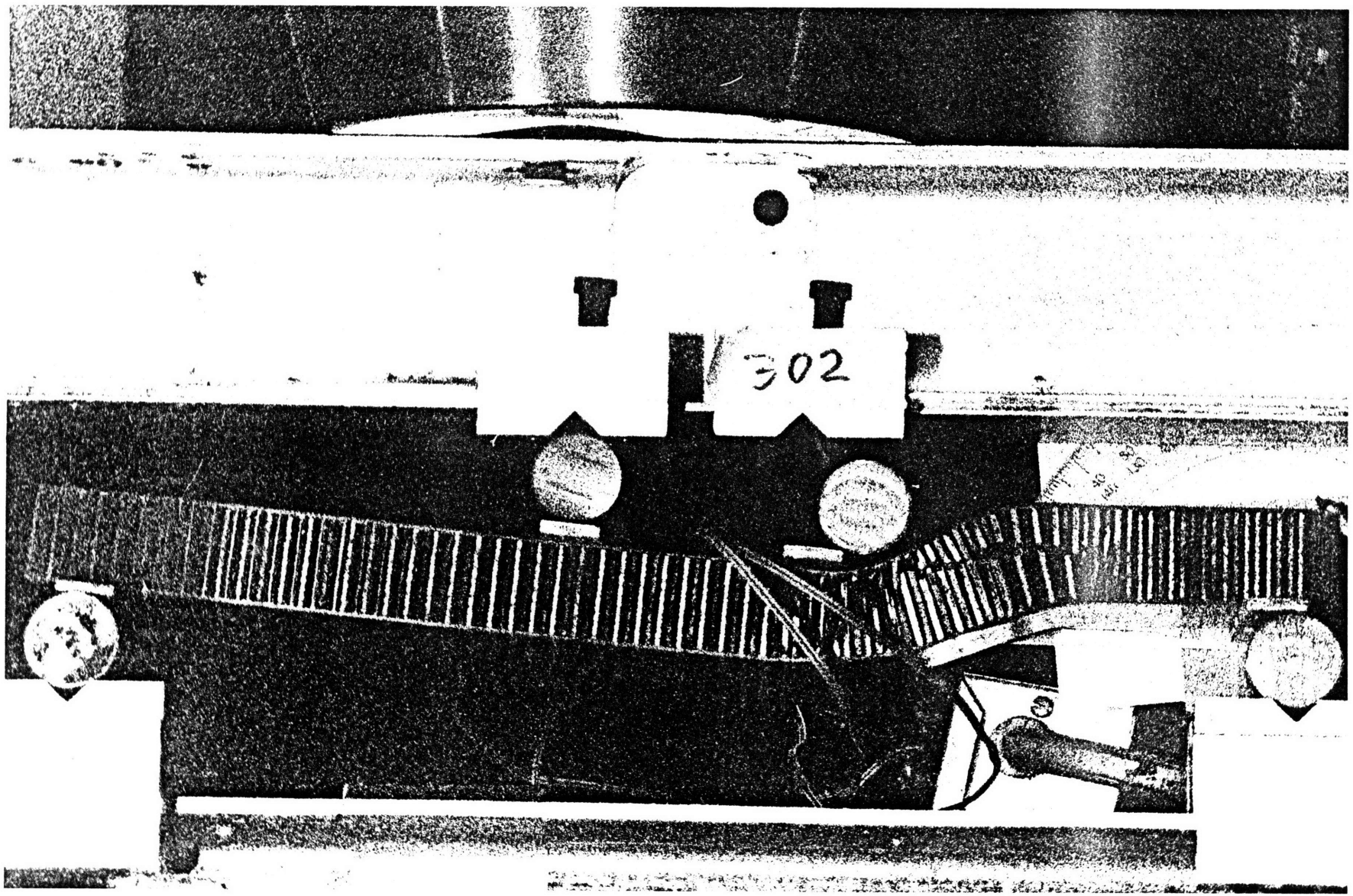

Figure A.12 Specimen # 302, [+-45]s: Core Shearing (rip) Failure.

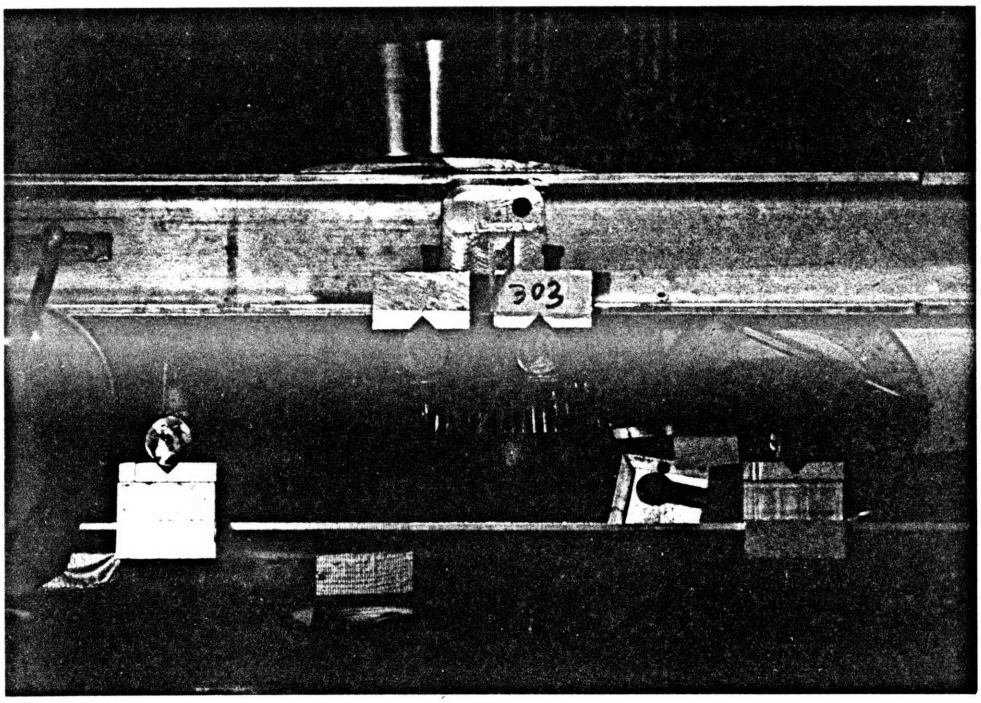

Figure A.13 Specimen #303; Core Crushing

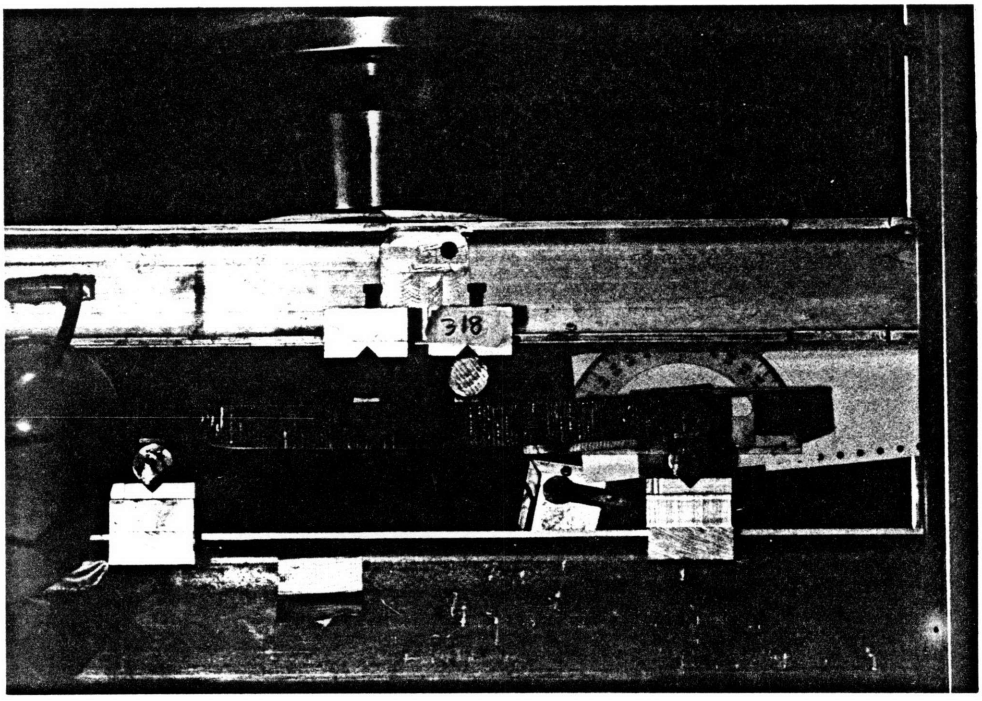

Figure A.14 Specimen #318; Core Shearing

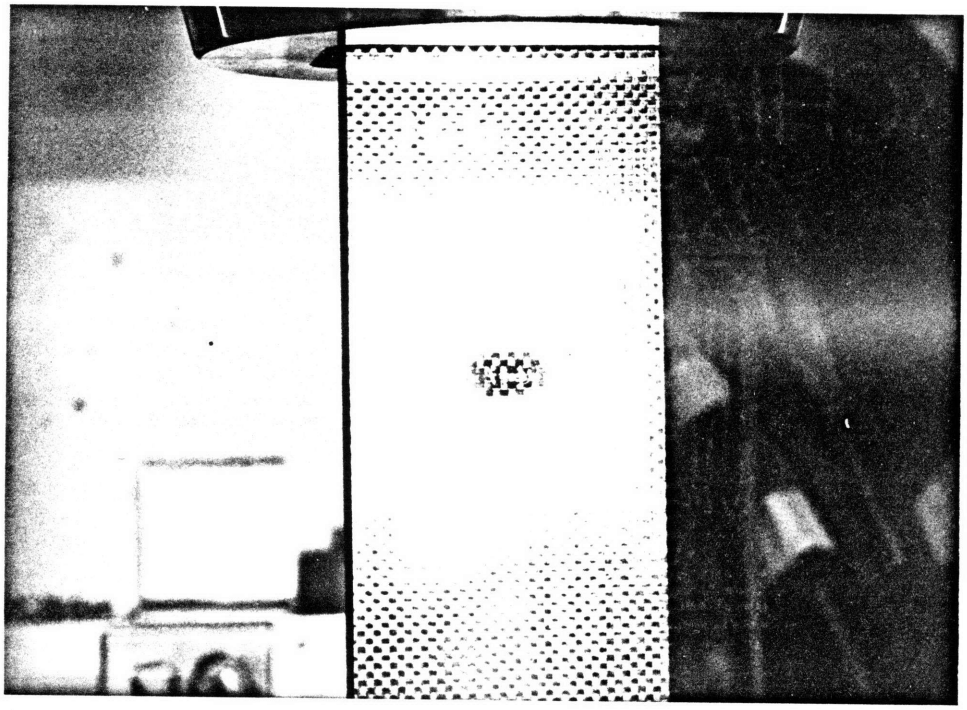

Figure A.15
Specimen #166 (0/90); Damage Growth Over Fatigue Life
N = 220, D = 30 mm, 2878lbs

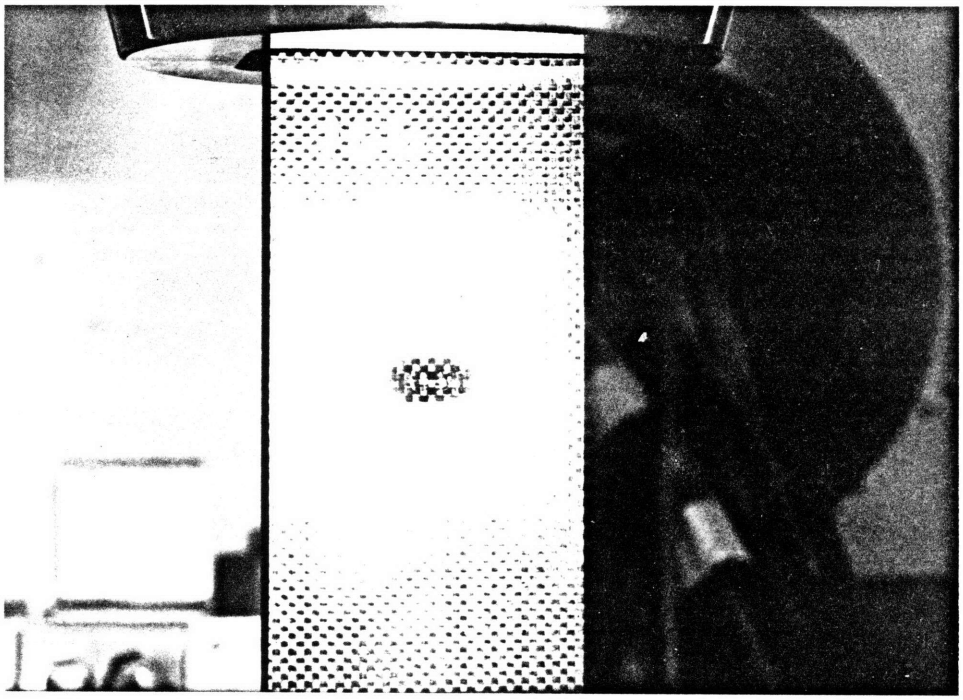

Figure A.15 (cont.)
Specimen #166 (0/90); Damage Growth Over Fatigue Life
N = 3000, D = 32 mm, 2878 lbs

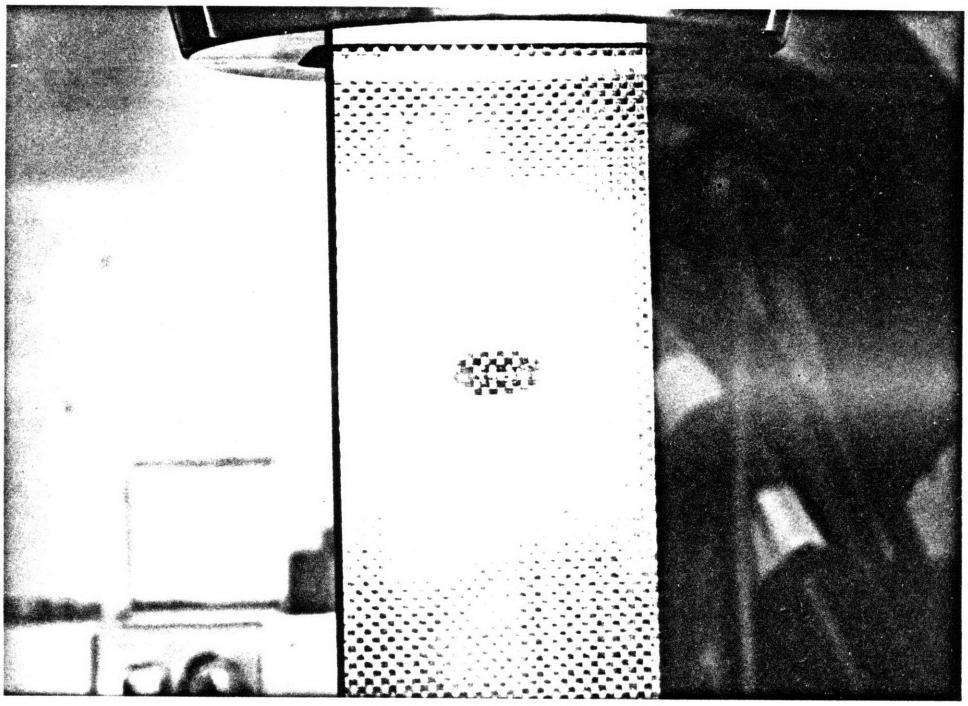

Figure A.15 (cont.)
Specimen #166 (0/90); Damage Growth Over Fatigue Life
N = 5000, D = 33 mm, 28781bs

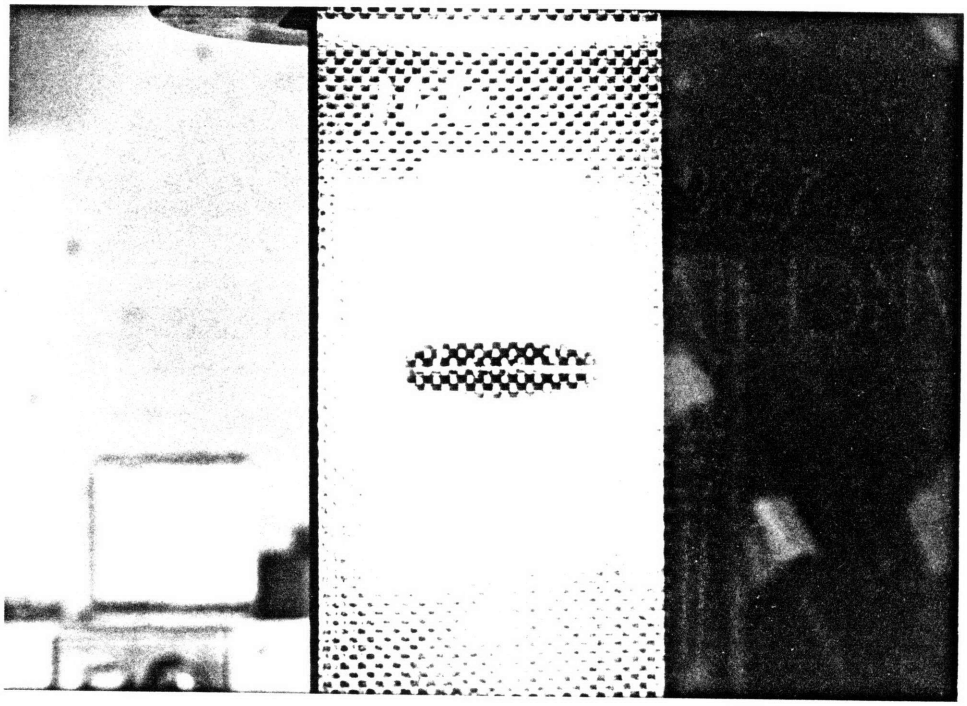

Figure A.15 (cont.)
Specimen #166 (0/90); Damage Growth Fatigue Life
N = 23,830, D = 40 mm, 2878 lbs

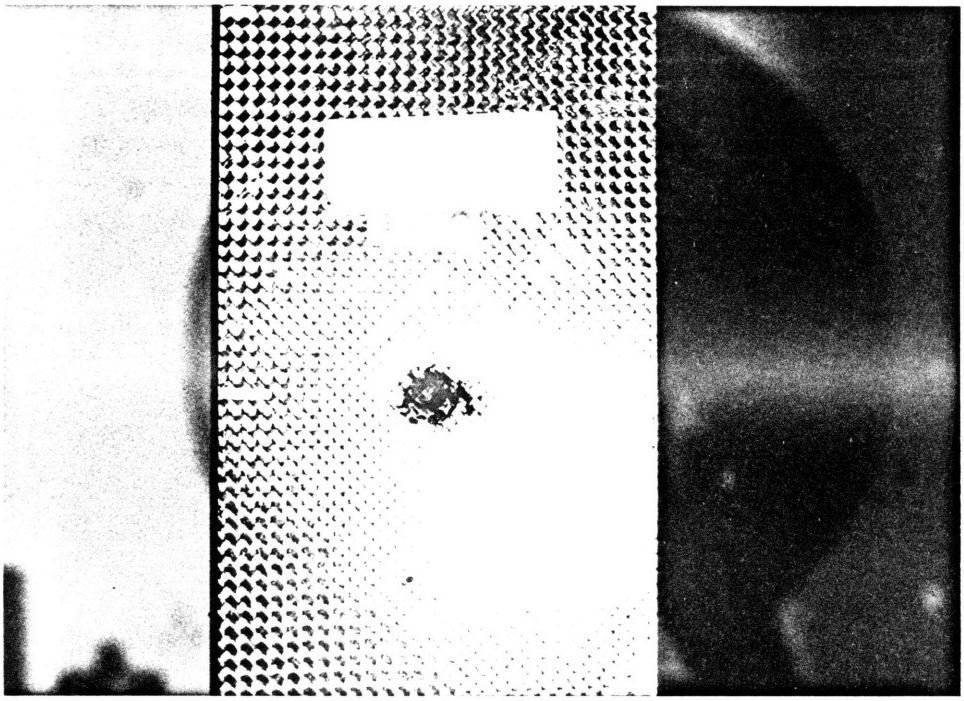

Figure A.16
Specimen #156 (+-45); Damage Growth Over Fatigue Life
N = 120, D = 20 mm, 2210 lbs

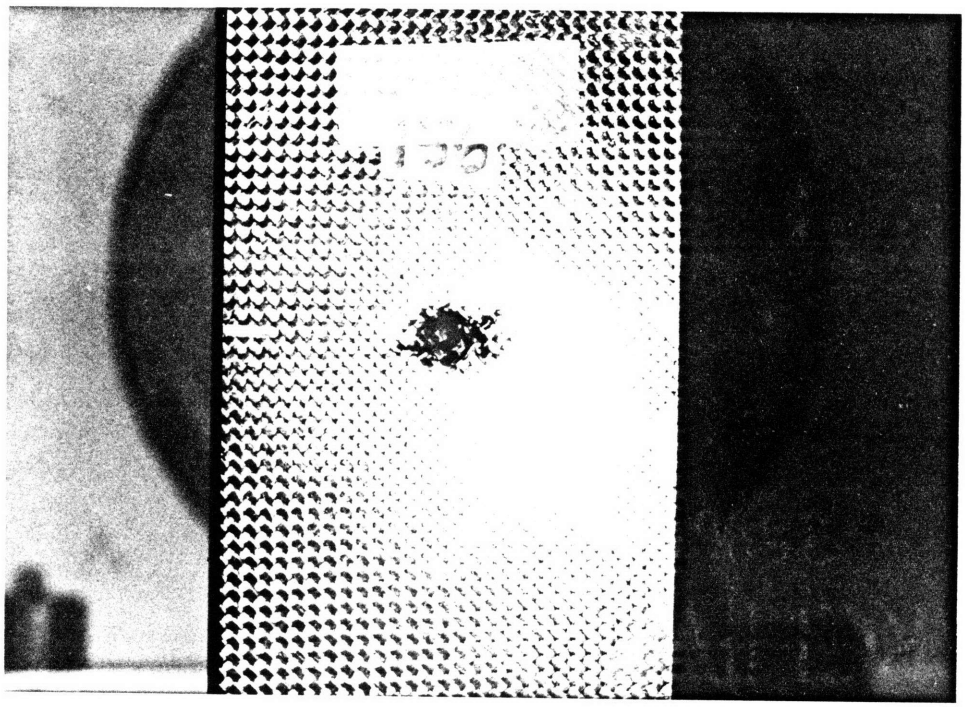

Figure A.16 (cont.)
Specimen #156 (+-45); Damage Growth Over Fatigue Life
N = 37,000, D = 22, 2210 lbs

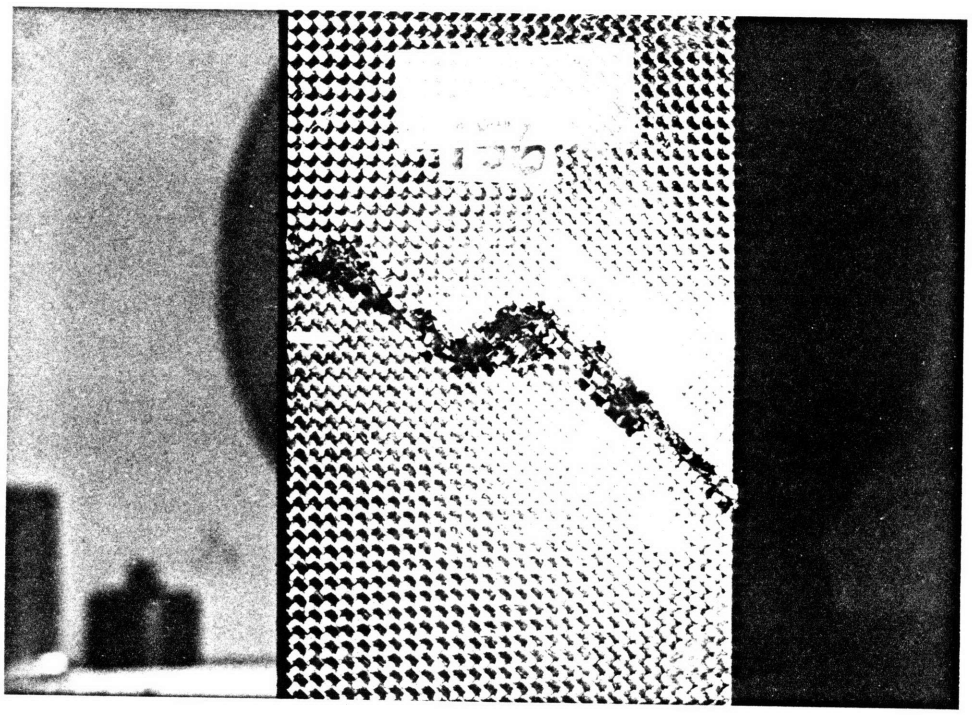

Figure A.16 (cont.)
Specimen #156 (+-45); Damage Growth Over Fatigue Life
N = 143,590 2210 lbs

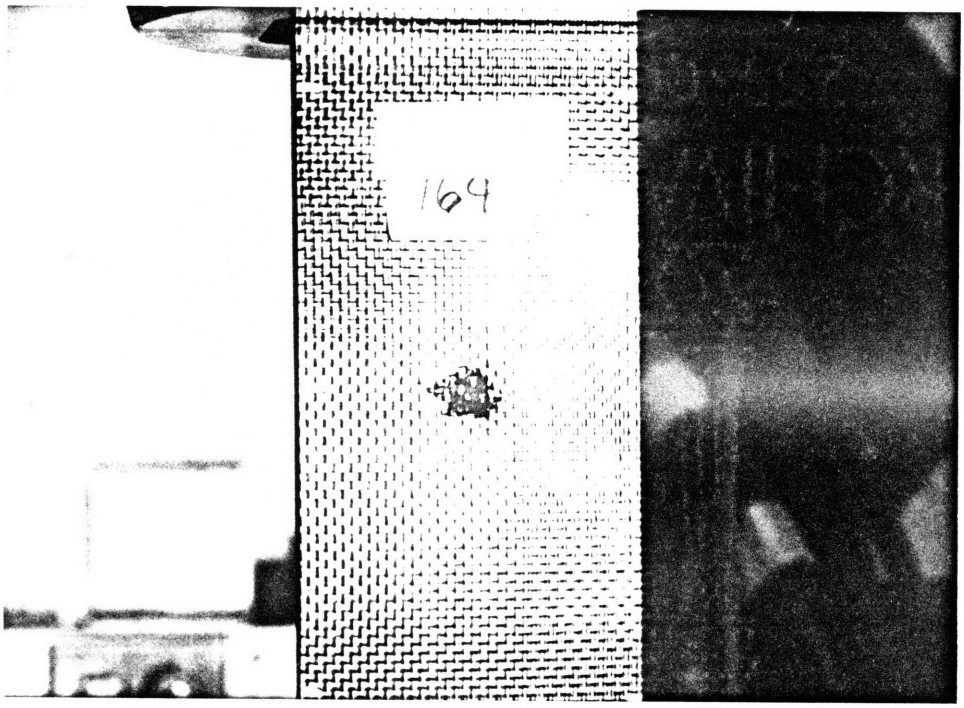

Figure A.17
Specimen #164 (0/90); Damage Growth Over Fatigue Life
N = 0.0 D = 14.5 mm, 2019 lbs

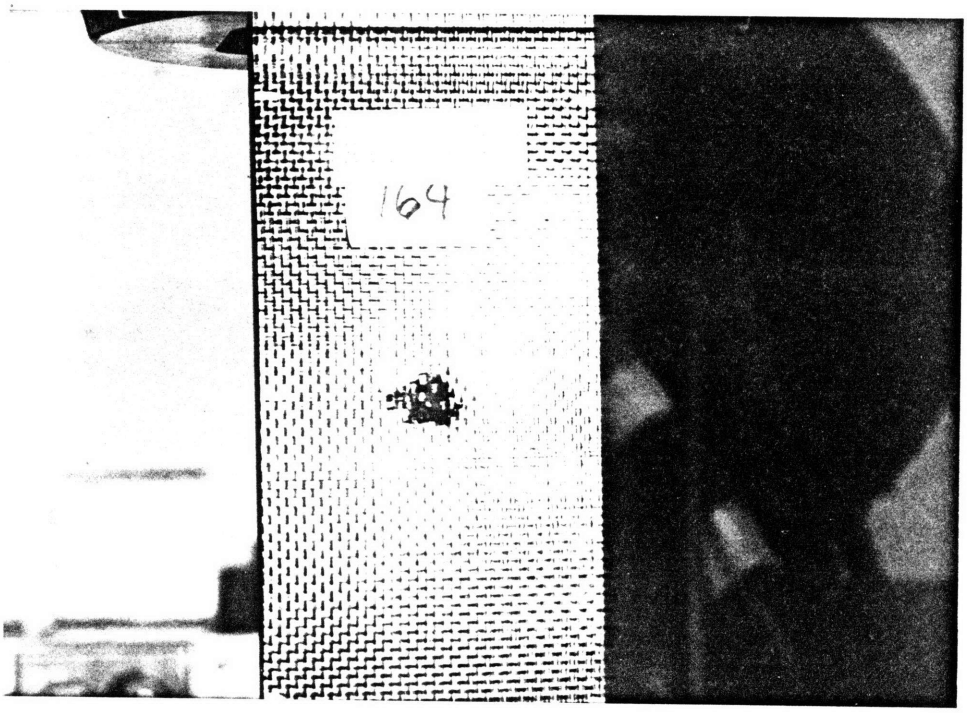

Figure A.17 (cont.)
Specimen #164 (0/90); Damage Growth Over Fatigue Life
N = 30, D = 21, 2019 lbs

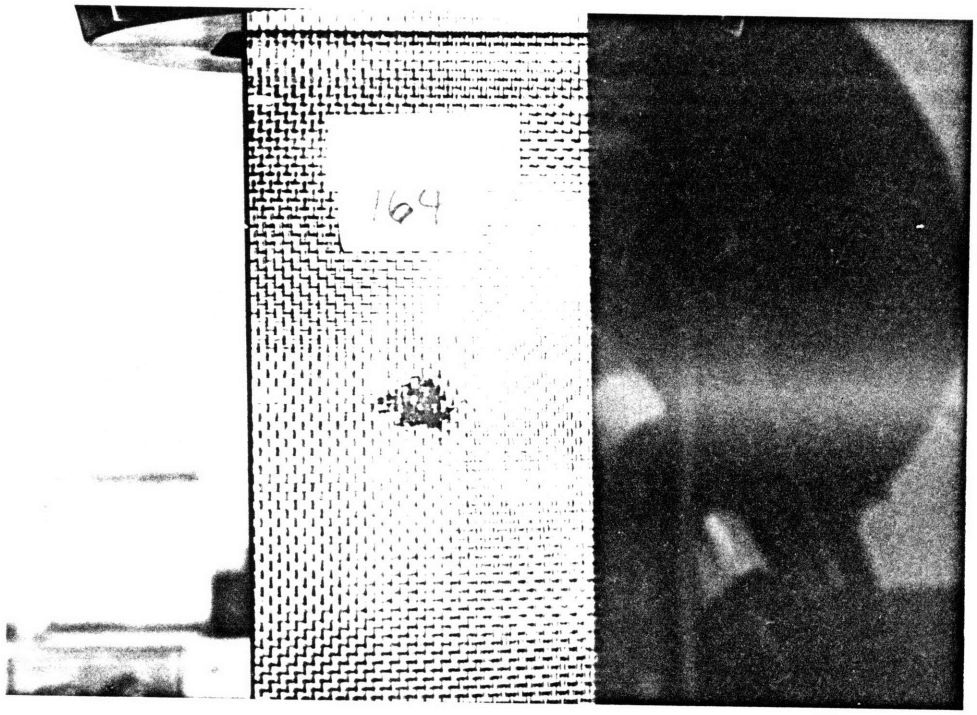

Figure A.17 (cont.)
Specimen #164 (0/90); Damage Growth Over Fatigue Life
N = 130, D = 22.5, 2019 lbs

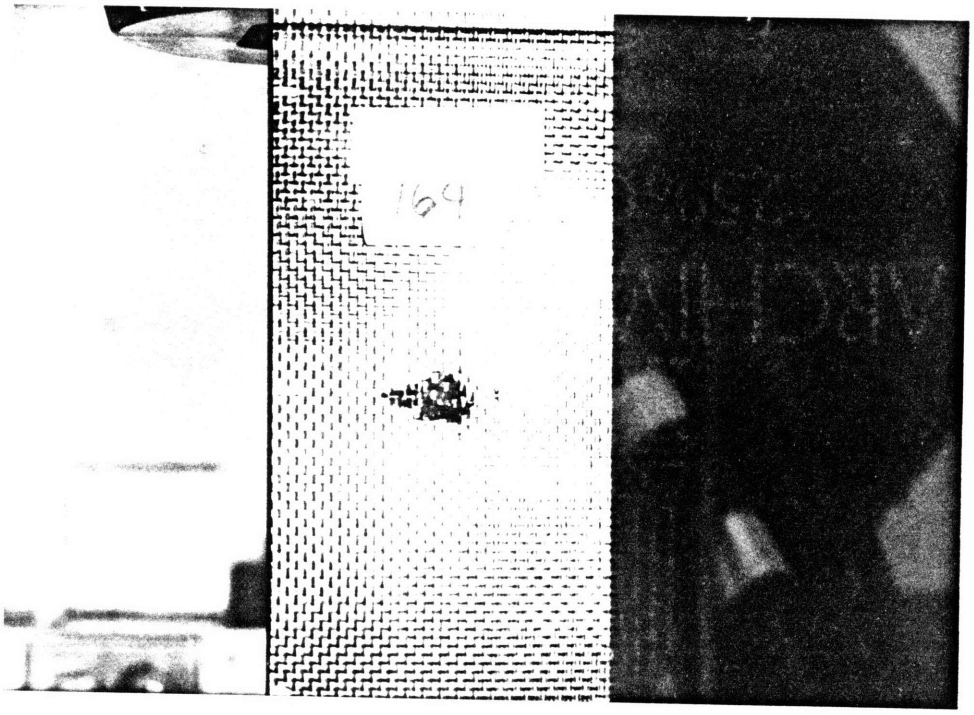

Figure A.17 (cont.)
Specimen #164 (0/90); Damage Growth Over Fatigue Life
N = 1000, D = 27, 2019 lbs

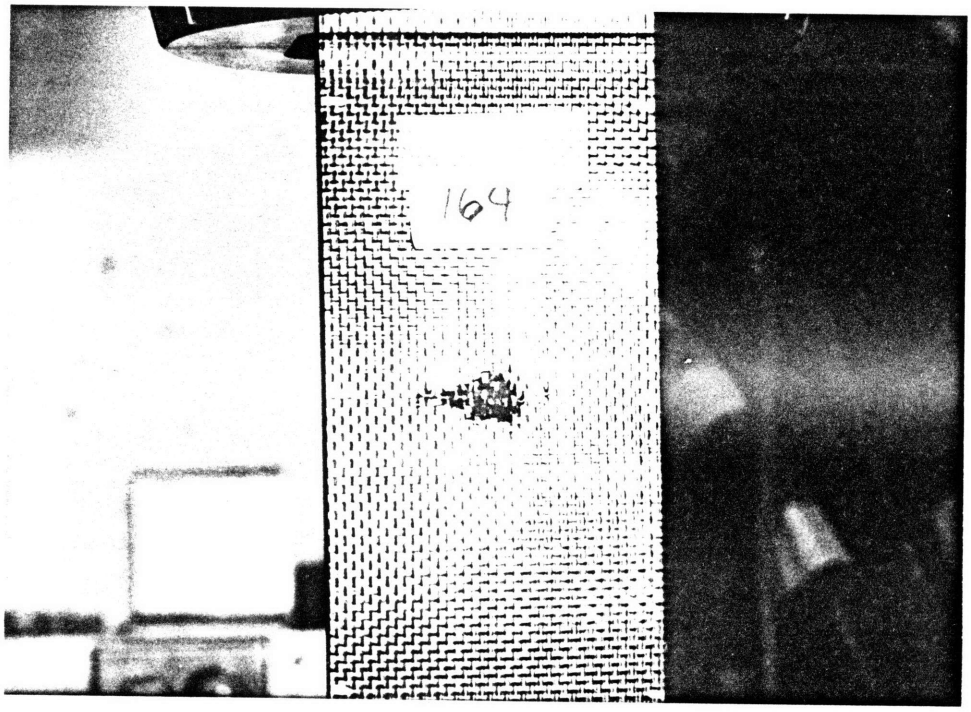

Figure A.17 (cont.)
Specimen #164 (0/90); Damage Growth Over Fatigue Life
N = 11,700, D = 32 mm, 2019 lbs

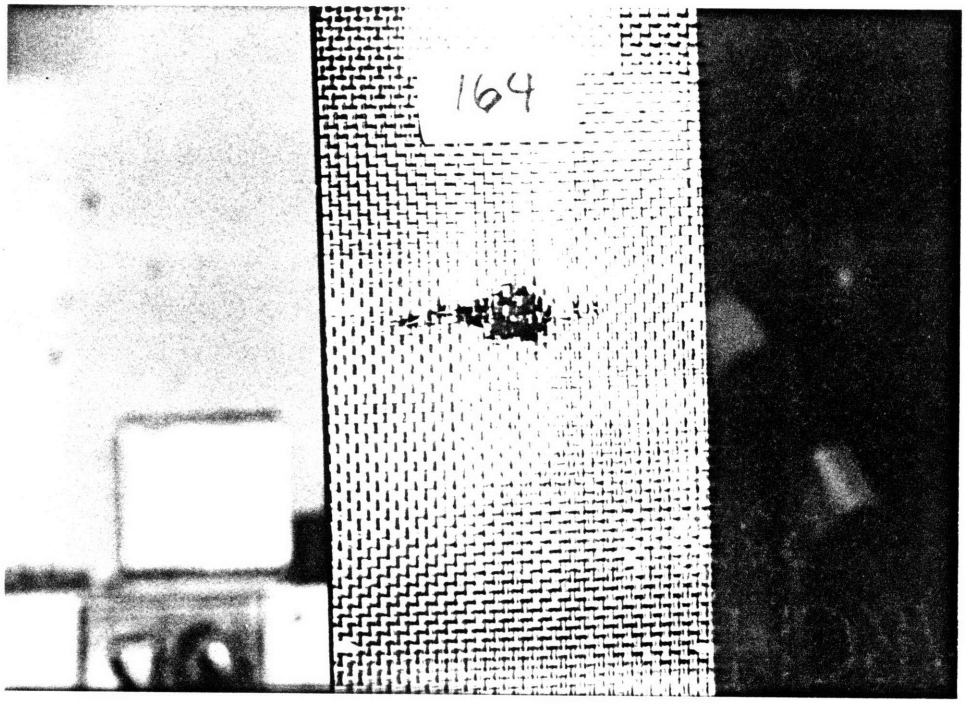

Figure A.17 (cont.)
Specimen #164 (0/90); Damage Growth Over Fatigue Life
N = 19,200 D = 36 mm 2019 lbs

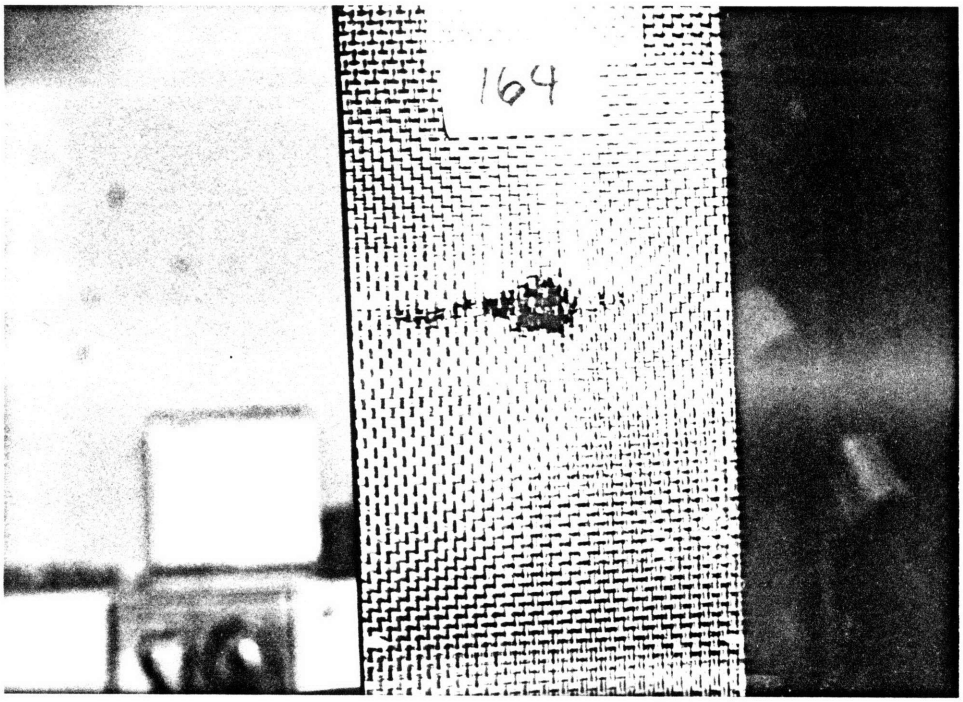

Figure A.17 (cont.)
Specimen #164 (0/90); Damage Growth Over Fatigue Life
N = 30,440 D = 45 mm 2019 lbs

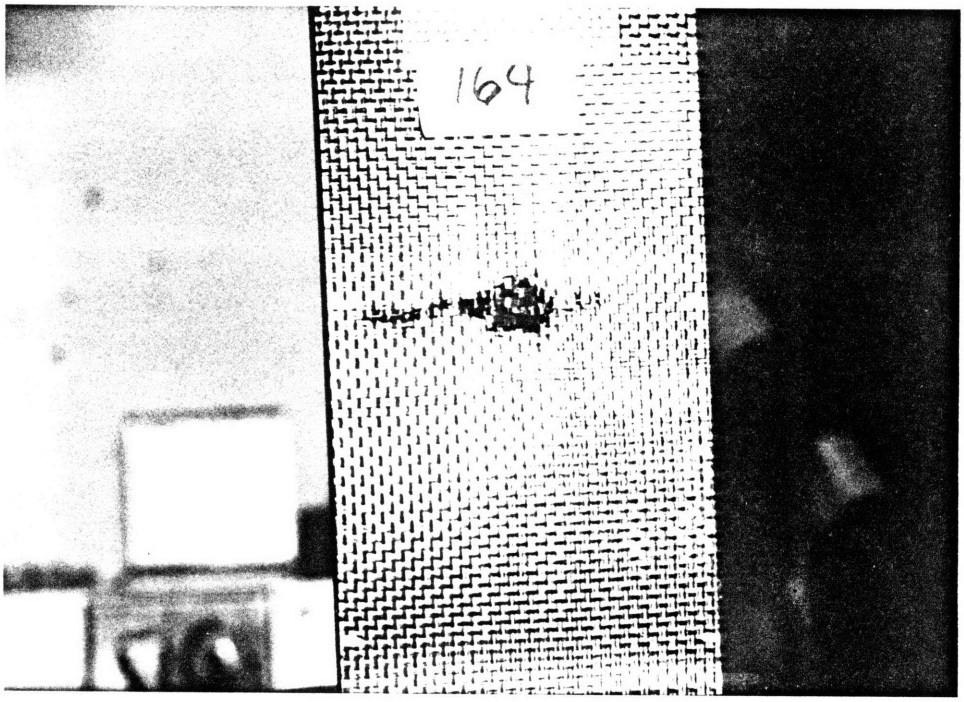

Figure A.17 (cont.)
Specimen #164 (0/90); Damage Growth Over Fatigue Life
N = 30,485 D = 50 2019 lbs

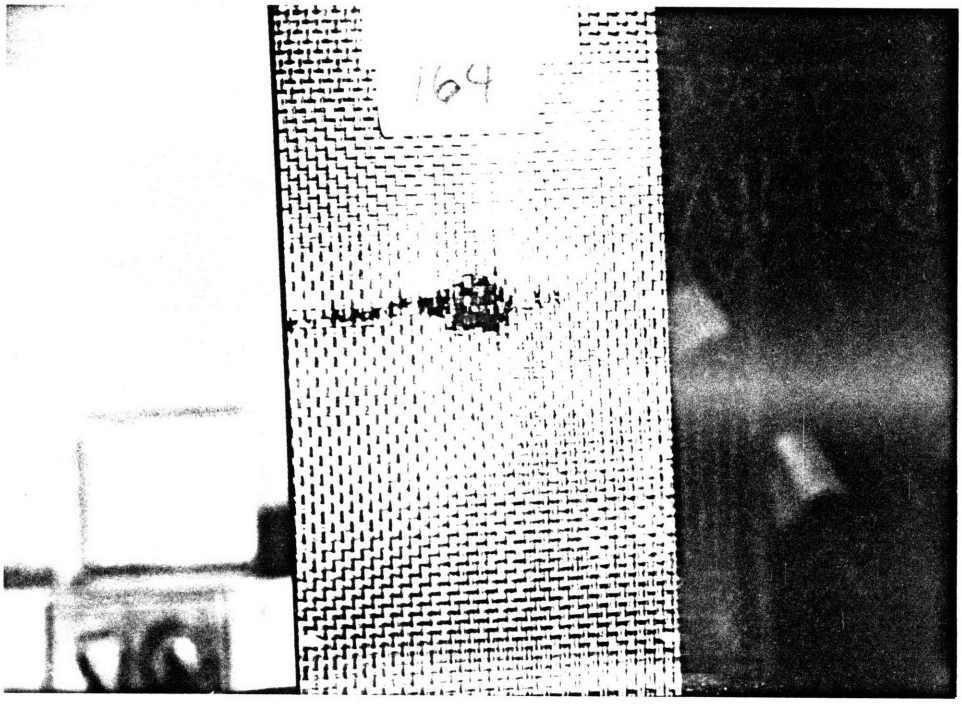

Figure A.17 (cont.)
Specimen #164 (0/90); Damage Growth Over Fatigue Life
N = 30,520 D = 53 mm 2019 lbs

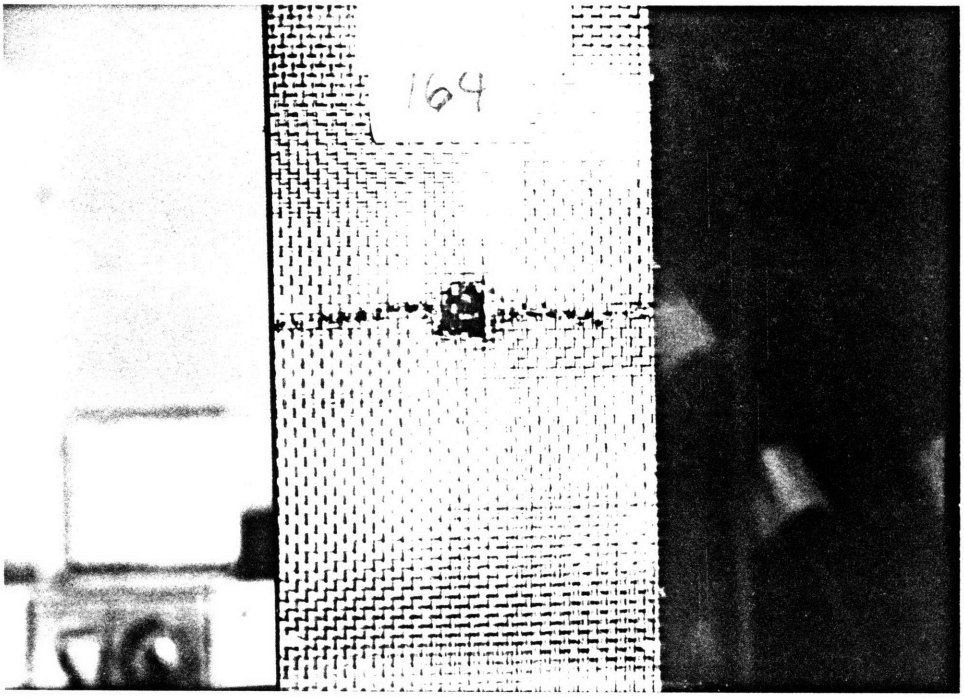

Figure A.17 (cont.)
Specimen #164 (0/90); Damage Growth Over Fatigue Life
N = 30,530

APPENDIX B: SUB-LAMINA GEOMETRY OF THE WOVEN PLY

In order to make use of the orthotropic properties of the plane weave ply and apply them to classical laminated plate theories, the woven ply can be viewed as an "imaginary" bi-ply with two equivilent principle material axes acting within the central plane of the ply. The sinusoidal bending of the fiber tows will be ignored for the "imaginary ply", and addressed later in this chapter. The final assumption is that the "imaginary" ply's mechanically effective thickness is half of its actual thickness. That is, one half of the lamina's filaments, which occupy one half of the lamina thickness, actually contribute to stiffness in the principle material direction. Figure 3.2(b) illustrates that fiber tows of thickness t/2 provide principle material stiffness in the fill direction and on both sides of the central plane. The warp tows provide no longitudinal filament stiffness in the paper direction, but they do occupy one half of the ply thickness, t. The imaginary ply is depicted in figure B.1.

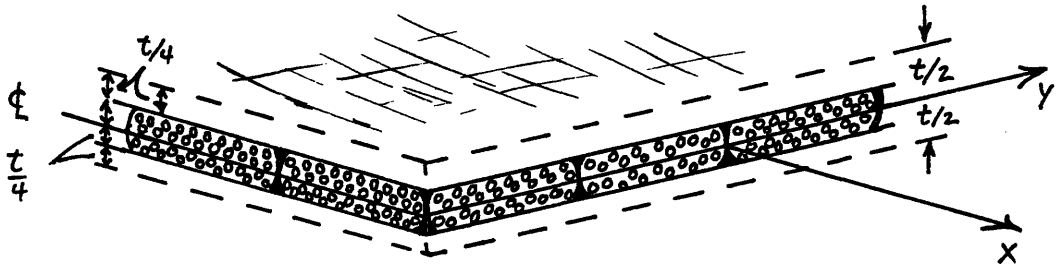

Figure B.1 The "imaginary bi-ply"

The assumptions made for the woven ply acting through the central plane and the effective mechanical thickness equal to t/2, are possible only if the filament tows are identical. A second geometric factor is the ratio between the tow thickness and its woven width. This determines the shape of the tow's sinusoidal bending. A large thickness to width ratio implies greater sinusoidal bending and succeptability to out-of-plane buckling. The nominal dimensions for AW193PW/3501-6 graphite/epoxy fabric are:

ply thickness .0076" (.193mm)

tow thickness .0038" (.0965mm)

tow width .0878" (2.23mm)

thickness/ width ratio = .0433 = 1 to 23.1

Figure B.2 illustrates the tow deflections and greatest angular deflection, Ω. Greater tow bending angles are possible but not likely, because fibers at the edge of the tow are expected to form a pointed cross section under the 40 psi curing pressure and free flowing epoxy matrix. A very thin elongated ellipse would be the likely tow cross section as the laminate is compressed to its minimum thickness during the pressurized cure cycle.

If one assumes that X percent of the filament tow width has a thickness of t/2 (or .0038 inch in this case) and that only the outer (100-X)/2 percent of the tow width has a tapered thickness, then Ω can be calculated. An assumption of (X + 10) percent on each tow will obviously yield a different angular deflection for the tow.

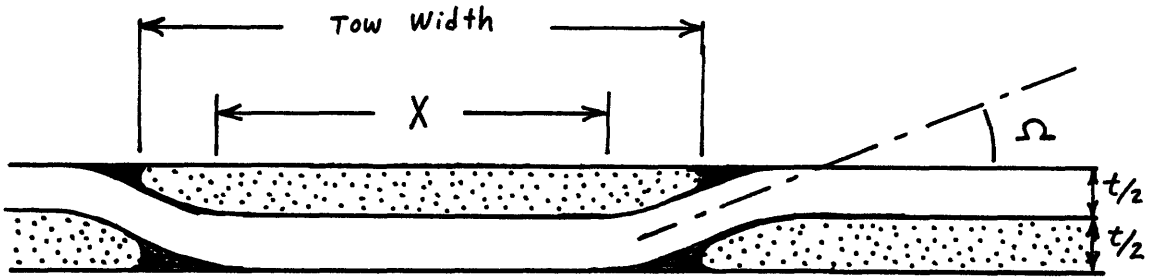

Figure B.2 Tow deflection angle within weave

If one assumes that X percent of the filament tow width has a thickness of t/2 (or .0038 inch in this case) and that only the outer (100-X)/2 percent of the tow width has a tapered thickness, then Ω can be calculated. An assumption of (X + 10) percent on each tow will obviously yield a different angular deflection for the tow.

Using this scheme, the maximum deflection angle Ω, from the central ply plane can be approximated for a given assumption, X. Table B.1 provides some values as an illustration. The maximum deflection angle is significant in that it represents a weakness in the retardation of tow and laminate buckling. It's inherant buckling mode shape makes it unstable and dependent upon the matrix to maintain stability as the tows carry longitudinal loads in the fill direction.

TABLE B.1
Tow Bending Within Fabric

Unaffected Tow Width,	X % :	75	80	85	90
Maximum Deflection Angle,	(deg.):	10.0	12.6	16.8	25.8

Thickness/ width for AW 193PW/3501-6 is 1/23. This ratio can be used to calculate other deflection angles for a given tow cross section with the following formula:

$$\Omega = \arcsin\left(1/[23(1-X)]\right) \qquad (B.1)$$

APPENDIX C: PANEL DEFLECTION GRAPHS

This appendix contains mid-panel deflection and angular deflection curves for specimen type and impact damage level.

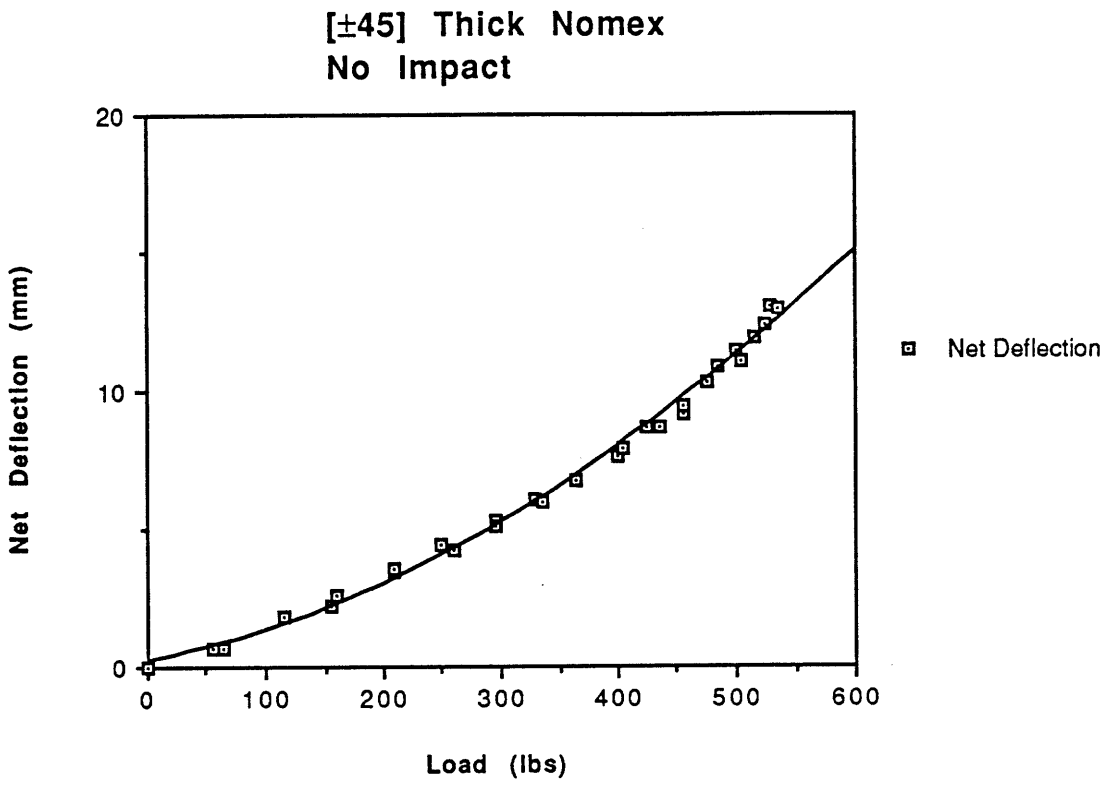

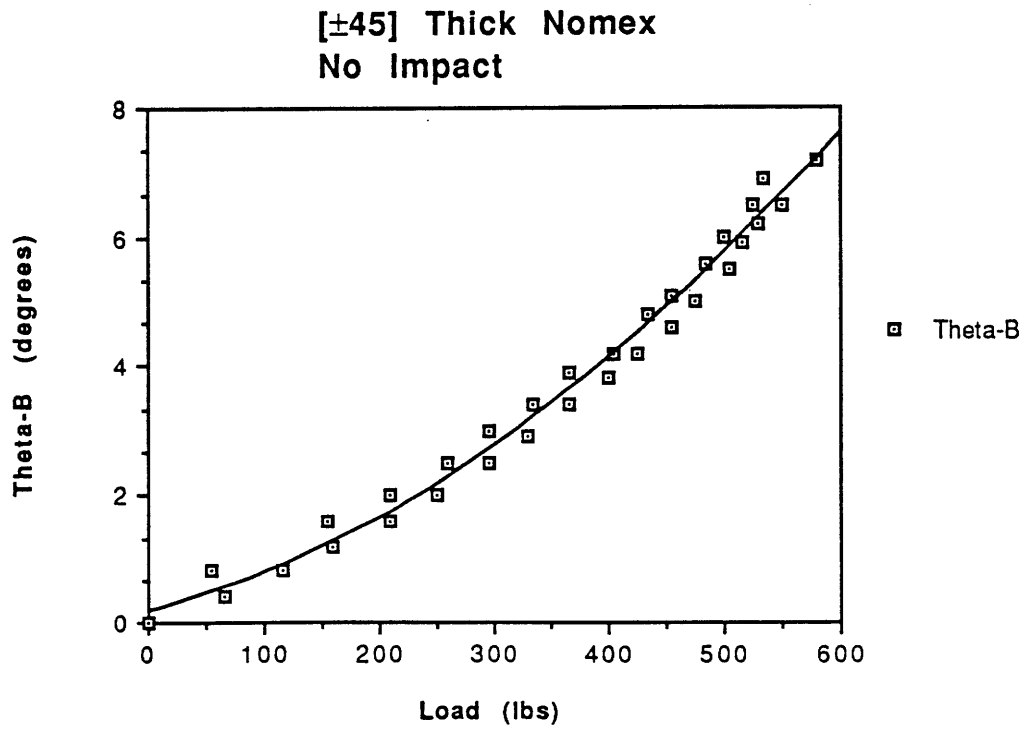

Figure C.1 [+-45] 1 inch; Undamaged: Deflection Curves

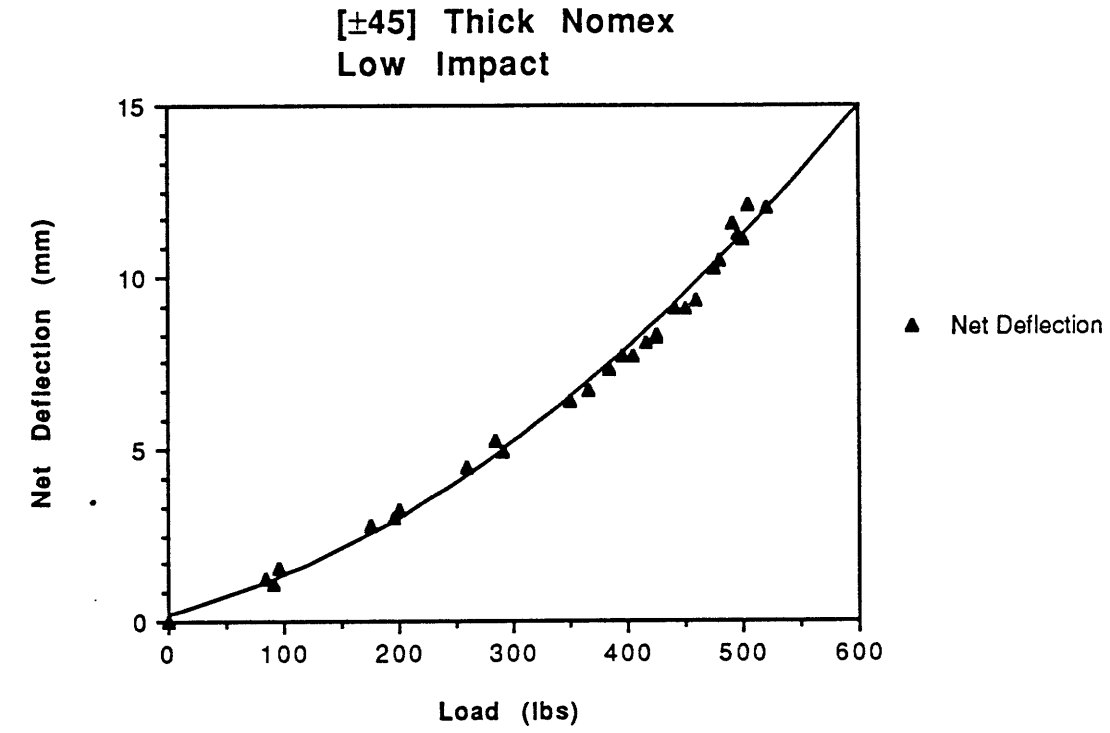

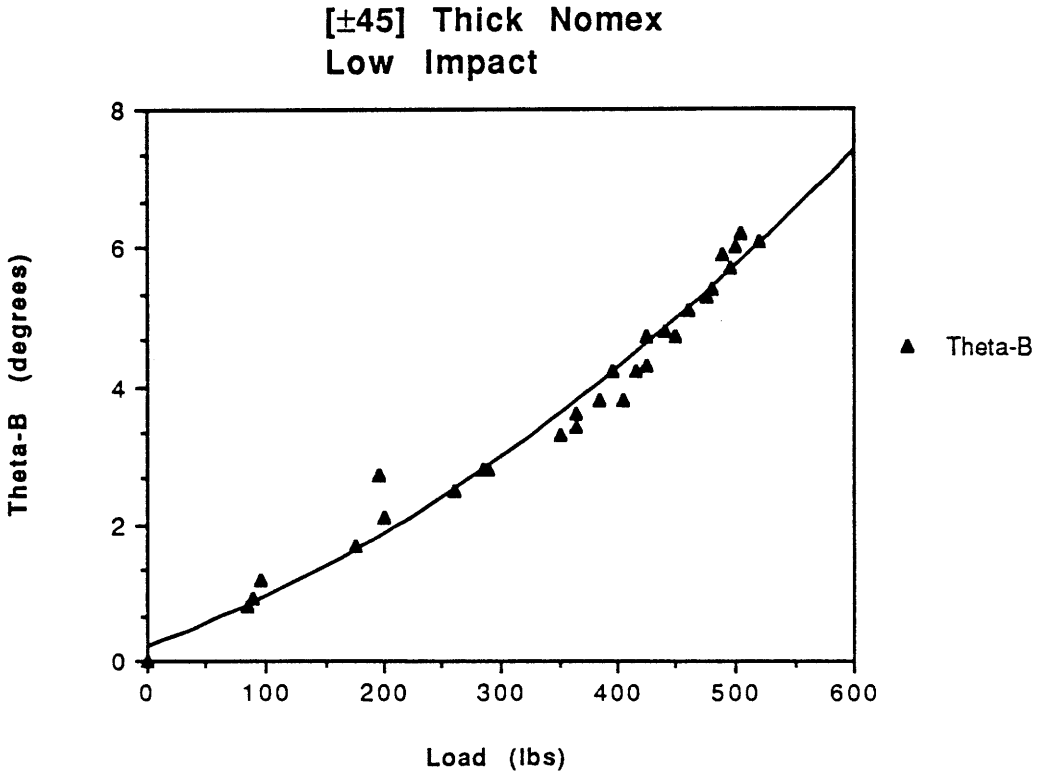

Figure C.2 [+-45] 1 inch; Low Damage: Deflection Curves

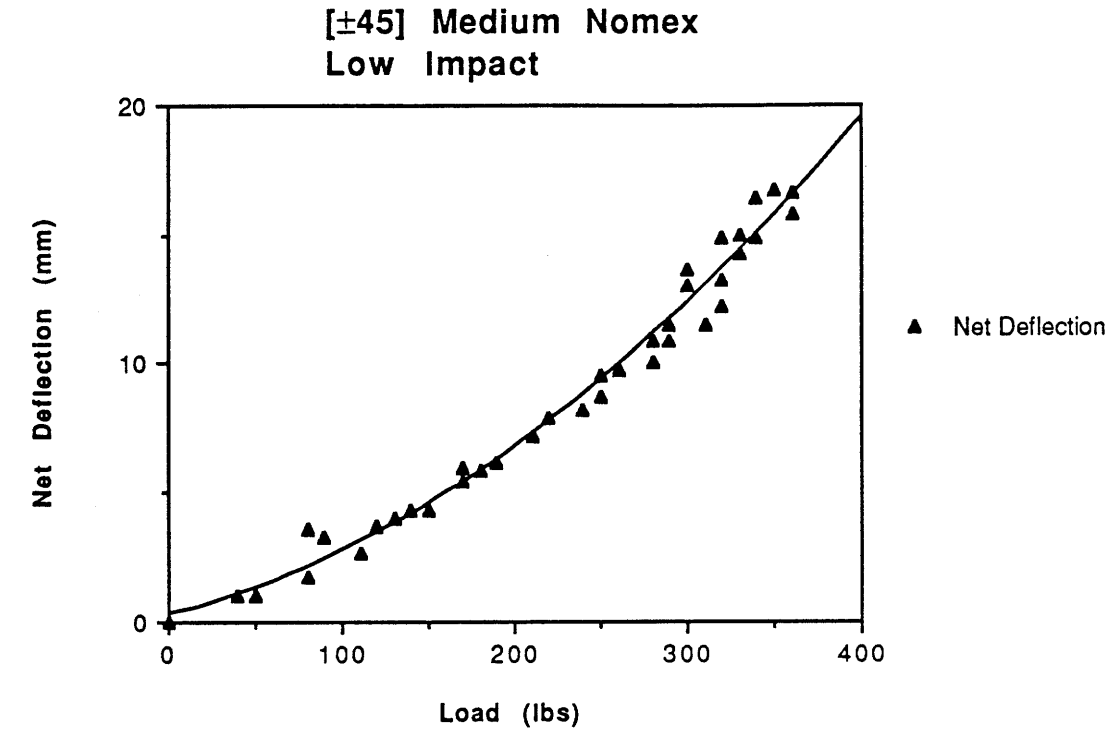

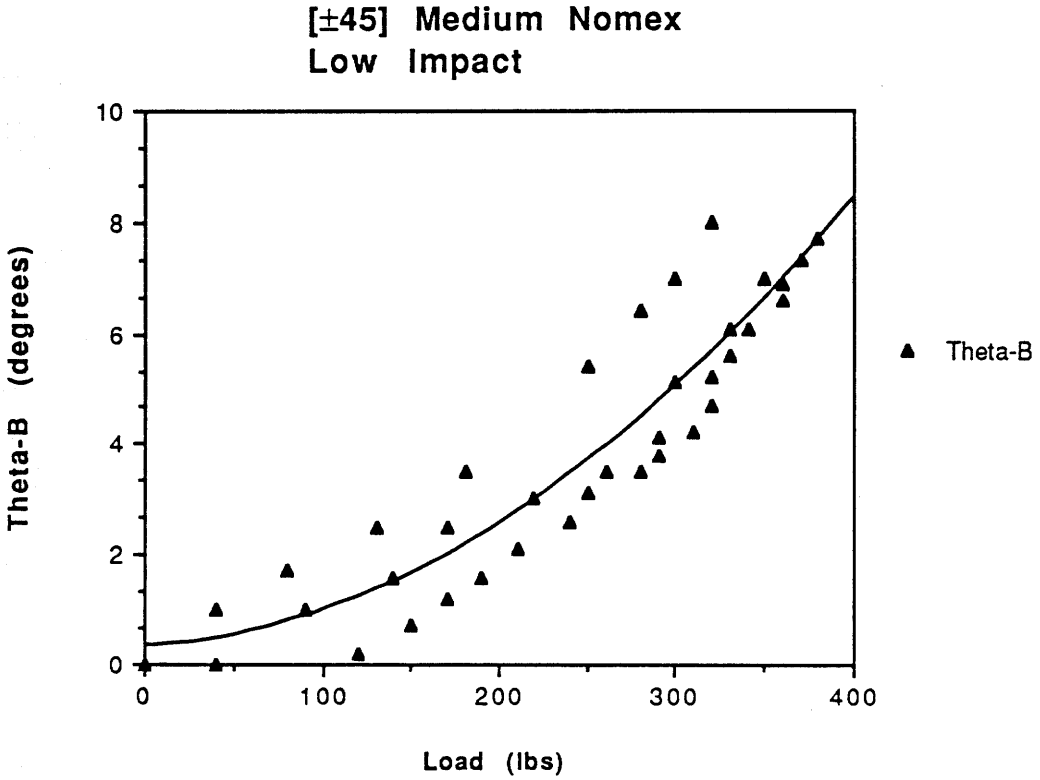

Figure C.3 [+-45] .687"; Low Damage: Deflection Curves

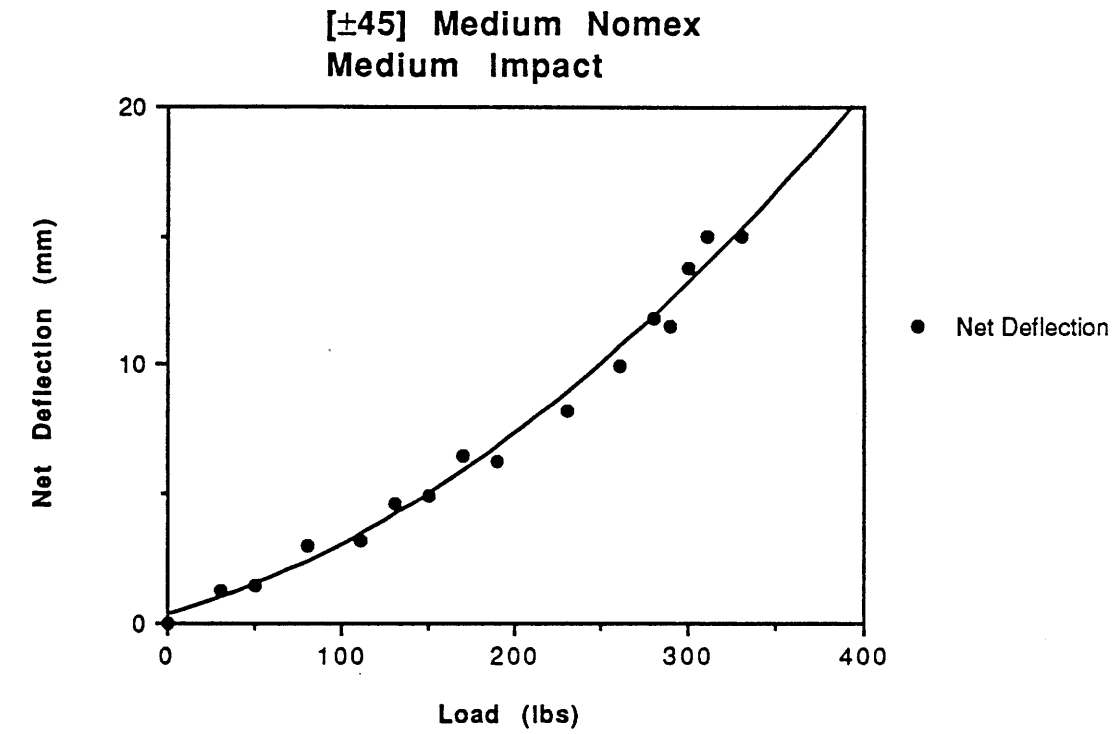

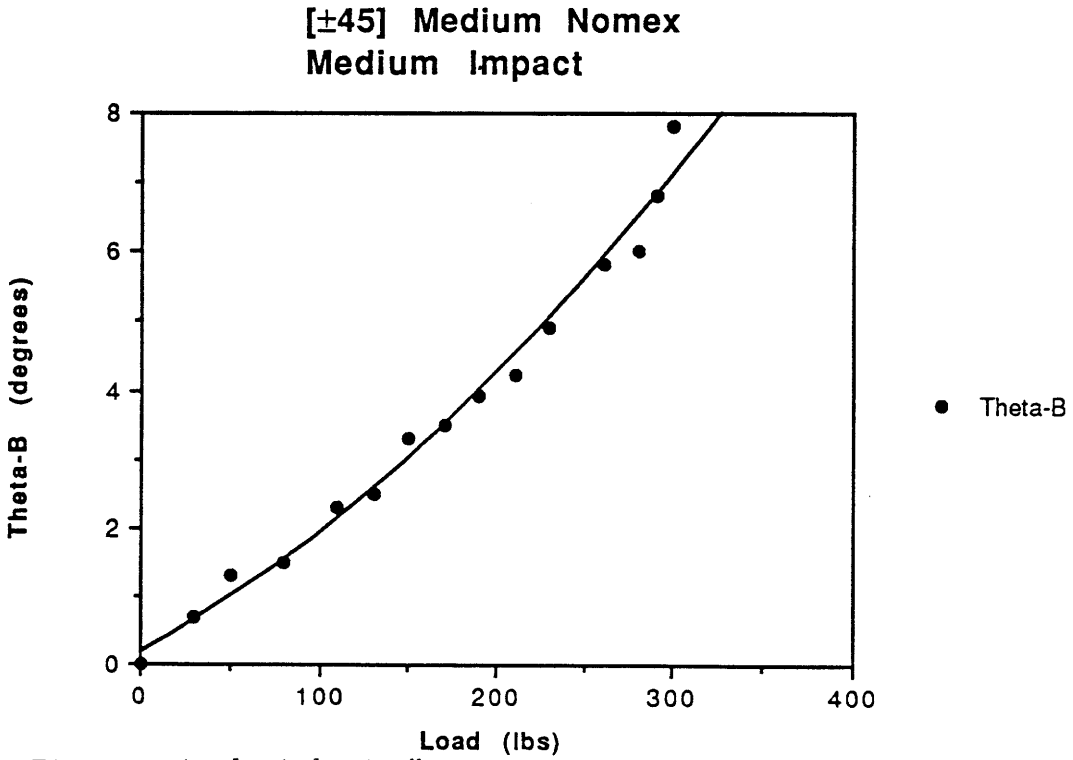

Figure C.4 [+-45] .687"; Medium Damage: Deflection Curves

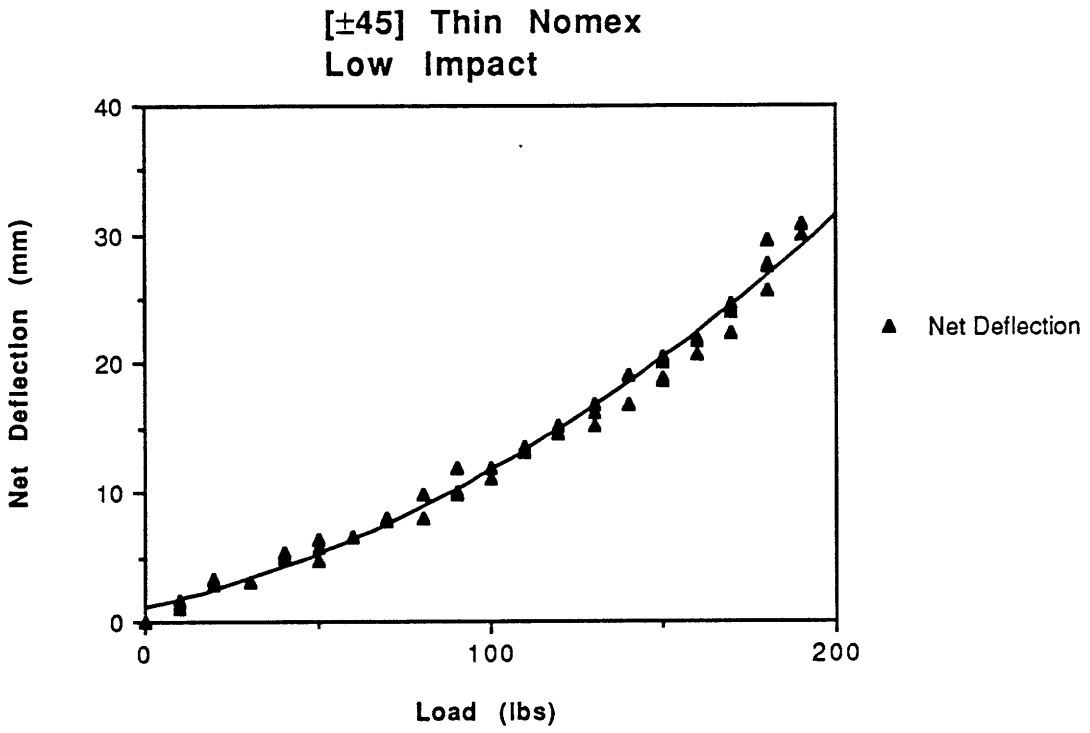

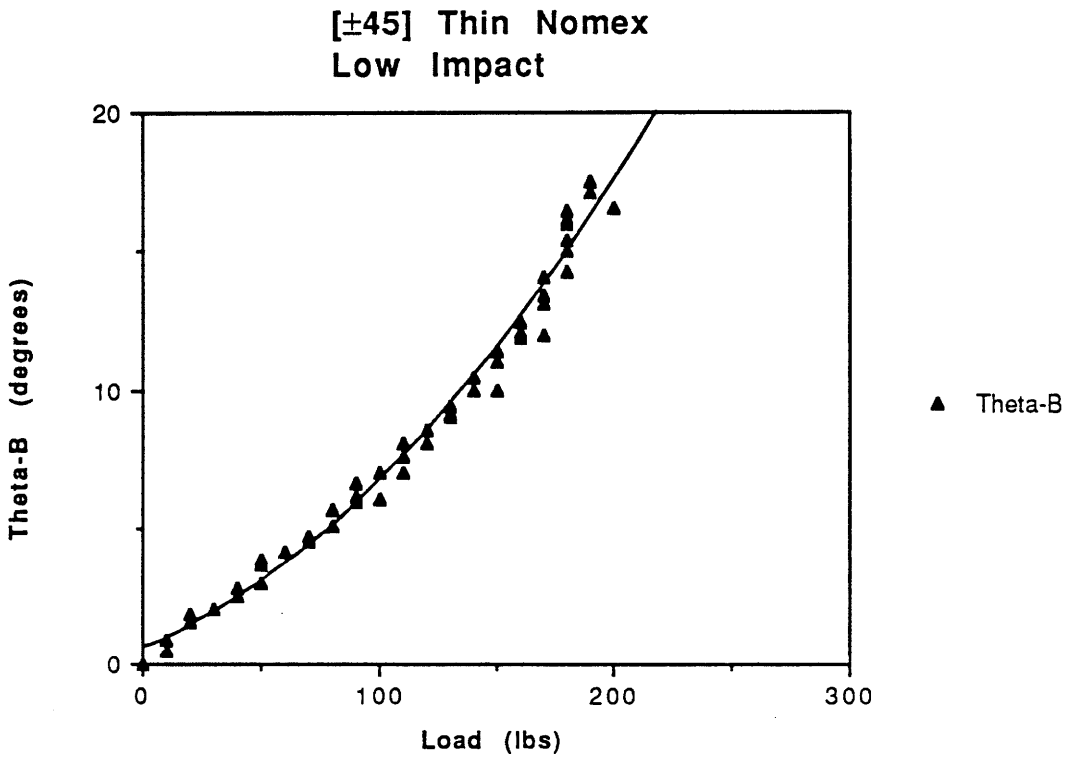

Figure C.5 [+-45] .375"; Low Damage: Deflection Curves

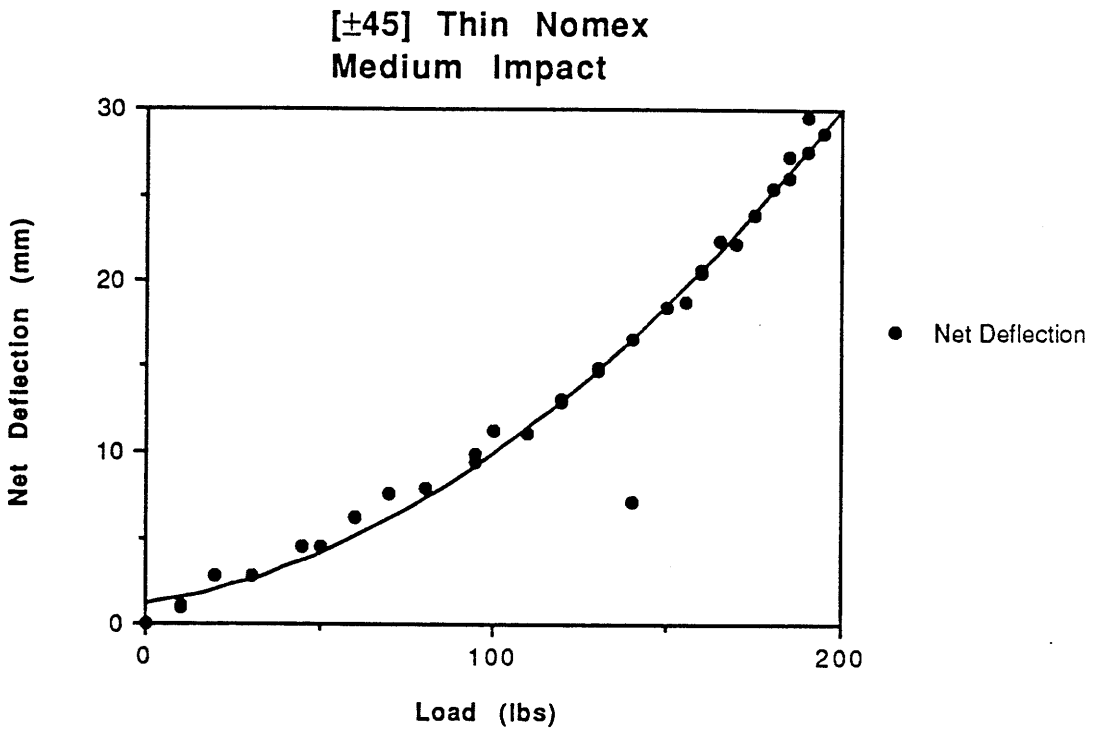

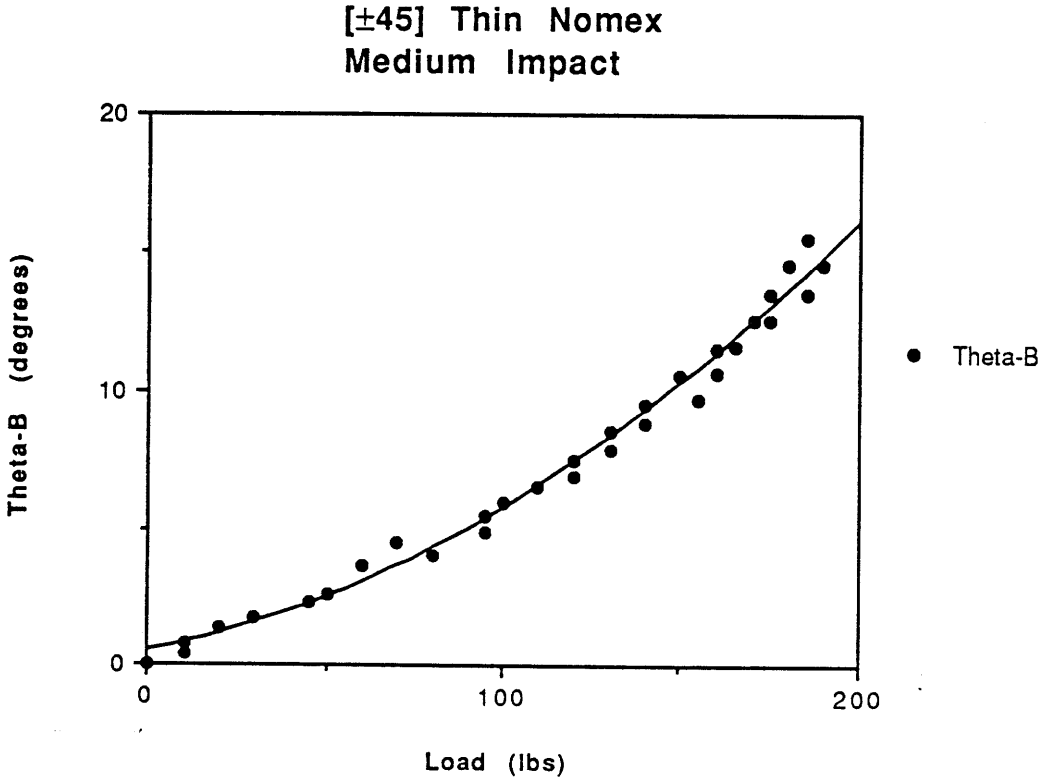

Figure C.6 [+-45] .375"; Medium Damage: Deflection Curves

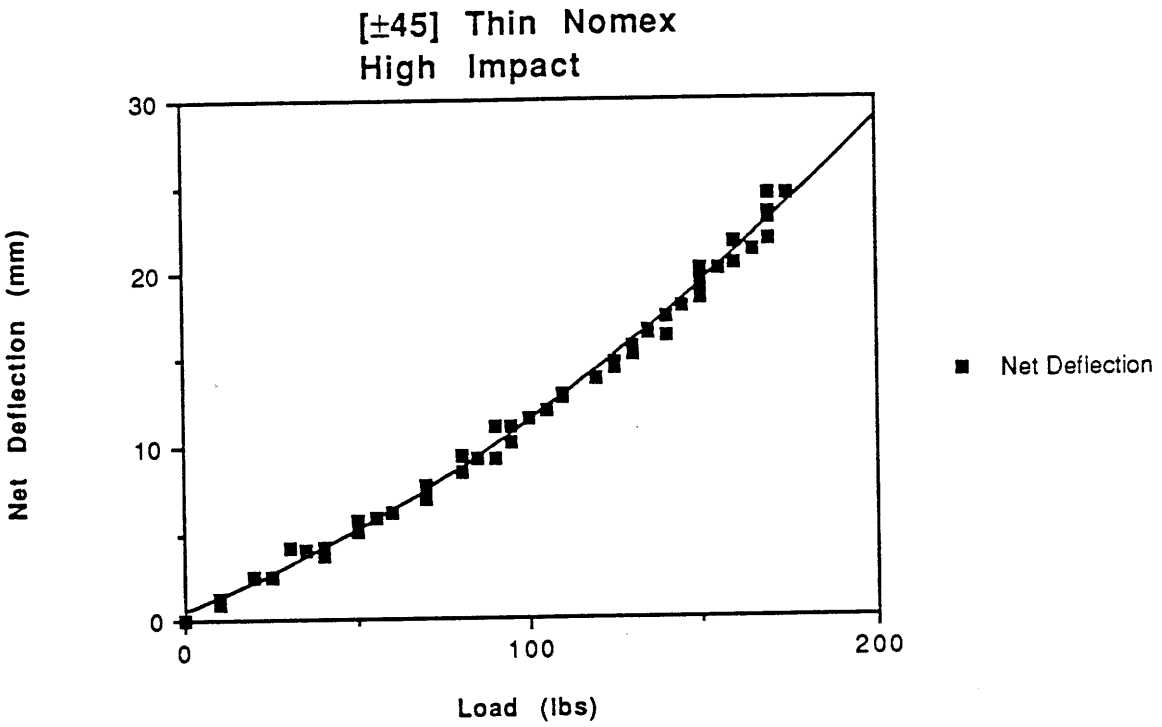

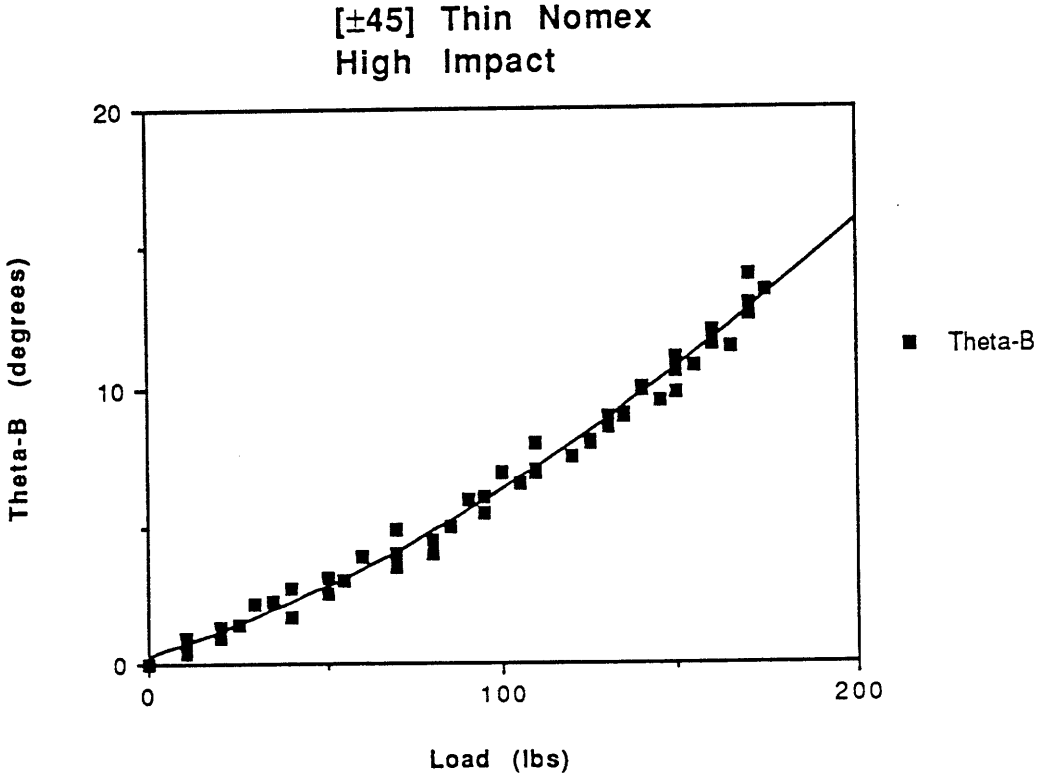

Figure C.7 [+-45] .375"; High Damage: Deflection Curves

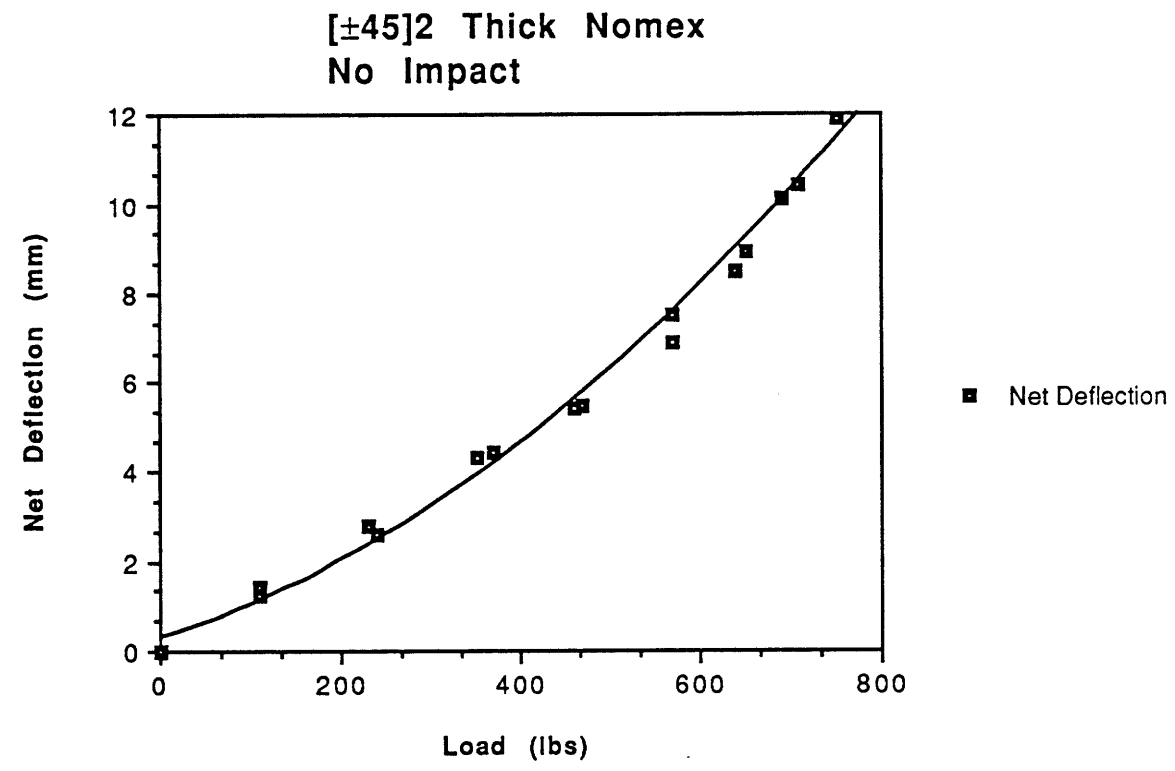

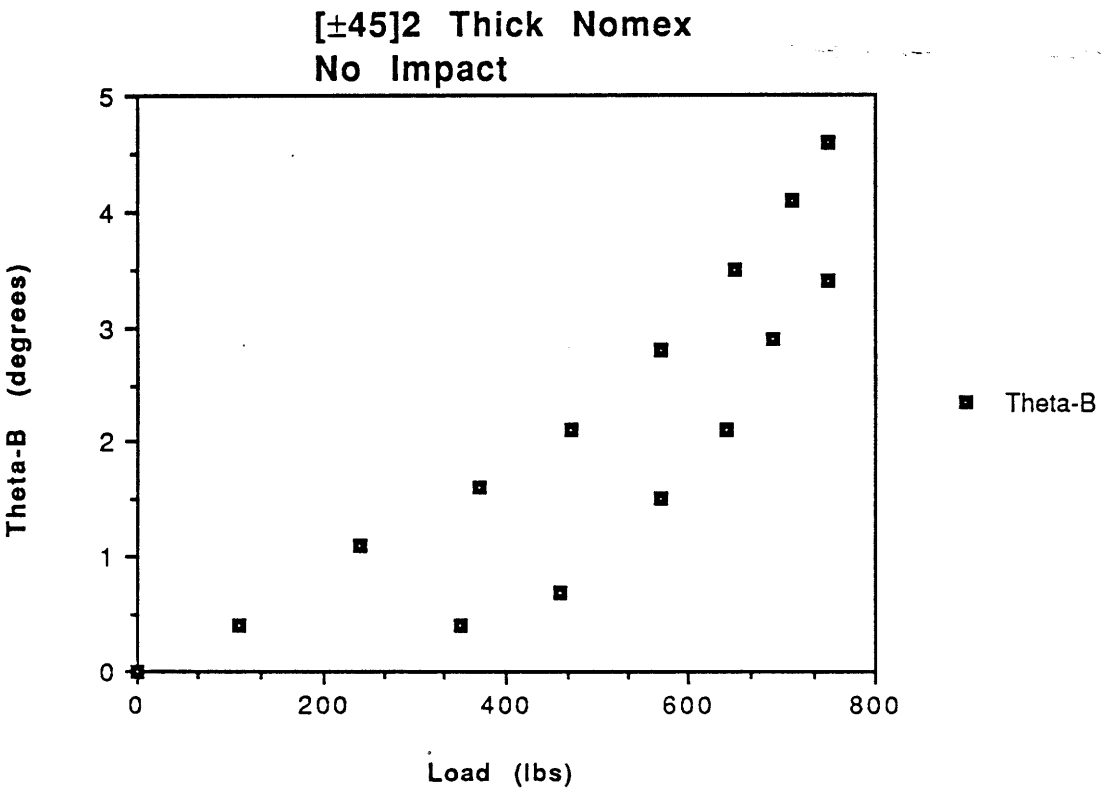

Figure C.8 [+-45]s 1.0 inch; Undamaged: Deflection Curves

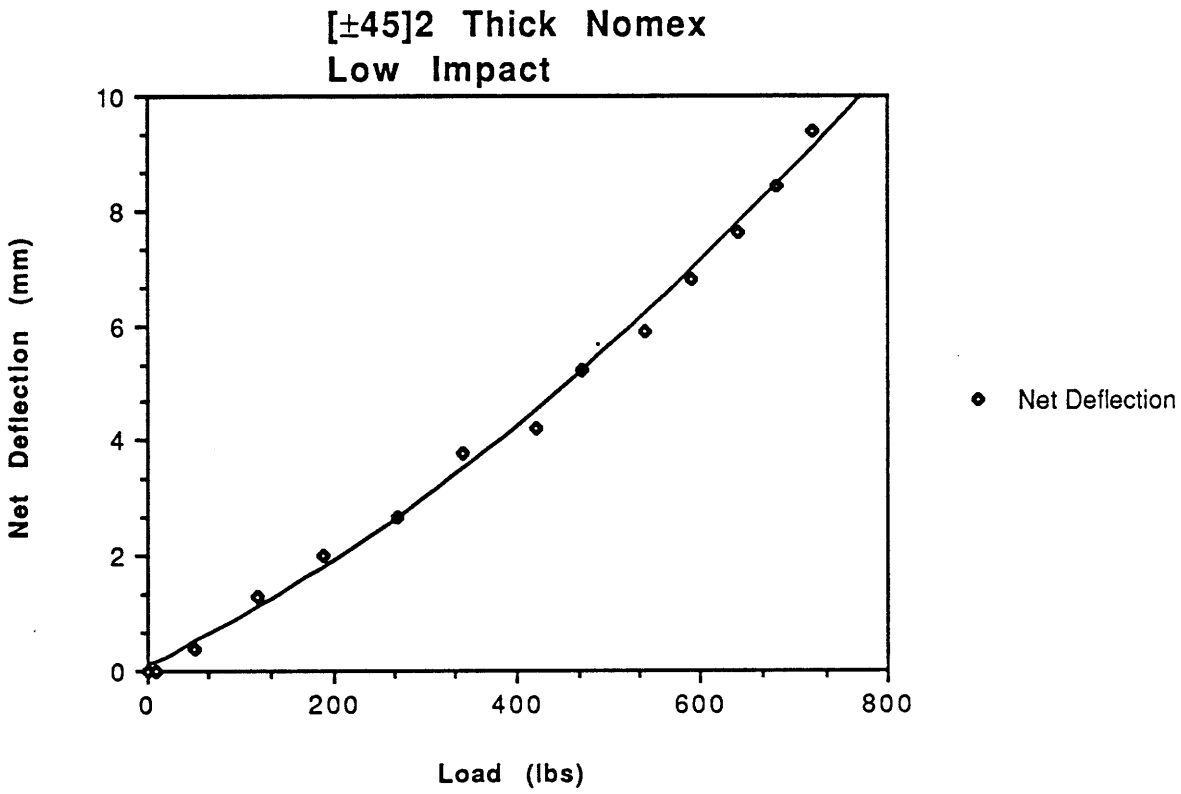

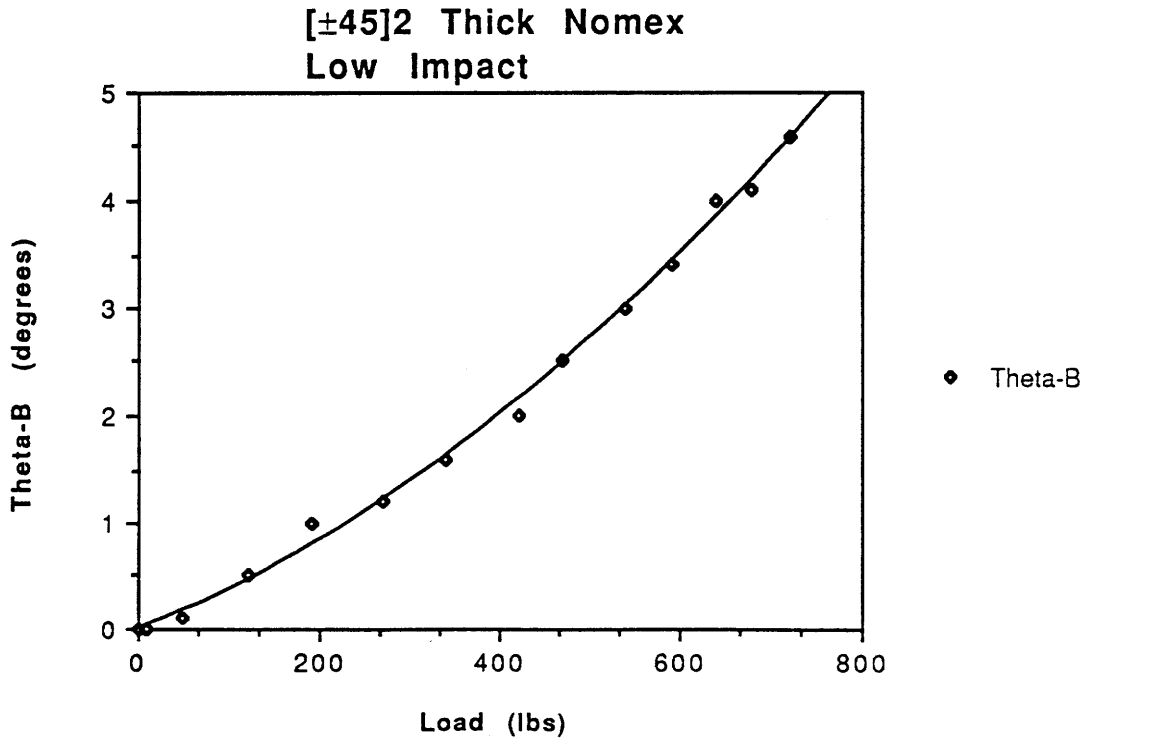

Figure C.9 [+-45]s 1.0 inch; Low Damage: Deflection Curves

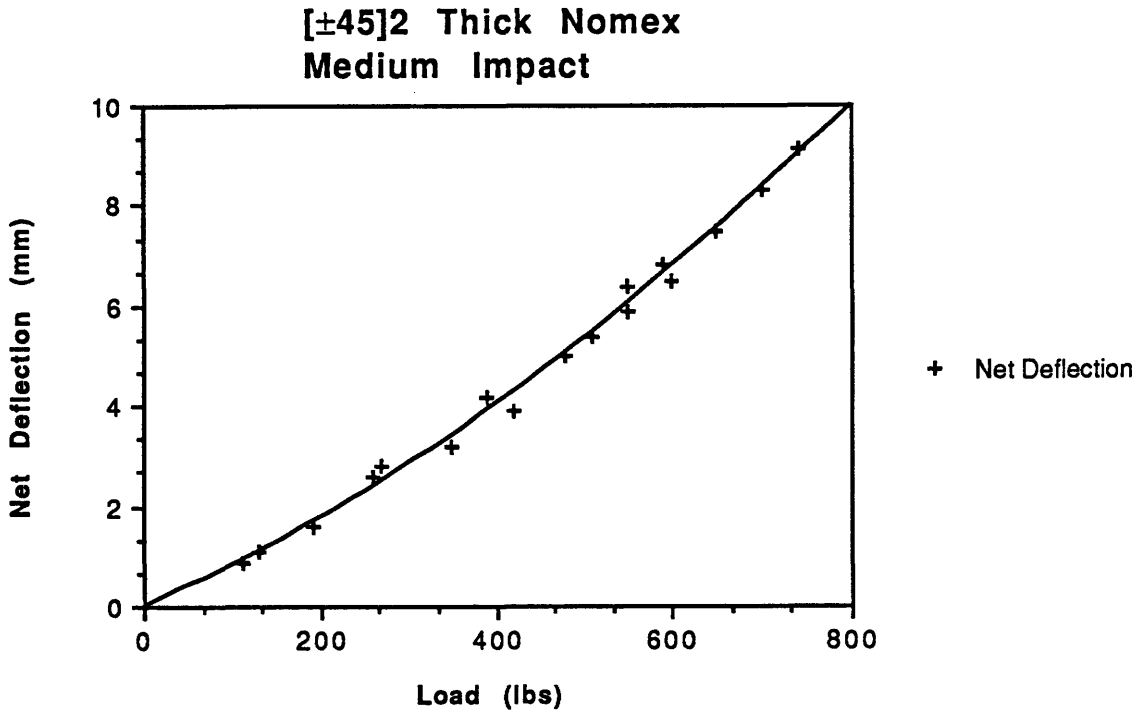

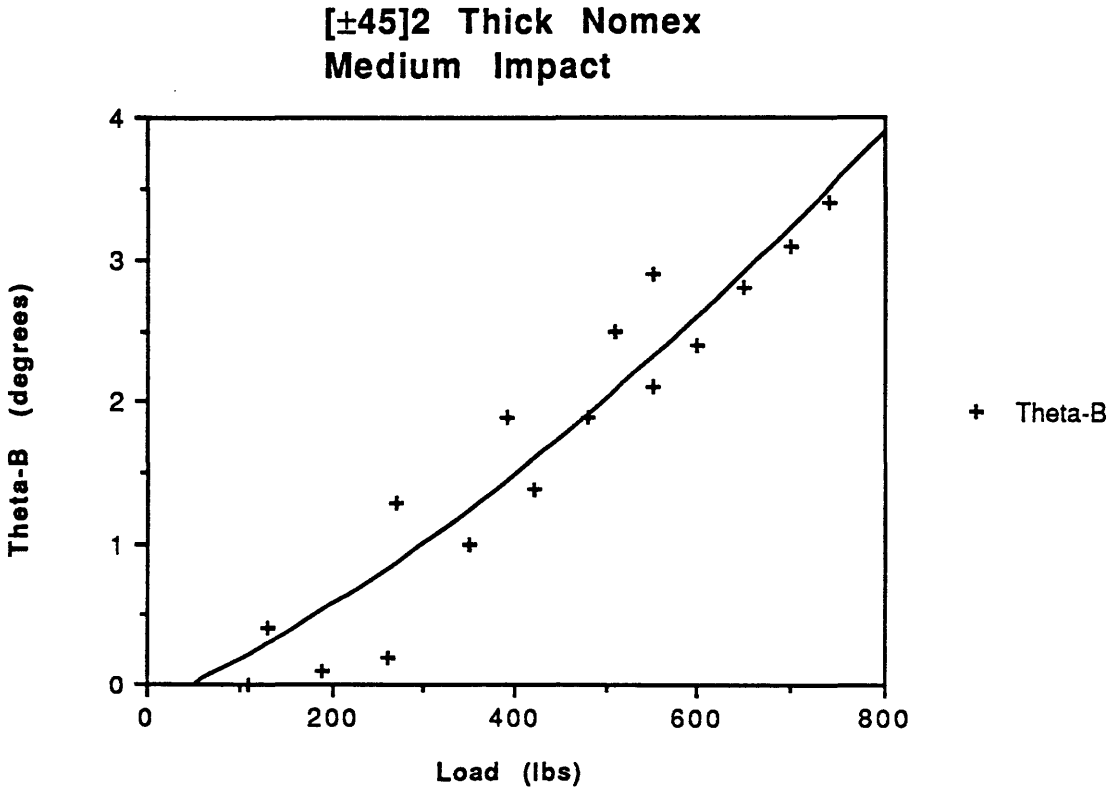

Figure C.10 [+-45]s 1.0 inch; Medium Impact: Deflection Curves

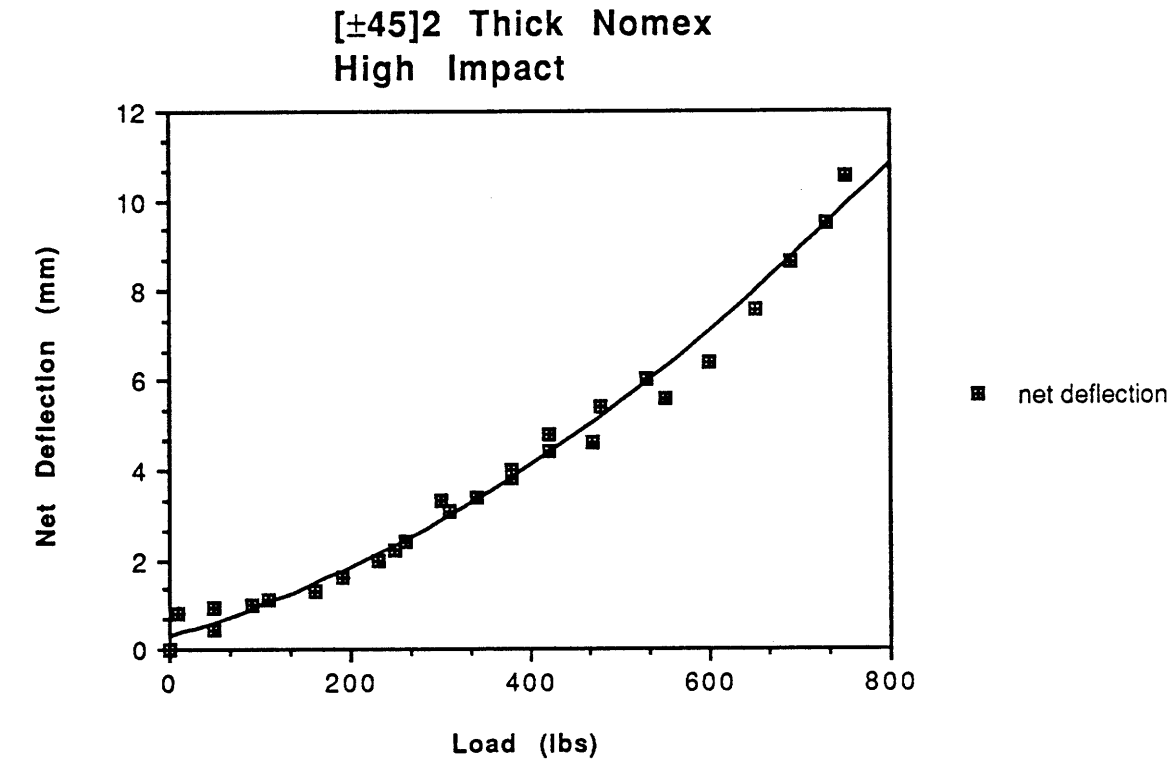

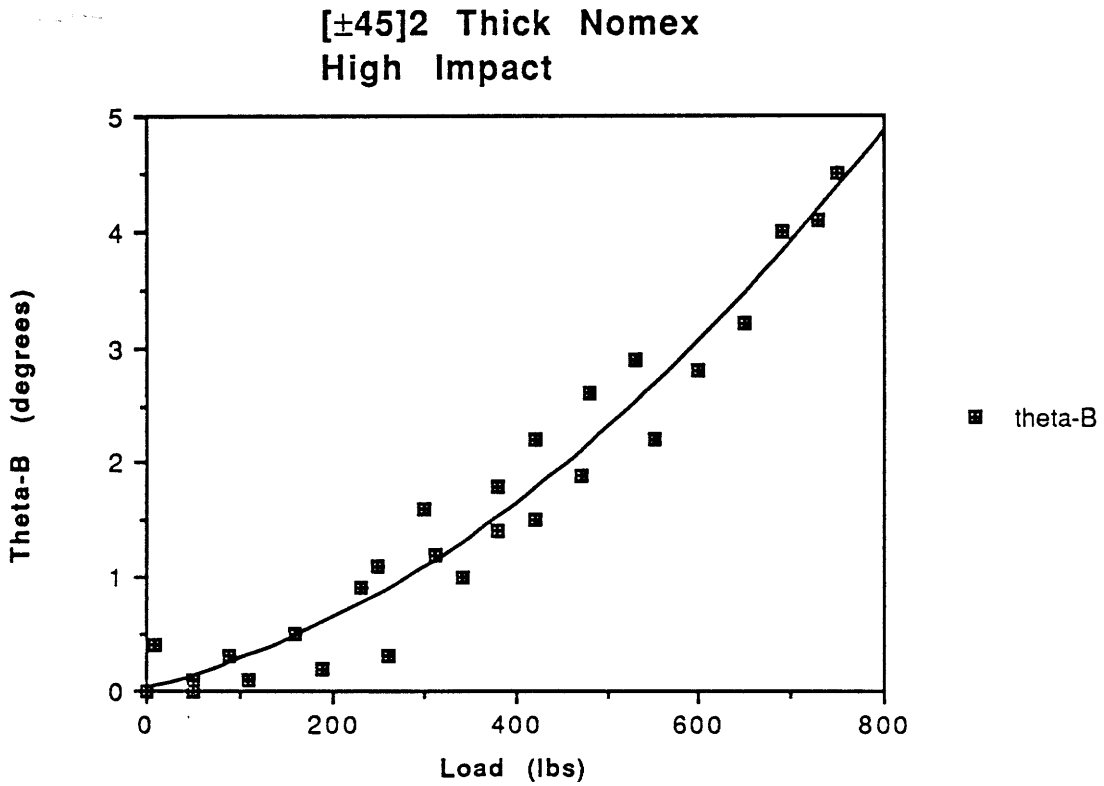

Figure C.11 [+-45]s 1.0 inch; High Damage: Deflection Curves

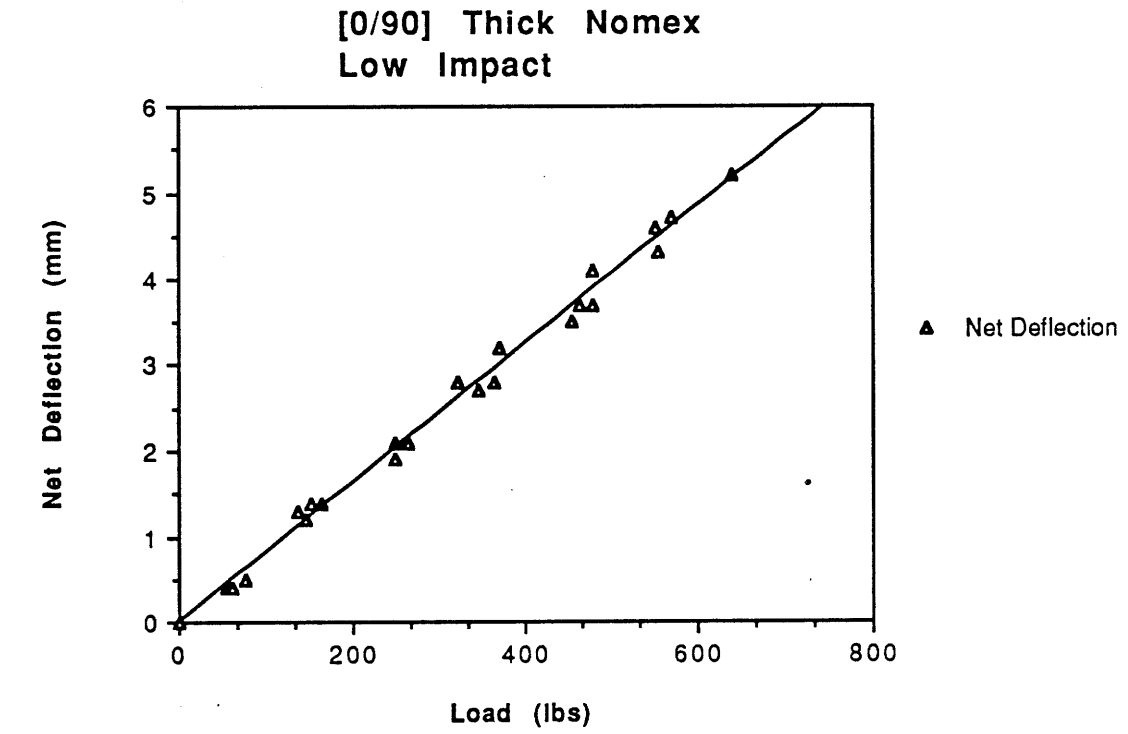

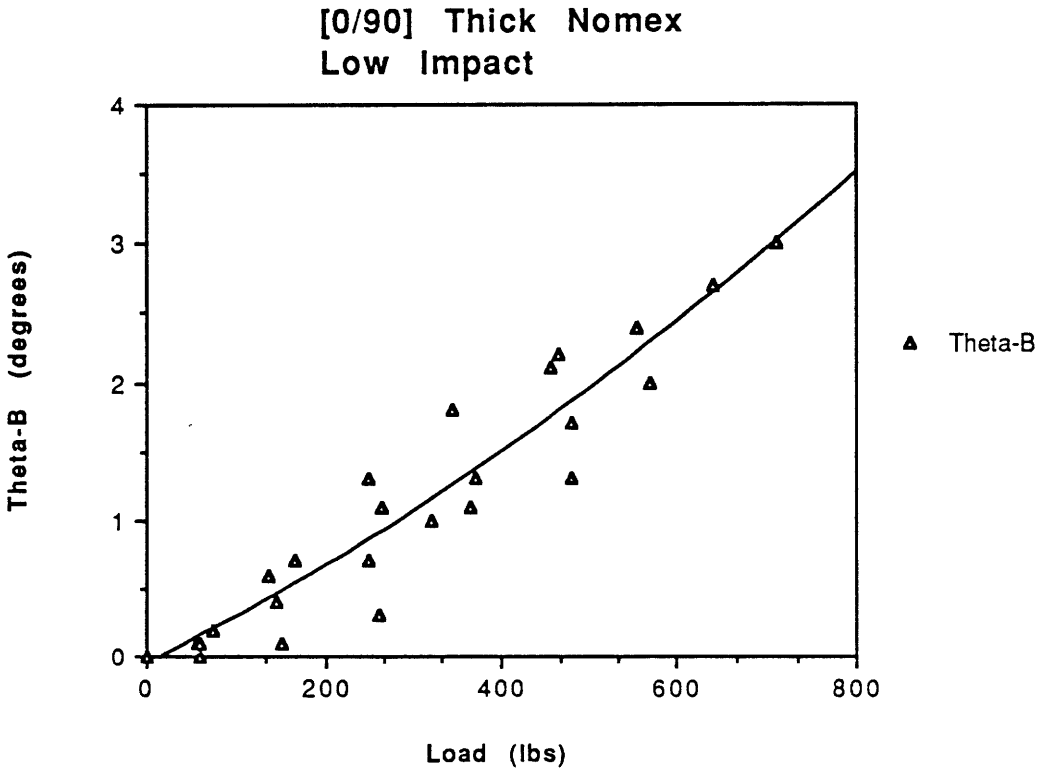

Figure C.12 [0/90] 1 inch; Low Damage: Deflection Curves

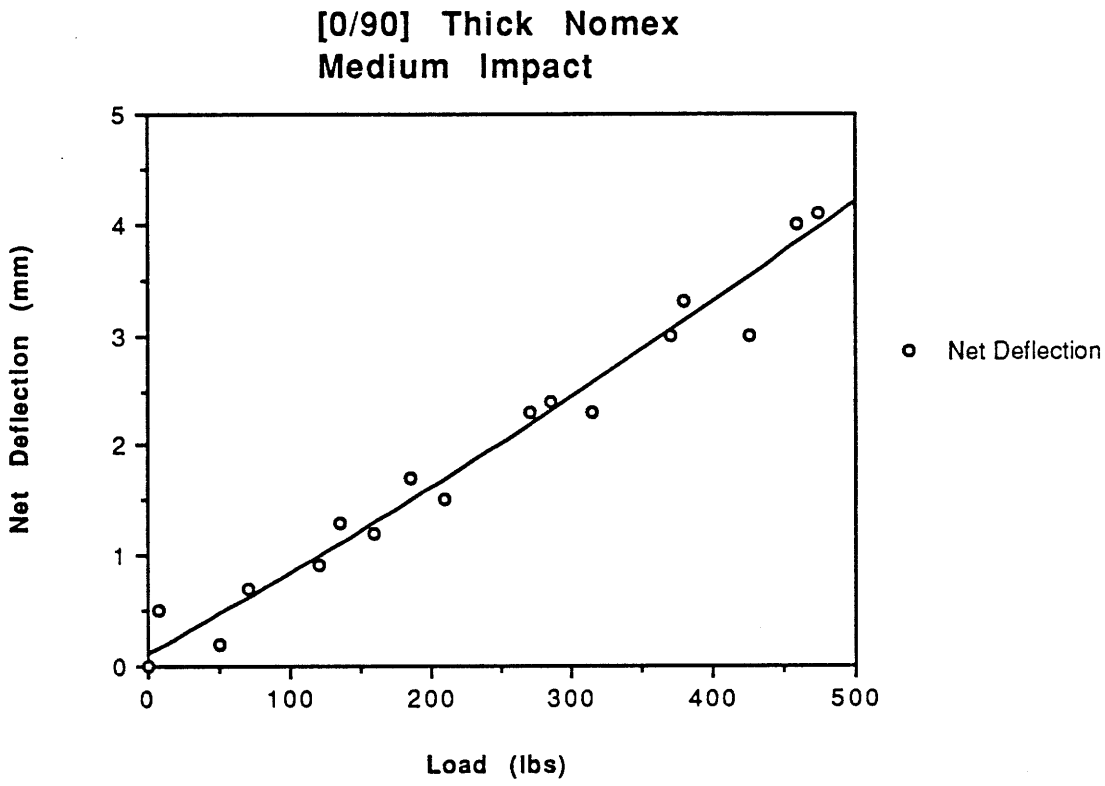

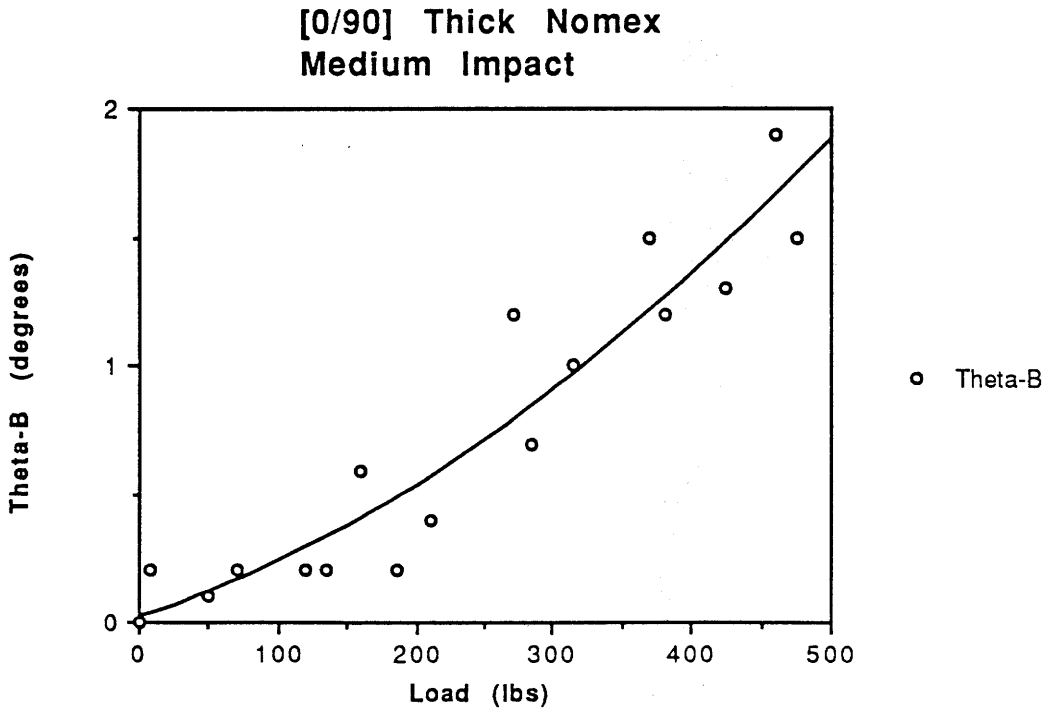

Figure C.13 [0/90] 1 inch; Medium Damage: Deflection Curves

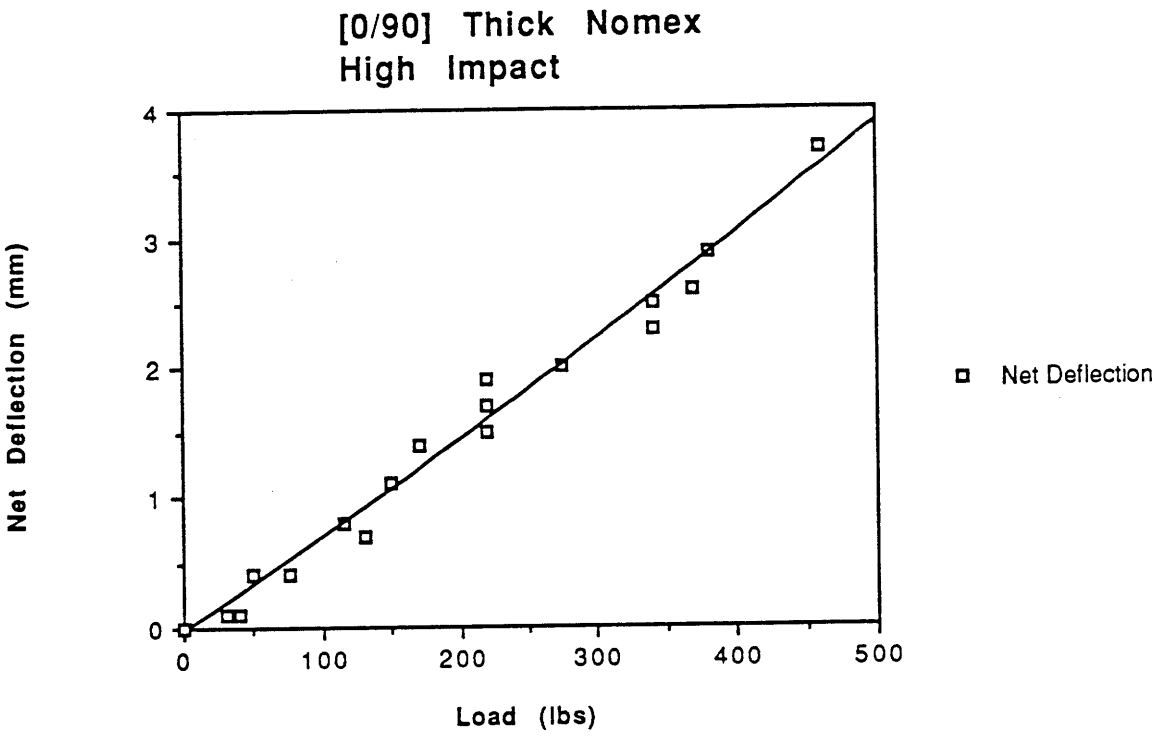

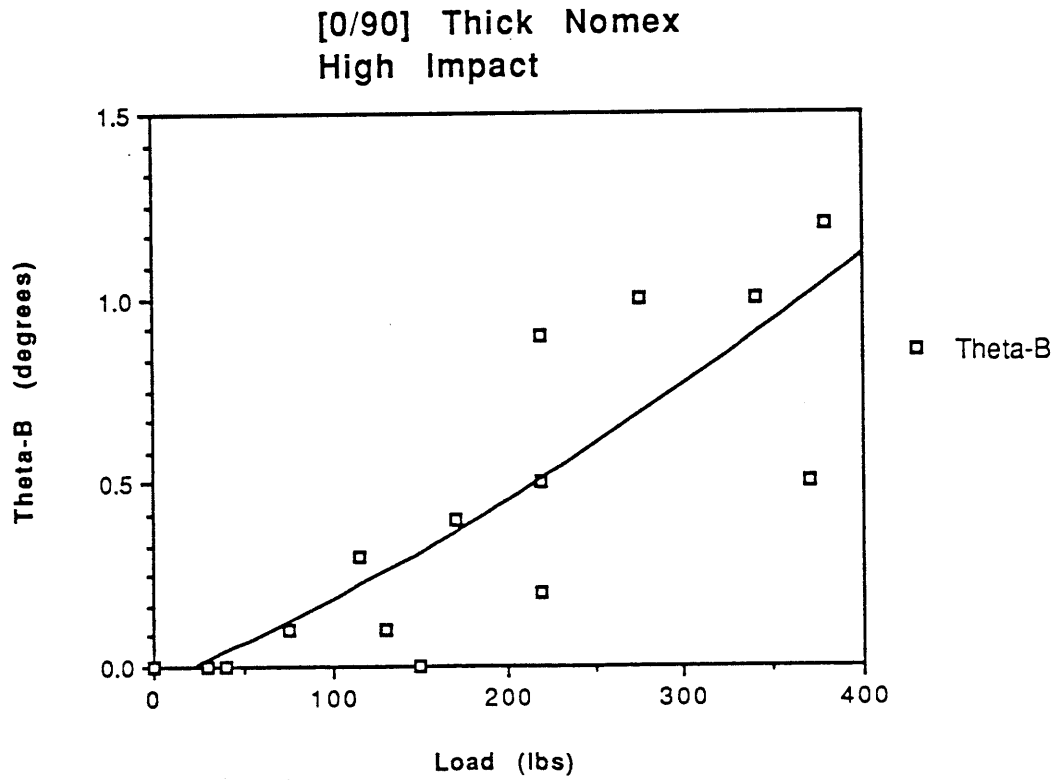

Figure C.14 [0/90] 1 inch; High Damage: Deflection Curves

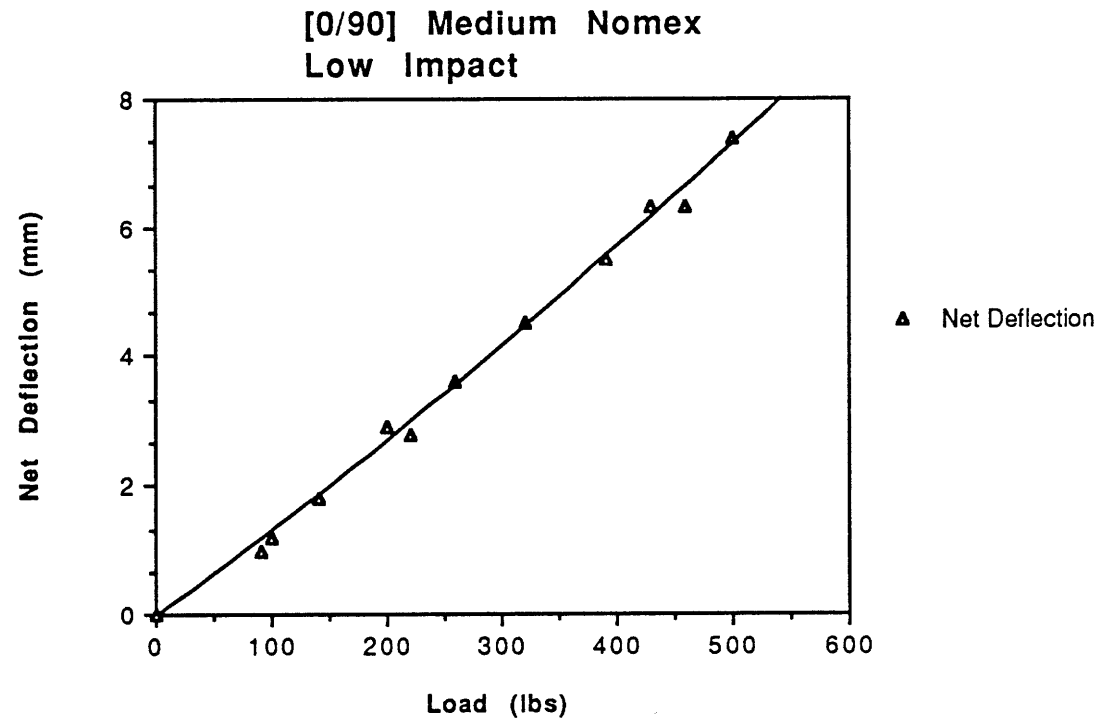

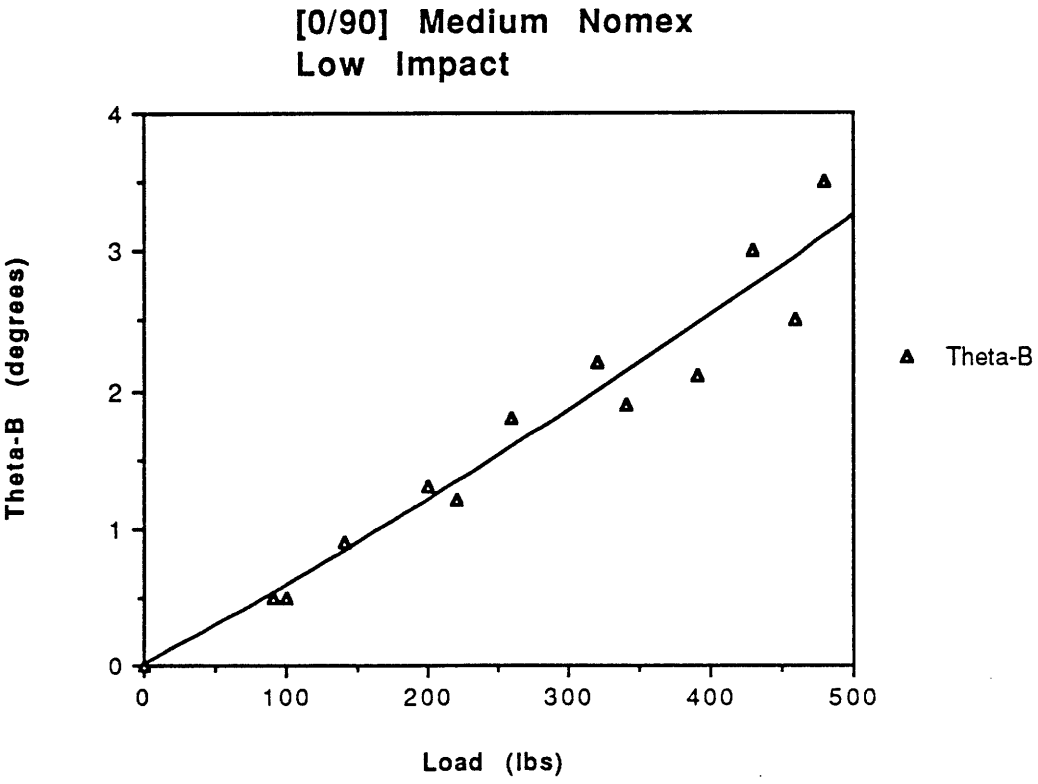

Figure C.15 [0/90] .687"; Low Damage: Deflection Curves

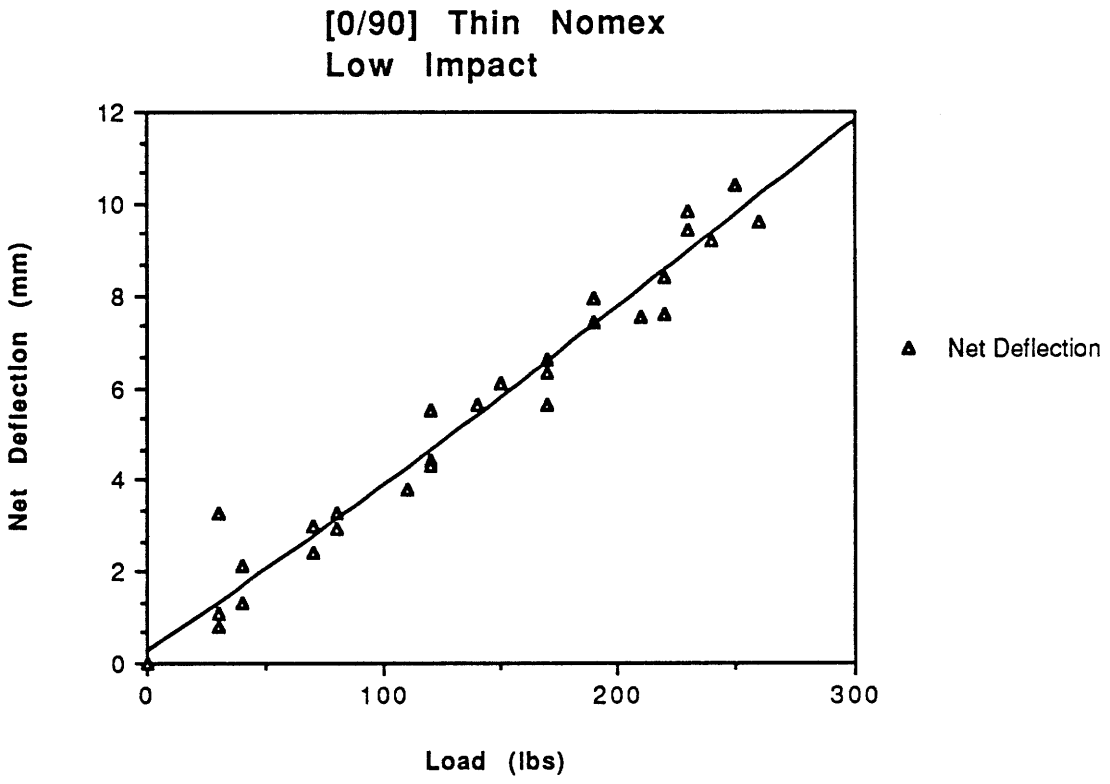

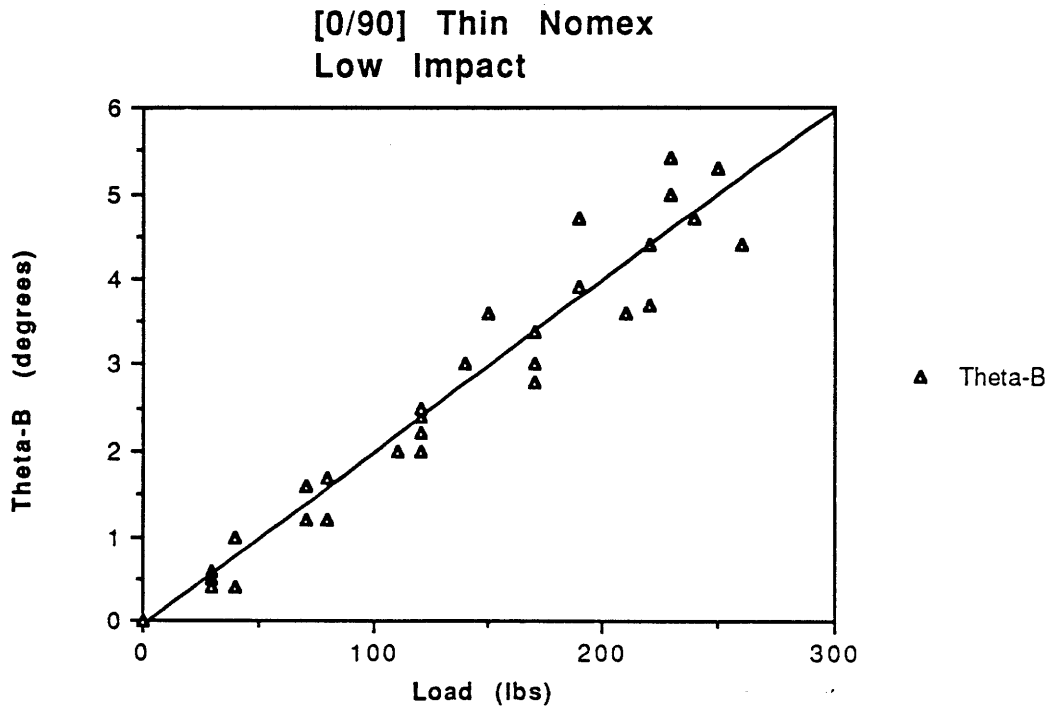

Figure C.16 [0/90] .375"; Low Impact: Deflection Curves

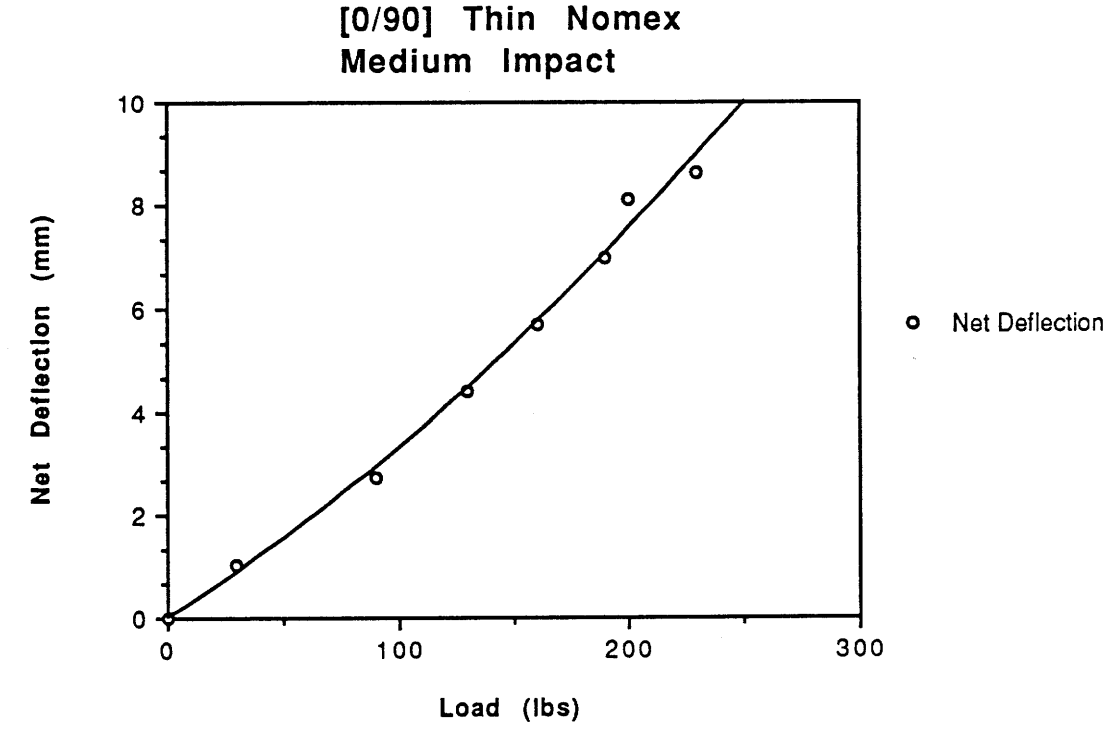

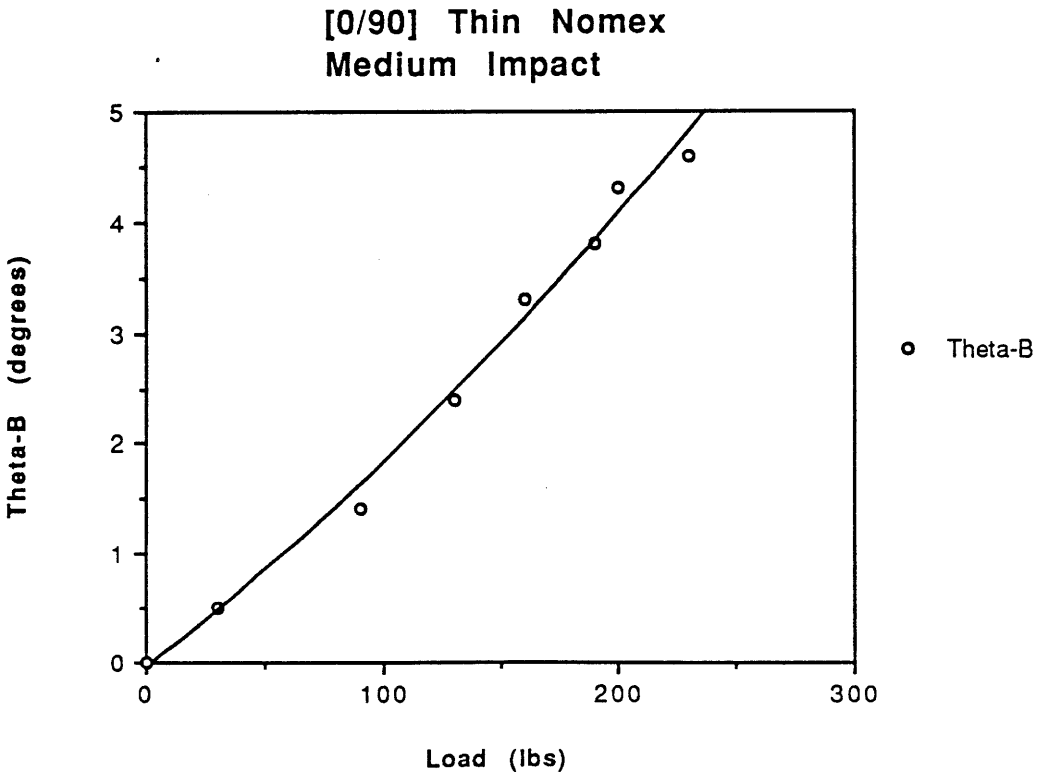

Figure C.17 [0/90] .375"; Medium Damage: Deflection Curves

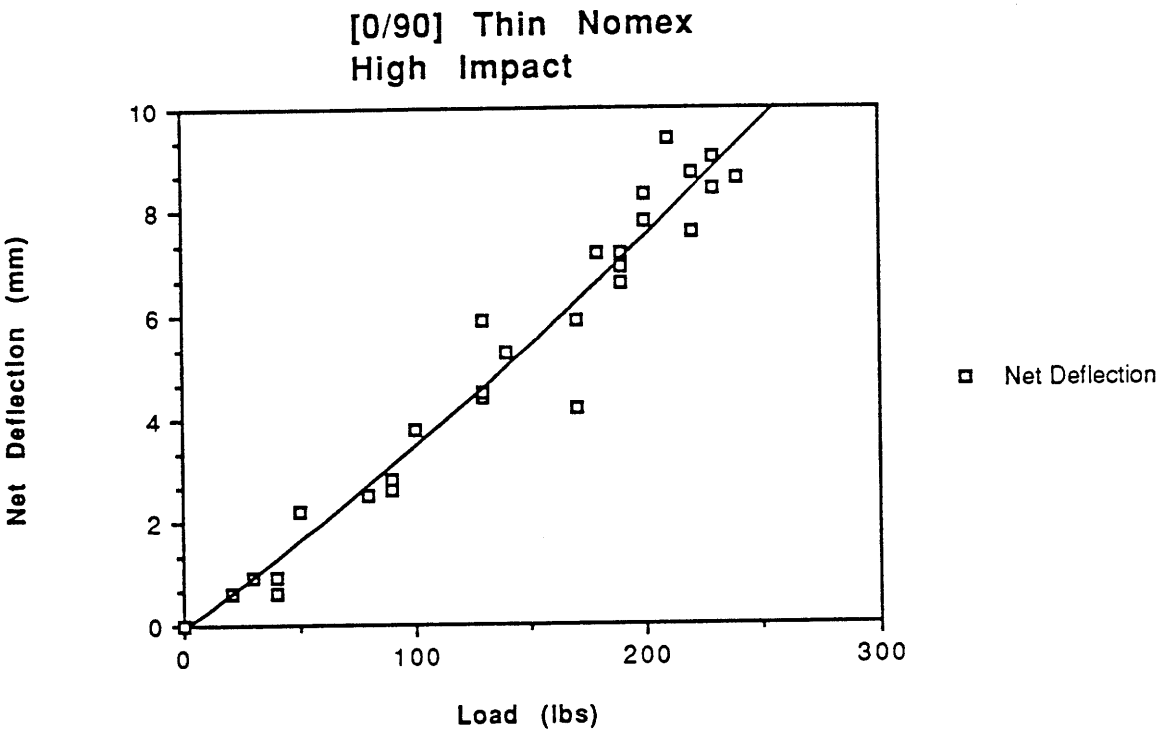

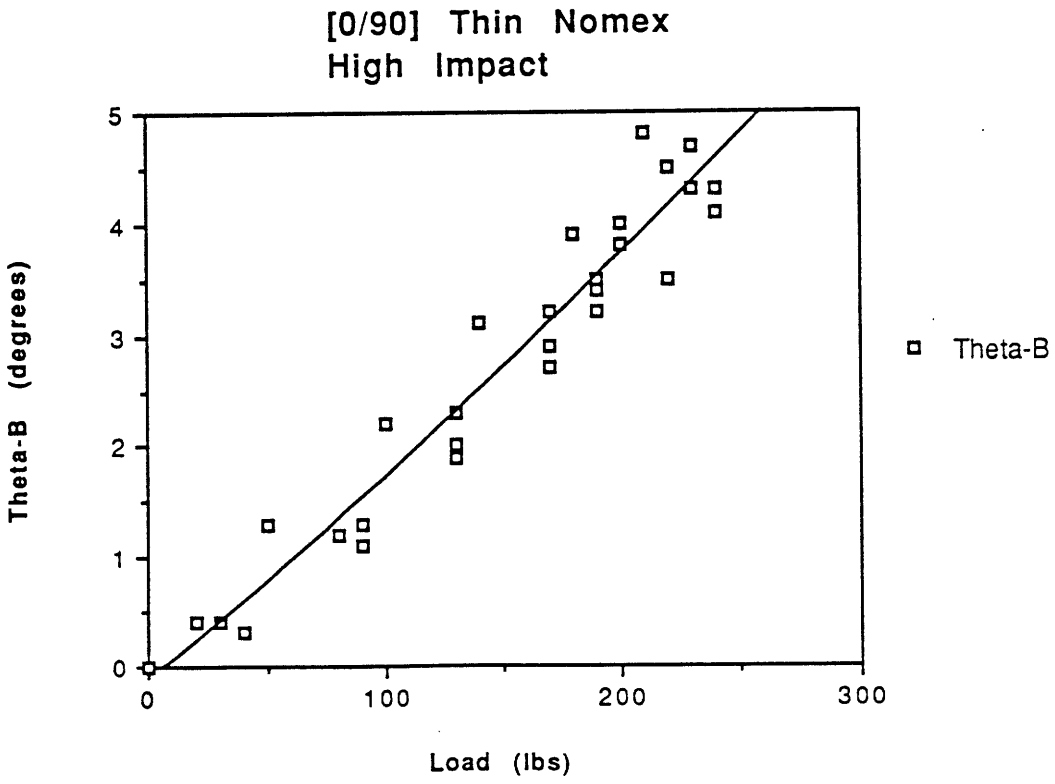

Figure C.18 [0/90] .375"; High Damage: Deflection Curves

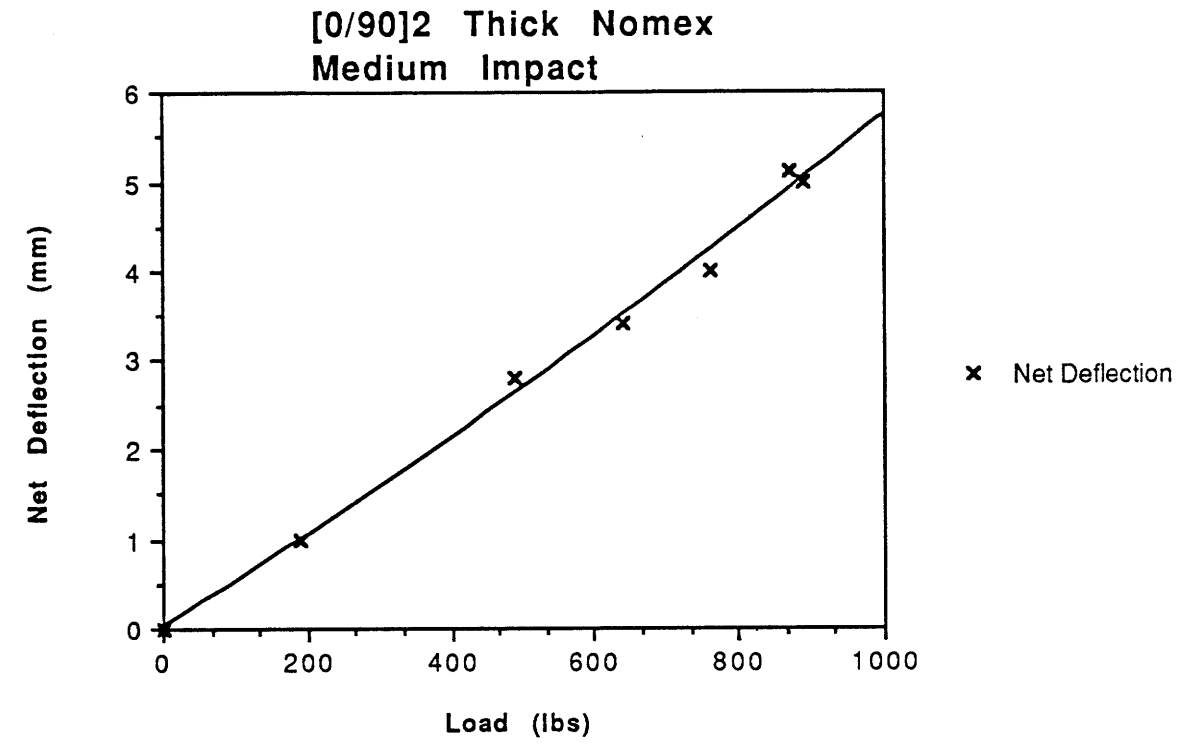

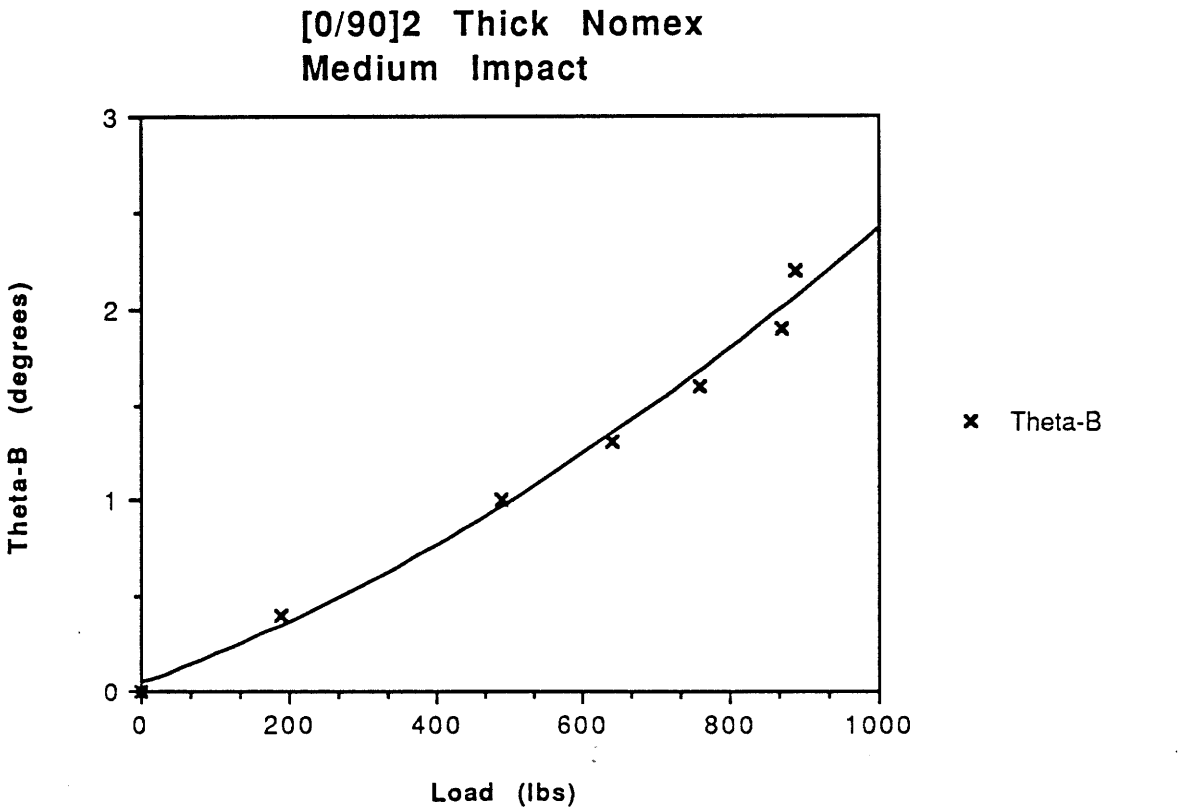

Figure C.19 [0/90]s 1 inch; Medium Damage: Deflection Curves

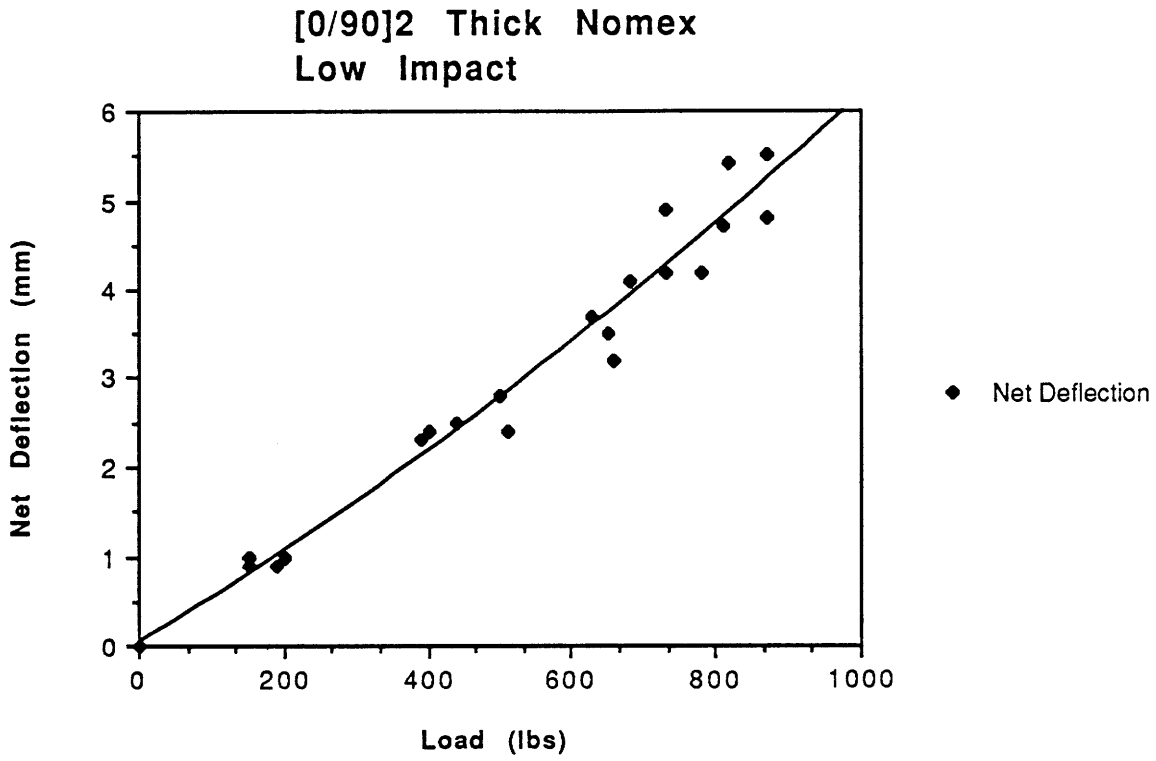

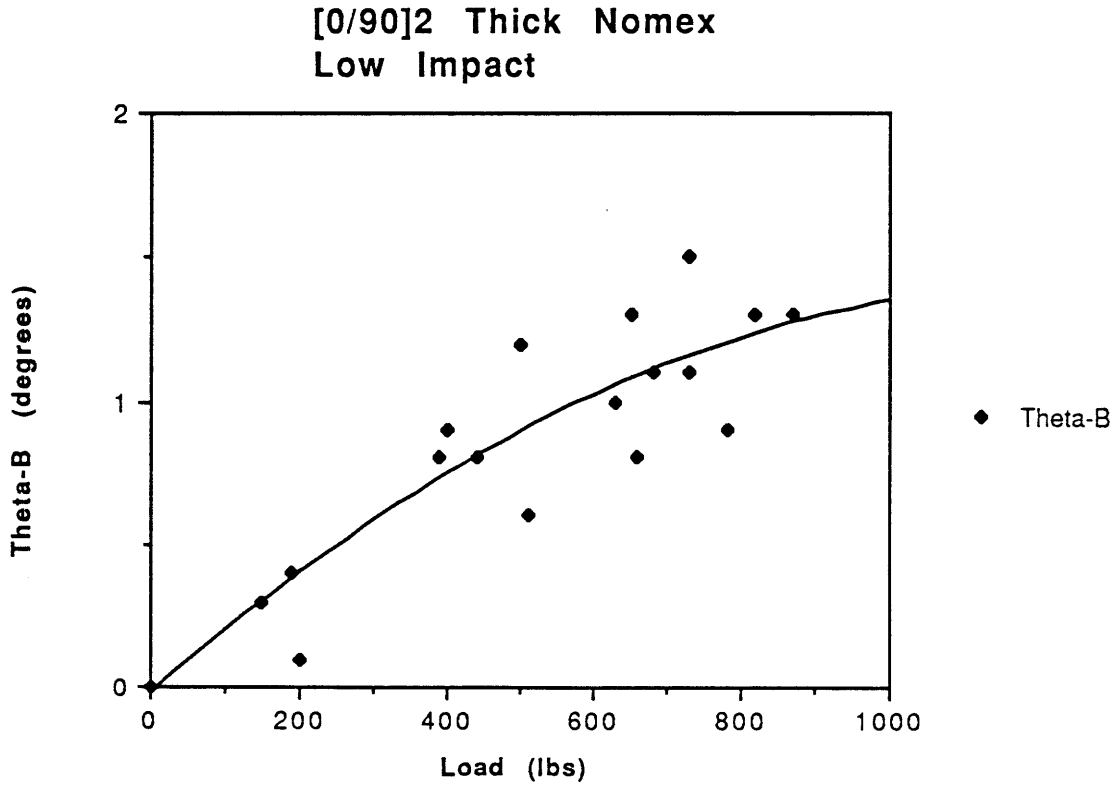

Figure C.20 [0/90]s 1 inch; Low Damage: Deflection Curves

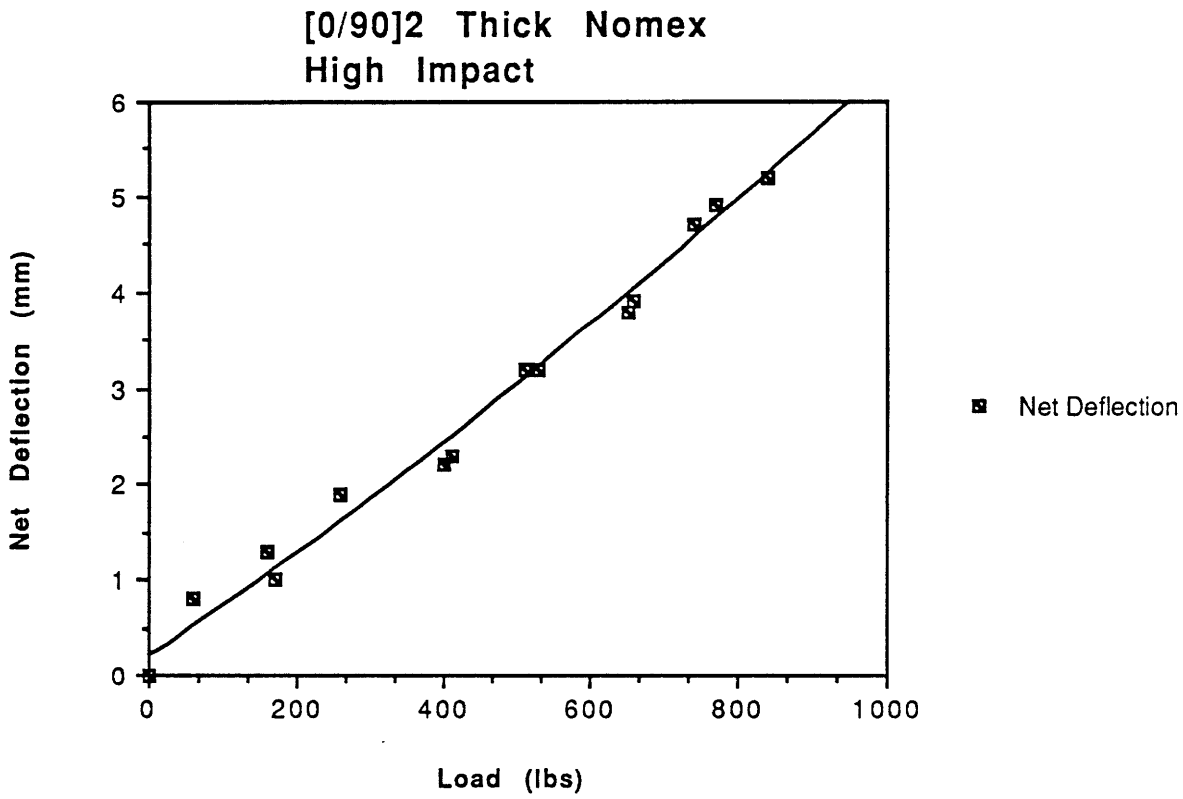

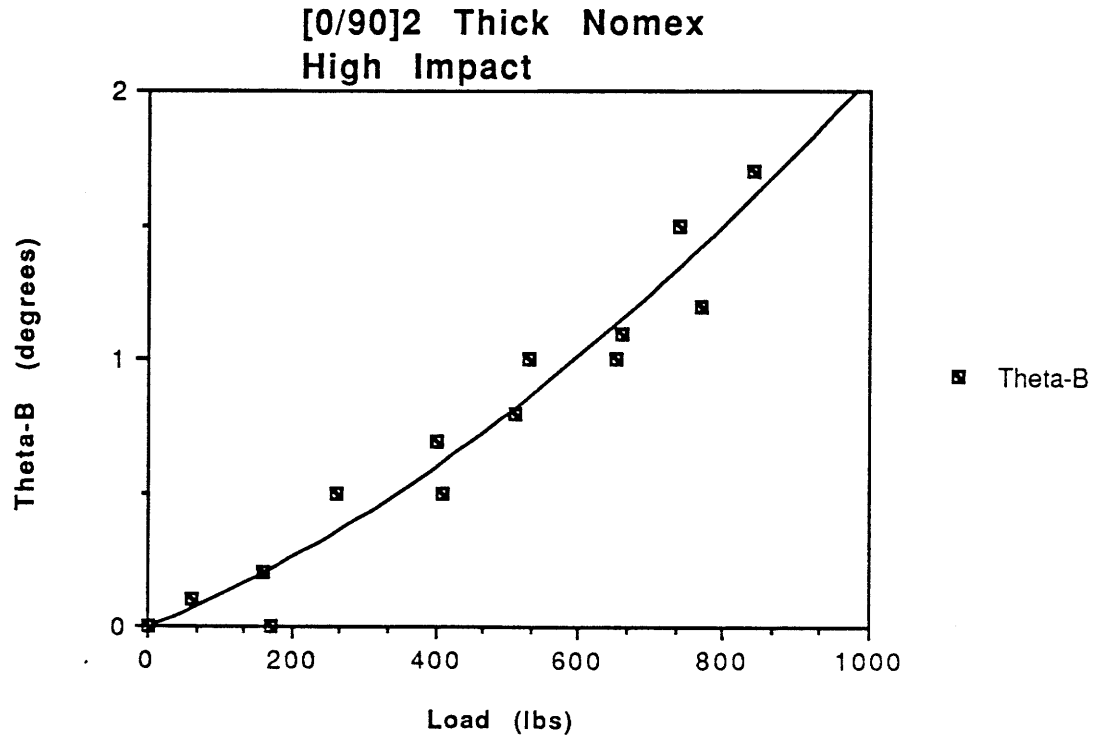

Figure C.21 [0/90]s 1 inch; High Damage: Deflection Curves